礼升生物发表文章目录

LISHENG

上海礼升生物

Shanghai Lisheng Biotech

类器官小课堂

微信扫一扫 了解更多类器官前沿资讯

扫一扫二维码，立即与创始人韩欣欣博士建立联系，共同开启生物科技新篇章！

礼升生物发表文章目录

Journal name	IF	Paper name	Date
Cell Transplantation	4.3	PARPi Decreased Primary Ovarian Cancer Organoid Growth Through Early Apoptosis and Base Excision Repair Pathway	2023.7
The Innovation	33.1	Landscape of human organoids Ideal model in clinics and research	2023.10
Cell organoid		Patient-derived skin tumor organoids with immune cells respond to metformin	2024.1
Cell organoid		Crossroad of ovarian cancer organoid culture Single cell suspension and mechanically sheared fragment	2024.5
Cell organoid		An advanced culture methodology suitable for the self-assemble and tissue-fragment derived intrahepatic cholangiocarcinoma organoids	2024.5
Cell organoid		Generation of patient-derived glioblastoma organoids_ a comparative study of enzymatic digestion and mechanical fragmentation methods	2024.5
Med Comm	10.7	Patient-derived ovarian cancer organoid carries immune microenvironment and blood vessel keeping high response to cisplatin	2024.6
Phytomedicine	6.7	Zengmian Yiliu formula suppresses cell cycle in immune-rich ovarian cancer patient-derived organoids	2025.4
Theranostics	12.4	The first abdominal aortic aneurysm organoid model replicates complex microenvironment for in vitro disease study	2025.8

Original Article

Cell Transplantation
Volume 32: 1–12

DOI: 10.1177/09636897231187996
journals.sagepub.com/home/cll
ssage

PARPi Decreased Primary Ovarian Cancer Organoid Growth Through Early Apoptosis and Base Excision Repair Pathway

Qi Cao[1*], Lanyang Li[2*], Yuqing Zhao[1], Chen Wang[2], Yanghua Shi[2], Xiang Tao[1], Chunhui Cai[2], and Xin-Xin Han[3]

Abstract

Ovarian cancer (OC), particularly high-grade serous cancer (HGSC), is the leading cause of mortality among gynecological cancers owing to the treatment difficulty and high recurrence probability. As therapeutic drugs approved for OC, poly ADP-ribose polymerase inhibitors (PARPi) lead to synthetic lethality by inhibiting single-strand DNA repair, particularly in homologous recombination-deficient cancers. However, even PARPi have distinct efficacies and are prone to have drug resistance, the molecular mechanisms underlying the PARPi resistance in OC remain unclear. A patient-derived organoid platform was generated and treated with a PARPi to understand the factors associated with PARPi resistance. PARPi significantly inhibits organoid growth. After 72 h of treatment, both the size of organoids and the numbers of adherent cells decreased. Moreover, immunofluorescence results showed that the proportion of Ki67 positive cells significantly reduced. When the PARPi concentration reached 200 nM, the percentage of Ki67$^+$/4′,6-diamidino-2-phenylindole (DAPI) cells decreased approximately 50%. PARPi treatment also affected the expression of genes involved in base excision repair and cell cycle. Functional assays revealed that PARPi inhibits cell growth by upregulating early apoptosis. The expression levels of several key genes were validated. In addition to previously reported genes, some promising genes *FEN1* and *POLA2*, were also be founded. The results demonstrate the complex effects of PARPi treatment on changes in potential genes relevant to PARPi resistance, and provide perspectives for further research on the PARPi resistance mechanisms.

Keywords

apoptosis, base excision repair, cell cycle, ovarian cancer organoid, PARPi

Introduction

Ovarian cancer (OC) is a common cancer in females, accounting for 2.5% of all females and has an extremely high mortality rate[1]. Owing to the difficulty of early diagnosis, OC is often diagnosed at an advanced stage and considered as intractable. Poly ADP-ribose polymerase (PARP) plays an important role in single-stranded DNA repair and base excision repair pathways[2]. PARP inhibitors (PARPi) prevent single-strand DNA breaks (SSB) repair and allows SSB accumulation to develop into double-strand breaks (DSB) that require homologous recombination (HR)[3,4]. This results in synthetic lethality in HR-deficient cancer cells, and has been widely studied[3]. Several PARPis, including olaparib, niraparib, and rucaparib[3], have been approved as a novel therapeutic option for treating OC in the clinical setting and presented significant excitement.

However, clinical treatment with PARPi remains intractable. PARPis are effective as maintain therapy for OC patients with BRCA mutations, but more than 40% of these patients still do not benefit from PARPi[5]. Platinum resistance has been reported in a patient with gBRCAmt recurrent OC

[1] Obstetrics and Gynecology Hospital of Fudan University, Shanghai, China
[2] Shanghai Lisheng Biotech, Shanghai, China
[3] Shanghai Key laboratory of Craniomaxillofacial Development and Diseases, Shanghai Stomatological Hospital and School of Stomatology, Fudan University, Shanghai, China

Submitted: January 13, 2023. Revised: June 29, 2023. Accepted: June 29, 2023.

*These authors contributed equally to this work

Corresponding Authors:
Chunhui Cai, Shanghai Lisheng Biotech, Shanghai, 200001, China.
Email: caichunhui@lishengbiotech.com

Xin-Xin Han, Shanghai Key laboratory of Craniomaxillofacial Development and Diseases, Shanghai Stomatological Hospital and School of Stomatology, Fudan University, Shanghai, 200092, China.
Email: xxhan@fudan.edu.cn

after PARPi resistance[6]. Thus, the increasing use of PARPi in clinical practice has increased PARPi resistance. Therefore, the mechanisms of PARPi resistance should be identified to address this problem and provide guidance for early prevention.

HR restoration, DNA replication fork stabilization, BRCA reversion mutations, increased drug efflux, PARP1 and PAR glycohydrolase (PARG) dissociation, and epigenetic molecular modifications are the most common mechanisms of PARPi resistance. Although multiple mechanisms are involved, these are only some mechanisms contributing to PARPi resistance[7]. As an increasing number of patients receive initial therapy and potential re-treatment with PARPi, a drug-susceptibility testing platform and a clear understanding of the mechanisms by which tumors acquire PARPi resistance are required.

By exploiting our patient-derived organoid platform, we developed organoid models with high similarity to clinical OC tissues. PARPi successfully inhibited organoid growth and reduced the proportion of Ki67-positive cancer cells; however, some Ki67-positive cells survived at high PARPi concentrations, indicating that PARPi resistance was reproduced on organoid platforms. In this study, we investigated the impact of PARPi treatment on OC organoids and attempted to identify the factors associated with PARPi resistance. Several genes involved in base excision repair and cell cycle pathways were also altered.

Materials and Methods

Patient Characteristics

We derived organoids from several representative patients and enrolled one patient with stage IV high-grade serous cancer (HGSC), who underwent surgery a bilateral salpingectomy in October 2022 and did not undergo any radiotherapy or chemotherapy before surgery. In this study, surgical samples were used in the experiments after collecting informed consent and approval from the Ethics Committee of the Obstetrics and Gynecology Hospital of Fudan University.

Organoid Culture

Fresh obtained clinical tissues were washed three times with an organoid washing buffer (LSTO00100201; Shanghai LiSheng Biotech, China) to rinse the mucus and debris. Then, the tissues were mechanically sheared using and Ovarian Cancer Tissue Sampling Kit (LSTO00100101, Shanghai LiSheng Biotech, China). Next, 3- to 6-mm tissue debris was seeded in 6-well culture plates (#3516, Costar) and cultured with 6-mL OC organoid medium (LSTO001004, Shanghai LiSheng Biotech, China) in a Heracell™ Vios 160i CR CO_2 incubator (51033770, ThermoFisher) at 37℃ under a humidified atmosphere with 5% CO_2. Approximately 50% medium was changed every 5 days, to provide sufficient nutrients for the organoids. After the tumor pieces developed into organoids, they were passaged every 15 days according to the manufacturer's instructions. If the pieces were circular and presented the characteristics of the parental tumor within 7 days, the culture was regarded as successful.

Drug Treatment Assay

The mechanically disrupted organoids were cultured in 6- and 24-well plates (#3516 and #3337, respectively; Costar) for 8 h and treated with the indicated concentrations of olaparib (AZD2281, Selleck). For gene expression analysis, RNA was extracted from a portion of the cells in 6-well plates cultured for 48 h and sequenced. The cells cultured for 24 and 72 h were analyzed by flow cytometry. To measure the growth and morphological changes in organoids, adherent cells in 24-well plates and organoids in 6-well plates were observed daily using a Leica DMi1 inverted microscope and imaged at 24, 48, and 72 h. Organoids in 6-well plates were sliced into frozen sections for immunofluorescence and histological analyses. The results were normalized to those of the dimethyl sulfoxide (DMSO) controls.

Histology and Immunofluorescence

Tissues and organoids were fixed in 4% paraformaldehyde (PFA) (BL539A, Biosharp) for 30 min, dehydrated with sucrose, and embedded in 7.5% gelatin for standard histology and immunofluorescence (IF). Frozen sections (10 mm) of the embedded samples were retrieved using citric acid (PH6.0). The adherent cells were fixed using 4% PFA for 20 min. Both adherent cells and frozen sections were permeabilized using 0.25% Triton X-100 in PBST, and blocked with Primary Antibody Dilution Buffer (E674004, Sangon Biotech, China). After overnight incubation with 1:1000 primary antibody Rabbit anti-PAX8 (10336-1-AP, Proteintech) and anti-Ki67 (MA5-14520, ThermoFisher) at 4°C, sections were washed two times in 0.125% PBST and incubated at room temperature with 1:1000 secondary antibody anti-rabbit (Cy3) (711-165-152, Jackson). Then, they were incubated with 4′,6-diamidino-2-phenylindole, dihydrochloride (DAPI) (D1306, ThermoFisher) stain solution at room temperature. After washing three times with 0.125% PBST, they were scanned using a Keyence BZ-X810 Fluorescence Microscope and the proportions of immunoreactive cells were counted. For H&E staining, the sections were washed twice and stained using a hematoxylin-eosin (HE) Stain Kit (G1120, Solarbio, China) according to the manufacturer's instructions.

Flow Cytometry

The adherent cells were collected and resuspended in fresh PBS. Apoptosis was analyzed by flow cytometry using an

Agilent NovoCyte Penteon instrument with an Annexin V/PI kit (BD Biosciences) according to the manufacturer's instructions.

RNA Sequencing

RNA was extracted from adherent cells and several floating organoids culture for 48 h using the RNA Easy Fast Tissue/ Cell Kit (4992732, Tiangen, China) and the purity was assessed using Qubit 3.0 Fluorometer (ThermoFisher, Waltham, England). After constructing the RNA library followed by NEBNext Ultra RNA library for Illumina (Biolab, England), RNA was sequenced on Illumina Hiseq 4000 using 150 bp paired-end reads. The sequencing results of fragments per kilobase of transcript per million mapped reads (FPKM) were analyzed. Differential gene expression analysis was performed using online software (Morpheus, https://software.broadinstitute.org/morpheus). An online database (g: Profiler) was used for analyzing the molecular functions, biological processes, and cell cycles.

Gene Expression Analysis

RNA was reverse-transcribed using FastKing gDNA Dispelling RT SuperMix (KR118, Tiangen, China). For quantitative real-time PCR (qPCR), gene-specific forward and reverse primers were used to amplify the samples with LightCycler 96 Instrument (Roche). The primer sequences are listed in Supplementary Table 1. The target gene expression levels were normalized to those of the housekeeping genes glyceraldehyde-3-phosphate dehydrogenase (GAPDH) and ribosomal protein 18 (18S). Relative gene expression levels were calculated as $2^{-(\Delta\Delta Ct)}$ values.

Statistical Analysis

To determine the cutoff points for qPCR and IHC, receiver operating characteristic curves were analyzed. The Student's *t*-test was used to determine significant differences between multiple statistical comparisons. Data analysis and graph drawing were performed using GraphPad Prism version 8. $*P < 0.05$ was considered significant.

Results

OC-Derived Organoids Were Highly Similar to Clinical Tissues

OC tissues obtained from consenting patient were dissociated and seeded in a commercial OC organoid culture medium (Fig. 1A). Histological image and immunohistological analyses were performed for one clinical tissue and one organoid to assess the similarity between the organoid and parental tumors. The morphology of organoids directly cultured from clinical tissues were highly coherent (Figs. 1B, 2A, B). PAX8 and Ki67 expression is frequently detected in ovarian carcinomas, and immunofluorescence is often used to confirm PAX8 and Ki67 positive tumors[8,9]. Immunofluorescence staining showed that the PAX8 and Ki67 expression levels in organoids remained consistent with those in clinical tissues (Figs. 1C–E, 2C, D). Our results were also consistent with the reported findings about Ki67 and PAX8 positive proportion in OC[9,10]. This result suggested that the organoids showed similar morphological and proliferative activity to patient tumors, indicating that our organoids have a high degree of consistency in patient tumor tissues. Hence, this organoid model may be useful for drug screening and other clinical tests.

PARPi Treatment Affects OC Organoids Morphology and Growth

Several organoids from one patient were tested for sensitivity to PARPi, as it is a useful U.S. Food and Drug Administration (FDA)-approved drug for OC treatment (Fig. 2E). This experiment was divided into three groups according to the drug concentration. Morphological changes in organoids or adherent cells were assessed at different time points. As expected, our organoids showed an increased sensitivity to PARPi (Fig. 3A). The organoids were treated with PARPi and cultured for 72 h, which resulted in progressively smaller organoids and less dense structures. Fibroblast-like cells that migrated from the organoids, and adhered to the culture plate were regarded as adherent cells. The number of adherent cells significantly reduced after PARPi treatment (Fig. 3A). Ki67 staining indicated a decreasing Ki67 positive cell proportion among adherent cells (Fig. 3B). Moreover, PARPi treatment decreased total cell number and Ki67 expression (Fig. 3C). Postoperatively, the patient received cisplatin and paclitaxel in accordance with the guidelines of the National Comprehensive Cancer Network and PARPi as candidates. Given the positive results of our studies and the completed chemotherapy of the patient, we suggest that PARPi might be a clinically viable choice for maintain therapy.

PARPi Promotes Early Apoptosis in OC Oragnoids

We assessed whether PARPi affected the apoptosis of organoids. After PARPi treatment for 24 h, the percentage of early and late apoptotic organoids was not significantly different among all groups (Fig. 4A). However, after 72 h, the drug treatment substantially induced early apoptosis and had a negligible effect on late apoptosis (Fig. 4B). Regardless of the concentration used, early apoptosis after 72 h treatment was four to five folds higher than that after 24 h treatment (Fig. 4C). These results suggest that early apoptosis significantly increased 72 h after PARPi administration, which may guide clinical practice.

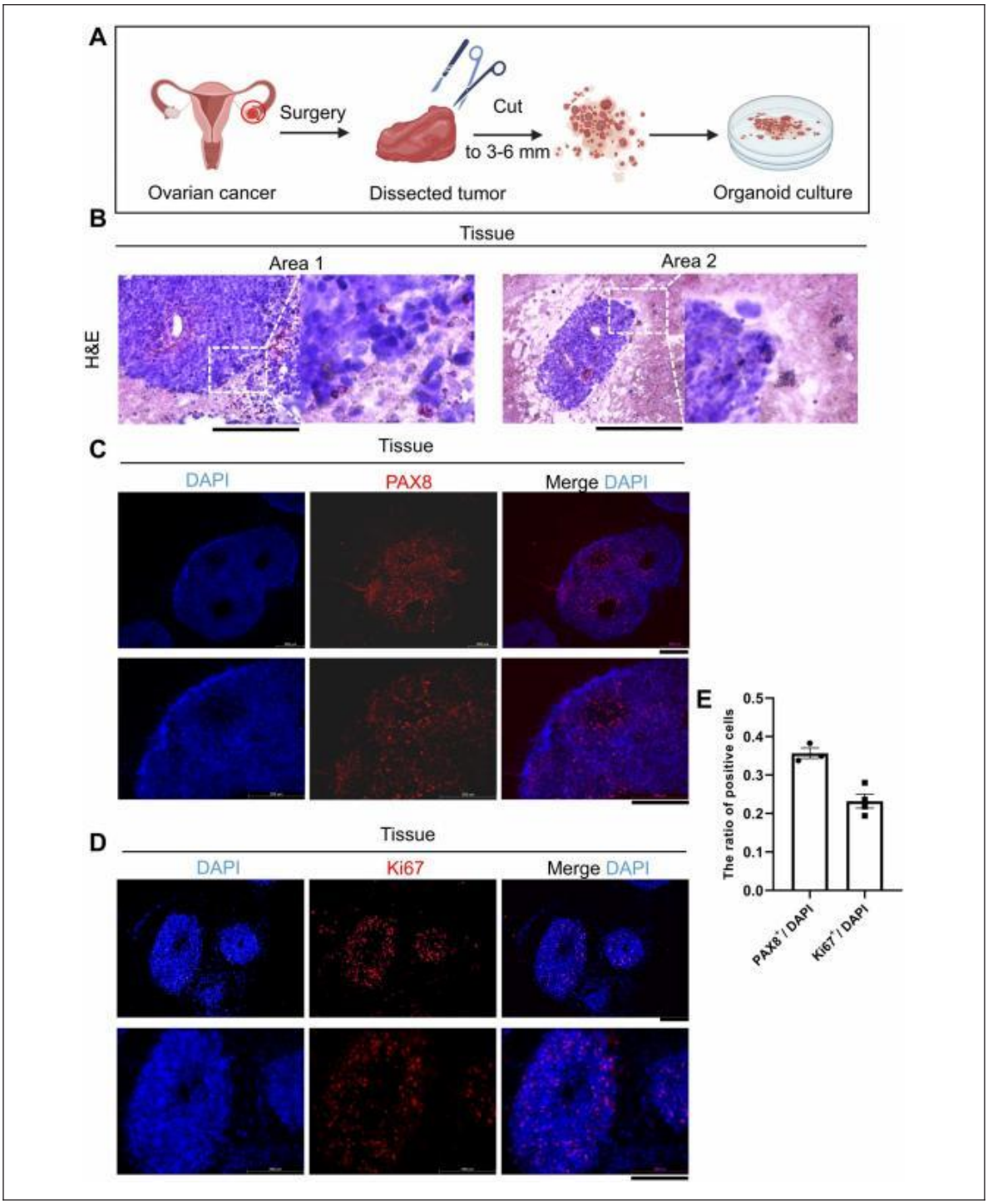

Figure 1. Detection of patient-derived tumor tissues. (A) Schematic diagram of OC organoid culture processing. (B) Representative H&E staining of clinical tissues. Scale bars: 200 μm. (C, D) Immunofluorescence results of PAX8 and Ki67 were shown. The expression level was showed by merged images. Scale bars: 200 μm. (E) Bar graphs describe the ratio of ovarian cancer marker positive cells to DAPI-stained cells in OC tissues. Dots represent individual data points. Quantitative analysis was presented as the mean ± SEM.

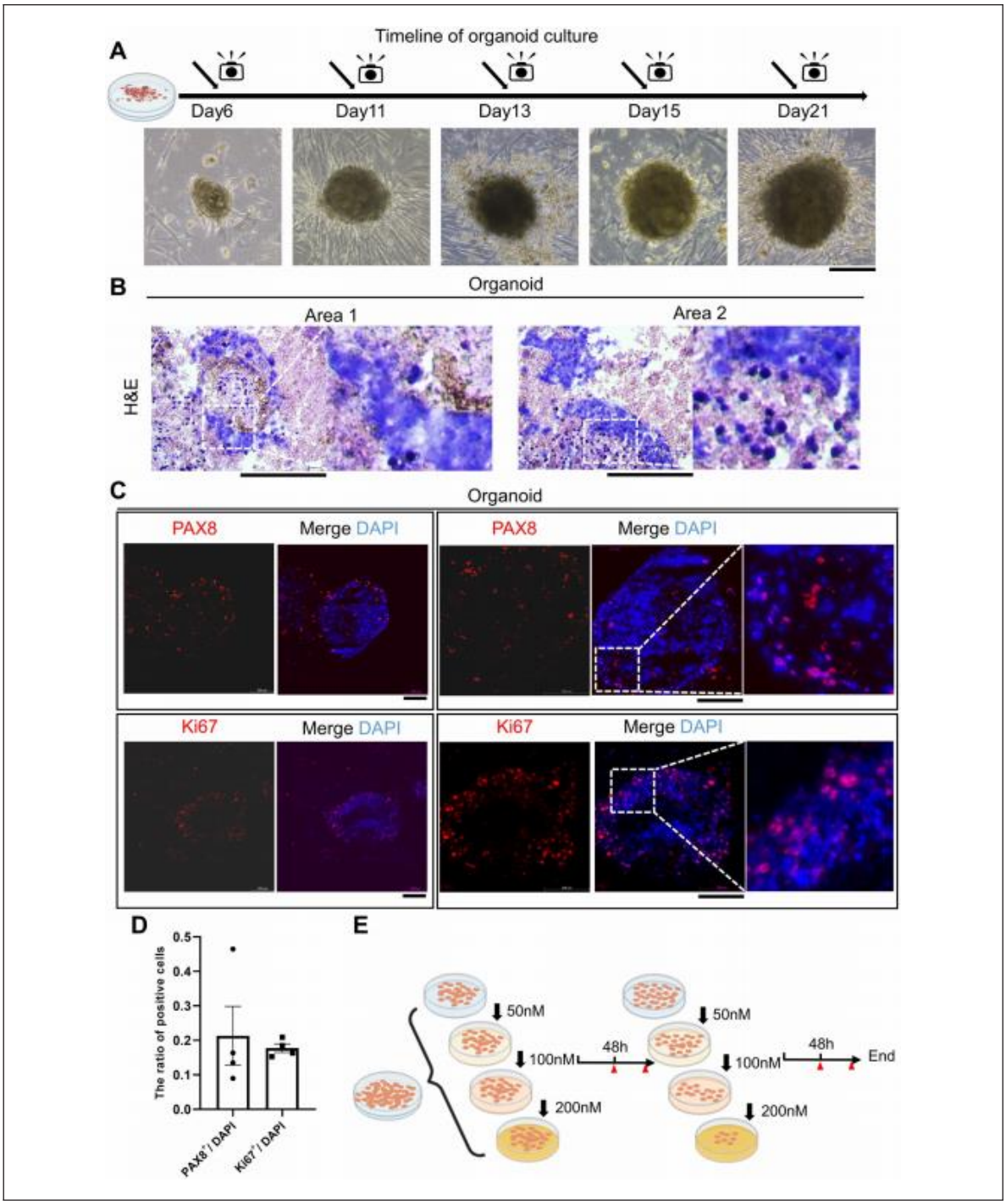

Figure 2. Detection of patient-derived OC organoids. (A) Bright view pictures of patient-derived ovarian organoids at different time points; (B) Representative H&E staining of OC organoids. (C) immunofluorescence results of PAX8 and Ki67 were shown. The expression level was showed by merged images. Scale bars: 200 μm. (D) Bar graphs describe the ratio of ovarian cancer marker positive cells to DAPI-stained cells in OC organoids. Dots represent individual data points. Quantitative analysis was presented as the mean ± SEM. (E) Schematic diagram of drug sensitivity assay processing.

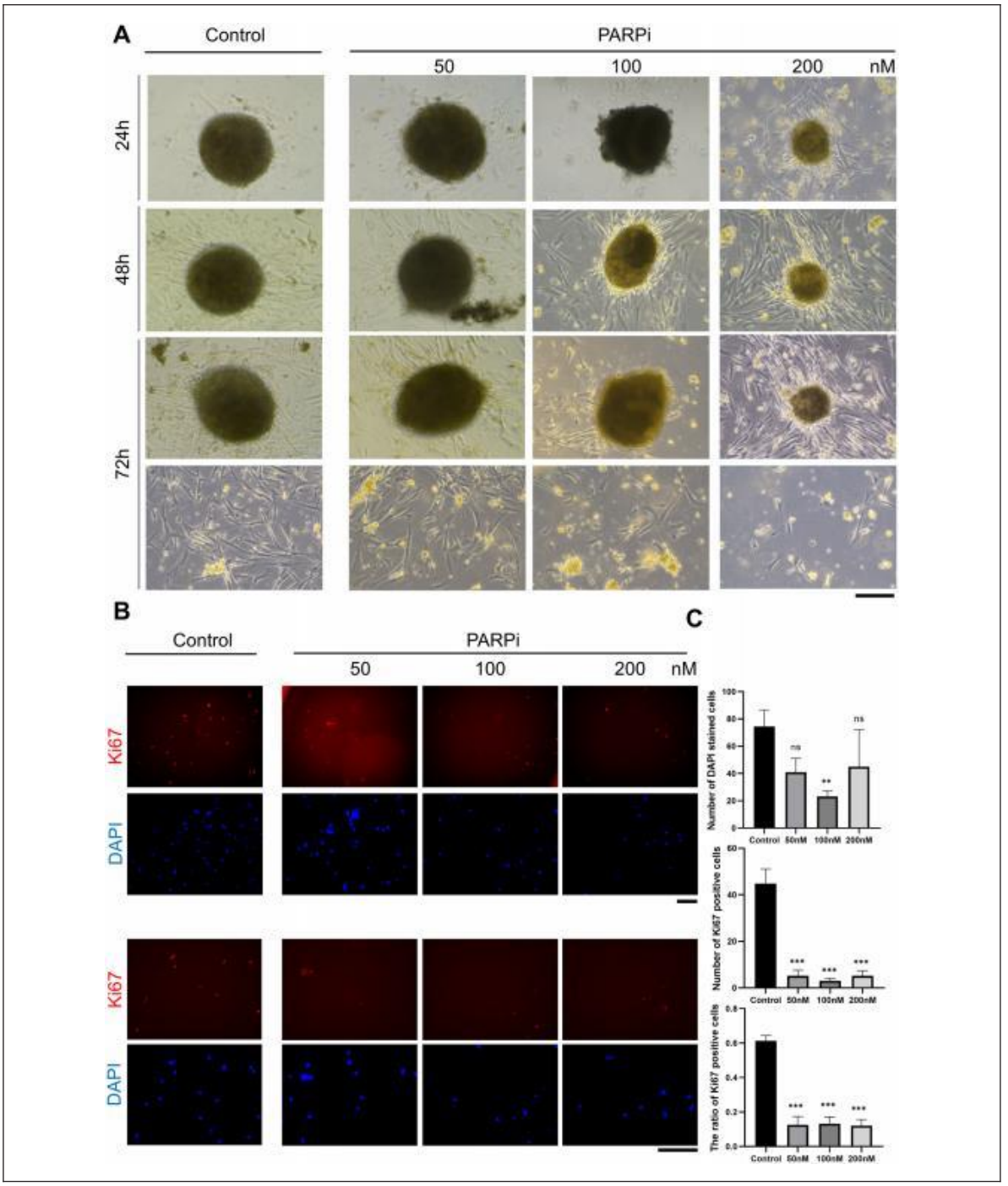

Figure 3. Morphological changes of organoids after PARPi treatment. (A) Representative bright field images of organoids after PARPi treatment were shown. The patient-derived organoids were inhibited by high-concentration PARPi, and treating for a long time did not represent a significant difference. Scale bars, 200 μm. (B) Representative images of Ki67 and DAPI immunofluorescence staining of adherent cells. Three indicated groups were divided to investigate dose sensitivity. (C) The expression level of ovarian cancer marker Ki67 and proportion of Ki67/DAPI in adherent cells after PARPi treatment was measured. Data are presented as the mean ± SEM (n = 3; *P < 0.05; **P < 0.0I; ***P < 0.00I; student's test).

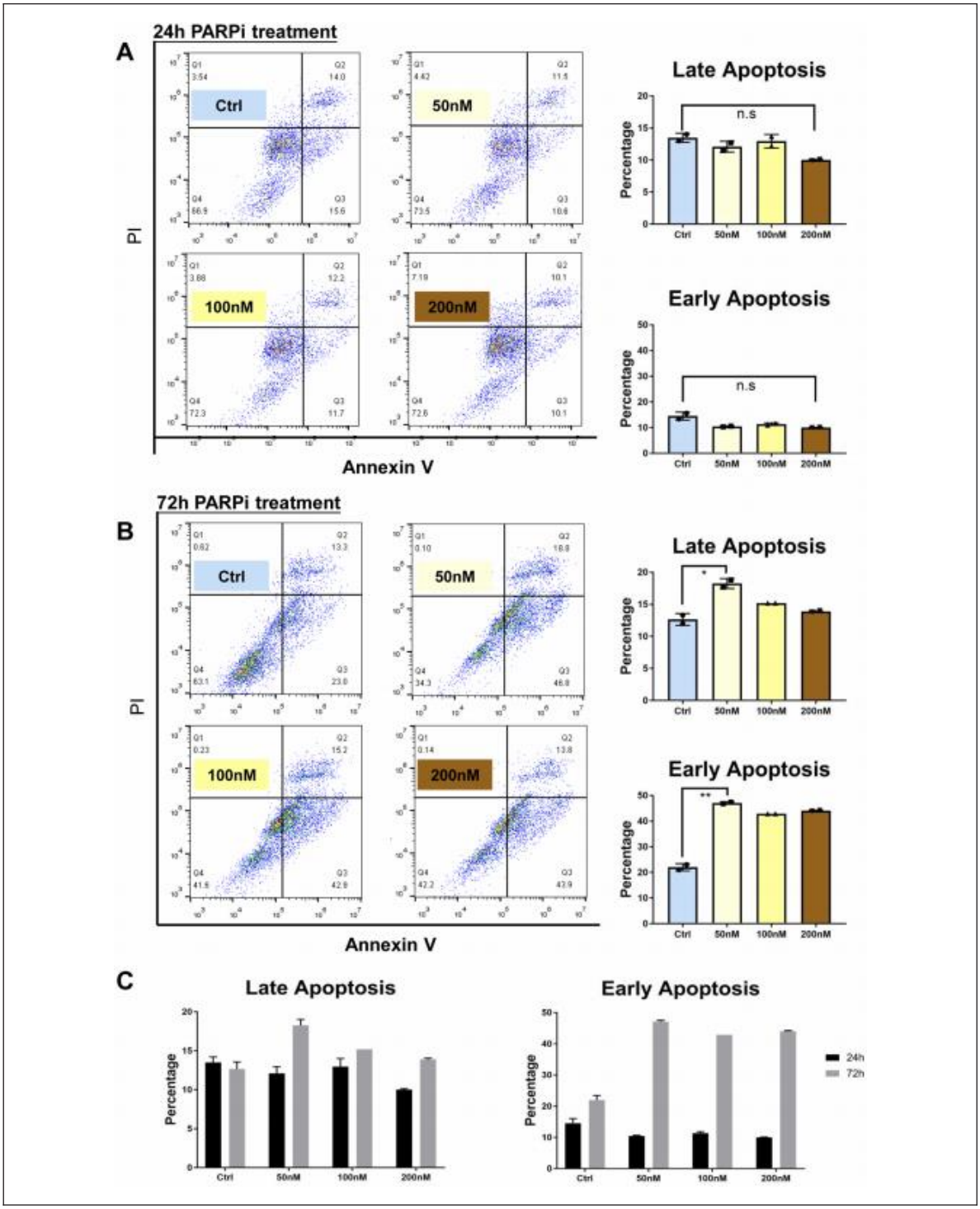

Figure 4. Analysis of apoptosis after PARPi treatment. (A) The apoptosis after 24 h PARPi treatment was evaluated and quantified. (B) The apoptosis after 72 h PARPi treatment was evaluated and quantified. (C) The percentages of apoptotic cells with different treatment concentration in early apoptosis and later apoptosis.

Gene Expression of Base Excision Repair and Cell Cycle Were Affected by PARPi

This study aimed to enhance the understanding of the effects of PARPi treatment on gene modulation. RNA sequencing (RNA-seq) was performed to determine changes in the organoid gene expression profile in one parental tumor sample and one derived organoid sample after treatment with 200 nM PARPi. We compared the transcriptomes of the PARPi-treated and control samples and found that at least 1,011 and 1,005 genes were upregulated and downregulated, respectively (Fig. 5A). Gene ontology (GO) was used to classify these differentially expressed genes (DEGs) into biological processes, molecular functions, and cellular components. The molecular function associated with upregulated genes was protein binding (Fig. 5B). The regulation of cellular progress in biological processes was also dramatically affected (Fig. 5C). Several pathways, such as the cell periphery, integral component of the membrane, and intrinsic component of the membrane, were downregulated. Genes belonging to these groups may be associated with PARPi treatment. Some PARPi-related upregulated and downregulated genes have never been reported. Considering the mechanism ofPARP inhibition, we selected several genes related to base excision repair and the cell cycle for FPKM analysis[11,12] (Fig. 5D, E). Among the identified upregulated genes, the expression of the cell proliferation gene *MCM2* decreased after treatment, which was consistent with gene expression level analysis because *MCM2* and PARP synergistically regulate cell proliferation[13] (Figs. 5E, 6B). To further verify the gene expression signatures before and after PARPi treatment, several gene expression levels were analyzed using qPCR with specific primers. *FEN1* and *SMUG1* are highly expressed and regarded as promising biomarkers in OC[14,15]. Therefore, changes in the expression of*FEN1* and *SMUG1*, as well as uracil-DNA glycosylases encoding gene *UNG*, after PARPi treatment were also evaluated to identify potential drug targets. *FEN1* and *UNG* were decreased after PARPi treatment. This suggests that these genes may be associated with the pathways targeted by PARPi. Interestingly, *MCM10* has no widely identified as a potential biomarker in OC, the decreasing trend of *MCM10* may provide evidence that *MCM10* is correlated with OC. *POLA2* is a therapeutic target in lung cancer, and *POLA2* mutation even causes gemcitabine resistance in lung cancer cells. Therefore, *POLA2* downregulation after PARPi treatment may have biological significance[16,17]. Representative DEGs of base excision repair and cell cycle were also validated by qRT-PCR analysis (Fig. 6A, B).

Discussion

We cultured organoids from pathological HGSC specimens and verified that the clinical and biochemical profiles of the organoids were similar to those of clinical tissues. PARPi treatment significantly inhibited the growth of HGSC organoids with increasing drug concentration and extended culture time. This is consistent with previous reports[18,19]. Immunohistochemical staining and immunofluorescence confirmed that PARPi treatment caused necrosis in the HGSC organoids. Further analysis revealed a significant increase in early and late apoptosis after 72 h of treatment. RNA-seq analysis revealed that PARPi treatment either upregulated or downregulated the expression of multiple genes. The expression of *UNG*, *POLA2*, *FEN1*, and *POLE3*, which are involved in base excision repair[20], were downregulated. The expression of *MCM10*, *CDKL5*, *MCM2*, *CDKN2B*, *CDK7*, *CDKN1C* related to the cell cycle[21,22], were also altered after PARPi treatment. Some of these results were confirmed by qPCR.

PARP plays a central role in single-stranded DNA base excision and repair[23,24]. Loss-of-function BRCA1/2 and HR result in DSBs are not normally repaired through HR repair (HRR). PARPi generally cause synthetic lethality by blocking SSB repair in tumor cells[23]. Therefore, given the mechanism of PARPi, BRCA 1/2 mutation or HR deficiency (HRD) indicate the application of PARPi[25,26]. However, some patients who meet these criteria experience rapid recurrence after PARPi treatment[27]. Therefore, a potentially efficient platform for assessing PARPi-sensitive inpatients is required.

A three-dimensional clinical tumor-derived organoid model was used to investigate the sensitivity of the patient to PARPi. After treatment with a PARPi for 72 h, we determined that the patient was highly sensitive to olaparib. The results showed that our organoid culture method is applicable for determining drug sensitivity and can provide guidance for clinical practice. This organoid platform can be combined with next generation sequencing (NGS) to detect drug therapy[28]. We recommend patients with BRCA1/2 mutations or HRD and still resistant to PARPi doing drug sensitivity test by organoid model. Therefore, improper PARPi treatment-mediated exacerbation and delay in optimal treatment could be avoided.

In this study, a small fraction of the cells and organoids remained viable after PARPi treatment, indicating PARPi resistance. Various mechanisms are involved in PARPi resistance[23,25]. The role of the tumor microenvironment in PARPi-resistant cancers remains unclear. Organoid models are one of the best methods for investigating the tumor microenvironment[29,30]. Studies on PARPi-resistant organoids can lay the foundation for further detailed research and provide effective strategies to overcome PARPi resistance.

Conclusion

Patient-derived organoids with certain OC marker expression levels and morphology similar to the original cancer tissues were used to investigate the effects of PARPi treatment on organoids and adherent cells from organoid cultures. The proportion of Ki67 positive cells significantly reduced after

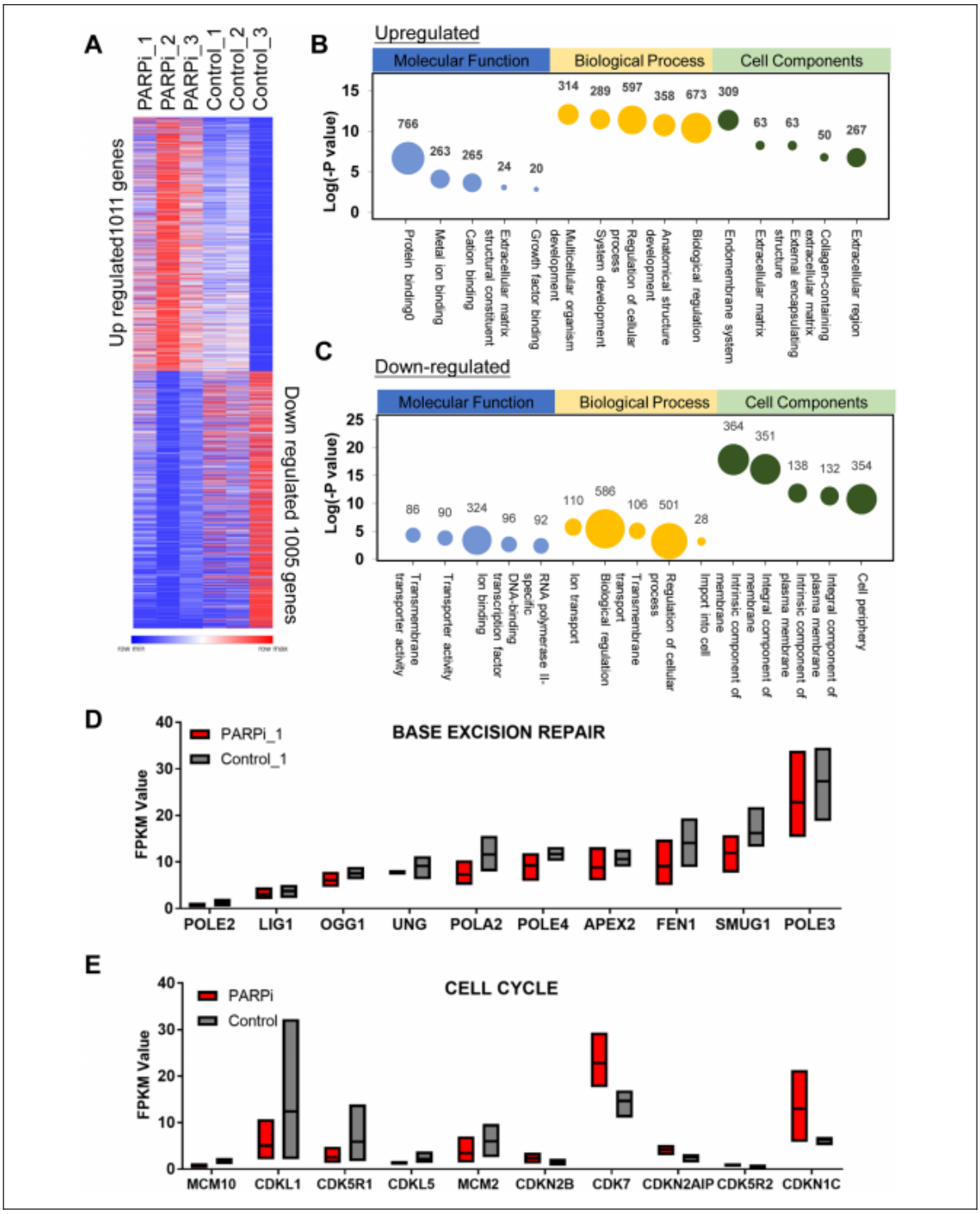

Figure 5. OC organoid have distinct transcriptomes after PARPi treatment. (A) Significantly upregulated and downregulated genes from control and PARPi treatment samples for the RNA sequencing results. (B, C) Gene ontology classification of organoid. Representatively upregulated or downregulated genes closely related molecular function, biological process, and cell components. The size of the bubbles indicates the number of associated genes. (D, E) Significantly changed genes linked base excision repair and cell cycle.

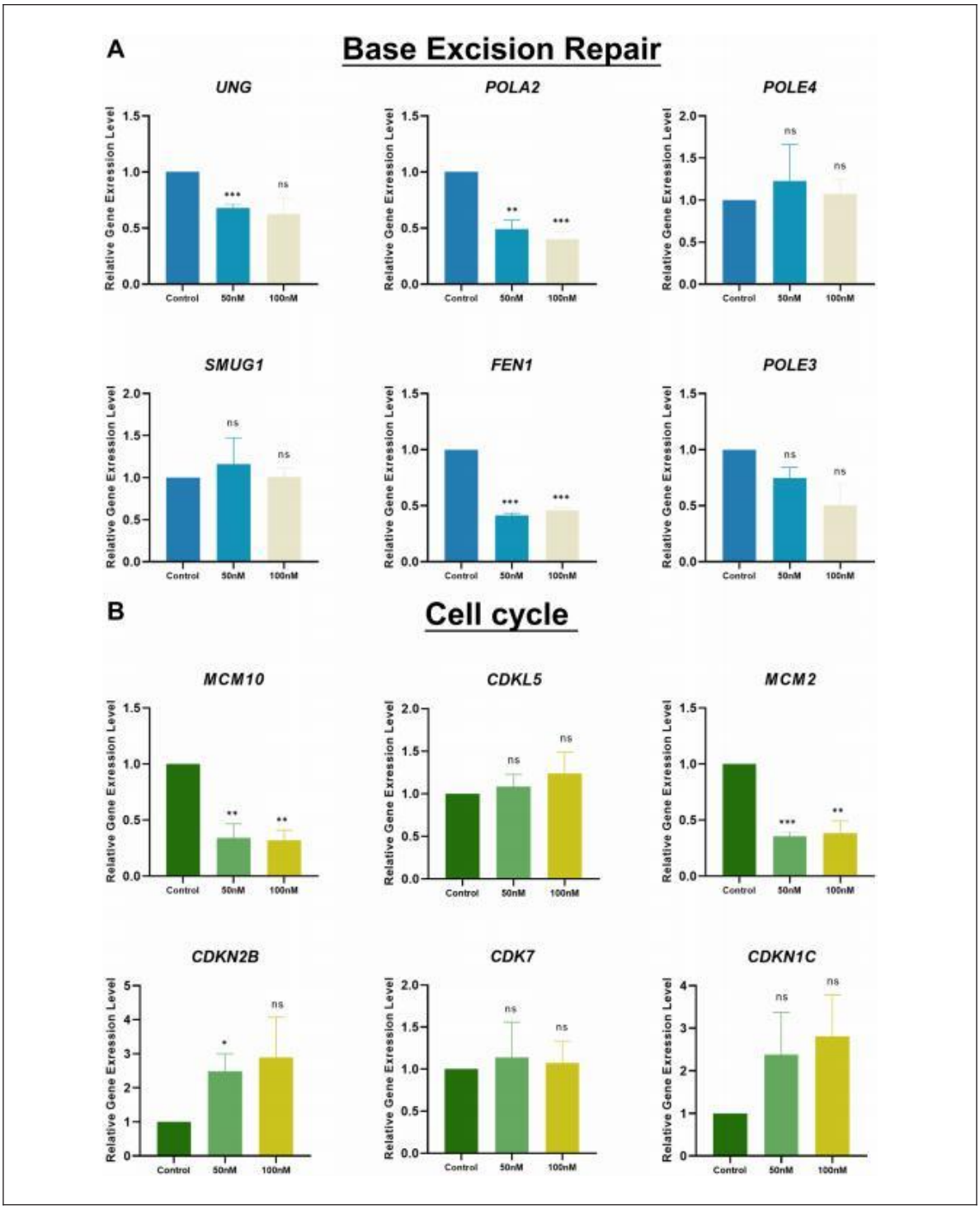

Figure 6. PARPi reduce cell proliferation and cell cycle in patient-derived organoid. (A, B) Expression level of 6 candidate genes linked to base excision repair pathways or cell cycle pathways after 48 h with different dosages of PARPi (0/50/100 nM) treatment. Data are presented as the mean ± SEM (n = 3; ns, no significance; *P < 0.05; **P < 0.01; ***P < 0.001; student's test).

PARPi treatment. Functional assays revealed that PARPi inhibits cell growth by upregulating apoptosis. Several pathways, such as cell cycle and base excision repair, have been highlighted as downstream targets of PARPi. Although further studies are needed, these results indicate the utility of our organoid platform and some potential genes related to PARPi resistance. Furthermore, these data provided clues for clarifying the PARPi resistance mechanisms and solving clinical problems.

Acknowledgments

The authors thank all the colleges in their laboratory. Figure 1A and 2E was generated using BioRender.

Author Contributions

H.X.X. and C.C.H. conceived and designed the experiments; C.Q., L.L.Y., W.C., S.Y.H., and T.X. performed the experiments; C.Q., L.L.Y., and C.C.H. analyzed the data; and C.Q., L.L.Y., C.C.H. and H.X.X. wrote the manuscript. All the authors approved the final manuscript.

Availability of Data and Material

All relevant data and materials used in this article and the Supplementary Materials are available from the corresponding author, CCH, on reasonable request.

Ethical Approval

This study was approved by the Ethics Committee of the Obstetrics and Gynecology Hospital of Fudan University (Obstetrics and Gynecology ethical approval number: 2022-04).

Statement of Human and Animal Rights

All human specimens were performed according to the Declaration of Helsinki and the Chinese guidelines of GB/T4352.1-2021 and GB/T38736-2020. Approved by the Ethics Committee of the Obstetrics and Gynecology Hospital ofFudan University, patients/subjects signed a written informed consent. All human tissues were collected with patient consent according to clinical SOPs.

Statement of Informed Consent

Patient consent was obtained from each patient.

Declaration of Conflicting Interests

The author(s) declared no potential conflicts of interest with respect to the research, authorship, and/or publication of this article.

Funding

The author(s) received no financial support for the research, authorship, and/or publication of this article.

ORCID iD

Chunhui Cai https://orcid.org/0000-0002-8700-4383

Supplemental Material

Supplemental material for this article is available online.

References

1. Ferlay J, Soerjomataram I, Dikshit R, Eser S, Mathers C, Rebelo M, Parkin DM, Forman D, Bray F. Cancer incidence and mortality worldwide: sources, methods and major patterns in GLOBOCAN 2012. Int J Cancer. 2015;136(5): E359–86.
2. Rouleau M, Patel A, Hendzel MJ, Kaufmann SH, Poirier GG. PARP inhibition: PARP1 and beyond. Nat Rev Cancer. 2010;10(4): 293–301.
3. Bryant HE, Schultz N, Thomas HD, Parker KM, Flower D, Lopez E, Kyle S, Meuth M, Curtin NJ, Helleday T. Specific killing of BRCA2-deficient tumours with inhibitors of poly(ADP-ribose) polymerase. Nature. 2005;434(7035): 913–7.
4. Franzese E, Centonze S, Diana A, Carlino F, Guerrera LP, Di Napoli M, De Vita F, Pignata S, Ciardiello F, Orditura M. PARP inhibitors in ovarian cancer. Cancer Treat Rev. 2019;73:1–9.
5. Audeh MW, Carmichael J, Penson RT, Friedlander M, Powell B, Bell-McGuinn KM, Scott C, Weitzel JN, Oaknin A, Loman N, Lu K, et al. Oral poly(ADP-ribose) polymerase inhibitor olaparib in patients with BRCA1 or BRCA2 mutations and recurrent ovarian cancer: a proof-of-concept trial. Lancet. 2010;376(9737): 245–51.
6. Zhao Q, Ni J, Dong J, Cheng X, Xiao L, Xue Q, Xu X, Guo W, Chen X. Platinum resistance after PARPi resistance in a gBRCAmt recurrent ovarian cancer patient: a case report. Reprod Sci. 2022;30:615–21.
7. Giudice E, Gentile M, Salutari V, Ricci C, Musacchio L, Carbone MV, Ghizzoni V, Camarda F, Tronconi F, Nero C, et al. PARP inhibitors resistance: mechanisms and perspectives. Cancers. 2022;14(6):1420.
8. Laury AR, Perets R, Piao H, Krane JF, Barletta JA, French C, Chirieac LR, Lis R, Loda M, Hornick JL, Drapkin R, et al. A comprehensive analysis of PAX8 expression in human epithelial tumors. Am J Surg Pathol. 2011;35(6): 816–26.
9. Giurgea LN, Ungureanu C, Mihailovici MS. The immunohistochemical expression of p53 and Ki67 in ovarian epithelial borderline tumors: correlation with clinicopathological factors. Rom J Morphol Embryol. 2012;53(4): 967–73.
10. Zhang S, Iyer S, Ran H, Dolgalev I, Gu S, Wei W, Foster CJR, Loomis CA, Olvera N, Dao F, Levine DA, et al. Genetically defined, syngeneic organoid platform for developing combination therapies for ovarian cancer. Cancer Discov. 2021;11(2): 362–83.
11. Mittica G, Ghisoni E, Giannone G, Genta S, Aglietta M, Sapino A, Valabrega G. PARP inhibitors in ovarian cancer. Recent Pat Anticancer Drug Discov. 2018;13(4): 392–410.
12. Vanacker H, Harter P, Labidi-Galy SI, Banerjee S, Oaknin A, Lorusso D, Ray-Coquard I. PARP-inhibitors in epithelial ovarian cancer: actual positioning and future expectations. Cancer Treat Rev. 2021;99:102255.
13. Xiao G, Lundine D, Annor GK, Canar J, Ellison V, Polotskaia A, Donabedian PL, Reiner T, Khramtsova GF, Olopade OI, Mazo A, et al. Gain-of-function mutant p53 R273H interacts with replicating DNA and PARP1 in breast cancer. Cancer Res. 2020;80(3): 394–405.

14. Abdel-Fatah TM, Russell R, Albarakati N, Maloney DJ, DorjsurenD, Rueda OM, Moseley P, Mohan V, Sun H, Abbotts R, Mukherjee A, et al. Genomic and protein expression analysis reveals flap endonuclease 1 (FEN1) as a key biomarker in breast and ovarian cancer. Mol Oncol. 2014;8(7): 1326–38.
15. Raja S, Van Houten B. The multiple cellular roles of SMUG1 in genome maintenance and cancer. Int J Mol Sci. 2021;22(4): 1981.
16. Koh V, Kwan HY, Tan WL, Mah TL, Yong WP. Knockdown of POLA2 increases gemcitabine resistance in lung cancer cells. BMC Genomics. 2016;17(Suppl 13): 1029.
17. Fan Z, Bai Y, Zhang Q, Qian P. CircRNA circ_POLA2 promotes lung cancer cell stemness via regulating the miR-326/GNB1 axis. Environ Toxicol. 2020;35(10): 1146–56.
18. Tao M, Wu X. The role of patient-derived ovarian cancer organoids in the study of PARP inhibitors sensitivity and resis- tance: from genomic analysis to functional testing. J Exp Clin Cancer Res. 2021;40(1): 338.
19. Tao M, Sun F, Wang J, Wang Y, Zhu H, Chen M, Liu L, Liu L, Lin H, Wu X. Developing patient-derived organoids to predict PARP inhibitor response and explore resistance overcoming strategies in ovarian cancer. Pharmacol Res. 2022;179:106232.
20. Yagüe-Capilla M, García-Caballero D, Aguilar-Pereyra F, Castillo-Acosta VM, Ruiz-Pérez LM, Vidal AE, González-Pacanowska D. Base excision repair plays an important role in the protection against nitric oxide- and in vivo-induced DNA damage in Trypanosoma brucei. Free Radic Biol Med. 2019;131:59–71.
21. CuiF, Hu J, Ning S, Tan J, Tang H. Overexpression of MCM10 promotes cell proliferation and predicts poor prognosis in prostate cancer. Prostate. 2018;78(16): 1299–310.
22. Liu Z, Li J, Chen J, Shan Q, Dai H, Xie H, Zhou L, Xu X, Zheng S. MCM family in HCC: MCM6 indicates adverse tumor features and poor outcomes and promotes S/G2 cell cycle progression. BMC Cancer. 2018;18(1): 200.
23. Li H, Liu ZY, Wu N, Chen YC, Cheng Q, Wang J. PARP inhibitor resistance: the underlying mechanisms and clinical implications. Mol Cancer. 2020;19(1): 107.
24. Lord CJ, Ashworth A. PARP inhibitors: synthetic lethality in the clinic. Science. 2017;355(6330): 1152–58.
25. Noordermeer SM, van Attikum H. PARP inhibitor resistance: a tug-of-war in BRCA-mutated cells. Trends Cell Biol. 2019;29(10): 820–34.
26. Stover EH, Fuh K, Konstantinopoulos PA, Matulonis UA, Liu JF. Clinical assays for assessment of homologous recombination DNA repair deficiency. Gynecol Oncol. 2020;159(3): 887–98.
27. Biegała Ł, Gajek A, Marczak A, Rogalska A. PARP inhibitor resistance in ovarian cancer: underlying mechanisms and therapeutic approaches targeting the ATR/CHK1 pathway. Biochim Biophys Acta Rev Cancer. 2021;1876(2): 188633.
28. Morice PM, Coquan E, Weiswald LB, Lambert B, Vaur D, Poulain L. Identifying patients eligible for PARP inhibitor treatment: from NGS-based tests to 3D functional assays. Br J Cancer. 2021;125(1): 7–14.
29. Neal JT, Li X, Zhu J, Giangarra V, Grzeskowiak CL, Ju J, Liu IH, Chiou SH, Salahudeen AA, Smith AR, Deutsch BC, et al. Organoid modeling of the tumor immune microenvironment. Cell. 2018;175(7): 1972–88.e16.
30. Xia T, Du WL, Chen XY, Zhang YN. Organoid models of the tumor microenvironment and their applications. J Cell Mol Med. 2021;25(13): 5829–41.

REVIEW

Landscape of human organoids: Ideal model in clinics and research

Xinxin Han,[1,2,11,*] Chunhui Cai,[2,11] Wei Deng,[3,4,11] Yanghua Shi,[2] Lanyang Li,[2] Chen Wang,[2] Jian Zhang,[2] Mingjie Rong,[2] Jiping Liu,[2] Bangjiang Fang,[3] Hua He,[5] Xiling Liu,[6] Chuxia Deng,[7,8,*] Xiao He,[9,*] and Xin Cao[10,*]

*Correspondence: xxhan@sibs.ac.cn (X.H.); cxdeng@um.edu.mo (C.D.); hexiao@ihep.ac.cn (X.H.); caox@fudan.edu.cn (X.C.)

Received: October 31, 2023; Accepted: March 29, 2024; Published Online: April 1, 2024; https://doi.org/10.1016/j.xinn.2024.100620

GRAPHICAL ABSTRACT

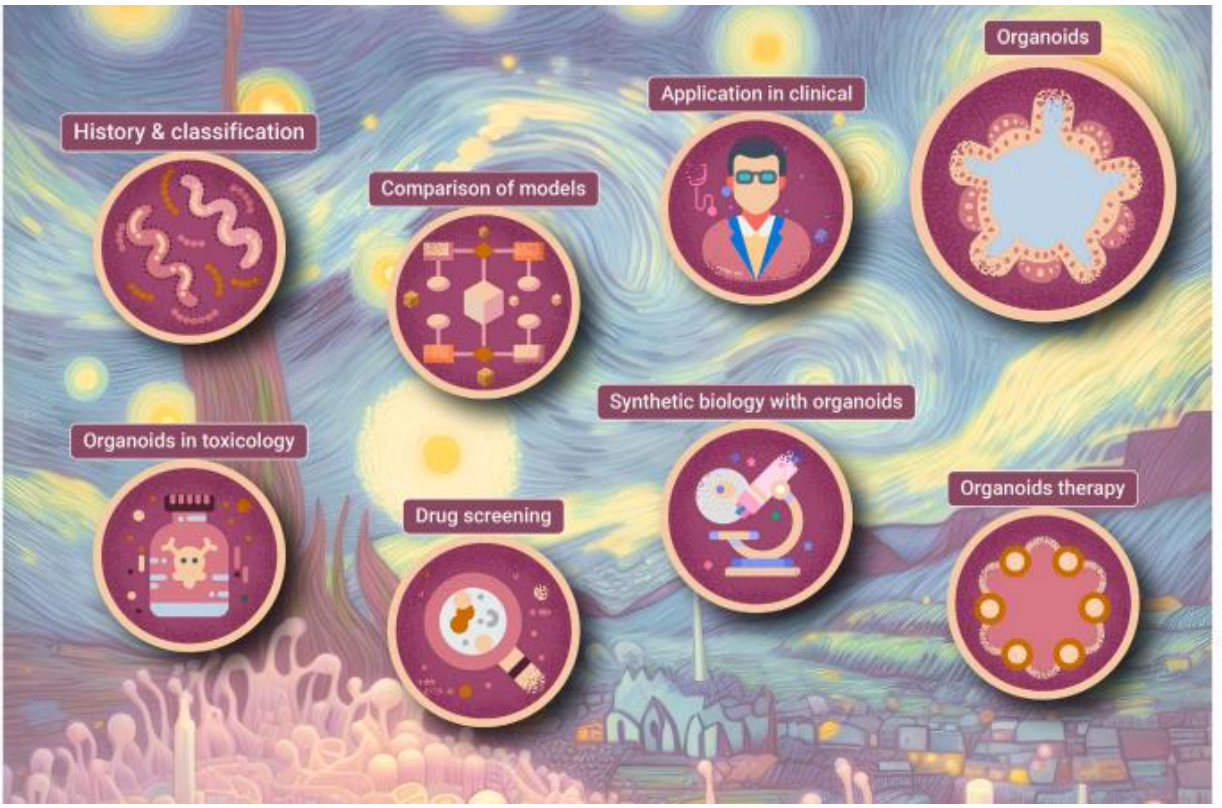

PUBLIC SUMMARY

- The landscape of organoids history: organoids mark a new and efficient model in tissue and organ level.
- Multiple applications of organoids in biomedicine and life healthcare.
- Organoids benefit to drug discovery, disease study, prevention, control, and therapy.
- Synthetic biology, artificial intelligence and automation integration broaden the role of organoids.

REVIEW

The Innovation

Landscape of human organoids: Ideal model in clinics and research

Xinxin Han,[1,2,11,*] Chunhui Cai,[2,11] Wei Deng,[3,4,11] Yanghua Shi,[2] Lanyang Li,[2] Chen Wang,[2] Jian Zhang,[2] Mingjie Rong,[2] Jiping Liu,[2] Bangjiang Fang,[3] Hua He,[5] Xiling Liu,[6] Chuxia Deng,[7,8,*] Xiao He,[9,*] and Xin Cao[10,*]

[1]Organ Regeneration X Lab, Lisheng East China Institute of Biotechnology, Peking University, Jiangsu 226200, China

[2]Shanghai Lisheng Biotech, Shanghai 200092, China

[3]LongHua Hospital, Shanghai University of Traditional Chinese Medicine, 725 Wanping South Road, Xuhui District, Shanghai 200032, China

[4]Department of Oncology, Shanghai Ninth People's Hospital, Shanghai Jiao Tong University School of Medicine, Shanghai 200125, China

[5]Department of Neurosurgery, Third Affiliated Hospital, Naval Medical University, Shanghai 200438, China

[6]Shanghai Key Laboratory of Forensic Medicine, Shanghai Forensic Service Platform, Academy of Forensic Science, Ministry of Justice, Shanghai 200063, China

[7]Cancer Center, Faculty of Health Sciences, University of Macau, Taipa, Macau SAR, China

[8]Ministry of Education Frontiers Science Center for Precision Oncology, University of Macau, Taipa, Macau SAR 999078, China

[9]CAS Key Lab for Biomedical Effects of Nanomaterials and Nanosafety, Institute of High Energy Physics, Chinese Academy of Sciences, Beijing 100049, China

[10]Zhongshan Hospital Institute of Clinical Science, Fudan University Shanghai Medical College, Shanghai 200032, China

[11]These authors contributed equally

*Correspondence: xxhan@sibs.ac.cn (X.H.); cxdeng@um.edu.mo (C.D.); hexiao@ihep.ac.cn (X.H.); caox@fudan.edu.cn (X.C.)

Received: October 31, 2023; Accepted: March 29, 2024; Published Online: April 1, 2024; https://doi.org/10.1016/j.xinn.2024.100620

Citation: Han X., Cai C., Deng W., et al., (2024). Landscape of human organoids: Ideal model in clinics and research. The Innovation 5(3), 100620.

In the last decade, organoid research has entered a golden era, signifying a pivotal shift in the biomedical landscape. The year 2023 marked a milestone with the publication of thousands of papers in this arena, reflecting exponential growth. However, amid this burgeoning expansion, a comprehensive and accurate overview of the field has been conspicuously absent. Our review is intended to bridge this gap, providing a panoramic view of the rapidly evolving organoid landscape. We meticulously analyze the organoid field from eight distinctive vantage points, harnessing our rich experience in academic research, industrial application, and clinical practice. We present a deep exploration of the advances in organoid technology, underpinned by our long-standing involvement in this arena. Our narrative traverses the historical genesis of organoids and their transformative impact across various biomedical sectors, including oncology, toxicology, and drug development. We delve into the synergy between organoids and avant-garde technologies such as synthetic biology and single-cell omics and discuss their pivotal role in tailoring personalized medicine, enhancing high-throughput drug screening, and constructing physiologically pertinent disease models. Our comprehensive analysis and reflective discourse provide a deep dive into the existing landscape and emerging trends in organoid technology. We spotlight technological innovations, methodological evolution, and the broadening spectrum of applications, emphasizing the revolutionary influence of organoids in personalized medicine, oncology, drug discovery, and other fields. Looking ahead, we cautiously anticipate future developments in the field of organoid research, especially its potential implications for personalized patient care, new avenues of drug discovery, and clinical research. We trust that our comprehensive review will be an asset for researchers, clinicians, and patients with keen interest in personalized medical strategies. We offer a broad view of the present and prospective capabilities of organoid technology, encompassing a wide range of current and future applications. In summary, in this review we attempt a comprehensive exploration of the organoid field. We offer reflections, summaries, and projections that might be useful for current researchers and clinicians, and we hope to contribute to shaping the evolving trajectory of this dynamic and rapidly advancing field.

INTRODUCTION

Organoid technology, the use of three-dimensional cultures derived from stem cells that closely mimic the architecture and functionality of native organs, represents a seminal advance in biomedical science, offering a revolutionary perspective on human physiology and pathology.[1] Organoid technology has profoundly impacted various fields, notably oncology and regenerative medicine, demonstrating unparalleled adaptability and precision.[2] Organoids, essentially miniature versions of organs, offer a highly physiologically relevant model for understanding human biology. This relevance is particularly critical in drug development, an area in which traditional models often fall short.[3] Compared to two-dimensional cell cultures or animal models, organoids provide a more accurate representation of human tissues, enabling more reliable and efficient drug screening and functional validation.[4] This feature is particularly valuable in the context of cancer research, where organoids can mimic the tumor microenvironment, providing insights into tumor-immune interactions and host-pathogen dynamics.[5] The clinical fidelity of organoids is higher than that of conventional models, as they can replicate the complex biological processes of human organs in vitro. This attribute enables the rapid functional testing of drugs, increasing the efficiency of the pathway from discovery to clinical application.[6] Additionally, organoids present a novel platform for in vitro gene-editing therapies. By leveraging CRISPR-Cas9 and other gene-editing tools, researchers can use organoids to model genetic diseases and test therapeutic strategies, significantly advancing the field of personalized medicine.[7,8] Our research findings emphasize the transformative potential of organoids in biomedical sciences. In the future, we expect organoids to play a pivotal role in advancing our understanding of human biology, evolving from cellular self-organization to integration with technologies such as synthetic biology and artificial intelligence (AI), offering substantial potential to revolutionize fields such as drug discovery, disease modeling, and personalized medicine. Progress in organoid technology continues to break barriers, offering insights once deemed unattainable. Accordingly, this review not only explores the current landscape of organoid technology but also offers a forward-looking perspective on the profound anticipated impact of organoids on future biomedical research.

ORGANOID HISTORY

Organoid research, originating in the early 20th century, explores the self-organizing properties of cells (Figure 1A). The initial studies involved cultivating mechanically dissociated sponge cells to create functional organisms in vitro. H.V. Wilson's observations in 1907 marked the inception of organoid research, revealing the self-organization and regeneration of dissociated sponge cells.[9–11] In subsequent decades, several groups performed dissociation-reaggregation experiments to generate different types of organs from dissociated amphibian pronephros and chick embryos,[12–14] demonstrating the ability of cells to self-organize and form organ-like structures in vitro.

In 1981, pluripotent stem cells (PSCs) were isolated from mouse embryos, a milestone in stem cell research.[15–18] In November 1998, human embryonic stem cells (ESCs) were derived from blastocysts, a breakthrough demonstrating human PSC derivation.[19] The development of human induced pluripotent stem cell (iPSC) technology further revolutionized the field.[20,21] The modern era of organoid technology truly began in the2000s with the development of iPSCs by Shinya Yamanaka's team at Kyoto University[22–25]: their pioneering work showed that mouse fibroblasts could be reprogrammed into a pluripotent state by introducing four transcription factors (Oct4, Sox2, Klf4, and c-Myc), generating the first iPSCs.[18,22]

In 2009, Hans Clevers introduced the term "organoid," emphasizing self-organization, particularly in cancer research.[26] The term "organoid" draws inspiration from the ancient Greek lexicon, where "organon" is the origin of "organ" andthe suffix "-oid" denotes resemblance or likeness. Therefore, "organoid" refers to something that resembles an organ. Researchers such as Lancaster and Knoblich expanded upon this seminal work.[27]They opined that the true essence of organoids lies not solely in their structural replication but in their ability to mirror the

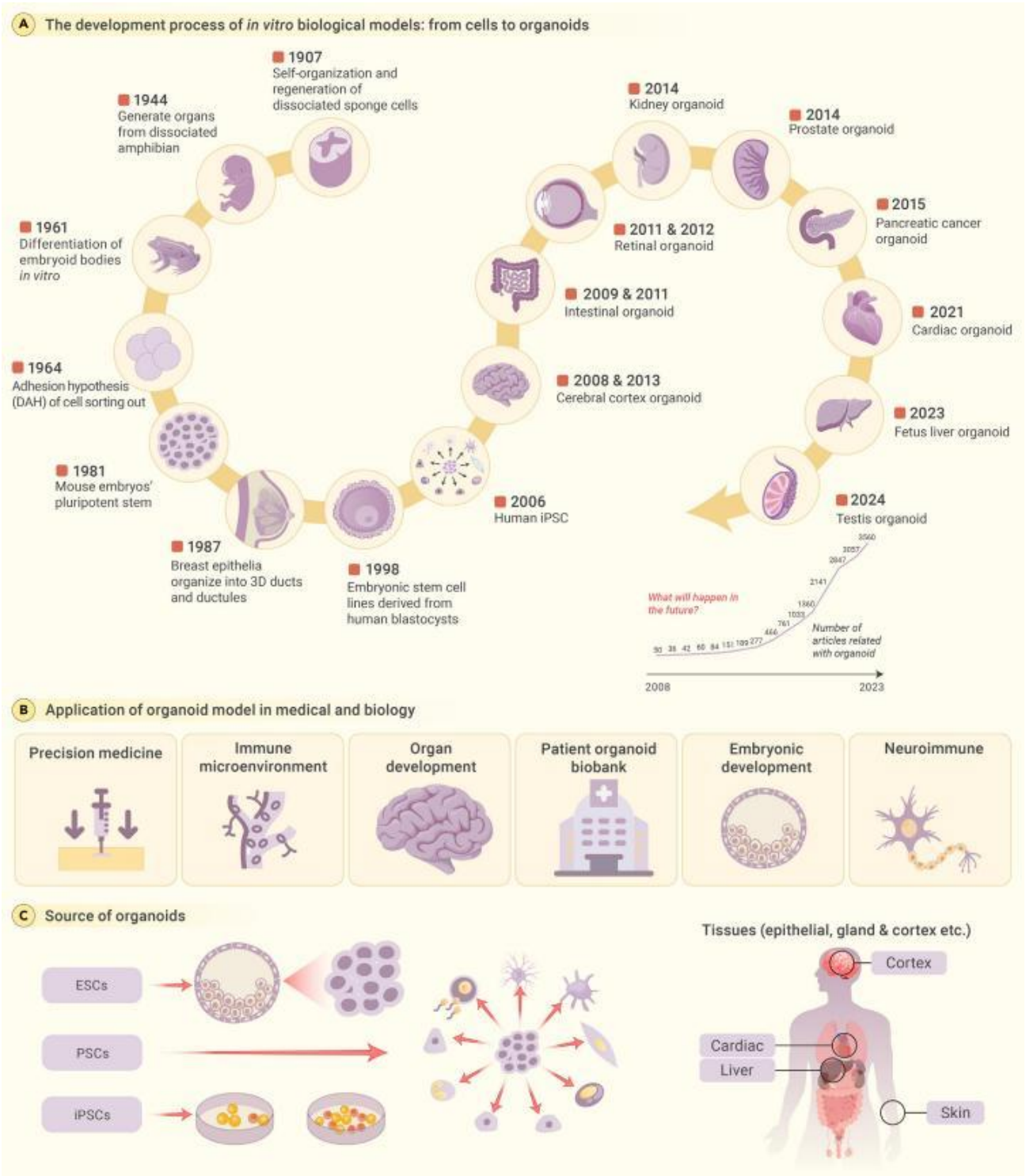

Figure 1. Unlocking organoids: A tale of historical discoveries and advanced taxonomies (A) The chronological history of the development of organoids. (B) Numerous novel applications of organoids have surfaced in the realm of life science research in recent years. (C) Further refinement is required in classification as a result of the diversification of organoid sources.

cellular diversity, specific functionalities, and even intricate cellular arrangements of the organs they represent.[28] Subsequently, the field of organoid technology advanced rapidly, ushering in a new era in scientific innovation.[29,30] Hans Clevers, intestinal organoids paved the way for new research on intestinal biology and disease mechanisms[31] and continue to be a valuable resource for investigating the molecular mechanisms underlying intestinal development and disease progression.[26,32] Cerebral organoids, created by Lancaster et al. in 2013, mimic human brain development and aid in understanding developmental brain disorders.[33]

In 2014, groundbreaking advances occurred in prostate organoid research, providing a robust platform for studying prostate cancer dynamics and therapeutic drug testing.[34,35] In 2015, kidney organoids derived from iPSCs provided insights into kidney development and disease modeling.[36,37] Subsequent years saw the burgeoning of organoid technology across various organ systems, includingthe pancreas. The development of pancreatic cancer organoidshasilluminated the pathophysiological mechanisms that underlie pancreatic ductal adenocarcinoma, fostering advancesin personalized medicine and targeted therapeutic strategies.[38,39] A surge in methodological refinements in retinal organoid cultivation have occurred since 2018. These organoids recapitulate the functionality of retinal cells, representing a significant leap forward from earlier models that lacked structural and functionalfidelity.[40,41] Most recently, cardiac organoids emerged, aiding in modeling heart diseases.[42,43]

Organoids have revolutionized biomedical research, enhancing drug assessments and personalized medicine.[44] In oncology, organoids have provided critical insights into the tumor immune microenvironment, propelling advancements in immunotherapy.[45] These three-dimensional cultures serve as pivotal tools in deciphering the complexities of organ and embryonic development, spotlighting essential elements of morphogenesis and the inception of life.[46] Moreover, the establishment of extensive organoid biobanks has supported personalized research approaches, offering a plethora of tissue-specific samples for in-depth study. In neuroimmune research, organoids have been instrumental in elucidating the intricate interplay between the nervous and immune systems, leading to new insights into a myriad of associated disorders.[47,48] The remarkable ability of organoids to replicate organ-level functions within controlled environments is responsible for their indispensable role in precision medicine, disease modeling, and regenerative medicine, enabling a transformative phase in modern medical research (Figure 1B).

The field of organoid development utilizes a variety of stem cell sources, each with unique characteristics. Among these are the well-known ESCs and the revolutionary iPSCs, both of which fall under the broader category of PSCs (Figure 1C). The versatile mesenchymal stem cells also play a crucial role in this domain.[49–55] Additionally, the world of clinical medicine offers a treasure trove of sources in the form of tissue specimens, both from individuals battling diseases and from healthy donors.[56,57] This range includes surgical specimens and other less obvious sources such as nasopharyngeal swabs, which have recently gained prominence.[58]

In conclusion, organoid research has introduced a new era in biomedical sciences, enhancing our understanding of life, disease, and therapies.

ORGANOIDS OUTSHINE CONVENTIONAL BIOMEDICAL MODELS

Biomedical researchers, in relentless pursuit of understanding life's complexity, have long sought models to mirror human physiology and pathology (Figure 2). Animal models, once pivotal in research,[59] present challenges due to interspecies differences and translational limitations.[60–62] Asthe limitations of animal models grew more apparent, the use of cell lines became prevalent.[63] However, cell lines, though scalable, have the disadvantages of genetic homogeneity and two-dimensional constraints.[64–66] In this complex scenario, the scientific community witnessed the emergence of organoids, three-dimensional structures derived from stem cells. These scaled-down models of organs are designed to bridge the gap between the simplicity of cell lines and the complexity of in vivo organisms, providing a clearer perspective on human biology.[57,67]

Patient-derived organoids, which resemble the original tissues, hold promise in biomedical research. These models are established from patient samples, retain their genetic complexity, and offer a rapid and cost-effective way to study diseases.[68] Patient-derived organoids maintain interpatient heterogeneity, making them valuable for personalized medicine, especially in cancer research;however, their applications extend beyond oncology. For example, endometrial organoids have been successfully established from both normal and diseased human endometrium, including tissue samples representing conditions such as endometriosis, endometrial hyperplasia, and endometrial cancer.[69] These organoids maintain tissue characteristics and genetic stability, which can facilitate the understanding of disease heterogeneity. For instance, organoids from patients with Mayer-Rokitansky-Ku··· ster-Hauser syndrome have revealed unique gene-expression patterns, highlighting their potential for personalized medicine.[70] This emphasizes the potential of endometrial organoidsto modelindividual patient pathologiesand contribute to personalized medicine. Endometrial organoids have shown promise in high-throughput drug screening: they can be used to test the efficacy and toxicity of new therapeutic agents in a controlled environment that closely mimics in vivo conditions.[69] By testing drugs on patient-specific organoids, researchers can identify the most effective treatments for individual patients.[69] This personalized strategy has the potential to transform endometrial disease treatment by customizing therapies to each patient's specific needs, thereby advancing precision medicine.[71,72]

In contrast, although patient-derived primary cell cultures closely resemble the original tumor,[73] they have a finite lifespan and limited replicative capacity. Their establishment can be challenging due to low success rates and slow growth, restricting the duration of drug-response testing.[74] Patient-derived xenograft models, which can take several months to establish and are costly to maintain, also exhibit genetic heterogeneity.[75] Moreover, the success rate of establishing these models can vary widely, making them less predictable than patient-derived organoids.[76] Genetically manipulated animal models are another alternative but present their own set of challenges.[77] These models take months or even years to develop, impose high maintenance costs, and exhibit genetic and cellular heterogeneity depending on the specific genetic modifications made.[78–80] The rigidity and complexity of these models make them less adaptable than the more versatile and representative patient-derived organoids.

Organoid technology has advanced beyond other in vitro techniques to become a leading approach within the field of personalized medicine.[81] Central to this advancement are iPSC-derived patient-specific organoids. These models have revolutionized our approach to understanding complex diseases by closely mirroring the genetic, cellular, and functional characteristics of a patient's tissue.[82–85] iPSC-derived organoids offer unique advantages in disease modeling, particularly due to their patient-specific nature.[84] They allow personalized disease modeling, which is crucial in understanding complex diseases such as cancers, neurological disorders, and rare genetic diseases. Moreover, iPSCs are amenable to genetic editing using CRISPR-Cas9, enabling the study of disease mechanisms and the development of targeted therapies.[82,83] iPSC-derived organoids have filled a gap in research opportunities by providing a more accurate, human-specific model, thereby revolutionizing the scope and methods of disease research. In Alzheimer's disease research, organoids replicate key disease features such as β-amyloid accumulation and tau protein buildup,[86,87] offering insights into molecular mechanisms and genetic factors such as APOE4.[83] Similarly, Parkinson's disease research benefits from the use of midbrain-specific organoids in exploring interactions involving dopamine-producing neurons.[88–91] The pathology of amyotrophic lateral sclerosis has been successfully mimicked in cerebral organoids using patient-derived protein extracts, illustrating TDP-43 aggregation and disease progression.[92] This model has also demonstrated the time-dependent spread of pathogenic TDP-43, inducing astrogliosis, cellular apoptosis, and DNA double-strand breaks in the recipient cerebral organoids. Accordingly, this model enables the in-depth exploration of genetic mechanisms and the development of targeted gene therapies for amyotrophic lateral sclerosis.[93–95]

The pharmaceutical industry, ever in search of therapeutic innovations, has embraced organoids as a powerful tool.[96–98] Patient-specific organoids, with their personalized genetic tapestries, have proven to be robust platforms for drug testing, providing a path for individualized therapeutic blueprints. Their high accuracy, consistency, reproducibility, and fidelity in drug-screening paradigms support their potential as vanguards of drug discovery.[99,100]

Furthermore, the convenience of subculturing and the potential for extended storage render organoids a favored option for extensive biobanking, accommodating a wide range of patient specimens.[101] Because of their differences from and synergies with other models, organoids illuminate a path toward personalized medicine, drug discovery, and a more profound understanding of life itself.

ORGANOIDS SOLVE CLINICAL DIFFICULTIES IN ONCOLOGY

Organoid technology introduces a new generation of detailed and accurate simulations, capturing the genetic traits and heterogeneity inherent in complex diseases such as cancer.[102–104] The ability of organoids to mimic diverse patient-specific responses is instrumental in dissecting the multifaceted nature of tumors, paving the way for targeted therapeutic interventions (Figure 3A). The detailed insights offered by these models are fostering new developments in biomedical research and pharmaceuticals, providing a novel approach to

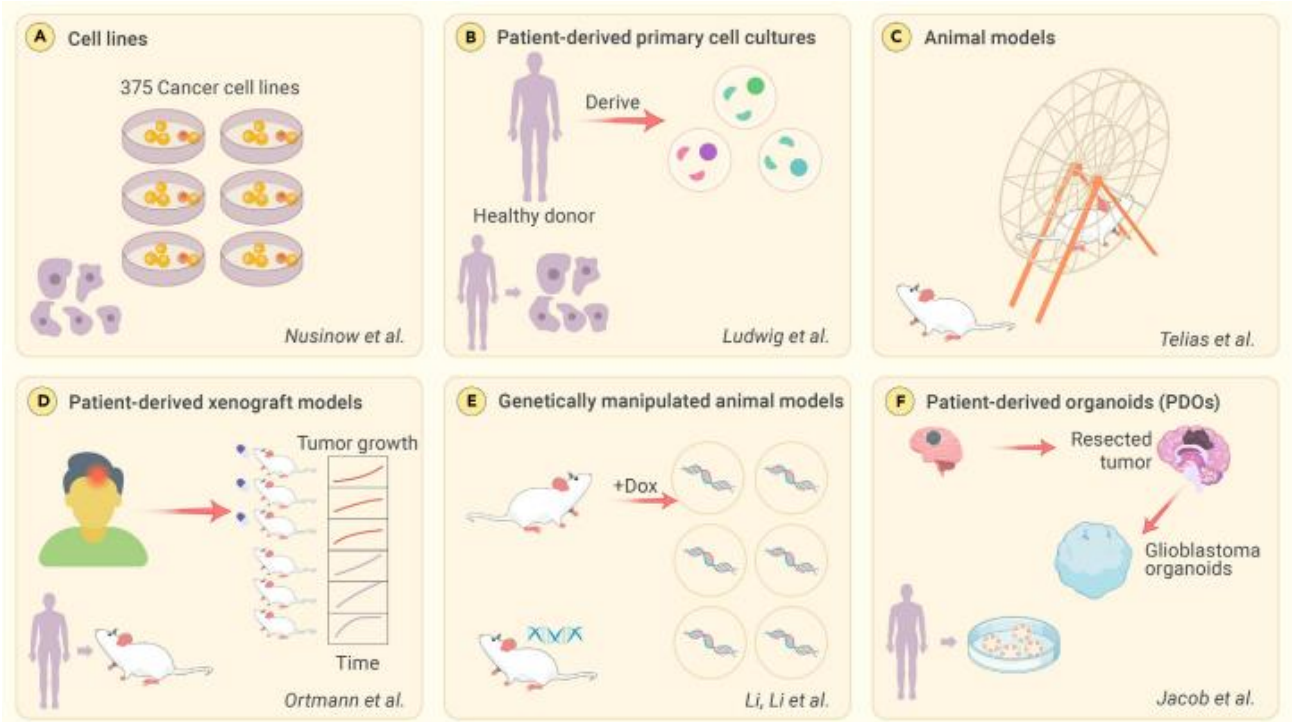

G

Lifespan	Immortal	20-50 Passages	10-40 Passages	0.5-2 years	0.5-2 years	0.5-2 years
Time to built	NA	1 week	1-2 weeks	Several weeks	Several months	1-2 years
Costs	$	$$	$$$$	$$$	$$$	$$$$
Success rate	+++	++	++	+	+	-
Genetic heterogeneity	-	+	+++	-	++	+
Inter-organ communication	-	-	-	+++	+++	+++
Drug screening	+++	+++	++	+	+	+
Biobank	+++	+++	++	-	-	-
Immune microenvironment	-	-	++	+++	++	+++
Pharmacodynamic consistency	?	?	?	?	?	?

Figure 2. Organoids represent significant improvements over existing biomedical models Organoids, the miniaturized facsimiles of organs, have redefined the landscape of biomedical models, presenting a more physiologically relevant alternative. Compared to other models, organoids not only boast a shorter construction cycle and a higher success rate but also excel in preserving individualized tissue characteristics of patients.

address complex clinical challenges, such as pancreatic cancer,[102,105] tumor drug resistance, recurrence, and metastasis.[103,106,107]

Pancreatic cancer presents a significant challenge in oncology, asitis characterized by late diagnosis and limited treatment options, an aggressive nature, a dense stroma, high heterogeneity, and a lack of effective screening techniques. These factors contribute to its poor prognosis as a clinically incurable disease.[108–110] The development of organoids, which are three-dimensional cell cultures replicating organ structure and function, introduces new possibilities in addressing this challenging cancer.[102] Patient-derived organoids have been successfully derived from pancreatic ductal adenocarcinoma patients,

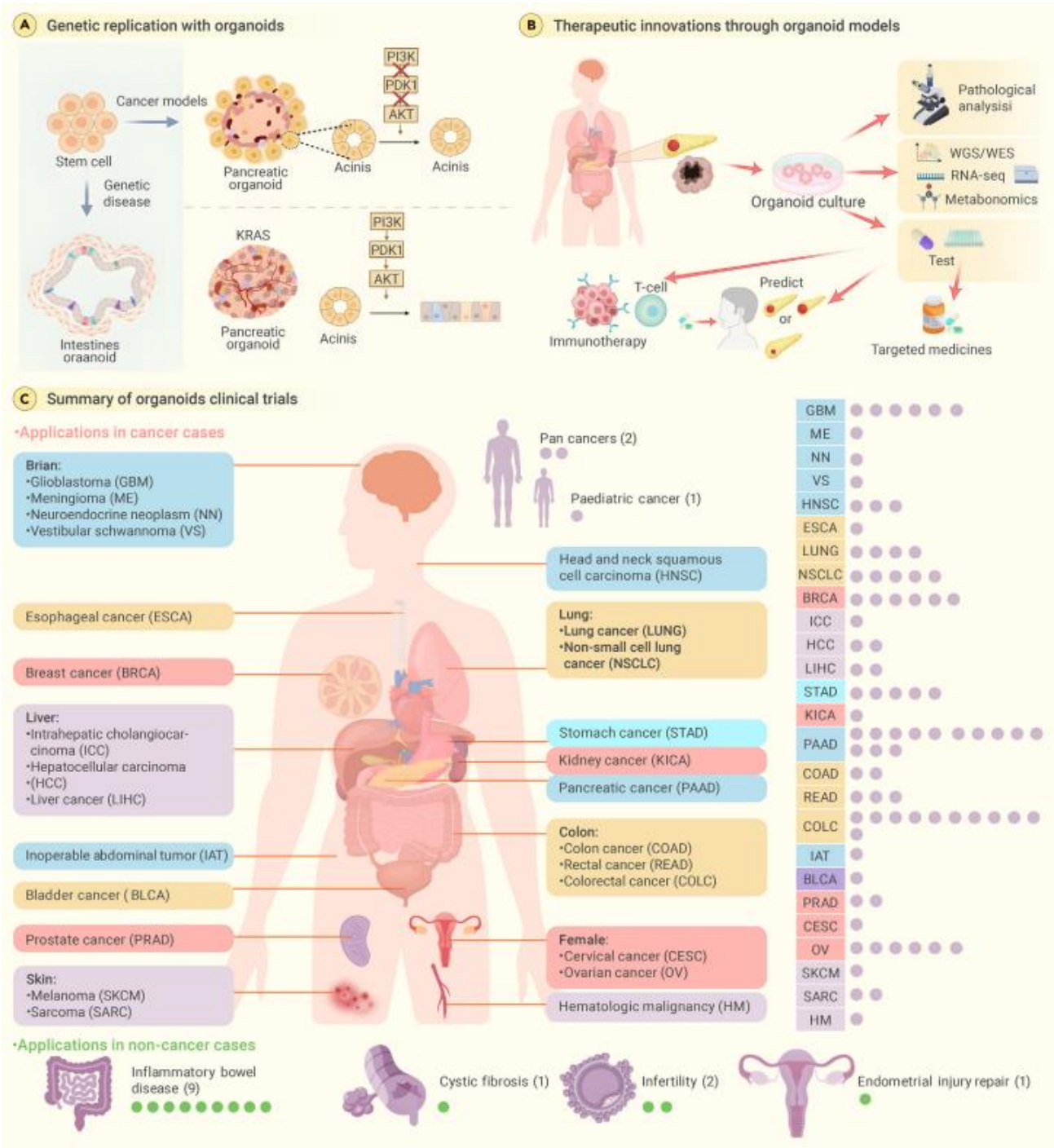

Figure 3. Organoid solves clinical difficulties in oncology: Pioneering models, therapies, and global trials (A) Utilizing organoids for genetic replication in a groundbreaking manner. Organoids are an innovative method that successfully generates genetically homogeneous models for cancers, specifically those that demonstrate resistance to medicine or repeated spread to other parts of the body. (B) Therapeutic innovations through organoid models. Utilizing the organoid-based genetic models, the scientific community is embarking on a journey of exploring and validating novel therapeutic regimens for tumors previously deemed untreatable. (C) Organoids at the forefront of global clinical endeavors. The global initiation of clinical trials that harness the capabilities of organoids testifies to their transformative potential.

demonstrating the ability to test the efficacy of various chemotherapy drugs.[111] In some cases, organoid drug responses have correlated with patient clinical responses.[102] Promising results have been observed in drug-screening experiments, where kinase inhibitors, which are drugs that block certain enzymes called kinases, have been shown to decrease the viability of patient-derived organoids, with CHK1 inhibitors exhibiting exceptional growth inhibition.[104] Organoids also show potential for treating drug-resistant tumors by maintaining key characteristics of primary tumors even after long-term passaging.[103,112] They facilitate the exploration of resistance mechanisms related to cancer stem cells and can be used to study drug-resistance mechanisms, personalized medicine,

and high-throughput drug-screening methodologies. Organoids have been successfully established from multiple human tumor types, such as breast, pancreatic, gastrointestinal, lung, prostate, ovarian, and bladder cancers.[106] They can be used to target key genes and cancer stem cells to reverse drug resistance in cancer and have been shown to accurately predict patient responses to targeted therapies and chemotherapies (Figure 3B).[113]

Organoid models have emerged as a crucial asset in the field of immunotherapy, an innovative type of cancer therapy that leverages the body's immune system to identify and eradicate cancer cells.[114—116] Organoid models have been instrumental in the generation and proliferation of tumor-reactive T cells derived from patient peripheral blood lymphocytes. Notably, these T cells exhibit a unique ability to target and annihilate autologous tumor organoids, emphasizing the promising role of organoids in the advancement of tailored immunotherapies.[117] Moreover, organoids have proven crucial in forecasting individualized responses to immunotherapeutic interventions. Because they preserve the genetic integrity of the original tumor samples, organoids offer a highly representative model for assessing the effectiveness of various immunotherapeutic agents and their synergistic combinations.[117,118] Research utilizing cancer organoids has shown that combination therapies markedly outperform monotherapy in terms of drug-response rates. This finding highlights the importance of organoids in refining treatment protocols and exploring novel therapeutic combinations.[117] Furthermore, the cocultivation of organoids with immune cells, including tumor-infiltrating lymphocytes and peripheral blood mononuclear cells, has yielded valuable insights into the tumor microenvironment and its intricate interactions with the immune system. This methodology is vital for the evaluation of immunotherapies and for elucidating the dynamics of tumor-immune interplay.[118] Advanced methodologies such as organoid-on-a-chip and three-dimensional bioprinting techniques have also been developed, enabling the creation of more elaborate cancer models.[119] These sophisticated models enable precise manipulation of the tumor microenvironment and effectively simulate multiorgan metastases in cancer, providing a more accurate testing ground for immunotherapeutic agents.[117] In summary, organoid models stand in the vanguard of cancer research and immunotherapy evaluation. This evolving technology is poised to become an essential instrument in the global battle against cancer, paving the way for more efficacious and personalized treatment for patients worldwide.[120—122]

Organoid-based clinical trials are gaining momentum internationally, with significant contributions from countries including China and the United States (Figure 3C).[1] Clinical trials, prospective observations, and randomized controlled trials using organoids cover a wide range of diseases, including cystic fibrosis and various types of cancers such as breast cancer, colorectal cancer, lung cancer, esophageal cancer, and liver cancer. These trials are at the forefront of translating laboratory findings into clinical therapies to address some of the most daunting challenges in modern medicine.[123] Numerous applications of organoid technology are currently undergoing rigorous clinical evaluations and hold promise for a new era of personalized and effective treatment strategies.[124] These trials highlight the potential of organoids to provide tangible solutions to some of the most perplexing medical challenges of our time.[125] The integration of organoid technology into mainstream healthcare could revolutionize treatment modalities and present unprecedented opportunities to improve patient outcomes. As these clinical trials progress, they pave the way for the next generation of medical breakthroughs, powered by the sophisticated simulations that only organoid technology can provide.

THE INTERSECTION OF SYNTHETIC BIOLOGY AND ORGANOID TECHNOLOGY

The path to realizing the full potential of organoid technology is fraught with complexities and inconsistencies. These challenges, along with technical difficulties in creation and analysis, have somewhat impeded widespread adoption. Synthetic biology, however, is a field poised to surmount these hurdles. Synthetic biology is introducing a new era by connecting innovative methodologies to the multifaceted world of organoids.[126] This nexus between synthetic biology and organoid research is a rapidly growing field that is expected to overhaul our comprehension of biological systems and inaugurate unique therapeutic strategies.[127]

Genetically encoded luorescent biosensors are revolutionizing real-time monitoring in organoid development,[128] enabling the measurement of protein kinase activity, pH levels, and lactate levels.[129] From studying cancer formation and progression by monitoring specific biochemical markers to investigating neurological disorders through precise measurements, these tools offer powerful insights into disease at a molecular level.[128,130] In gastrointestinal organoid culture, bioengineered sensors or biosensors have been integrated to enable measurements specific to gastrointestinal organoids.[131]

Advances in synthetic biology include the creation of tunable synthetic matrices using materials such as polyethylene glycol and hyaluronic acid to enhance organoid growth and functionality.[132] Bioengineered hydrogels, such as those that emulate the esophageal microenvironment or support ovarian follicle culture, play crucial roles in promoting cell differentiation and organoid-like structure formation (Figure 4A). Synthetic biology, driven by advances in biomaterials such as hydrogels, is crucial for the development of organoid technology.[133] Cruz-Acuña et al. developed a bioengineered hydrogel system that mimics the esophageal microenvironment, promoting the differentiation of PSCs into esophageal epithelial cells.[134] Nason-Tomaszewski et al. created fibrous hydrogels to support organoid-like structure formation and oocyte survival in ovarian follicle culture.[135] Nguyen et al. utilized tryptophan zipper peptides to craft bioactive hydrogels with antimicrobial properties, promoting mammalian cell growth and inducing polarity changes in human intestinal organoids.[136] The concept of "assembloids" represents a further advance in bottom-up construction.[137] These organoids, derived from spatially organized multiple cell types, mimic the complexity of actual organs. By combining different cellular components, assembloid technology provides a high-throughput platform for generating functional human organoids. For example, researchers have created multilayer bladder assembloids that mimic the interactions between epithelium and stroma found in mature adult bladders.[138] These assembloids not only exhibit functional characteristics but also enable the modeling of specific conditions, such as urinary tract infections and urothelial carcinoma (Figure 4B).

Organoids also present a unique advantage in the field of synthetic biology, namely, the production of a myriad of biological products.[139] The unique milieu of these miniature organ structures mimics physiological conditions within the human body, facilitating the ex vivo production of complex molecules with high biocompatibility.[140] For example, organoid technology shows great promise in antibody production by mimicking immune system components to produce specific antibodies against pathogens in vitro. This accelerates therapeutic development and enables research into immune response.[141] In another area of synthetic biology, organoid technology has revolutionized toxin production for medical research. The cultivation of organoids capable of producing snake venom is an important advance that offers potential for antivenom development, pharmacological research, and therapeutic applications. Organoids derived from snake venom gland cells provide an in vivo-like model for venom production.[142] This study represents a significant stride in venom research, as these new organoids can serve as a viable platform that not only fosters a deeper understanding of venom biology but also propels the development of antivenoms and other therapeutic agents.[143] In summary, organoid technology is carving a new niche in the production of synthetic biology products and is expected to propel the development of innovative drugs and therapeutic strategies in the future (Figure 4C). Recently, Kim et al. reported another significant advance in the field of synthetic biology and organoid technology.[144,145] Researchers created human enamel organoids from iPSCs to mimic tooth development. These organoids, which resemble ameloblasts, formed enamel in response to the presence of calcium and interacted with dental mesenchyme to enable mineralization. They also displayed differentiation potential and regenerative abilities. This advance in synthetic biology introduces new possibilities for dental treatments and research.[144,145]

Synthetic biology, an evolving field, shows promise for the generation of diverse biochemical compounds, which is crucial for therapeutic development. The main challenge is efficiently identifying compounds with high biological activity and therapeutic value, and an emerging solution is using organoids in high-throughput screening systems. Organoids, which mimic the functions of real organs in three-dimensional structures, provide a platform for more accurately evaluating synthetic compounds. For instance, a study by Yang et al. emphasizes that organoids provide a three-dimensional

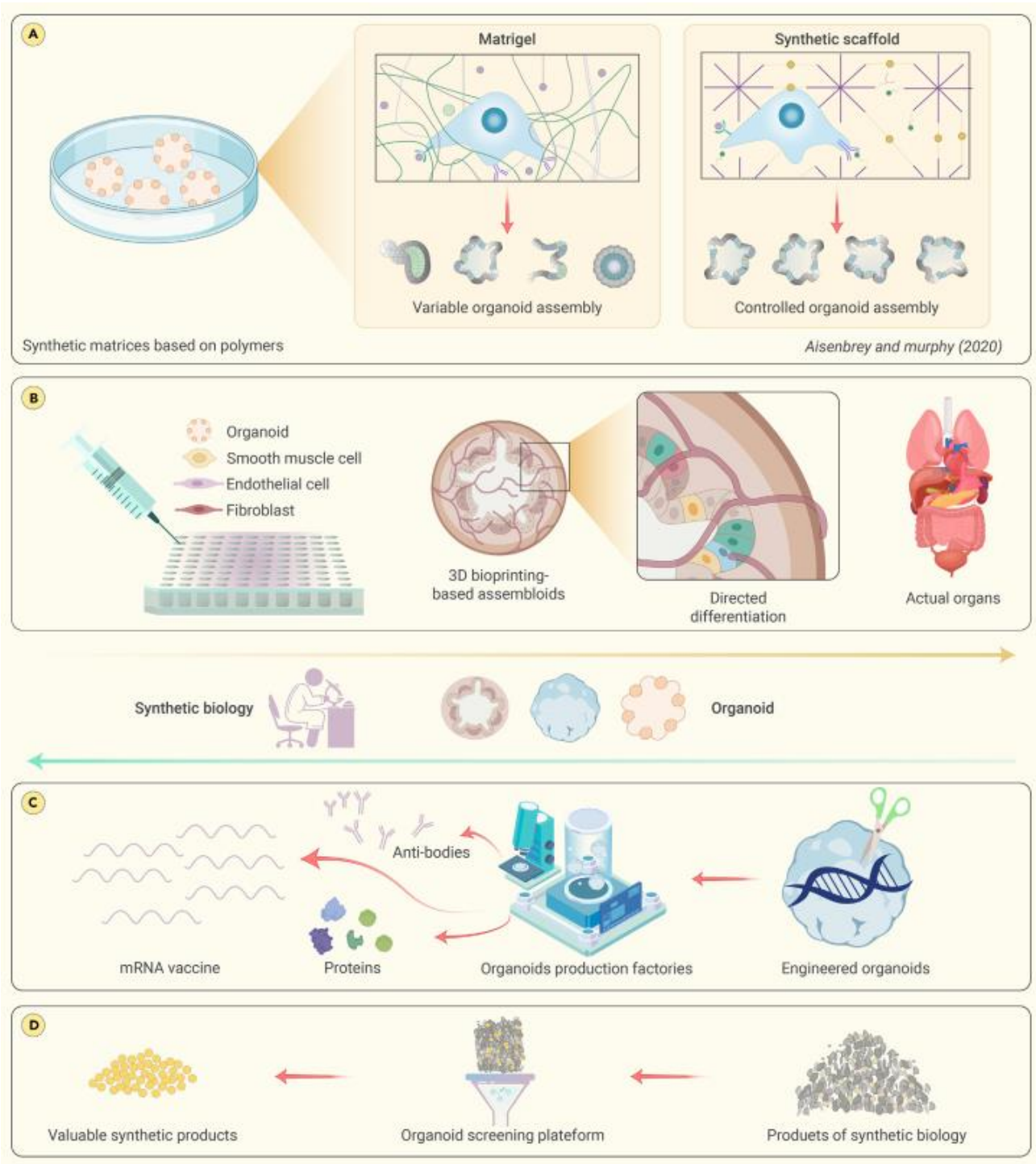

Figure 4. The intersection of synthetic biology and organoid (A) Synthetic biology aids in creating various auxiliary matrices and scaffolds. These structures provide an optimized environment, enhancing the growth and development of organoids. (B) By combining different cellular components, assembloids mimic the complexity of actual organs. (C) The utilization of organoid technology is establishing a distinct and specialized role within the realm of synthetic biology product manufacture. (D) Organoids, which are three-dimensional multicellular constructs that replicate the activity of actual organs, offer a distinct prospect for enhanced and streamlined screening procedures of synthetic drugs.

platform suitable for high-throughput drug screening, potentially bridging the gap between basic research and clinical practice.[146] The integration of compound production by synthetic biology and the screening capabilities of organoids could revolutionize therapeutic development. The synergy between generating diverse biological compounds and efficiently screening them for the most promising candidates could significantly expedite drug discovery, bringing effective treatments to patients more quickly and reliably (Figure 4D).

In conclusion, the fusion of synthetic biology and organoid research represents a monumental advance in biomedicine, presenting new avenues for studying and manipulating organoids. This intersection is poised toreshape our understanding of human biology and disease, paving the way for transformative clinical applications and developments in biomedical research.

ORGANOIDS: REVOLUTIONIZING THE LANDSCAPE OF TOXICOLOGY RESEARCH

Toxicology research, which is instrumental in evaluating the safety of pharmaceutical drugs, industrial chemicals, cosmetics, and food additives, has traditionally relied on animal models and two-dimensional cell cultures. The application of organoidsin toxicology allows the exploration of tissue-specific responses totoxicants, which was hitherto impossible with the above traditional methods.[147] The primary use of organoid models in toxicology lies in drug development and toxicity testing.[148] Conventional in vitro and animal models frequently fail to precisely forecast toxicity in humans, causing late-stage drug failures and unforeseen adverse effects after market release. However, the ability to generate organoids that mimic the complexity and functionality of human organs presents new opportunities for understanding toxicity mechanisms at a cellular and molecular level. The significant contributions of organoids to toxicology include their use in drug-toxicity testing, where liver organoids have aided in predicting drug-induced liver injuries—a major cause of drug withdrawal from the market.[149]

Liver organoids have proven to be a valuable in vitro tool for drug testing, including toxicity assessment.[150] Another study discusses the potential of using human PSC-derived organoids for high-fidelity drug-induced liver injury screening.[151] Moreover, organoids derived from pluripotent or tissue-resident adult stem cells can self-organize into three-dimensional structures, closely mirroring the in vivo architecture and functionality of various organs.[152] This ability allows organoids to mimic the effects of toxin damage on specific tissues, providing platforms for the specialized study of toxicity pathways. For instance, brain organoids comprising various neuronal and glial subtypes facilitate the analysis of the neurodevelopmental and neurodegenerative effects of drug toxicity.[153] Likewise, intestinal organoids have been utilized to study gastrointestinal toxicity, such as the mucosal damage induced by compounds like non-steroidal anti-inlammatory drugs.[154] In addition, the creation of patient-specific organoids exhibits tremendous potential in personalized medicine.[148] These organoids can help define individual susceptibility to various toxins, which could transform toxicity testing by facilitating personalized risk assessment and intervention strategies (Figure 5A).

The potential application of organoid models extends further to the field of environmental toxicology. Organoids facilitate research on how environmental toxins affect human health.[148] For instance, lung organoids have been used to study the impact of air-pollution particles on lung tissues, providing a realistic representation of human lung exposure to environmental hazards (Figure 5B).[155]

Technological advances, including microluidics and high-throughput screening systems, promise a bright future for organoids in toxicology. Microluidic platforms can provide increased control over the organoid microenvironment,[156] fostering the examination of dynamic processes and cell interactions (Figure 5C). High-throughput screening systems can expedite the testing of numerous compounds, enabling efficient and cost-effective toxicological assessments. The incorporation of multiorganoid systems also shows great promise. By amalgamating different types of organoids, researchers can construct more intricate and interconnected models to simulate the interaction among organs in the human body.[157,158] The system was able to demonstrate drug metabolism, interorgan crosstalk, and adverse drug reactions, offering a comprehensive assessment beyond what single-organ models can provide.[159] This strategy can enrich our understanding of systemic toxicity and the effects of toxins on multiple organs. Moreover, organoid engineering can help overcome some of the limitations of current organoid models. By incorporating additional cell types, such as immune or vascular cells, researchers can increase the physiological relevance of organoids and simulate the responses of human tissue to toxicants.[147] However, organoid models pose substantial challenges due to their complexity and variability. The differentiation of organoids into multiple cell types can luctuate, leading to inconsistent study results.[160,161] Additionally, the lack of vascularizationin organoidscan impede toxin delivery, skewing the interpretation of toxicological results.[147]

In conclusion, organoid models in toxicology present immense potential. Addressing the challenges of standardization, scalability, physiological relevance, and ethical considerations will be pivotal to fully exploiting organoids in toxicology research. With continued technological advancement and interdisciplinary collaborations, organoid models present an opportunity to revolutionize toxicology, leading to more accurate and efficient testing of harmful substances and thereby significantly increasing human health and safety.

THE ORGANOID EPOCH: A PARADIGM SHIFT IN DRUG DEVELOPMENT

Organoid technology has played a pivotal role in the advancement and evaluation of new pharmaceuticals. While organoids are not directly involved in the creation of novel drugs, they are essential for facilitating the discovery of promising drug candidates via drug screening and testing.[162,163] Specifically, organoids derived from colorectal cancer patients have been instrumental in assessing responses to inhibitors of tankyrases, enzymes that are crucial in Wnt signaling and are frequently disrupted in colorectal cancer. This testing has led to the identification of new drug candidates targeting the Wnt pathway.[68] Moreover, organoids from breast and lung cancer patients with certain mutations have been valuable in predicting sensitivity to PARP inhibitors, drugs that focus on DNA-repair mechanisms,[68,164,165] contributing significantly to the development of individualized treatment plans involving PARP inhibitors. An additional study revealed that organoids possessing ARID1A missense mutations exhibited particular sensitivity to ATR inhibitors, which affect the DNA-damage response. This discovery holds significant promise for the development of new ATR-targeting drugs for cancers with ARID1A mutations.[166] Furthermore, organoids from endometrial and metastatic tumors responded to STAT3 inhibitors, hinting at the potential for novel drugs that target STAT3 signaling in endometrial adenocarcinoma.[167] Organoid lines from mesothelioma patients retained biomarkers and histological features of the patients, tumors.[168] In drug testing with cisplatin and pemetrexed, the organoids mirrored the patients, responses, demonstrating the potential of organoids in predicting treatment outcomes for mesothelioma. Finally, organoids from appendiceal carcinoma were used in immunotherapy trials, paving the way for the creation of new immunotherapeutic agents tailored to the unique characteristics of appendiceal tumors.[167] In every facet of pharmaceutical development, organoids manifest indispensable significance, providing robust support and verification from foundational research to clinical trials and all the way to the guidance of personalized medication, facilitating all-encompassing success in drug innovation.

The emergence of organoids in high-throughput drug screening has transformed drug discovery by enabling the targeted identification of effective molecules from large compound libraries.[162,163] Recent advances in automation and systematic platforms have made organoids a gold standard in drug screening with the potential to streamline drug-discovery pipelines.[169—171] Their ability to efficiently identify the most effective molecules from large compound libraries is transformative, and organoids are poised to become an integral part of drug-discovery pipelines. A large-scale organoid-based screening platform was used to test 1,172 Food and Drug Administration-approved compounds on pancreatic cancer organoids, and 22 drugs with anticancer effects were identified. This effort underscored the importance of three-dimensional culture-based platforms for drug screening, as some drugs that were effective in organoids did not show the same effects in two-dimensional cultures.[166] One of the most critical aspects of drug development is the early identification of toxicological profiles. Traditional animal models often fail to capture the full spectrum of human-specific toxicities, leading to costly failures in late-stage clinical trials. Organoids, because of their human-derived cells and tissue-specific architectures, constitute a more accurate model for assessing drug toxicity.[172,173] Kidney organoids,[174,175] for instance, have been used to evaluate nephrotoxicity, which is a significant concern in human pharmacology. Organoids are crucial and powerful tools not only for testing compound efficacy and toxicity but also for understanding disease mechanisms and validating therapeutic targets.[176] In cancer research, patient-derived tumor organoids play an important role in validating oncogenes and tumor-suppressor genes, thereby offering insights into drug mechanisms. In a study by Hirt et al.[177] reported by Mainardi and Bernards,[166] a newly derived pancreatic organoid biobank comprising 31 three-dimensional cell lines derived from tumors and nine from healthy tissue was used to investigate novel drug-gene interactions with potential translational value. The evaluation of drug responses in a context that mimics human physiology is crucial for the success

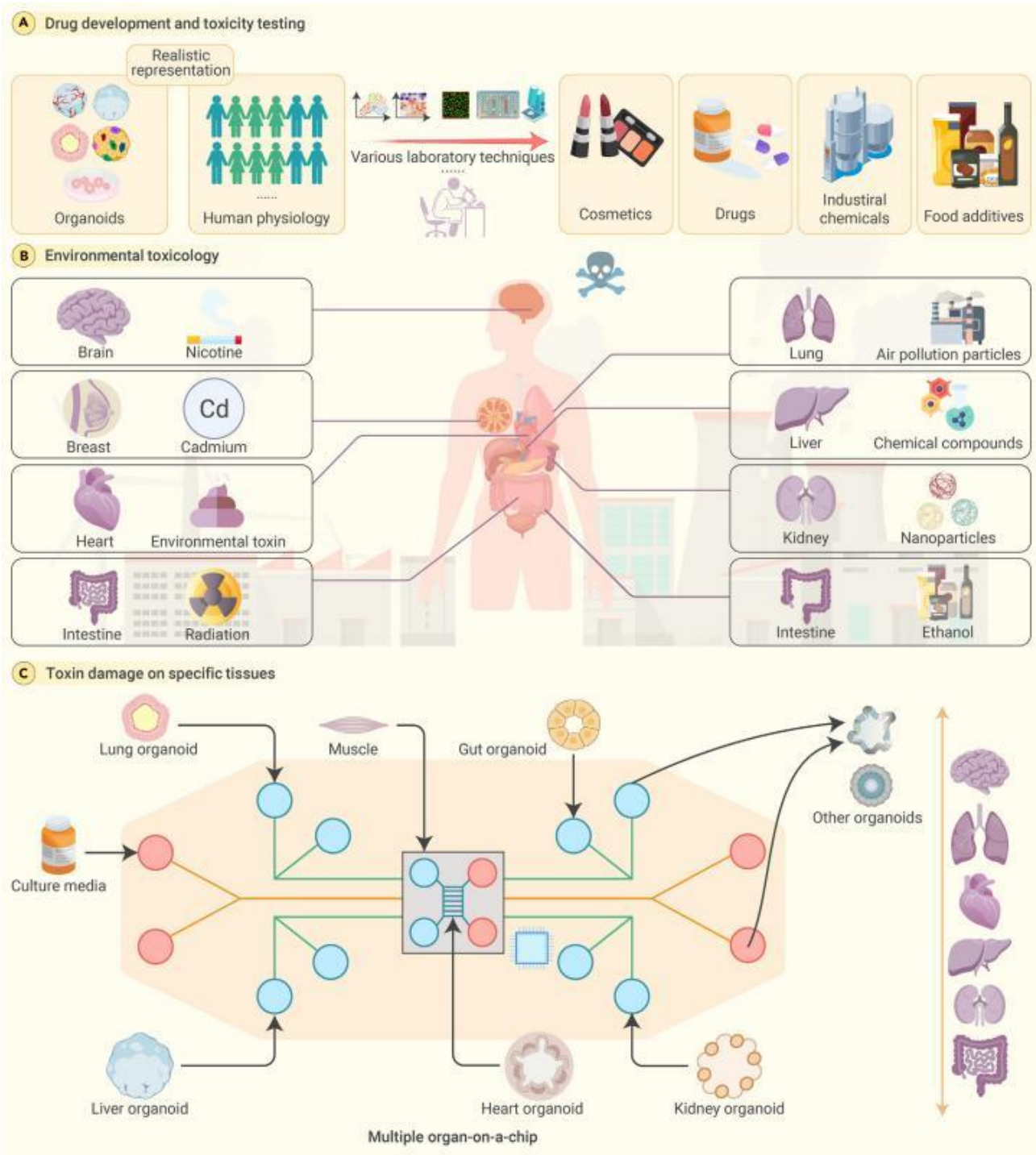

Figure 5. Organoids: Transforming the field of toxicology research (A) Organoids represent a significant advancement in accurately predicting human reactions to common items, surpassing the reliability of conventional models. Stem cell-derived organoids provide a more precise reproduction of human tissue structure and physiological reactions, making them suitable for assessing the safety of common consumer goods. (B) The environmental sentinel: organoids detecting global toxic threats. Organoids serve as powerful tools for detecting environmental toxins, including those affecting the brain. (C) Toward a comprehensive human model: multiorgan chips for effective toxicology. Microluidic platforms and multiorganoid systems are at the forefront of simulating complex human physiology.

of any therapeutic intervention. The advantages of organoids in drug responses can even be applied to clinical trials of new drugs.[81,178] Clinical trials are the bottleneck of drug development, with significant time and resource investments followed by high failure rates. Organoids have the potential to increase the success rate of clinical trials by providing a more accurate representation of patients, diseased tissue and predicting their responses to specific therapies.[179] Organoids derived from patients enrolled in a trial could be used in parallel to evaluate drug responses, helping to adapt or modify the trial,s course in real time. This

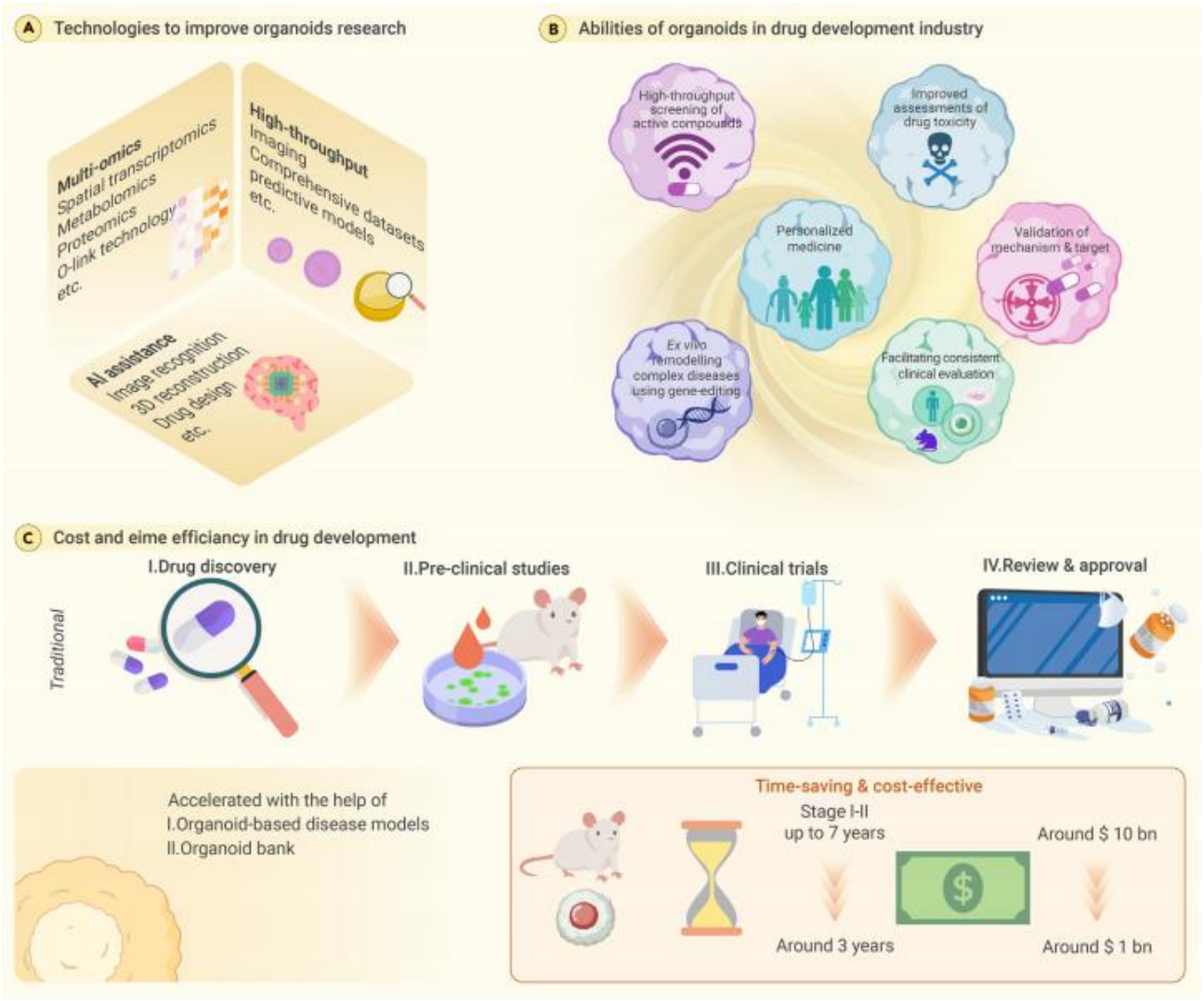

Figure 6. The organoid epoch: A paradigm shift in drug development (A) Organoid technology: advancing drug development across all stages. Organoids are crucial in inluencing the drug-development sector, providing extensive assistance throughout the entire process. (B) The various applications of organoid models in biological research. Organoids play a pivotal role in the drug-development industry, offering a wide range of applications that streamline and enhance the process. (C) Comparing the cost and time efficiency of drug development: traditional methods with organoid-based approaches. Organoids represent a fundamental change in medication development, providing notable benefits compared to conventional approaches.

personalized approach to clinical trials holds great promise for improving patient outcomes and reducing the time and cost associated with drug development.[180] The aim of personalized medicine is to tailor treatments to individual patients based on their genetic and physiological characteristics. In oncology, patient-derived tumor organoids can be used to screen for effective chemotherapy agents, thereby personalizing treatment plans.[180–183] The ability to evaluate drug responses in patient-specific organoids holds great promise for improving treatment outcomes and reducing adverse effects. Immunotherapies have revolutionized cancer treatment, but their efficacy varies among patients. Organoids constitute a powerful platform for studying the immune microenvironment and developing novel immunotherapies.[184,185] Researchers can assess the efficacy of immunotherapeutic treatments by coculturing organoids with immune cells, such as tumor-infiltrating lymphocytes.[184] The study of tumor-infiltrating lymphocytes within organoids has also introduced new avenues for personalized immunotherapies tailored to the specific immunological landscape of each patient,s tumor.[186,187] The ability to model complex diseases ex vivo has been significantly advanced by the advent of organoid technology and gene-editing techniques. For instance, CRISPR-Cas9 has been instrumental in creating lung cancer models by introducing specific mutations into lung organoids.[188] Such models offer a multifaceted approach to understanding complex diseases and have therefore been particularly useful in studying developmental and genetic diseases (Figures 6A and 6B).

Ex vivo modeling of complex diseases in organoids, aided by advanced gene-editing techniques, represents a cost-effective and ethical alternative to traditional drug-development methods. Organoids accurately replicate human physiology, thereby reducing the time and costs associated with drug discovery (Figure 6C).[189] Their utility in academic research and clinical application is significant, offering the potential to revolutionize the field and pave the way for more efficient therapeutic advancements.

ORGANOIDS ADVANCE BIOMEDICAL FIELDS ACROSS THE BOARD

The field of biomedical research has achieved a significant leap forward with the advent of organoid technology. Their versatility and adaptability make thema valuable tool for a wide range of research applications, with the potential to reshape therapeutic approaches to a range of clinical challenges (Figure 7A). The promise of organoids is particularly palpable in the realm of diabetes treatment. Researchers are abuzz regarding the creation of islet-like organoids that respond to glucose, which herald a potential paradigm shift in diabetes

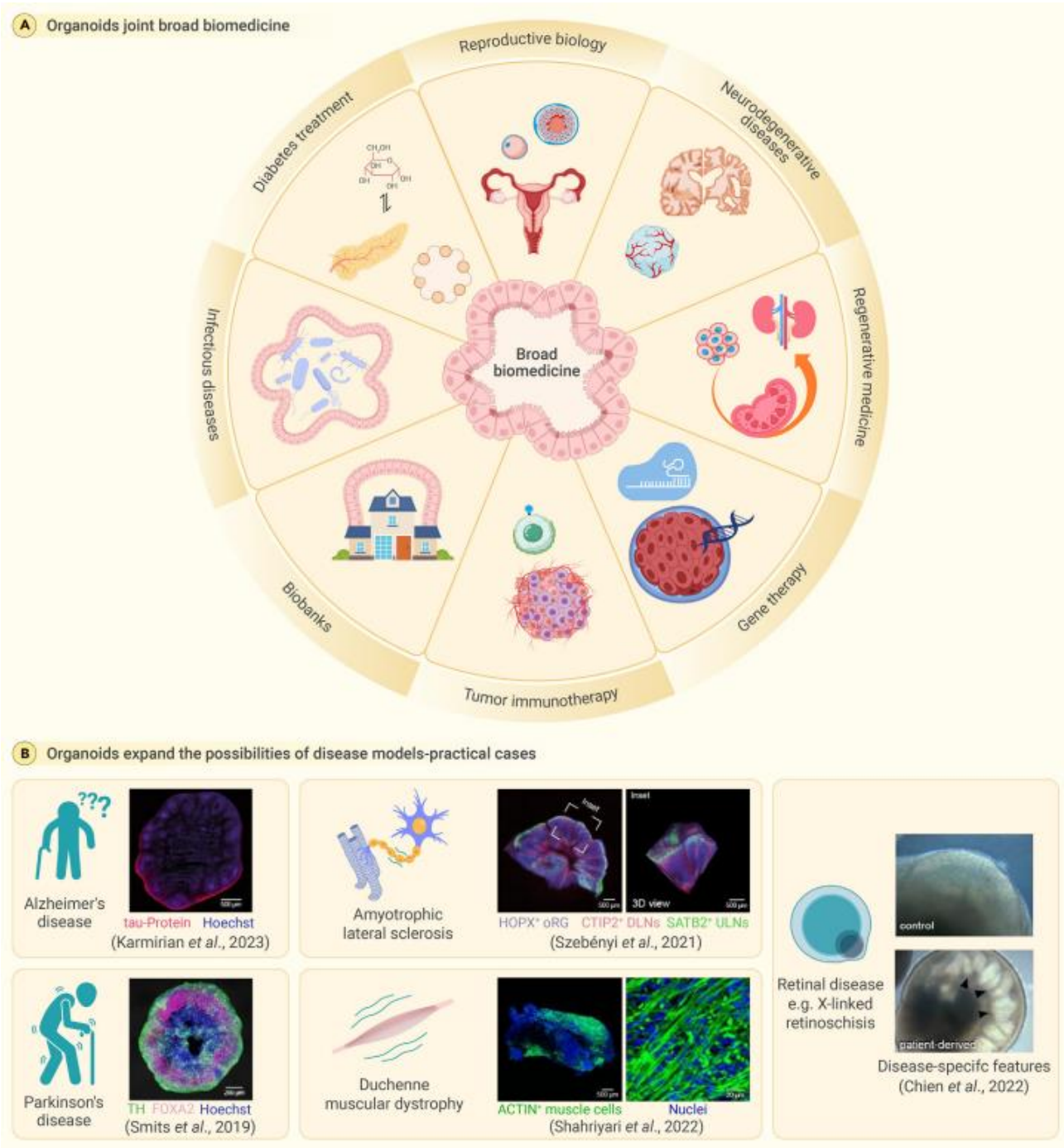

Figure 7. The multifaceted impact of organoid technology in biomedical science (A) The domain of biomedical research has experienced a substantial advancement with the introduction of organoid technology. The valuable attributes of versatility and adaptability possessed by these tools render them highly useful in a diverse array of research applications. Consequently, they hold great potential for revolutionizing therapeutic strategies aimed at addressing a wide range of clinical difficulties. (B) The application of organoids has greatly expanded the scope of disease inquiry. Technological advancements have made it possible to explore scientific realms that were previously inaccessible, especially when with regard to situations that are unique to humans.

management.[190] These organoidshouse a diverse array of cells: insulin-producing β cells, glucagon-producing a cells, somatostatin-producing δ cells, and pancreatic polypeptide-producing g cells.[191] Their efficacy was tested by transplantation into diabetic mice,[192] where these organoids mimicked native pancreaticβ cells, releasing insulin in response to blood glucose luctuations and stabilizing glucose levels. Despite the promise of this approach, challenges remain, such as scaling up organoid production and maintaining their long-term functionality.

Regenerative medicine, which is synonymous with restoration and healing, has found in organoids a robust and versatile ally.[125] These structures are pioneering advancesin tissue repair,[50,53,193,194] transplantation, and overall regenerative strategies.[53] In inlammatory bowel disease research, organoids are

providing insights into tissue-regeneration mechanisms, paving the way for innovative treatments.[125] Organoid transplantation is also presenting new possibilities. A prime example is the transplantation of human intestinal organoids into mice,[195] which resulted not only in the successful integration of the organoids but also in physiological improvements in the recipient mice. Similarly, research into human kidney organoids transplanted into rats has shown promising results,[196,197] including enhanced vascularization and function. Such studies hint at a future in which organ transplant waiting lists could be significantly reduced, with organoids serving as a viable alternative. In biobanking, organoids are revolutionizing the collection, preservation, and utilization of normal and pathological specimens, improving disease modeling and drug screening.[198] Organoids also enable the preservation and study of viruses or microorganisms that are difficult to culture in traditional cell lines, providing more accurate models for research on tropism and immunity induction.[199—201]

The intersection of organoids and infectious disease research is also particularly compelling. Organoids offer a dynamic platform for studying host-pathogen interactions, paving the way for deeper insights and innovative treatments.[202—204] For instance, organoids have been pivotal in the study of respiratory viruses.[205] Their application in research related to inluenza and respiratory syncytial virus isjust the tip of the iceberg.[204] However, research on SARS-CoV-2 is where the potential of organoids is truly showcased.[206—209] Researchers have used lung and intestinal organoids to gain a nuanced understanding of how the virus invades human cells.[210—213] These studies are revealing vital data about viral entry, replication, and spread. Furthermore, organoids provide a platform for testing potential drugs against the virus, accelerating the drug-discovery process.[214,215] Beyond viral infection, organoids have a role to play in bacterial and parasitic infection research.[202,216] Their three-dimensional structure, mirroring that of human tissue, offers a unique environment to study the dynamics of bacterial infections ata cellular level. Additionally, in parasitic research, organoids are illuminating host-helminth interactions,[217] unveiling the intricate relationships between parasites and their human hosts.

Moreover, organoid models are a powerful tool for studying female fertility and reproductive biology. These organoids, derived from tissues in the female reproductive tract, enable research on normal reproductive processes and pathologies such as endometriosis, endometrial cancer, and ovarian cancer.[156,218—220] Ovarian organoids facilitate the investigation of oocyte growth and maturation along with hormonal stimulation responses.[220] Fallopian tube, endometrial, and cervical organoids are utilized to study various aspects of female reproductive health, including the development and function of the fallopian tubes, the menstrual cycle, endometriosis, endometrial hyperplasia, cervical clear cell carcinoma, and the impact of infections such as Chlamydia trachomatis and human papillomavirus. Additionally, organoids derived from pathological tissues have aided in understanding reproductive disorders and have been valuable for drug screening.[156,218,220] Organoids also model early developmental events, such as implantation, and can be used to investigate interactions between different cell types such as trophoblast cells and the maternal decidua. Recent studies have also involved the development and characterization of trophoblast organoids and decidual organoids from human placental samples, which serve as models to study the maternal-fetal interface.[221] These organoids have been used to investigate innate immune signaling and the differential antiviral defenses present at the maternal-fetal interface. Moreover, organoids have been employed to study the effects of environmental toxicants on female fertility and reproductive health.[219] They offer a physiologically relevant and controlled system for the examination of intricate cellular processes within acontextually appropriate environment, offering the potential to revolutionize thefieldof reproductive medicine.

Duchenne muscular dystrophy, a debilitating genetic disorder, is also the subject of promising advances due to organoids. Using gene-editing technologies, researchers have been able to correct genetic mutations in iPSC-derived muscle cells, which constitutes a monumental advance in the development of effective treatments for Duchenne muscular dystrophy (Figure 7B).[82,83] Organoid-based research has also enabled the development of innovative therapeutic strategies for retinal diseases, which have historically been challenging to treat.[84,85] Leveraging organoids, scientists have been able to explore the potential of gene augmentation therapy using systems such as CRISPR-Cas9. One notable success has been the promise shown in treating Leber congenital amaurosis, a severe form of inherited blindness: targeted gene therapies have demonstrated potential in restoring vision.[83]

In summary, the versatile applications of organoids are undeniablysetting the stage for groundbreaking advancement in biomedical research. As we continue to harness their potential, the bridge between laboratory-based discoveries and real-world clinical applications is becoming more robust. The future promises a new era of personalized medicine with organoids at its core, offering hope for myriad clinical challenges.

TECH-INFUSED ORGANOIDS: THE NEW VANGUARD OF BIOMEDICINE

Recent technological advances are further empowering organoid systems and enabling the derivation of new biological insights. New tools in single-cell omics, imaging, genetics, and AI are being integrated with organoid platforms. Single-cell RNA sequencing (scRNA-seq) and other omics tools enable the high-resolution dissection of organoid composition and function (Figure8).[222] Advanced imaging techniques allow the dynamic visualization of organoid morphogenesis and cell-cell interactions.[223] AI and machine learning provide computational power to extract complex patterns and build predictive models from multidimensional organoid data.[224] The integration of organoids with these emerging technologies has created a new generation of “organs-on-chips” that recapitulate tissue- and organ-level physiology in unprecedented detail.[225,226]

Genetic engineering in organoids is a rapidly advancing field that combines organ-like complexity with molecular precision. Methods such as viral (retroviral, lentiviral, adenoviral) and nonviral (electroporation, lipofection) delivery systems enable gene manipulation in organoids,[227] and CRISPR-Cas9 is revolutionizing precise gene editing.[228] RNA interference is also used to modulate gene expression.[227]

Organoids are vital in high-throughput screening for assessing cell viability and metabolic activity. Enzyme-linked immunosorbent assays quantify biomarkers, while image-based profiling techniques such as epiluorescence and confocal microscopy are used to analyze organoid morphology and functional changes after treatment.[163,229] High-content analysis dissects developmental processes and disease progression at the cellular level, integrating omics data and multidimensional imaging for a comprehensive view of organoid responses to drug treatments. z-stack imaging provides a complete cross-sectional view of three-dimensional organoids, increasing the accuracy of drug efficacy and toxicity assessments.[229] Computational methods model cellular interactions and biomechanical properties in organoids, facilitating the optimization of culture conditions and the prediction of drug-treatment outcomes.[230] Human liver organoids derived from PSCs have been successfully used to model drug-induced liver injury, aiding in antifibrosis drug screening and the identification of compounds with significant antifibrotic effects, such as SD208 and imatinib.[230]

The integration of single-cell omics and organoid technologies has significantly advanced our understanding of organ development, disease mechanisms, and potential therapeutic approaches. This synergy has been especially effective in the field of neurobiology and brain organoid research. Fleck et al. investigated the gene-regulatory network underlying human cerebral organoid development and used multiomics single-cell data to develop an algorithm called Pando to infer the gene-regulatory network, thereby revealing the involvement of different transcription factors at various stages of cerebral organoid development. Their research emphasizes the conservation of developmental programs across species and the predictive capability of multiregion human cerebral organoids as model systems.[231] Vento-Tormo emphasized the revolutionary upgrade that organoid technology,[232] combined with single-cell profiling, has brought to the field of human development. This combination allows a deeper understanding of cell-cell communication and cellular heterogeneity, as evidenced by the work of Camp et al. in studying human liver organoids using scRNA-seq.[232] Yin et al. further elaborated on the strengths of combining scRNA-seq and organoid technologies, highlighting applications such as the discovery of novel cell types and gene markers, the recapitulation of cellular heterogeneity, the delineation of cell-differentiation pathways, and the modeling of diseases.[233] Single-cellomics technologies also enable the high-resolution dissection of cellular heterogeneity within organoid systems. scRNA-seq has been transformative in decoding organoid composition and identifying novel cell states. For example, scRNA-seq was used to map the cell lineages and transitional states in intestinal organoids, reconstructing the differentiation trajectories from stem cells to all intestinal epithelial cell types.[222] In patient-derived organoids, a recent study adopted an integrative approach combining scRNA-seq, epigenomic single-nucleotide polymorphism (SNP)-to-gene mapping, and genome-wide association study

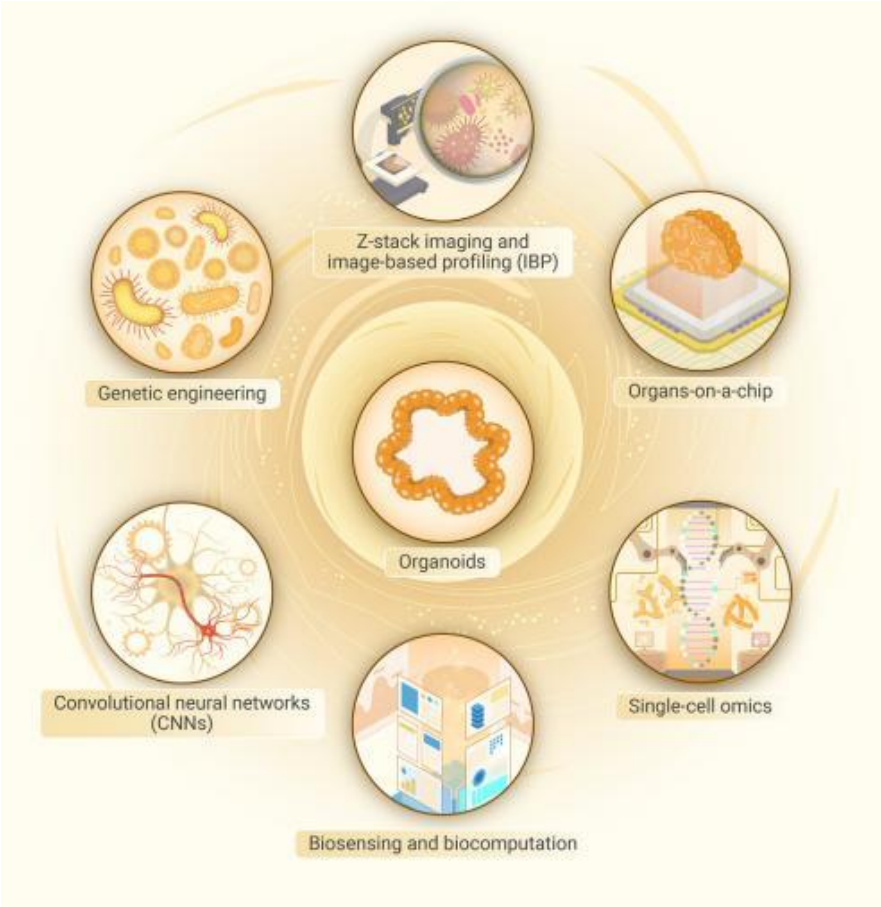

Figure 8. Tech-infused organoids: The cutting-edge advancement in biomedicine Organoids are now being enhanced with cutting-edge technical advancements. The integration of several disciplines in joint efforts has led to the development of organoids that are equipped with cutting-edge technology. This advancement holds the potential to bring about a significant transformation in the field of biomedicine.

summary statistics to deduce the cellular subtypes and molecular pathways by which genetic variants affect disease phenotypes.[234] In summary, the integration of single-cell omics with organoid technologies provides a robust platform for modeling organ development and diseases. This combination has proven effective in revealing the cellular and molecular intricacies of organogenesis and disease pathogenesis.[235] These advancements not only deepen our understanding of human biology but also pave the way for the development of novel therapeutic strategies.

The field of single-cell omics faces challenges in data interpretation due to the complexity of merging high-dimensional single-cell data with spatial information. The integration of AI and deep-learning algorithms can help streamline this process, enabling the identification of intricate patterns and interactions that are not easily discernible through traditional methods. Combining organoids with AI and deep learning enables innovative approaches to analyzing complex biological datasets and constructing predictive models. Organoids produce extensive multidimensional data, including cellular imaging, omics profiles, phenotypic readouts, and time series, and AI offers the computational power to extract meaningful patterns from this data overload.[236]

One major application is automated image analysis using convolutional neural networks, which can segment and classify cells in organoid imaging data orders of magnitude faster than human annotation.[237] AI also enables phenotypic profiling from images. A deep-learning model was trained to predict the emergence of retinal tissue morphology and cell types in optic cup organoids over time.[238] In the absence of reliable markers for assessing organoid vitality, researchers recently devised an innovative approach using AI algorithms to analyze a spectrum of phenotypic parameters. Remarkably, the AI-driven method can ascertain organoid aging solely through bright-field imaging. This approach eliminates the cumbersome steps of preparing single-cell suspensions and performing senescence-associated β-galactosidase staining, thereby streamlining quality control processes and making biobank operations more efficient.[224]

Beyond merely visualizing images, AI can concurrently reconstruct multiple parameters from multiomicsdata in organoids. These data are then integrated with complementary datasets, such as functional metricsand patient records, all derived from the same experimental conditions. The resulting repository is a large multimodal database. AI algorithms sift through this complex data to identify patterns and correlations, elucidating connections within diverse multiparametric information that may be challenging for human analysts to interpret. Overall, the integration of organoids with AI and deep learning constitutes an exciting new frontier.

The integration of organoids with microluidics and sensors has enabled the development of "organs-on-chips" that recapitulate key aspects of human tissue physiology in vitro. These biomimetic systems incorporate organoids into microengineered devices with tissue-tissue interfaces, luid low, and real-time monitoring to model organ function and disease.[225] One example is the gut-on-a-chip, which combines intestinal organoids with a microluidic device lined by endothelial and immune cells to model the intestinal epithelium. This system faithfully reproduces the microenvironment of the living intestine, including peristalsis-like motions and cyclic strain from breathing. Using this model, researchers showed that cyclic strain promotes intestinal stem cell differentiation and epithelial permeability. Thus, the gut-on-a-chip provides a powerful platform to study intestinal absorption, inlammation, gut-microbe interactions, and more.[239—241] Another study by Campisi et al. presents a three-dimensional self-organized microvascular model of the blood-brain barrier using human iPSC-derived endothelial cells, brain pericytes, and astrocytes in a fibrin gel. This microluidic system replicates in vivo neurovascular organization, exhibiting lower permeability than conventional in vitro models, and thus provides a physiologically relevant and robust platform for drug discovery and the prediction of neurotherapeutic transport efficacy.[242] Hajal et al. developed a human blood-brain barrier model within microluidic devices by incorporating endothelial cells, brain pericytes, and astrocytes in a three-dimensional gel matrix. This model forms three-dimensional vessel architectures that resemble the natural blood-brain barrier, with gene-expression profiles and permeability values comparable to those observed in vivo.[243] Accordingly, this blood-brain barrier model facilitates the quantitative assessment of molecular permeabilities and is suitable for use in both academic and industrial research to predict transport across the blood-brain barrier. These studies exemplify significant advances in organ-on-a-chip technology, specifically in modeling the blood-brain barrier.[244] This progress underscores the potential of organ-on-a-chip technology to revolutionize biomedical research and therapeutic development.

Another exciting emerging application of organoids is the modeling of neural networks for biocomputation. Like their in vivo counterparts, the organized neuronal networks generated within brain organoids can perform specialized information processing.[245] Researchers now plan to develop brain organoids that can serve as "biocomputers" for tasks such as pattern recognition and classification.[246] In one pioneering study, a proof of concept of using brain organoids for biosensing and biocomputation was demonstrated. A recent publication in the journal Neuron revealed groundbreaking research conducted by Brett Kagan

and his team at Cortical Labs, demonstrating that organoid neural networks cultured in vitro can learn to play the classic arcade game Pong.[247] These so-called mini-brains, composed of interconnected neural cells, exhibit the ability to perceive and interact with their surrounding environment. Utilizing a computer interface, the neural networks were trained to detect the position of the game's digital sphere and manipulate a virtual paddle accordingly. Remarkably, the assemblage of brain cells acquired this skill within 5 min. Biocomputing with brain organoids could potentially be faster, more efficient, and more powerful than silicon-based computing and AI, requiring only a fraction of the energy.[248] This technology could enable brain-inspired AI and powerful models for studying neural information processing.

Looking forward, the integration of organoids with new technologies has immense potential to transform biomedicine and human health. Such advances could power a new generation of preclinical disease models for drug screening, enable regenerative therapies using laboratory-grown tissues, and provide platforms for precision medicine. Realizing this potential will require collaborative multidisciplinary efforts at the intersection of stem cell biology, bioengineering, and data science. An exciting future lies ahead as organoids and emerging technologies combine to elucidate human biology in unprecedented detail.

CONCLUSION AND OUTLOOK

The advent of organoid technology marks a watershed in biomedical research, transcending previous boundaries of scientific inquiry. This innovation has revolutionized our understanding of human biology and introduced unprecedented avenues in disease management, addressing obstacles once considered insurmountable. At the cusp of this burgeoning field, the possibilities seem limitless, with organoid technology poised to reshape healthcare, research methodologies, and ethical considerations concerning human life.

Throughout this review, we have highlighted the multifaceted impact of organoids, emphasizing their utility in personalized medicine, drug discovery, and disease modeling. The bespoke nature of organoid systems, particularly patient-derived organoids, has introduced a new era of precision in biomedical research. By closely mimicking the intricate architecture and functionality of human organs, organoids offer a more representative model for human physiology and pathology, surpassing traditional in vitro and animal models. The capacity of organoids to replicate complex biological processes, such as the tumor immune microenvironment and host-pathogen interactions, positions them as a vanguard in further elucidating disease mechanisms and therapeutic responses.

Looking to the future, the integration of organoids with cutting-edge technologies such as synthetic biology, AI, and gene editing heralds a transformative phase in biomedical innovation. This synergy holds promise for unlocking new therapeutic pathways, advancing drug development, and providing profound new insights into complex diseases. The potential of organoids to serve as platforms for rapid drug testing and functional experimentation, coupled with their compatibility with gene-editing techniques, signifies a quantum leap in medical research.

In summary, organoid technology stands at the forefront of a revolution in the biomedical field. Its impact on human society will be profound, and its future applications appear boundless. As researchers and clinicians continue to harness the power of this technology, we anticipate a future replete with groundbreaking discoveries and innovative treatments that will ultimately reshape our approach to understanding and curing human diseases.

REFERENCES

1. Yang, S., Hu, H., Kung, H., et al. (2023). Organoids: The current status and biomedical applications. MedComm 4(3): e274. https://doi.org/10.1002/mco2.274.
2. Barbuzano, J. (2017). Organoids: A new window into disease, development and discovery. Harvard Stem Cell Institute News. https://hsci.harvard.edu/organoids.
3. Melzer, M.K., Resheq, Y., Navaee, F., et al. (2023). The application of pancreatic cancer organoids for novel drug discovery. Expert Opin. Drug Discov. 18(4): 429—444. https://doi.org/10.1080/17460441.2023.2194627.
4. Taverna, J.A., Hung, C.N., Williams, M., et al. (2024). Ex vivo drug testing of patient-derived lung organoids to predict treatment responses for personalized medicine. Lung Cancer 190: 107533. https://doi.org/10.1016/j.lungcan.2024.107533.
5. Tsai, S., McOlash, L., Palen, K., et al. (2018). Development of primary human pancreatic cancer organoids, matched stromal and immune cells and 3D tumor microenvironment models. BMC Cancer 18(1): 335. https://doi.org/10.1186/s12885-018-4238-4.
6. Kumar, S.S., Sreedharan, S.N., Patil, S., et al. (2020). The potential role of organoids in pathology and oncology research. Pathol. Oncol. Res. 26(2): 1353—1354. https://doi.org/10.1007/s12253-019-00642-z.
7. Driehuis, E., and Clevers, H. (2017). CRISPR/Cas 9 genome editing and its applications in organoids. Am. J. Physiol. Gastrointest. Liver Physiol. 312(3): G257—G265. https://doi.org/10.1152/ajpgi.00410.2016.
8. Duan, J., Penzes, P., and Gejman, P. (2019). From genetic association to disease biology: 2d and 3d human iPSC models of neuropsychiatric disorders and Crispr/Cas9 genome editing. Eur. Neuropsychopharmacol 29: S763—S764. https://doi.org/10.1016/j.euroneuro.2017.06.120.
9. Eerkes-Medrano, D., Feehan, C.J., and Leys, S.P. (2015). Sponge cell aggregation: checkpoints in development indicate a high level of organismal complexity. Invertebr. Biol. 134(1): 1—18. https://doi.org/10.1111/ivb.12072.
10. Wilson, H.V. (1910). Development of sponges from dissociated tissue cells. Bulletin of the Bureau of Fisheries 30: 1—35.
11. Wilson, H.V. (1907). A new method by which sponges may be artificially reared. Science 25(649): 912—915. https://doi.org/10.1126/science.25.649.912.
12. Corrò, C., Novellasdemunt, L., and Li, V.S.W. (2020). A brief history of organoids. Am. J. Physiol. Cell Physiol. 319(1): C151—C165. https://doi.org/10.1152/ajpcell.00120.2020.
13. Okabayashi, K., and Asashima, M. (2006). In vitro organogenesis using amphibian pluripotent cells. Proc. Jpn. Acad. Ser. B Phys. Biol. Sci. 82(7): 197—207.
14. Zwilling, E. (1964). Development of fragmented and of dissociated limb bud mesoderm. Dev. Biol. 9(1): 20—37. https://doi.org/10.1016/0012-1606(64)90012-0.
15. Axelrod, H.R. (1984). Embryonic stem cell lines derived from blastocysts by a simplified technique. Dev. Biol. 101(1): 225—228. https://doi.org/10.1016/0012-1606(84)90133-7.
16. Evans, M.J., and Kaufman, M.H. (1981). Establishment in culture of pluripotential cells from mouse embryos. Nature 292(5819): 154—156. https://doi.org/10.1038/292154a0.
17. Martin, G.R. (1981). Isolation of a pluripotent cell line from early mouse embryos cultured in medium conditioned by teratocarcinoma stem cells. Proc Natl Acad Sci 78(12): 7634—7638. https://doi.org/10.1073/pnas.78.12.7634.
18. Takahashi, K., and Yamanaka, S. (2006). Induction of pluripotent stem cells from mouse embryonic and adult fibroblast cultures by defined factors. Cell 126(4): 663—676. https://doi.org/10.1016/j.cell.2006.07.024.
19. Thomson, J.A., Itskovitz-Eldor, J., Shapiro, S.S., et al. (1998). Embryonic stem cell lines derived from human blastocysts. Science 282(5391): 1145—1147. https://doi.org/10.1126/science.282.5391.1145.
20. Chang, E.A., Jin, S.W., Nam, M.H., et al. (2019). Human induced pluripotent stem cells : clinical significance and applications in neurologic diseases. J. Korean Neurosurg. Soc. 62(5): 493—501. https://doi.org/10.3340/jkns.2018.0222.
21. Chhabra, A. (2017). Derivation of human induced pluripotent stem cell (iPSC) lines and mechanism of pluripotency: historical perspective and recent advances. Stem Cell Rev. Rep. 13(6): 757—773. https://doi.org/10.1007/s12015-017-9766-9.
22. Takahashi, K., Tanabe, K., Ohnuki, M., et al. (2007). Induction of pluripotent stem cells from adult human fibroblasts by defined factors. Cell 131(5): 861—872.https://doi.org/10.1016/j.cell.2007.11.019.
23. Ludwig, T.E., Kujak, A., Rauti, A., et al. (2018). 20 Years of human pluripotent stem cell research: it all started with five lines. Cell Stem Cell 23(5): 644—648. https://doi.org/10.1016/j.stem.2018.10.009.
24. Ochi, M. (2013). Shinya Yamanaka's 2012 Nobel Prize and the radical change in orthopedic strategy thanks to his discovery of iPS cells. Acta Orthop. 84(1): 1—3. https://doi.org/10.3109/17453674.2013.765642.
25. Omole, A.E., and Fakoya, A.O.J. (2018). Ten years of progress and promise of induced pluripotent stem cells: historical origins, characteristics, mechanisms, limitations, and potential applications. PeerJ 6: e4370. https://doi.org/10.7717/peerj.4370.
26. Sato, T., Vries, R.G., Snippert, H.J., et al. (2009). Single Lgr5 stem cells build crypt-villus structures in vitro without a mesenchymal niche. Nature 459(7244): 262—265. https://doi.org/10.1038/nature07935.
27. Lancaster, M.A., and Knoblich, J.A. (2014). Organogenesis in a dish: modeling development and disease using organoid technologies. Science 345(6194): 1247125. https://doi.org/10.1126/science.1247125.
28. Purnell, B.A. (2014). The making of bodies part by part. Science 345(6194): 280. https://doi.org/10.1126/science.345.6194.280-j.
29. Bender, E. (2015). Q&A: Hans Clevers. Nature 521(7551): S15. https://doi.org/10.1038/521S15a.
30. (2013). A gutsy approach to stem cells and signalling: an interview with Hans Clevers. Dis Model Mech 6(5): 1053—1056. https://doi.org/10.1242/dmm.013367.
31. Sinha, G. (2017). The organoid architect. Science 357(6353): 746—749. https://doi.org/10.1126/science.357.6353.746.
32. Pleguezuelos-Manzano, C., Puschhof, J., Van Den Brink, S., et al. (2020). Establishment and culture of human intestinal organoids derived from adult stem cells. Curr. Protoc. Immunol. 130(1): e106. https://doi.org/10.1002/cpim.106.
33. Lancaster, M.A., Renner, M., Martin, C.A., et al. (2013). Cerebral organoids model human brain development and microcephaly. Nature 501(7467): 373—379. https://doi.org/10.1038/nature12517.
34. (2014). Prostate cancer organoids make debut. Cancer Discov. 4(11): 1248. https://doi.org/10.1158/2159-8290.CD-NB2014-143.
35. Karthaus, W.R., Iaquinta, P.J., Drost, J., et al. (2014). Identification of multipotent luminal progenitor cells in human prostate organoid cultures. Cell 159(1): 163—175. https://doi.org/10.1016/j.cell.2014.08.017.
36. Takasato, M., Er, P.X., Chiu, H.S., et al. (2015). Kidney organoids from human iPS cells contain multiple lineages and model human nephrogenesis. Nature 526(7574): 564—568. https://doi.org/10.1038/nature15695.

37. Morizane, R., Lam, A.Q., Freedman, B.S., et al. (2015). Nephron organoids derived from human pluripotent stem cells model kidney development and injury. Nat. Biotechnol. 33(11): 1193–1200. https://doi.org/10.1038/nbt.3392.
38. Boj, S.F., Hwang, C.I., Baker, L.A., et al. (2016). Model organoids provide new research opportunities for ductal pancreatic cancer. Mol. Cell. Oncol. 3(1): e1014757. https://doi.org/10.1080/23723556.2015.1014757.
39. Huang, L., Holtzinger, A., Jagan, I., et al. (2015). Ductal pancreatic cancer modeling and drug screening using human pluripotent stem cell– and patient-derived tumor organoids. Nat. Med. 21(11): 1364–1371. https://doi.org/10.1038/nm.3973.
40. Fligor, C.M., Langer, K.B., Sridhar, A., et al. (2018). Three-dimensional retinal organoids facilitate the investigation of retinal ganglion cell development, organization and neurite outgrowth from human pluripotent stem cells. Sci. Rep. 8(1): 14520. https://doi.org/10.1038/s41598-018-32871-8.
41. Xian, B., Luo, Z., Li, K., et al. (2019). Dexamethasone provides effective immunosuppression for improved survival of retinal organoids after epiretinal transplantation. Stem Cells Int. 2019: 7148032. https://doi.org/10.1155/2019/7148032.
42. Lewis-Israeli, Y.R., Wasserman, A.H., Gabalski, M.A., et al. (2021). Self-assembling human heart organoids for the modeling of cardiac development and congenital heart disease. Nat. Commun. 12(1): 5142. https://doi.org/10.1038/s41467-021-25329-5.
43. Richards, D.J., Li, Y., Kerr, C.M., et al. (2020). Human cardiac organoids for the modelling of myocardial infarction and drug cardiotoxicity. Nat. Biomed. Eng. 4(4): 446–462. https://doi.org/10.1038/s41551-020-0539-4.
44. Liu, L., Yu, L., Li, Z., et al. (2021). Patient-derived organoid (PDO) platforms to facilitate clinical decision making. J. Transl. Med. 19(1): 40. https://doi.org/10.1186/s12967-020-02677-2.
45. Dominijanni, A., Mazzocchi, A., Shelkey, E., et al. (2020). Bioengineered tumor organoids. Curr. Opin. Biomed. Eng. 13: 168–173. https://doi.org/10.1016/j.cobme.2020.03.005.
46. Hosseini, Z.F., Nelson, D.A., Moskwa, N., et al. (2019). Generating embryonic salivary gland organoids. Curr. Protoc. Cell Biol. 83(1): e76. https://doi.org/10.1002/cpcb.76.
47. Sun, X.Y., Ju, X.C., Li, Y., et al. (2022). Generation of vascularized brain organoids to study neurovascular interactions. Elife 11: e76707. https://doi.org/10.1101/2022.01.04.474960.
48. Fagerlund, I., Dougalis, A., Shakirzyanova, A., et al. (2021). Microglia-like cells promote neuronal functions in cerebral organoids. Cells 11(1): 124. https://doi.org/10.3390/cells11010124.
49. Jensen, K.B., and Little, M.H. (2023). Organoids are not organs: sources of variation and misinformation in organoid biology. Stem Cell Rep. 18(6): 1255–1270. https://doi.org/10.1016/j.stemcr.2023.05.009.
50. Turhan, A.G., Hwang, J.W., Chaker, D., et al. (2021). iPSC-derived organoids as therapeutic models in regenerative medicine and oncology. Front. Med. 8: 728543. https://doi.org/10.3389/fmed.2021.728543.
51. McCauley, H.A., and Wells, J.M. (2017). Pluripotent stem cell-derived organoids: using principles of developmental biology to grow human tissues in a dish. Development 144(6): 958–962. https://doi.org/10.1242/dev.140731.
52. Rowe, R.G., and Daley, G.Q. (2019). Induced pluripotent stem cells in disease modelling and drug discovery. Nat. Rev. Genet.20(7):377–388.https://doi.org/10.1038/s41576-019-0100-z.
53. Kim, W., Gwon, Y., Park, S., et al. (2023). Therapeutic strategies of three-dimensional stem cell spheroids and organoids for tissue repair and regeneration. Bioact. Mater. 19: 50–74. https://doi.org/10.1016/j.bioactmat.2022.03.039.
54. Lee, C.T., Bendriem, R.M., Wu, W.W., et al. (2017). 3D brain Organoids derived from pluripotent stem cells: promising experimental models for brain development and neurodegenerative disorders. J. Biomed. Sci. 24(1): 59. https://doi.org/10.1186/s12929-017-0362-8.
55. Li, Z.A., Shang, J., Xiang, S., et al. (2022). Articular tissue-mimicking organoids derived from mesenchymal stem cells and induced pluripotent stem cells. Organoids 1(2): 135–148. https://doi.org/10.3390/organoids1020011.
56. Azar, J., Bahmad, H.F., Daher, D., et al. (2021). The use of stem cell-derived organoids in disease modeling: an update. Int. J. Mol. Sci. 22(14): 7667.
57. Kim, J., Koo, B.K., and Knoblich, J.A. (2020). Human organoids: model systems for human biology and medicine. Nat. Rev. Mol. Cell Biol. 21(10): 571–584. https://doi.org/10.1038/s41580-020-0259-3.
58. Nio, Y., and Takebe, T. (2019). Organoid models of development and disease towards therapy. In Medical Applications of iPS Cells: Innovation in Medical Sciences. Current Human Cell Research and Applications, H. Inoue and Y. Nakamura, eds. (Springer), pp. 149–168. https://doi.org/10.1007/978-981-13-3672-0_9.
59. Li, L., Bowling, S., McGeary, S.E., et al. (2023). A mouse model with high clonal barcode diversity for joint lineage, transcriptomic, and epigenomic profiling in single cells. Cell 186(23): 5183–5199.e22. https://doi.org/10.1016/j.cell.2023.09.019.
60. Marshall, L.J., Bailey, J., Cassotta, M., et al. (2023). Poor translatability of biomedical research using animals — A narrative review. Altern. Lab. Anim. 51(2): 102–135. https://doi.org/10.1177/02611929231157756.
61. Domínguez-Oliva, A., Hernández-Ávalos, I., Martínez-Burnes, J., et al. (2023). The importance of animal models in biomedical research: current insights and applications. Animals 13(7): 1223. https://www.ncbi.nlm.nih.gov/pmc/articles/PMC10093480/.
62. Barroca, N.C.B., Della Santa, G., Suchecki, D., et al. (2022). Challenges in the use of animal models and perspectives for a translational view of stress and psychopathologies. Neurosci. Biobehav. Rev. 140: 104771. https://doi.org/10.1016/j.neubiorev.2022.104771.
63. Nusinow, D.P., Szpyt, J., Ghandi, M., et al. (2020). Quantitative proteomics of the cancer cell line encyclopedia. Cell 180(2): 387–402.e16. https://doi.org/10.1016/j.cell.2019.12.023.
64. Lorsch, J.R., Collins, F.S., and Lippincott-Schwartz, J. (2014). Fixing problems with cell lines: technologies and policies can improve authentication. Science 346(6216): 1452–1453. https://doi.org/10.1126/science.1259110.
65. Kaur, G., and Dufour, J.M. (2012). Cell lines: valuable tools or useless artifacts. Spermatogenesis 2(1): 1–5. https://doi.org/10.4161/spmg.19885.
66. Li, J., Settivari, R.S., and LeBaron, M.J. (2019). Genetic instability of in vitro cell lines: implications for genetic toxicity testing. Environ. Mol. Mutagen. 60(6): 559–562. https://doi.org/10.1002/em.22280.
67. Mead, B.E., and Karp, J.M. (2019). All models are wrong, but some organoids may be useful. Genome Biol. 20(1): 66. https://doi.org/10.1186/S13059-019-1677-4.
68. Rae, C., Amato, F., and Braconi, C. (2021). Patient-derived organoids as a model for cancer drug discovery. Int. J. Mol. Sci. 22(7): 3483. https://doi.org/10.3390/ijms22073483.
69. Gu, Z.Y., Jia, S.Z., Liu, S., et al. (2020). Endometrial organoids: A new model for the research of endometrial-related diseases. Biol. Reprod. 103(5): 918–926. https://doi.org/10.1093/biolre/ioaa124.
70. Brucker, S.Y., Hentrich, T., Schulze-Hentrich, J.M., et al. (2022). Endometrial organoids derived from Mayer-Rokitansky-Ku… ster-Hauser syndrome patients provide insights into disease-causing pathways. Dis. Model. Mech. 15(5): dmm049379. https://doi.org/10.1242/dmm.049379.
71. Chen, P., Zhang, X., Ding, R., et al. (2021). Patient-derived organoids can guide personalized-therapies for patients with advanced breast cancer. Adv. Sci. 8(22): 2101176. https://doi.org/10.1002/advs.202101176.
72. Boretto, M., Maenhoudt, N., Luo, X., et al. (2019). Patient-derived organoids from endometrial disease capture clinical heterogeneity and are amenable to drug screening. Nat. Cell Biol. 21(8): 1041–1051. https://doi.org/10.1038/s41556-019-0360-z.
73. Ludwig, L.S., Lareau, C.A., Ulirsch, J.C., et al. (2019). Lineage tracing in humans enabled by mitochondrial mutations and single-cell genomics. Cell 176(6): 1325–1339.e22. https://doi.org/10.1016/j.cell.2019.01.022.
74. Richter, M., Piwocka, O., Musielak, M., et al. (2021). From donor to the lab: a fascinating journey of primary cell lines. Front. Cell Dev. Biol. 9: 711381. https://doi.org/10.3389/fcell.2021.711381.
75. Chen, X., Shen, C., Wei, Z., et al. (2021). Patient-derived non-small cell lung cancer xenograft mirrors complex tumor heterogeneity. Cancer Biol. Med. 18(1): 184–198. https://doi.org/10.20892/j.issn.2095-3941.2020.0012.
76. Ortmann, J., Rampášek, L., Tai, E., et al . (2021). Assessing therapy response in patient-derived xenografts. Sci. Transl. Med. 13(620): eabf4969. https://doi.org/10.1126/scitranslmed.abf4969.
77. Telias, M., Sit, K.K., Frozenfar, D., et al. (2022). Retinoic acid inhibitors mitigate vision loss in a mouse model of retinal degeneration. Sci. Adv. 8(11): eabm4643. https://doi.org/10.1126/sciadv.abm4643.
78. Oh, B.Y., Hong, H.K., Lee, W.Y., et al. (2017). Animal models of colorectal cancer with liver metastasis. Cancer Lett. 387: 114–120. https://doi.org/10.1016/j.canlet.2016.01.048.
79. Tagaya, H., Ishikawa, K., Hosokawa, Y., et al. (2019). A method of producing genetically manipulated mouse mammary gland. Breast Cancer Res. 21(1): 1. https://doi.org/10.1186/s13058-018-1086-8.
80. Arends, M.J., White, E.S., and Whitelaw, C.B.A. (2016). Animal and cellular models of human disease. J. Pathol. 238(2): 137–140. https://doi.org/10.1002/path.4662.
81. Takahashi, T. (2019). Organoids for drug discovery and personalized medicine. Annu. Rev. Pharmacol. Toxicol. 59(1): 447–462. https://doi.org/10.1146/annurev-pharmtox-010818-021108.
82. Costamagna, G., Comi, G.P., and Corti, S. (2021). Advancing drug discovery for neurological disorders using iPSC-derived neural organoids. Int. J. Mol. Sci. 22(5): 2659. https://doi.org/10.3390/ijms22052659.
83. Zhao, J., Fu, Y., Yamazaki, Y., et al. (2020). APOE4 exacerbates synapse loss and neurodegeneration in Alzheimer's disease patient iPSC-derived cerebral organoids. Nat. Commun. 11(1): 5540. https://doi.org/10.1038/s41467-020-19264-0.
84. Olgasi, C., Cucci, A., and Follenzi, A. (2020). iPSC-derived liver organoids: A Journey from drug screening, to disease modeling, arriving to regenerative medicine. Int. J. Mol. Sci. 21(17): 6215. https://doi.org/10.3390/ijms21176215.
85. Blaszkiewicz, J., and Duncan, S.A. (2022). Advancements in disease modeling and drug discovery using iPSC-derived hepatocyte-like cells. Genes 13(4): 573. https://doi.org/10.3390/genes13040573.
86. Bubnys, A., and Tsai, L.H. (2022). Harnessing cerebral organoids for Alzheimer's disease research. Curr. Opin. Neurobiol. 72:120–130.https://doi.org/10.1016/j.conb.2021.10.003.
87. Karmirian, K., Holubiec, M., Goto-Silva, L., et al. (2023). Modeling Alzheimer's disease using human brain organoids. In Alzheimer's Disease, 2561, J. Chun, ed. (Springer US), pp. 135–158. https://doi.org/10.1007/978-1-0716-2655-9_7.
88. Galet, B., Cheval, H., and Ravassard, P. (2020). Patient-derived midbrain organoids to explore the molecular basis of Parkinson's disease. Front. Neurol. 11: 1005. https://doi.org/10.3389/fneur.2020.01005.
89. McComish, S.F., MacMahon Copas, A.N., and Caldwell, M.A. (2022). Human brain-based models provide a powerful tool for the advancement of Parkinson's disease research and therapeutic development. Front. Neurosci. 16: 851058. https://doi.org/10.3389/fnins.2022.851058.
90. Smits, L.M., Reinhardt, L., Reinhardt, P., et al. (2019). Modeling Parkinson's disease in midbrain-like organoids. Npj Park Dis 5(1): 5. https://doi.org/10.1038/s41531-019-0078-4.
91. Smits, L.M., and Schwamborn, J.C. (2020). Midbrain organoids: a new tool to investigate Parkinson's disease. Front. Cell Dev. Biol. 8: 359. https://doi.org/10.3389/fcell.2020.00359.
92. Tamaki, Y., Ross, J.P., Alipour, P., et al. (2023). Spinal cord extracts of amyotrophic lateral sclerosis spread TDP-43 pathology in cerebral organoids. A.J. Myers, ed. 19(2): e1010606. https://doi.org/10.1371/journal.pgen.1010606.

93. Szebényi, K., Wenger, L.M.D., Sun, Y., et al. (2021). Human ALS/FTD brain organoid slice cultures display distinct early astrocyte and targetable neuronal pathology. Nat. Neurosci. 24(11): 1542—1554. https://doi.org/10.1038/s41593-021-00923-4.

94. Du, H., Huo, Z., Chen, Y., et al. (2023). Induced pluripotent stem cells and their applications in amyotrophic lateral sclerosis. Cells 12(6): 971. https://doi.org/10.3390/cells12060971.

95. Ghasemi, M. (2022). Gene therapy in amyotrophic lateral sclerosis. MDPI 11(13): 2066.

96. Miranda, C.C., and Cabral, J.M.S. (2020). Organoids for Cell Therapy and Drug Discovery. Instituto Superior Técnico 1: 461—471. https://linkinghub.elsevier.com/retrieve/pii/B9780128191781000459.

97. Choo, N., Ramm, S., Luu, J., et al. (2021). High-throughput imaging assay for drug screening of 3D prostate cancer organoids. SLAS Discov. 26(9): 1107—1124. https://doi.org/10.1177/24725552211020668.

98. Rauth, S., Karmakar, S., Batra, S.K., et al. (2021). Recent advances in organoid development and applications in disease modeling. Biochim. Biophys. Acta. Rev. Cancer 1875(2): 188527. https://doi.org/10.1016/j.bbcan.2021.188527.

99. Ortolano, N. (2022). Organoids bring drug discovery and development to the culture hood. 10x Genomics. https://www.10xgenomics.com/blog/organoids-bring-drug-discovery-and-development-to-the-culture-hood.

100. Urs, S. (2023). Organoid technology: a reliable tool for drug screening. Crown Biosci Blog. https://blog.crownbio.com/organoid-technology-a-reliable-tool-for-drug-screening.

101. Jacob, F., Salinas, R.D., Zhang, D.Y., et al. (2020). A patient-derived glioblastoma organoid model and biobank recapitulates inter- and intra-tumoral heterogeneity. Cell 180(1): 188—204.e22. https://doi.org/10.1016/j.cell.2019.11.036.

102. Sereti, E., Papapostolou, I., and Dimas, K. (2023). Pancreatic cancer organoids: an emerging platform for precision medicine? Biomedicines 11(3): 890. https://doi.org/10.3390/biomedicines11030890.

103. Pernik, M.N., Bird, C.E., Traylor, J.I., et al. (2021). Patient-derived cancer organoids for precision oncology treatment. J. Pers. Med. 11(5): 423. https://doi.org/10.3390/jpm11050423.

104. Watanabe, S., Yogo, A., Otsubo, T., et al. (2022). Establishment of patient-derived organoids and a characterization-based drug discovery platform for treatment of pancreatic cancer. BMC Cancer 22(1): 489. https://doi.org/10.1186/s12885-022-09619-9.

105. Choi, J.I., Jang, S.I., Hong, J., et al. (2021). Cancer-initiating cells in human pancreatic cancer organoids are maintained by interactions with endothelial cells. Cancer Lett. 498: 42—53. https://doi.org/10.1016/j.canlet.2020.10.012.

106. Xu, H., Jiao, D., Liu, A., et al. (2022). Tumor organoids: applications in cancer modeling and potentials in precision medicine. J. Hematol. Oncol. 15(1): 58. https://doi.org/10.1186/s13045-022-01278-4.

107. Nagle, P.W., Plukker, J.T.M., Muijs, C.T., et al. (2018). Patient-derived tumor organoids for prediction of cancer treatment response. Semin. Cancer Biol. 53: 258—264. https://doi.org/10.1016/j.semcancer.2018.06.005.

108. Bazeed, A.Y., Day, C.M., and Garg, S.(2022). Pancreatic cancer: challengesand opportunities in locoregional therapies. Cancers 14(17): 4257. https://doi.org/10.3390/cancers14174257.

109. Zeng, S., Pöttler, M., Lan, B., et al. (2019). Chemoresistance in Pancreatic Cancer. Int. J. Mol. Sci. 20(18): 4504. https://doi.org/10.3390/ijms20184504.

110. Liot, S., Balas, J., Aubert, A., et al. (2021). Stroma involvement in pancreatic ductal adenocarcinoma: an overview focusing on extracellular matrix proteins. Front. Immunol. 12: 612271. https://doi.org/10.3389/fimmu.2021.612271.

111. Piro, G., Agostini, A., Larghi, A., et al. (2021). Pancreatic cancer patient-derived organoid platforms: a clinical tool to study cell- and non-cell-autonomous mechanisms of treatment response. Front. Med. 8: 793144. https://doi.org/10.3389/fmed.2021.793144.

112. Harada, K., and Sakamoto, N.(2022). Cancer organoid applications to investigate chemotherapy resistance. Front. Mol. Biosci. 9: 1067207. https://doi.org/10.3389/fmolb.2022.1067207.

113. Su, C., Olsen, K.A., Bond, C.E., et al. (2023). The efficacy of using patient-derived organoids to predict treatment response in colorectal cancer. Cancers 15(3): 805. https://doi.org/10.3390/cancers15030805.

114. Luckett, K.A., and Ganesh, K. (2023). Engineering the immune microenvironment into organoid models. Annu. Rev. Cancer Biol. 7(1): 171—187. https://doi.org/10.1146/annurev-cancerbio-061421-040659.

115. Sun, C.P., Lan, H.R., Fang, X.L., et al. (2022). Organoid models for precision cancer immunotherapy. Front. Immunol. 13: 770465. https://doi.org/10.3389/fimmu.2022.770465.

116. Wang, J., Chen, C., Wang, L., et al. (2022). Patient-derived tumor organoids: new progress and opportunities to facilitate precision cancer immunotherapy. Front. Oncol. 12: 872531. https://doi.org/10.3389/fonc.2022.872531.

117. Fan, H., Demirci, U., and Chen, P. (2019). Emerging organoid models: leaping forward in cancer research. J. Hematol. Oncol. 12(1): 142. https://doi.org/10.1186/s13045-019-0832-4.

118. Magré, L., Verstegen, M.M.A., Buschow, S., et al. (2023). Emerging organoid-immune co-culture models for cancer research: from oncoimmunology to personalized immunotherapies. J. Immunother. Cancer 11(5): e006290. https://doi.org/10.1136/jitc-2022-006290.

119. Saiding, Q., Ma, J., Ke, C., et al. (2022). From "organs on a chip" to "patient on a chip.". Innovation 3(5): 100282. https://doi.org/10.1016/j.xinn.2022.100282.

120. Subtil, B., Iyer, K.K., Poel, D., et al. (2023). Dendritic cell phenotype and function in a 3D co-culture model of patient-derived metastatic colorectal cancer organoids. Front. Immunol. 14: 1105244. https://doi.org/10.3389/fimmu.2023.1105244.

121. Zhu, Y., Kang, E., Wilson, M., et al. (2022). 3D tumor spheroid and organoid to model tumor microenvironment for cancer immunotherapy. Organoids 1(2): 149—167. https://doi.org/10.3390/organoids1020012.

122. Miebach, L., Berner, J., and Bekeschus, S. (2022). In vivo model in cancer research and tumor immunology. Front. Immunol. 13: 1006064. https://doi.org/10.3389/fimmu.2022.1006064.

123. Zhao, X., Jiang, Y., Liu, C., et al. (2022). Organoid technology and clinical applications in digestive system cancer. Engineering 9: 123—130. https://doi.org/10.1016/j.eng.2021.04.017.

124. Takebe, T., Wells, J.M., Helmrath, M.A., et al. (2018). Organoid center strategies for accelerating clinical translation. Cell Stem Cell 22(6): 806—809. https://doi.org/10.1016/j.stem.2018.05.008.

125. Choi, W.H., Bae, D.H., and Yoo, J. (2023). Current status and prospects of organoid-based regenerative medicine. BMB Rep. 56(1): 10—14. https://doi.org/10.5483/BMBRep.2022-0195.

126. Glykofrydis, F., and Elfick, A. (2022). Exploring standards for multicellular mammalian synthetic biology. Trends Biotechnol. 40(11): 1299—1312. https://doi.org/10.1016/j.tibtech.2022.06.001.

127. Sorrentino, G., Rezakhani, S., Yildiz, E., et al. (2020). Mechano-modulatory synthetic niches for liver organoid derivation. Nat. Commun. 11(1): 3416. https://doi.org/10.1038/s41467-020-17161-0.

128. Ovechkina, V.S., Zakian, S.M., Medvedev, S.P., et al. (2021). Genetically encoded luorescent biosensors for biomedical applications. Biomedicines 9(11): 1528. https://doi.org/10.3390/biomedicines9111528.

129. Yousafzai, M.S., and Hammer, J.A. (2023). Using biosensors to study organoids, spheroids and organs-on-a-chip: a mechanobiology perspective. Biosensors 13(10): 905. https://doi.org/10.3390/bios13100905.

130. Lin, W., Mehta, S., and Zhang, J. (2019). Genetically encoded luorescent biosensors illuminate kinase signaling in cancer. J. Biol. Chem. 294(40): 14814—14822. https://doi.org/10.1074/jbc.REV119.006177.

131. Kim, G.A., Ginga, N.J., and Takayama, S. (2018). Integration of sensors in gastrointestinal organoid culture for biological analysis. Cell. Mol. Gastroenterol. Hepatol. 6(1): 123—131.e1. https://doi.org/10.1016/j.jcmgh.2018.03.002.

132. Poudel, H., Sanford, K., Szwedo, P.K., et al. (2022). Synthetic matrices for intestinal organoid culture: implications for better performance. ACS Omega 7(1): 38—47. https://doi.org/10.1021/acsomega.1c05136.

133. Zhang, Y., Li, D., Liu, Y., et al. (2024). 3D-bioprinted anisotropic bicellular living hydrogels boost osteochondral regeneration via reconstruction of cartilage—bone interface. Innovation 5(1): 100542. https://doi.org/10.1016/j.xinn.2023.100542.

134. Cruz-Acuña, R., Kariuki, S.W., Sugiura, K., et al. (2023). Engineered hydrogel reveals contribution of matrix mechanics to esophageal adenocarcinoma and identifies matrix-activated therapeutic targets. J. Clin. Invest. 133(23): e168146. https://doi.org/10.1172/JCI168146.

135. Nason-Tomaszewski, C.E., Thomas, E.E., Matera, D.L., et al. (2024). Extracellular matrix-templating fibrous hydrogels promote ovarian tissue remodeling and oocyte growth. Bioact. Mater. 32: 292—303. https://doi.org/10.1016/j.bioactmat.2023.10.001.

136. Nguyen, A.K., Molley, T.G., Kardia, E., et al. (2023). Hierarchical assembly of tryptophan zipper peptides into stress-relaxing bioactive hydrogels. Nat. Commun. 14(1): 6604. https://doi.org/10.1038/s41467-023-41907-1.

137. Huang, R., Shang, L., and Zhao, Y. (2021). Biomimic organ architectures and functions by assembling organoid models. Sci. Bull. 66(9): 862—864. https://doi.org/10.1016/j.scib.2021.02.008.

138. Kim, E., Choi, S., Kang, B., et al. (2020). Creation of bladder assembloids mimicking tissue regeneration and cancer. Nature 588(7839): 664—669. https://doi.org/10.1038/s41586-020-3034-x.

139. Mukherjee, A., Sinha, A., Maibam, M., et al. (2022). Organoids and commercialization. In Organoid Bioengineering - Advances, Applications and Challenges, 13, M.K. Paul, ed.. https://doi.org/10.5772/intechopen.104706.

140. Hernandez-Gordillo, V., Kassis, T., Lampejo, A., et al. (2020). Fully synthetic matrices for in vitro culture of primary human intestinal enteroids and endometrial organoids. Biomaterials 254: 120125. https://doi.org/10.1016/j.biomaterials.2020.120125.

141. Wagar, L.E., Salahudeen, A., Constantz, C.M., et al. (2021). Modeling human adaptive immune responses with tonsil organoids. Nat. Med. 27(1): 125—135. https://doi.org/10.1038/s41591-020-01145-0.

142. Sang, Y., Miller, L.C., Nelli, R.K., et al. (2021). Harness organoid models for virological studies in animals: a cross-species perspective. Front. Microbiol. 12: 725074. https://doi.org/10.3389/fmicb.2021.725074.

143. Puschhof, J., Post, Y., Beumer, J., et al. (2021). Derivation of snake venom gland organoids for in vitro venom production. Nat. Protoc. 16(3): 1494—1510. https://doi.org/10.1038/s41596-020-00463-4.

144. Kim, K.H., Kim, E.J., Kim, H.Y., et al. (2023). Fabrication of functional ameloblasts from hiPSCs for dental application. Front. Cell Dev. Biol. 11: 1164811. https://doi.org/10.3389/fcell.2023.1164811.

145. Alghadeer, A., Hanson-Drury, S., Patni, A.P., et al. (2023). Single-cell census of human tooth development enables generation of human enamel. Dev. Cell 58(20): 2163—2180.e9. https://doi.org/10.1016/j.devcel.2023.07.013.

146. Yang, J., Huang, S., Cheng, S., et al. (2021). Application of ovarian cancer organoids in precision medicine: key challenges and current opportunities. Front. Cell Dev. Biol. 9: 701429. https://doi.org/10.3389/fcell.2021.701429.

147. Li, M., Gong, J., Gao, L., et al. (2022). Advanced human developmental toxicity and teratogenicity assessment using human organoid models. Ecotoxicol. Environ. Saf.235: 113429. https://doi.org/10.1016/j.ecoenv.2022.113429.

148. Caipa Garcia, A.L., Arlt, V.M., and Phillips, D.H. (2022). Organoids for toxicology and genetic toxicology: applications with drugs and prospects for environmental carcinogenesis. Mutagenesis 37(2): 143—154. https://doi.org/10.1093/mutage/geab023.

149. Matsui, T., and Shinozawa, T.(2021). Human organoids for predictive toxicology research and drug development. Front. Genet. 12: 767621. https://doi.org/10.3389/FGENE.2021.767621.

150. Haaker, M.W., Kruitwagen, H.S., Vaandrager, A.B., et al. (2020). Identification of potential drugs for treatment of hepatic lipidosis in cats using an in vitro feline liver organoid system. J. Vet. Intern. Med. 34(1): 132–138. https://doi.org/10.1111/jvim.15670.
151. Shinozawa, T., Kimura, M., Cai, Y., et al. (2021). High-fidelity drug-induced liver injury screen using human pluripotent stem cell–derived organoids. Gastroenterology 160(3): 831–846.e10. https://doi.org/10.1053/j.gastro.2020.10.002.
152. Truskey, G.A. (2018). Human microphysiological systems and organoids as in vitro models for toxicological studies. Front. Public Health 6: 185. https://doi.org/10.3389/FPUBH.2018.00185.
153. Seo, Y., Bang, S., Son, J., et al. (2022). Brain physiome: a concept bridging in vitro 3D brain models and in silico models for predicting drug toxicity in the brain. Bioact. Mater. 13: 135–148. https://doi.org/10.1016/j.bioactmat.2021.11.009.
154. Shin, W., and Kim, H.J. (2022). 3D in vitro morphogenesis of human intestinal epithelium in a gut-on-a-chip or a hybrid chip with a cell culture insert. Nat. Protoc. 17(3): 910–939. https://doi.org/10.1038/s41596-021-00674-3.
155. Winkler, A., Santo, N., Madaschi, L., et al. (2021). Lung organoids and microplastic fibers: a new exposure model for emerging contaminants. Preprint at bioRxiv. https://www.biorxiv.org/content/10.1101/2021.03.07.434247v2.
156. Heidari-Khoei, H., Esfandiari, F., Hajari, M.A., et al. (2020). Organoid technology in female reproductive biomedicine. Reprod. Biol. Endocrinol. 18(1): 64. https://doi.org/10.1186/s12958-020-00621-z.
157. Lichou, F., and Trynka, G. (2020). Functional studies of GWAS variants are gaining momentum. Nat. Commun. 11(1): 6283. https://doi.org/10.1038/s41467-020-20188-y.
158. Menon, R., and Richardson, L. (2022). Organ-on-a-chip for perinatal biology experiments. Placenta Reprod. Med. 1: 98.
159. Ingber, D.E. (2022). Human organs-on-chips for disease modelling, drug development and personalized medicine. Nat. Rev. Genet. 23(8): 467–491. https://doi.org/10.1038/s41576-022-00466-9.
160. Espinosa Angarica, V., and Del Sol, A. (2016). Modeling heterogeneity in the pluripotent state: a promising strategy for improving the efficiency and fidelity of stem cell differentiation. Bioessays 38(8): 758–768. https://doi.org/10.1002/bies.201600103.
161. Hemeryck, L., Hermans, F., Chappell, J., et al. (2022). Organoids from human tooth showing epithelial stemness phenotype and differentiation potential. Cell. Mol. Life Sci. 79(3): 153. https://doi.org/10.1007/s00018-022-04183-8.
162. Zhang, S., Shen, J., Wang, X., et al. (2023). Integration of organoids in peptide drug discovery: Rise of the high-throughput screening. VIEW 4. https://doi.org/10.1002/viw.20230010.
163. Lampart, F.L., Iber, D., and Doumpas, N. (2023). Organoids in high-throughput and high-content screenings. Front. Chem. Eng.5:1120348.https://doi.org/10.3389/fceng.2023.1120348.
164. Campaner, E., Zannini, A., Santorsola, M., et al. (2020). Breast cancer organoids model patient-specific response to drug treatment. Cancers 12(12): 3869. https://doi.org/10.3390/CANCERS12123869.
165. Kim, M., Mun, H., Sung, C.O., et al. (2019). Patient-derived lung cancer organoids as in vitro cancer models for therapeutic screening. Nat. Commun. 10(1): 3991. https://doi.org/10.1038/s41467-019-11867-6.
166. Mainardi, S., and Bernards, R. (2022). A large-scale organoid-based screening platform to advance drug repurposing in pancreatic cancer. Cell Genom. 2(2): 100100. https://doi.org/10.1016/j.xgen.2022.100100.
167. Yang, R., and Yu, Y. (2023). Patient-derived organoids in translational oncology and drug screening. Cancer Lett. 562: 216180. https://doi.org/10.1016/j.canlet.2023.216180.
168. Ito, F., Kato, K., Yanatori, I., et al. (2023). Matrigel-based organoid culture of malignant mesothelioma reproduces cisplatin sensitivity through CTR1. BMC Cancer 23(1): 487. https://doi.org/10.1186/s12885-023-10966-4.
169. Dhakal, B., Li, C.M.Y., Li, R., et al. (2022). The antianginal drug perhexiline displays cytotoxicity against colorectal cancer cells in vitro: a potential for drug repurposing. Cancers 14(4): 1043. https://doi.org/10.3390/cancers14041043.
170. Boehnke, K., Iversen, P.W., Schumacher, D., et al.(2016). Assay establishment and validation of a high-throughput screening platform for three-dimensional patient-derived colon cancer organoid cultures. SLAS Discov 21(9): 931–941. https://doi.org/10.1177/1087057116650965.
171. Renner, H., Grabos, M., Becker, K.J., et al. (2020). A fully automated high-throughput workflow for 3D-based chemical screening in human midbrain organoids. Elife 9: e52904. https://doi.org/10.7554/eLife.52904.
172. Karabicici, M., Akbari, S., Ertem, O., et al. (2023). Human liver organoid models for assessment of drug toxicity at the preclinical stage. Endocr., Metab. Immune Disord.: Drug Targets 23(14): 1713–1724. https://doi.org/10.2174/1871530323666230411100121.
173. Dilz, J., Auge, I., Groeneveld, K., et al. (2023). A proof-of-concept assay for quantitative and optical assessment of drug-induced toxicity in renal organoids. Sci. Rep. 13(1): 6167. https://doi.org/10.1038/s41598-023-33110-5.
174. Karp, S., Pollak, M., and Subramanian, B. (2022). Disease modeling with kidney organoids. Micromachines 13(9): 1384. https://doi.org/10.3390/mi13091384.
175. Astashkina, A.I., Mann, B.K., Prestwich, G.D., et al. (2012). Comparing predictive drug nephrotoxicity biomarkers in kidney 3-D primary organoid culture and immortalized cell lines. Biomaterials 33(18): 4712–4721. https://doi.org/10.1016/j.biomaterials.2012.03.001.
176. Shamshirgaran, Y., Jonebring, A., Svensson, A., et al. (2021). Rapid target validation in a Cas9-inducible hiPSC derived kidney model. Sci. Rep. 11(1): 16532. https://doi.org/10.1038/s41598-021-95986-5.
177. Hirt, C.K., Booij, T.H., Grob, L., Simmler, P., Toussaint, N.C., Keller, D., Taube, D., Ludwig, V., Goryachkin, A., and Pauli, C. (2022). Drug screening and genome editing in human pancreatic cancer organoids identifies drug-gene interactions and candidates for off-label treatment. Cell Genom 2: 100095. https://doi.org/10.1016/j.xgen.2022.100095.
178. Zhou, Z., Cong, L., and Cong, X. (2021). Patient-derived organoids in precision medicine: drug screening, organoid-on-a-chip and living organoid biobank. Front. Oncol. 11: 762184. https://doi.org/10.3389/fonc.2021.762184.
179. Grossman, J.E., Muthuswamy, L., Huang, L., et al. (2022). Organoid sensitivity correlates with therapeutic response in patients with pancreatic cancer. Clin. Cancer Res. 28(4): 708–718. https://doi.org/10.1158/1078-0432.CCR-20-4116.
180. Vlachogiannis, G., Hedayat, S., Vatsiou, A., et al. (2018). Patient-derived organoids model treatment response of metastatic gastrointestinal cancers. Science 359(6378): 920–926. https://doi.org/10.1126/science.aao2774.
181. Acklin-Wehnert, S., Dayanidhi, D., Czito, B.G., et al. (2023). Feasibility of establishing and drug screening patient-derived rectal organoid models from pretreatment rectal cancer biopsies. J. Clin. Oncol. 41(4_suppl): 176. https://doi.org/10.1200/jco.2023.41.4_suppl.176.
182. Zhang, Y., Houchen, C.W., and Li, M. (2022). Patient-derived organoids pharmacotyping guides precision medicine for pancreatic cancer. Clin. Cancer Res. 28(15): 3176–3178. https://doi.org/10.1158/1078-0432.CCR-22-1083.
183. Gerhards, N.M., and Rottenberg, S. (2018). New tools for old drugs: functional genetic screens to optimize current chemotherapy. Drug Resist. Updat. 36: 30–46. https://doi.org/10.1016/j.drup.2018.01.001.
184. Neal, J.T., Li, X., Zhu, J., et al. (2018). Organoid modeling of the tumor immune microenvironment. Cell 175(7): 1972–1988.e16. https://doi.org/10.1016/j.cell.2018.11.021.
185. Liu, C., Qin, T., Huang, Y., et al. (2020). Drug screening model meets cancer organoid technology. Transl. Oncol. 13(11): 100840. https://doi.org/10.1016/j.tranon.2020.100840.
186. Zou, F., Tan, J., Liu, T., et al. (2021). The CD39 positive hepatitis B virus surface protein (HBVs)-targeted CAR-T and personalized tumor-reactive CD8+ T cells exhibit potent anti-hepatocellular carcinoma (HCC) activity. Mol. Ther. 29(5): 1794–1807. https://doi.org/10.1016/j.ymthe.2021.01.021.
187. Sahin, U. (2018). Studying tumor-reactive T cells: a personalized organoid model. Cell Stem Cell 23(3): 318–319. https://doi.org/10.1016/j.stem.2018.08.015.
188. Weidinger, P. (2017). Modeling Lung Tumorigenesis Using CRISPR/Cas9-Based Genome Editing in Ex Vivo 3D Organoids (University of Applied Sciences Technikum, Wien). PhD Thesis. https://www.marshallplan.at/images/All-Papers/MP-2017/Weidinger+Pia_747.PDF.
189. Weeber, F., Ooft, S.N., Dijkstra, K.K., et al. (2017). Tumor organoids as a pre-clinical cancer model for drug discovery. Cell Chem. Biol. 24(9): 1092–1100. https://doi.org/10.1016/J.CHEMBIOL.2017.06.012.
190. Yoshihara, E., O'Connor, C., Gasser, E., et al. (2020). Immune-evasive human islet-like organoids ameliorate diabetes. Nature 586(7830): 606–611. https://doi.org/10.1038/s41586-020-2631-z.
191. Tahbaz, M., and Yoshihara, E. (2021). Immune protection of stem cell-derived islet cell therapy for Treating Diabetes. Front. Endocrinol. 12: 716625. https://doi.org/10.3389/fendo.2021.716625.
192. Zhou, J., and Huang, X. (2023). Scientists target human stomach cells for diabetes therapy. WCM Newsroom. https://news.weill.cornell.edu/news/2023/05/scientists-target-human-stomach-cells-for-diabetes-therapy.
193. Arjmand, B., Rabbani, Z., Soveyzi, F., et al. (2023). Advancement of organoid technology in regenerative medicine. Regen. Eng. Transl. Med. 9(1): 83–96. https://doi.org/10.1007/s40883-022-00271-0.
194. Qian, S., Mao, J., Liu, Z., et al. (2022). Stem cells for organoids. Smart Med. 1(1): e20220007. https://doi.org/10.1002/SMMD.20220007.
195. Watanabe, S., Kobayashi, S., Ogasawara, N., et al. (2022). Transplantation of intestinal organoids into a mouse model of colitis - Nature Protocols. Nat. Protoc. 17(3): 649–671. https://doi.org/10.1038/s41596-021-00658-3.
196. Grassi, L., Alfonsi, R., Francescangeli, F., et al. (2019). Organoids as a new model for improving regenerative medicine and cancer personalized therapy in renal diseases - Cell Death & Disease. Cell Death Dis. 10: 201. https://doi.org/10.1038/s41419-019-1453-0.
197. Reviewed by Emily Henderson, B.S. (2022). World's first-in-human research using organoid transplantation yields good results. News-Medicalnet. https://www.news-medical.net/news/20220822/Worlds-first-in-human-research-using-organoid-transplantation-yields-good-results.aspx.
198. Boers, S.N., Van Delden, J.J., Clevers, H., et al. (2016). Organoid biobanking: identifying the ethics. EMBO Rep. 17(7): 938–941. https://doi.org/10.15252/embr.201642613.
199. Sridhar, A., Simmini, S., Ribeiro, C.M.S., et al. (2020). A perspective on organoids for virology research. Viruses 12(11): 1341. https://doi.org/10.3390/v12111341.
200. Lensink, M.A., Boers, S.N., Jongsma, K.R., et al. (2021). Organoids for personalized treatment of cystic fibrosis: professional perspectiveson the ethics and governance of organoid biobanking. J. Cyst. Fibros. 20(3): 443–451. https://doi.org/10.1016/j.jcf.2020.11.015.
201. Kim, M.B., Hwangbo, S., Jang, S., et al. (2022). Bioengineered co-culture of organoids to recapitulate host-microbe interactions. Mater. Today. Bio 16: 100345. https://doi.org/10.1016/j.mtbio.2022.100345.
202. Roodsant, T., Navis, M., Aknouch, I., et al. (2020). A human 2D primary organoid-derived epithelial monolayer model to study host-pathogen interaction in the small intestine. Front. Cell. Infect. Microbiol. 10: 272. https://doi.org/10.3389/fcimb.2020.00272.
203. Pellegrino, E., and Gutierrez, M.G. (2021). Human stem cell-based models for studying host-pathogen interactions. Cell Microbiol. 23(7): e13335. https://doi.org/10.1111/cmi.13335.
204. Dutta, D., and Clevers, H. (2017). Organoid culture systems to study host–pathogen interactions. Curr. Opin. Immunol. 48: 15–22. https://doi.org/10.1016/j.coi.2017.07.012.
205. Hong, K.J., and Seo, S.H. (2018). Organoid as a culture system for viral vaccine strains. Clin. Exp. Vaccine Res. 7(2): 145–148. https://doi.org/10.7774/cevr.2018.7.2.145.

206. Yang, J., Gong, Y., Zhang, C., et al. (2022). Co-existence and co-infection of inluenza a viruses and coronaviruses: public health challenges. Innovation 3(5): 100306. https://doi.org/10.1016/j.xinn.2022.100306.

207. Li, X.F., Cui, Z., Fan, H., et al. (2022). A highly immunogenic live-attenuated vaccine candidate prevents SARS-CoV-2 infection and transmission in hamsters. Innovation 3(2): 100221. https://doi.org/10.1016/j.xinn.2022.100221.

208. Liu, W., Jia, J., Dai, Y., et al. (2022). Delineating COVID-19 immunological features using single-cell RNA sequencing. Innovation 3(5): 100289. https://doi.org/10.1016/j.xinn.2022.100289.

209. Li, T., Huang, T., Guo, C., et al. (2021). Genomic variation, origin tracing, and vaccine development of SARS-CoV-2: A systematic review. Innovation 2(2): 100116. https://doi.org/10.1016/j.xinn.2021.100116.

210. Ramírez-Flores, C.J., and Knoll, L.J. (2021). Human intestinal enteroids as a model for SARS-CoV-2 infection and antiviral drug screening. M.J. Evans, ed. 17(11): e1010080. https://doi.org/10.1371/journal.ppat.1010080.

211. Bartfeld, S. (2021). Organoids as host models for infection biology – a review of methods. Exp. Mol. Med. 53: 1471–1482. https://www.nature.com/articles/s12276-021-00629-4.

212. Huang, Y., Huang, Z., Tang, Z., et al. (2021). Research progress, challenges, and breakthroughs of organoids as disease models. Front. Cell Dev. Biol. 9: 740574. https://doi.org/10.3389/fcell.2021.740574.

213. Blutt, S.E., and Estes, M.K. (2022). Organoid models for infectious disease. Annu. Rev. Med. 73(1): 167–182.

214. Masmoudi, F., Santos-Ferreira, N., Pajkrt, D., et al. (2023). Evaluation of 3D human intestinal organoids as a platform for EV-A71 antiviral drug discovery. Cells 12(8): 1138. https://doi.org/10.3390/cells12081138.

215. Ramezankhani, R., Solhi, R., Chai, Y.C., et al. (2022). Organoid and microluidics-based platforms for drug screening in COVID-19. Drug Discov. Today 27(4): 1062–1076. https://doi.org/10.1016/j.drudis.2021.12.014.

216. Bartfeld, S. (2016). Modeling infectious diseases and host-microbe interactions in gastrointestinal organoids. Dev. Biol. 420(2): 262–270. https://doi.org/10.1016/j.ydbio.2016.09.014.

217. Duque-Correa, M.A., Maizels, R.M., Grencis, R.K., et al. (2020). Organoids – new models for host–helminth interactions. Trends Parasitol. 36(2): 170–181. https://doi.org/10.1016/j.pt.2019.10.013.

218. Thompson, R.E., Bouma, G.J., and Hollinshead, F.K. (2022). The roles of extracellular vesicles and organoid models in female reproductive physiology. Int. J. Mol. Sci. 23(6): 3186. https://doi.org/10.3390/ijms23063186.

219. (2022). S18.3: Building organoid and microluidic models to identify toxicant risks to female reproduction. Am. J. Reprod. Immunol. 87(S1): 72–73. https://doi.org/10.1111/aji.90_13546.

220. Alzamil, L., Nikolakopoulou, K., and Turco, M.Y. (2021). Organoid systems to study the human female reproductive tract and pregnancy. Cell Death Differ. 28(1): 35–51. https://doi.org/10.1038/s41418-020-0565-5.

221. Yang, L., Semmes, E.C., Ovies, C., et al. (2021). Innate immune signaling in trophoblast and decidua organoids defines differential antiviral defenses at the maternal-fetal interface. Preprint at BioRxiv. https://doi.org/10.1101/2021.03.29.437467.

222. Brazovskaja, A., Treutlein, B., and Camp, J.G. (2019). High-throughput single-cell transcriptomics on organoids. Curr. Opin. Biotechnol. 55: 167–171. https://doi.org/10.1016/j.copbio.2018.11.002.

223. Hof, L., Moreth, T., Koch, M., et al. (2021). Long-term live imaging and multiscale analysis identify heterogeneity and core principles of epithelial organoid morphogenesis. BMC Biol. 19(1): 37. https://doi.org/10.1186/s12915-021-00958-w.

224. Yang, R., Du, Y., Kwan, W., et al. (2023). A quick and reliable image-based AI algorithm for evaluating cellular senescence of gastric organoids. Cancer Biol. Med. 20: 519–536. Published Online. https://doi.org/10.20892/j.issn.2095-3941.2023.0099.

225. Leung, C.M., De Haan, P., Ronaldson-Bouchard, K., et al. (2022). A guide to the organ-on-a-chip. Nat Rev Methods Primer 2(1): 33. https://doi.org/10.1038/s43586-022-00118-6.

226. Guenat, O.T., Geiser, T., and Berthiaume, F. (2020). Clinically relevant tissue scale responses as new readouts from organs-on-a-chip for precision medicine. Annu. Rev. Anal. Chem. 13(1): 111–133. https://doi.org/10.1146/annurev-anchem-061318-114919.

227. Teriyapirom, I., Batista-Rocha, A.S., and Koo, B.K. (2021). Genetic engineering in organoids. J. Mol. Med. 99(4): 555–568. https://doi.org/10.1007/s00109-020-02029-z.

228. Lim, S.W., Fang, X., Cui, S., et al. (2023). CRISPR-Cas9-Mediated correction of SLC12A3 gene mutation rescues the Gitelman's disease phenotype in a patient-derived kidney organoid system. Int. J. Mol. Sci. 24(3): 3019. https://doi.org/10.3390/ijms24033019.

229. Li, X., Fu, G., Zhang, L., et al. (2022). Assay establishment and validation of a high-throughput organoid-based drug screening platform. Stem Cell Res. Ther. 13(1): 219. https://doi.org/10.1186/s13287-022-02902-3.

230. Wu, X., Jiang, D., Yang, Y., et al. (2023). Modeling drug-induced liver injury and screening for anti-hepatofibrotic compounds using human PSC-derived organoids. Cell Regen. 12(1): 6. https://doi.org/10.1186/s13619-022-00148-1.

231. Fleck, J.S., Jansen, S.M.J., Wollny, D., et al. (2021). Inferring and perturbing cell fate regulomes in human cerebral organoids. Preprint at BioRxiv. https://doi.org/10.1101/2021.08.24.457460.

232. Vento-Tormo, R. (2023). Single-cell omics meets organoid cultures. Nat. Rev. Genet. 24(8): 492. https://doi.org/10.1038/s41576-023-00622-9.

233. Yin, Y., Liu, P.Y., Shi, Y., et al. (2021). Single-cell sequencing and organoids: a powerful combination for modelling organ development and diseases. In Reviews of Physiology, Biochemistry and Pharmacology, S.H.F. Pedersen, ed. (Springer International Publishing), pp. 189–210. https://doi.org/10.1007/112_2020_47.

234. Jagadeesh, K.A., Dey, K.K., Montoro, D.T., et al. (2022). Identifying disease-critical cell types and cellular processes by integrating single-cell RNA-sequencing and human genetics. Nat. Genet. 54(10): 1479–1492. https://doi.org/10.1038/s41588-022-01187-9.

235. Jin, F., Liu, M., Zhang, D., et al. (2023). Translational perspective on bone-derived cytokines in inter-organ communications. Innovation 4(1): 100365. https://doi.org/10.1016/j.xinn.2022.100365.

236. Du, X., Chen, Z., Li, Q., et al. (2023). Organoids revealed: morphological analysis of the profound next generation in-vitro model with artificial intelligence. Biodes. Manuf. 6(3): 319–339. https://doi.org/10.1007/s42242-022-00226-y.

237. Kassis, T., Hernandez-Gordillo, V., Langer, R., et al. (2019). OrgaQuant: human intestinal organoid localization and quantification using deep convolutional neural networks. Sci. Rep. 9(1): 12479. https://doi.org/10.1038/s41598-019-48874-y.

238. Kegeles, E., Naumov, A., Karpulevich, E.A., et al. (2020). Convolutional neural networks can predict retinal differentiation in retinal organoids. Front. Cell. Neurosci. 14: 171. https://doi.org/10.3389/fncel.2020.00171.

239. Bein, A., Shin, W., Jalili-Firoozinezhad, S., et al. (2018). Microluidic organ-on-a-chip models of human intestine. Cell. Mol. Gastroenterol. Hepatol. 5(4): 659–668. https://doi.org/10.1016/j.jcmgh.2017.12.010.

240. Valiei, A., Aminian-Dehkordi, J., and Mofrad, M.R.K. (2023). Gut-on-a-chip models for dissecting the gut microbiology and physiology. APL Bioeng. 7(1): 011502. https://doi.org/10.1063/5.0126541.

241. Kasendra, M., Tovaglieri, A., Sontheimer-Phelps, A., et al. (2018). Development of a primary human small intestine-on-a-chip using biopsy-derived organoids. Sci. Rep. 8(1): 2871. https://doi.org/10.1038/s41598-018-21201-7.

242. Campisi, M., Shin, Y., Osaki, T., et al. (2018). 3D self-organized microvascular model of the human blood-brain barrier with endothelial cells, pericytes and astrocytes. Biomaterials 180: 117–129. https://doi.org/10.1016/j.biomaterials.2018.07.014.

243. Hajal, C., Offeddu, G.S., Shin, Y., et al. (2022). Engineered human blood–brain barrier microluidic model for vascular permeability analyses. Nat. Protoc. 17(1): 95–128. https://doi.org/10.1038/s41596-021-00635-w.

244. Tian, M., Ma, Z., and Yang, G.Z. (2024). Micro/nanosystems for controllable drug delivery to the brain. Innovation 5(1): 100548. https://doi.org/10.1016/j.xinn.2023.100548.

245. Pereira, A., Garcia, J.W., and Muotri, A. (2023). Neural stimulation of brain organoids with dynamic patterns: a sentiomics approach directed to regenerative neuromedicine. NeuroSci 4(1): 31–42. https://doi.org/10.3390/neurosci4010004.

246. Serruya, M.D. (2017). Connecting the brain to itself through an emulation. Front. Neurosci. 11: 373. https://doi.org/10.3389/fnins.2017.00373.

247. Kagan, B.J., Kitchen, A.C., Tran, N.T., et al. (2022). In vitro neurons learn and exhibit sentience when embodied in a simulated game-world. Neuron 110(23): 3952–3969.e8. https://doi.org/10.1016/j.neuron.2022.09.001.

248. Smirnova, L., Caffo, B.S., Gracias, D.H., et al. (2023). Organoid intelligence (OI): the new frontier in biocomputing and intelligence-in-a-dish. Front. Sci. 1: 1017235. https://doi.org/10.3389/fsci.2023.1017235.

ACKNOWLEDGMENTS

This work was supported by the National Natural Science Foundation of China (82373719, 82173662, and 32200581), the National Key R&D Program of China (2023YFC3605702 and 2023YFC2308002), and the Extraordinary 2025 Elite Project of Fudan University.

AUTHOR CONTRIBUTIONS

X. Han, C.D., X. He, and X.C. provided direction and guidance throughout the preparation of this manuscript. X. Han, C.C., and W.D. collected and interpreted studies and were major contributors to writing and editing of the manuscript. B.F., Y.S., L.L., C.W., J.Z., M.R., J.L., H.H., and X.L. participated in discussions, language editing, and manuscript revision. All authors read and approved the final manuscript.

DECLARATION OF INTERESTS

The authors declare no competing interests.

LEAD CONTACT WEBSITE

https://www.researchgate.net/profile/Xin-Cao-26.

Cell Organoid

Article

https://doi.org/10.26599/CO.2024.9410001

Patient-derived skin tumor organoids with immune cells respond to metformin

Authors

Yanghua Shi, Jiping Liu, Lanyang Li, Chen Wang, Jian Zhang, ..., Jun Chen*, Chunhui Cai*, Xinxin Han*

Correspondence

Jun Chen, chenjun125125@126.com; Chunhui Cai, caichunhui@lishengbiotehc.com; Xinxin Han, xxhan@sibs.ac.cn

In Brief

Here, we developed patient–derived skin tumor organoids mimicking clinical tissues, showcasing diverse cell types and immune interactions. Single–cell sequencing identified 11 cell types, highlighting fidelity to in vivo counterparts. Bermatofibrosarcoma protuberans (DFSP) organoids revealed metforminIs unique immune signaling modulation, aiding drug testing and mechanistic exploration.

Graphical abstract

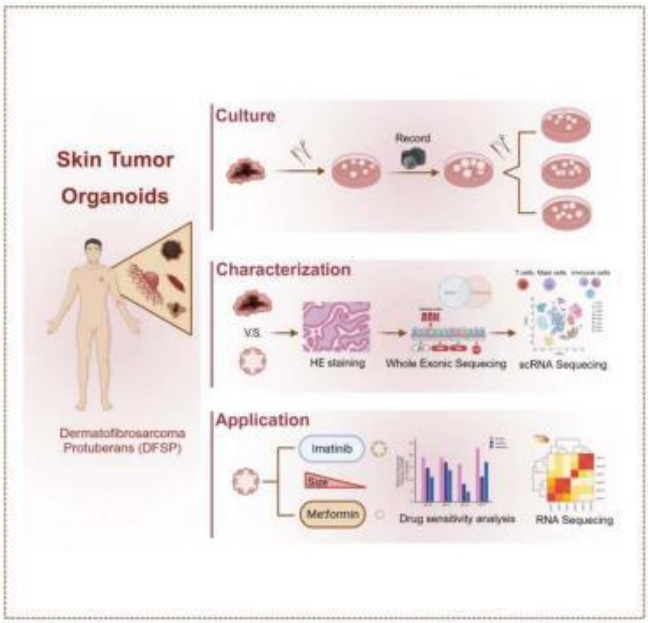

Highlights

- Patient–derived skin tumor organoids replicate clinical tissue characteristic
- Single–cell sequencing identifies 11 distinct cell types in skin organoids
- Bermatofibrosarcoma protuberans (DFSP) organoids used to test responses to imatinib and metformin
- Metformin inhibits the growth of DFSP organoids via immune signaling pathway

LISHENG 上海礼升生物 Shanghai Lisheng Biotech

Cell Organoid

Article

https://doi.org/10.26599/CO.2024.9410001

Patient-derived skin tumor organoids with immune cells respond to metformin

Yanghua Shi[1,§], Jiping Liu[1,§], Lanyang Li[1], Chen Wang[1], Jian Zhang[1], Mingjie Rong[1], Yamin Rao[2], Xiaobo Zhou[3], Di Sun[4], Jun Chen[3,*], Chunhui Cai[1,*], and Xinxin Han[1,5,*]

[1] *Shanghai Lisheng Biotech, Shanghai 200092, China*

[2] *Department of Pathology, Shanghai Ninth People's Hospital, affiliated to Shanghai Jiao Tong University School of Medicine, Shanghai 200011, China*

[3] *Department of Dermatology and Dermatologic Surgery, Shanghai Ninth People's Hospital, affiliated to Shanghai Jiao Tong University School of Medicine, Shanghai 200011, China*

[4] *Department of Plastic and Reconstructive Surgery, Shanghai Ninth People's Hospital, affiliated to Shanghai Jiao Tong University School of Medicine, Shanghai 200011, China*

[5] *Organ Regeneration X Lab, LiSheng East China Institute of Biotechnology, Peking University, Nantong 226299, China*

§ *Yanghua Shi and Jiping Liu contributed equally to this work.*

Received: 23 January 2024 / **Revised:** 26 March 2024 / **Accepted:** 6 April 2024

ABSTRACT

Surgery is the primary treatment for skin tumors, but it can result in scarring and distress for patients. Developing alternative therapeutic methods necessitates suitable *in vitro* models, which are currently limited in accurately representing the *in vivo* cell types and microenvironment of skin tumors. Here, we present a practical approach for creating patient-derived skin tumor organoids that effectively replicate the histological characteristics and mutational profiles observed in clinical tissues. Utilizing single-cell sequencing, we identified up to 11 distinct cell types within the organoid samples, encompassing various skin system cells and immune cells. Furthermore, we demonstrate the applicability of bermatofibrosarcoma protuberans (DFSP) organoids for assessing their responses to imatinib and metformin. Our findings reveal that metformin, in contrast to imatinib, can modulate the expression of downstream genes through immune signaling pathways. Our results underscore the ability of DFSP organoids to preserve key features of clinical tissues, including the presence of multiple cell types, especially immune cells. Importantly, our organoids provide a convenient approach for investigating the effects of drugs and elucidating underlying molecular mechanisms.

KEYWORDS

skin tumor, keloid, dermatofibrosarcoma protuberans (DFSP), patient-derived organoid (PDO), drug screening, immune cells therapy, metformin, imatinib

Introduction

Surgical intervention remains the primary treatment for skin tumors, despite its potential to result in scarring and patient distress. The development of alternative therapeutic methods necessitates suitable *in vitro* models, which are currently limited in accurately representing the *in vivo* cell types and microenvironment of skin tumors. The skin serves as a crucial barrier between the body and the external environment, playing a pivotal role in protecting against pathogens and environmental insults[1-3]. The intricate network of immune cells residing in the skin, plays a central role in maintaining skin homeostasis and defending against pathogens[4-6]. In addition to their role in protection, immune cells in the skin are also involved in the pathogenesis of various skin diseases, contributing to both inflammatory and autoimmune conditions[7-9]. The establishment of a useful *in vitro* skin tumor model incorporating original immune cells may provide insights into the complex interplay between the skin and the immune system, unraveling the mechanisms underlying skin tumors, and facilitating the development of effective therapeutic strategies.

Dermatofibrosarcoma protuberans (DFSP) is an uncommon cutaneous sarcoma with a high local recurrence rate, low metastatic rate, and low mortality, and its incidence has remained stable over the years[10]. Both Mohs surgery and wide local excision (WLE) are viable surgical options for treating DFSP. Mohs surgery may minimize reconstruction needs due to smaller

* Address correspondence to Jun Chen, chenjun125125@126.com; Chunhui Cai, caichunhui@lishengbiotehc.com; Xinxin Han, xxhan@sibs.ac.cn

Cite this article as Shi, Y. H., et al. *Cell Organoid*, **2024**, 1: 9410001.

average defect sizes and may result in fewer complications, but may also result in asymmetry. Immediate flap reconstruction, especially in larger defects, can achieve aesthetic results for DFSP patients without compromising the detection of disease recurrence[11–13]. Given the high recurrence rate of DFSP and its low mortality, the development of alternative treatment modalities, such as systemic (oral) or localized (topical) pharmacotherapy, is of paramount importance to enhance clinical outcomes. However, the research on in vitro models for DFSP is still insufficient[14]. Recently, some novel patient-derived models have been established. Two cell lines, NCC-DFSP1-C1 and NCC-DFSP2-C1, were derived from two patients with DFSP. These cell lines preserved the unique collagen type I alpha 1 chain (COL1A1) -PDGFB translocation characteristic of DFSP, which causes constitutive activation of the platelet-derived growth factor β (PDGFB) signaling pathway. In vitro screening studies identified anticancer drugs that showed antiproliferative effects at considerably low concentrations in the DFSP cell lines. These cell lines could be used for developing novel therapeutic strategies to treat DFSP[15]. Although some progress has been made, there is still an urgent need to develop an *in vitro* three-dimensional (3D) model for DFSP including the immune microenvironment in order to better understand the biology of this disease and develop effective treatment methods.

In the field of cancer research, organoids, also known as tumoroids, serve as an important component for the discovery of potential therapeutic targets and the identification of novel compounds[16]. They have been shown to more accurately recapitulate the structures, specific functions, molecular characteristics, genomic alterations, expression profiles, and tumor microenvironment of primary tumors [17]. Patient-derived organoids (PDOs) have been used as a tool for personalized medical decisions to predict patients' responses to therapeutic regimens and potentially improve treatment outcomes[18]. In skin tumor study, researchers used hydrogel-based engineering techniques to develop patient-specific sarcoma organoids, including DFSP[19]. The organoids were screened for chemotherapy efficacy, and a subset was enriched with a patient-matched immune system for screening of immunotherapy efficacy. The study concluded that a large subset of sarcoma organoids does not respond to chemotherapy or immunotherapy, as seen in clinical practice[19]. Specifically, skin organoids can not only highly simulate the physiological structure and function of skin tissue, better restore the real skin ecology under different *in vitro* environments, but also be applied to skin development research, skin disease pathology research and drug screening and other fields[20,21].

Imatinib, a tyrosine kinase inhibitor, has been identified as a safe and effective treatment for DFSP[22]. It has shown significant efficacy in advanced cases of DFSP, reducing tumor size preoperatively and lessening surgical morbidity associated with the removal of residual DFSP[23]. The drug works by targeting the COL1A1-PDGFB fusion gene, a result of the distinctive rearrangement of chromosomes 17 and 22 that underlies the development of DFSP[24]. However, the use of imatinib as a neoadjuvant therapy, aimed at reducing tumor size for complex surgical cases, requires careful patient selection and consideration of potential risks and benefits, especially when the tumor is in a cosmetically or functionally significant area or when incomplete excision could lead to high local risk. Despite imatinib' s general tolerability and favorable therapeutic index, the pharmacological benefits and toxicity risks for each patient must be evaluated[23].

In our study, we present a rapid method for the generation of skin tumor organoids without the use of enzymes or Matrigel. Our organoids exhibited proliferative capacity across multiple generations, reaching a substantial volume comparable to 2 mm^3. Histological and genomic analyses revealed the resemblance between the organoids and clinical tissues. Single-cell sequencing data identified 11 distinct cell types within the skin tumor organoids, encompassing immune cells and various skin cell types. RNA sequencing of four distinct DFSP organoids further confirmed the diverse cell populations within our cultured organoids. Additionally, we evaluated the responsiveness of our organoids to imatinib and metformin, both of which effectively inhibited the growth of DFSP organoids. Notably, metformin was found to modulate the expression of immune signaling pathways. Collectively, these findings underscore the potential utility of our patient-derived skin tumor organoids for drug testing and mechanistic studies.

Results

Culture of skin tumor organoids from patient tumors without enzymatic dissociation

In order to maintain the native micro-environment of tumor tissues, and to decrease the risk of clonal selection of specific cell populations, we developed a method to generate skin tumor organoids without enzymatic dissociation of tumor tissues into single cells (Fig. 1a). Furthermore, we did not use Matrigel or other biomaterials to support organoid growth, the skin tumor organoids were cultured either suspend or adherent or both in the culture medium. Freshly resected skin tumor tissue was collected from patients after surgery with full informed consent (Fig. S1(a) in the Electronic Supplementary Material (ESM)). The tissue samples were soaked in a washing solution for 3 minutes and then transferred to a 50 mL centrifuge tube for three rounds of washing. After decanting the excess liquid, the tissue blocks were placed in a 10 cm culture dish, and 100–200 μL of culture medium was added. The tissue blocks were then cut into approximately 0.5–1 mm^3 microtissue blocks and transferred to a new 10 cm culture dish, with 1 mL of culture medium added to resuspend the microtissue blocks. Finally, 15 mL of culture medium was added to maintain the organoid culture (Fig. 1a). Image records were taken for each skin tumor organoid to observe morphological differences among patients. A total of 10 tumor samples detected on skin were collected after surgery from the center part of lesion area, including 2 keloid patients, 1 melanoma patient, 1 malignant schwannoma patient, and 6 DFSP patients (Figs. S1(a) and S1(b) in the ESM). Due to the rarity of DFSP, a skin cancer with no reliable *in vitro* study method, we focused on the culture and characterization of DFSP organoids in our subsequent study.

To evaluate the growth characteristics of organoids from different patients, images were captured at various time points (Fig. 1b and Fig. S1(c) in the ESM). Once the organoid volume reached 2 mm^3 or the margin became smooth, we sub-cultured large organoids into smaller ones using a mechanical dissociation method (Fig. 1a). Quantitative analysis of organoid volumes using ImageJ revealed proliferative capacity in both P0 and P1 (Fig. 1c).

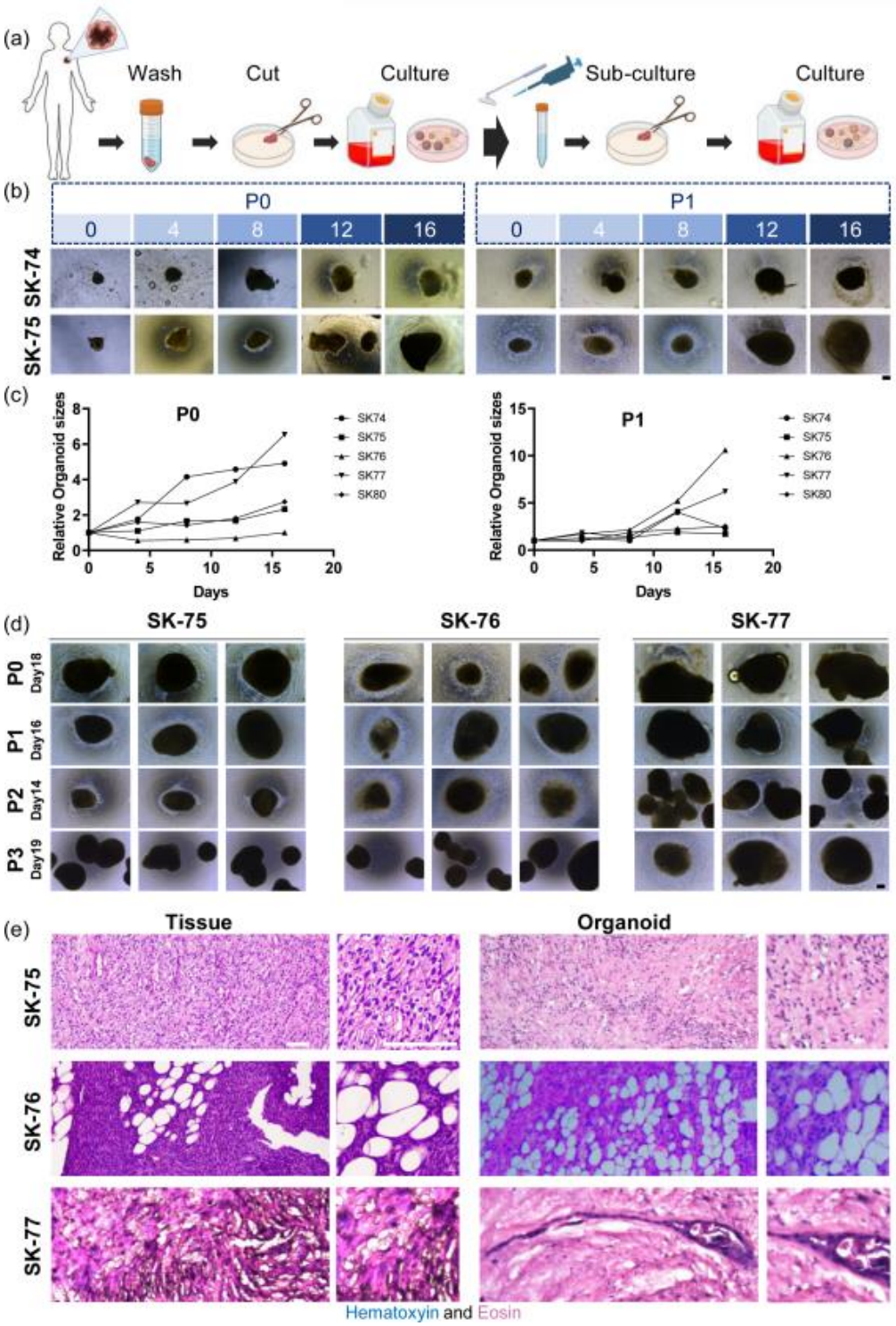

Figure 1. Culture and characterization of skin tumor organoids. (a) Schematic diagram of organoid culture and passaging process. (b) Growth records of organoids from different patients, with organoids at P0 on the left and at P1 on the right; scale bar = 200 μm. (c) Statistical chart of organoid growth volume at different generations. (d) Bright–field images of DFSP organoids at different generations from P0 to P3; scale bar = 200 μm. (e) Comparative histological images of clinical tissue and organoids stained with H&E staining; scale bar = 50 μm.

The growth curves for SK75 and SK80 organoids were similar in both generations; however, for SK74 and SK77 organoids, the P0 generation exhibited higher cell growth ability than P1. Conversely, for SK76 organoids, the P0 generation showed lower cell growth ability than P1. Our observations indicated that the growth speed and maximum volume of cultured organoids did not correlate with different generations (Fig. 1d).

To determine whether DFSP organoids resemble their clinical tumor tissues, we conducted histological examinations. Hematoxylin and eosin (H&E) staining revealed cellular types and distribution within the DFSP organoids that closely resembled those found in clinical tissues (Fig. 1e). Additionally, we observed morphological inter-patient heterogeneity. DFSP organoids exhibited spindle-shaped cancer cells (SK75), multiple adipocytes (SK76), and disordered cells (SK77).

Characterization of genetic mutations between DFSP organoids and tissues

To assess whether DFSP organoids maintain genomic alterations of tumor tissues, we performed whole exome sequencing (WES) of three pairs of samples (SK74/SK75/SK77) from different patients (Fig. 2a). The number and locations of genetic mutations in the exons between their clinical tissues and organoids were analyzed. The WES results showed around 80% concordance rate of mutation sites between the clinical tissues and organoid samples from the same patient (Fig. 2b). The organoids of patients SK74 and SK77 exhibited more mutation sites (Fig. 2a). Subsequently, we performed an overlap analysis of mutation sites from the three different patients (Fig. 2c), and the data showed that the complete overlap of mutation sites among the three patients compared to their respective mutation site numbers was not very high, being less than 40% (Fig. 2d). This result reflects the sample heterogeneity among different patients and reveals the complexity of the disease. According to a literature reference describing DFSP gene alterations[25], we extracted the highly frequent mutation sites in this disease to create a heatmap and found that the three patients selected in our study all conformed to the conclusions mentioned in the published article, and maintained a high degree of consistency between the organoids and tissues (Fig. 2e). Finally, we also conducted an in-depth analysis of our own WES data to identify some specific gene mutation sites, which included both SNPs (Fig.2f) and Indels (Fig. 2g). These mutation proportions were consistent between the tissues and organoids of the same patient, but were significantly different among samples from different patients. For example, the SNP of *PRSS3* was only found in SK74 and SK75, while SK77 had a higher proportion ofIndel mutations in *PRSS3* (Figs. 2fand 2g).

Single-cell sequencing data reveals immune cells within the skin tumor organoids

In order to explore the cellular microenvironment and molecular characteristics of distinct skin tumors, we conducted single-cell sequencing on keloid and DFSP organoids. Given the similar appearance of keloid and DFSP patients, which can lead to misdiagnosis, it was crucial to discern the molecular variances between them. Organoids were collected from two patients for each disease once the cultured organoid size reached 2 mm^3. By comparing our single-cell data from the four organoid samples with publicly available single-cell sequencing data from skin samples, we were able to identify up to 11 different cell types in our organoid samples (Fig. 3a)[26]. These cell types encompassed common skin system cell types such as endothelia, fibroblast, glandular, keratinocyte, melanocytes, and muscle fiber, as well as immune cells like lymphatic endothelia, mast cells, and T cells. Examination of the single-cell data from the four organoid samples individually revealed an abundance of fibroblast cells in the DFSP organoids, while immune-related cells were relatively scarce. Conversely, the keloid organoids displayed a higher presence of keratinocyte and T cells, indicating diverse immune microenvironments in cultured organoids from different diseases (Fig. 3b). Furthermore, weighted gene co-expression network analysis (WGCNA) of gene expression in keloid and DFSP organoids demonstrated unique gene expression characteristics for each patient (Figs. S2a and S2b in the ESM).

Cell-type heterogeneity and molecular signatures by DFSP organoids

To further investigate cell-type heterogeneity in DFSP organoids, we conducted RNA-seq analysis on four distinct sets of organoids once the cultured organoid size reached 2 mm^3 in their P0 generation, including SK74, SK75, SK76 and SK77 (Fig. S1b in the ESM). Each organoid underwent two independent experimental replicates, with the second experiment including two parallel controls, resulting in three datasets for each organoid. The clustering analysis of the RNA-seq data was consistent with our sample collection (Fig. 3d). Both principal component analysis (PCA) and gene clustering analysis revealed substantial heterogeneity among the four organoids (Figs. 3e and 3f). Upon annotating the RNA-seq data with network information, the distribution of different cell types in the four organoids was visually discernible (Fig. 3g). For SK74 and SK75, cell-types distribution results by RNA-seq analysis were similar as the single cell sequencing results. Notably, the SK77 organoid, collected at 20 days, emerged as the youngest among the group, exhibited a comparatively higher proportion of each cell type, whereas the remaining three organoids displayed distinct dominant cell populations (Fig. 3g). Subsequent WGCNA partitioned the differentially expressed genes of the four organoids into eight distinct modules (Fig. S2c in the ESM). The gene expression profiles also demonstrated marked disparities between SK77 and the other samples. KEGG/GO analysis unveiled the upregulated signaling pathways in each module (Fig. S2d in the ESM), with the turquoise module specifically upregulated in the SK77 sample. Notably, the Defense response to virus and Angiogenesis pathways were significantly upregulated. A comprehensive investigation of key genes in these pathways may yield potential therapeutic targets in the future. This heterogeneity may stem from inter-individual variations among patients or differences in organoids validation time points[17, 27–29].

Imatinib and metformin effectively inhibit the growth of DFSP organoids

To assess the suitability of DFSP organoids for drug sensitivity screening and drug discovery, we conducted experiments using the clinically approved drug Imatinib and the potential anti-cancer drug metformin. Metformin has been repurposed for several emerging applications, including as an anti-cancer agent[30]. It has been found to have anti-cancer effects and is associated with reduced risk of cancer and decreased cancer-related mortality in patients with diabetes[31]. Treatment of the organoids individually

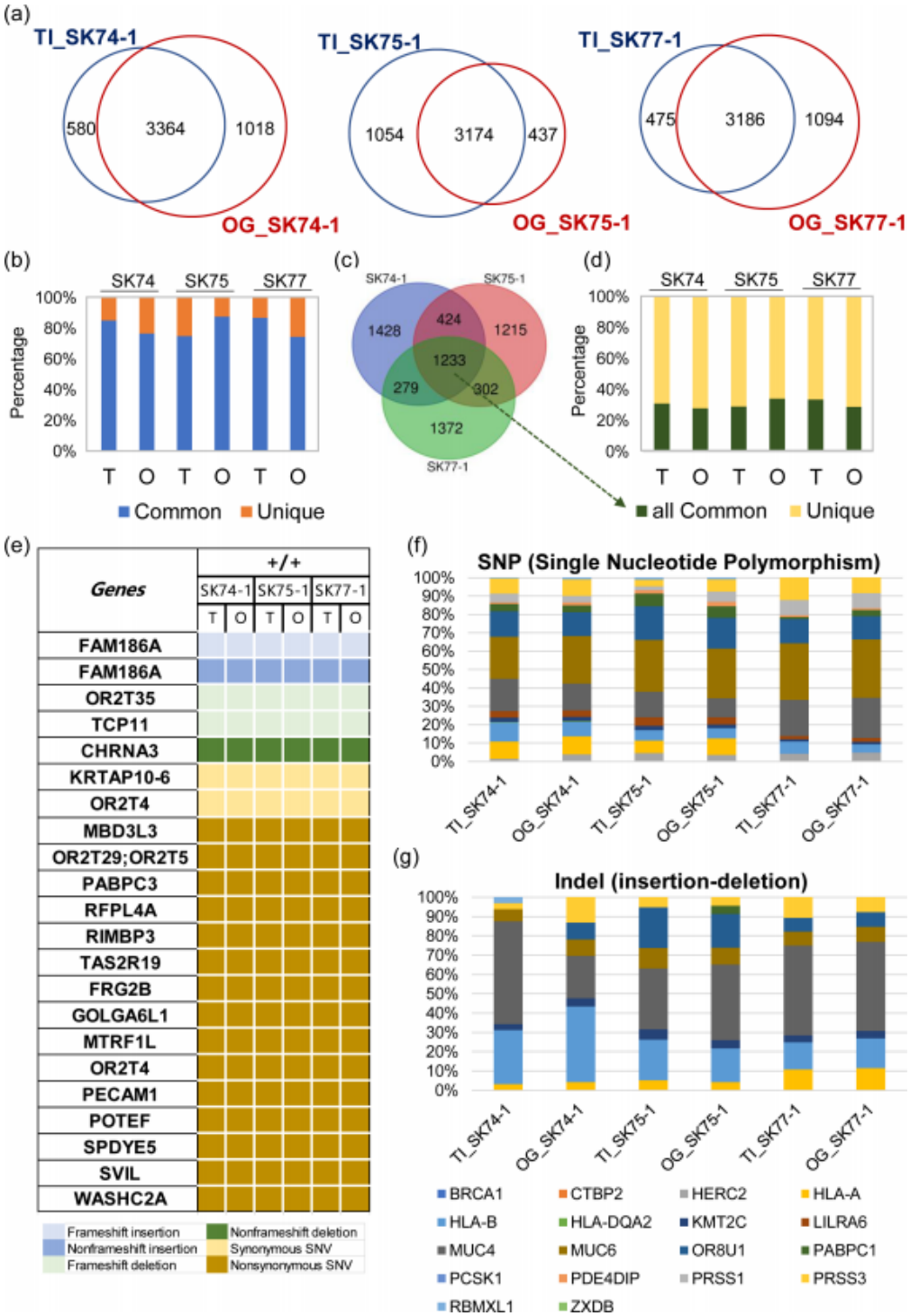

Figure 2. Comparison of WES data between organoids and tissues. (a) Venn diagram showing WES gene mutation sites in clinical tissue and organoids. (b) High consistency between clinical tissue and organoids from the same patient, with an overlap rate close to 80% (n = 3, SK74/SK75/SK77). (c) Venn diagram of WES gene mutation sites from three different patients. (d) Low overlap rate of WES mutation sites among three different patients, less than 40%, demonstrating patient heterogeneity. (e) Consistency between clinical tissue and organoid samples was observed, as reported by Peng et al. in their study on genomic alterations of dermatofibrosarcoma protuberans. (f) WES data analysis revealed different mutation sites of certain genes among different patients.

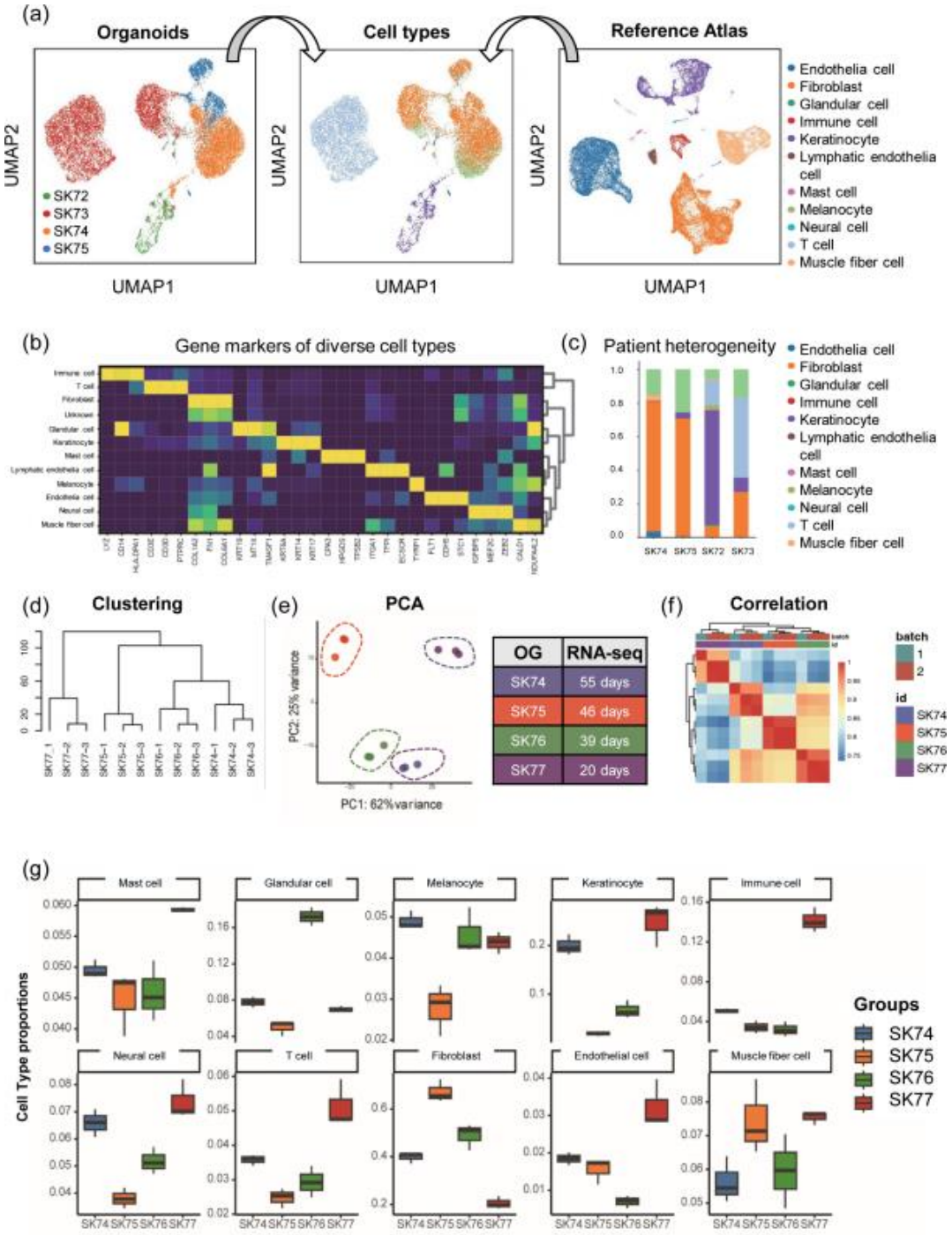

Figure 3. Diverse cell types in the cultured skin organoids. (a) Cell type definition based on comparison with public network data. (b) Identification of marker genes for different cell types. (c) Variation in cell type composition and proportions across the four organoids. (d) Three replicates of each of the four organ types were clustered and collected at different time points. (e) RNA–seq data was analyzed using PCA. (f) Gene clustering analysis was performed on the four organoids. (g) The proportions of different cell types varied across the four organ types.

with Imatinib (SK74/SK75/SK76) revealed significant inhibition of organoid sphere enlargement in SK74/SK75 compared to the control group (Fig. 4a). Notably, distinct phenotypic variations were observed under drug inhibition, with SK74 exhibiting rapid

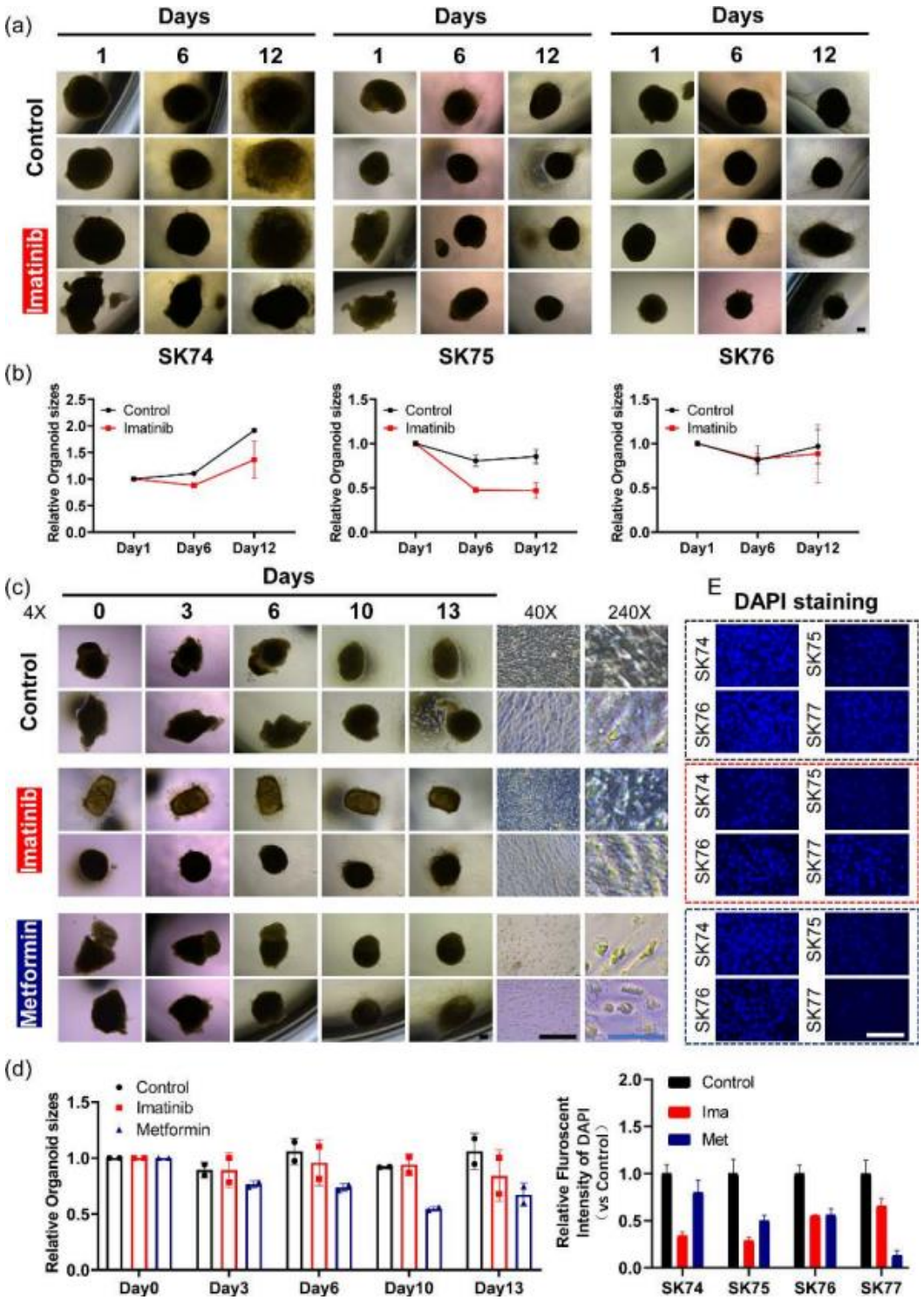

Figure 4. Imatinib and metformin effectively inhibit the growth of DFSP organoids. (a) Treatment of three DFSP organoids with imatinib resulted in a noticeable reduction in organoid sphere volume in two organoids, SK74 and SK75, with no significant effect observed in SK76; scale bar = 200 μm. (b) Statistical line graph depicting organoid volume sizes. (c) Record of organoid growth after treatment with imatinib and metformin, showing a significant decrease in the number of adherent cells in the drug–treated groups on the thirteenth day; black scale bar = 200 μm; blue scale bar = 50 μm. (d) Statistical bar graph representing organoid volume sizes. (e) Bar graph showing the number of adherent cells counted after DAPI staining; scale bar = 200 μm.

organoid sphere volume increase and edge-differentiated cell morphology in the control group. In contrast, SK75 organoid spheres became more compact with no significant volume increase, and imatinib led to the appearance of smaller organoid spheres (Fig. 4b). Furthermore, treatment of the SK77 organoids with the previously untested drug metformin resulted in effective inhibition of organoid sphere volume from the sixth day to the thirteenth day. This was accompanied by a significant decrease in cell numbers, along with notable changes in cell morphology and size (Figs. 4c and 4d). Subsequent testing on additional organoids confirmed the therapeutic efficacy of both drugs after 13 days of treatment, as evidenced by DAPI staining data of the adherent cells (Fig. 4e). These drug experiments provided compelling evidence that DFSP organoids can serve as a valuable method for drug sensitivity testing and new drug screening.

Metformin inhibited DFSP organoids via immune related pathways

Based on the pronounced phenotypic responses of DFSP organoids to imatinib and metformin, we sought to further elucidate the molecular mechanisms underpinning the pharmacological actions of these agents. To this end, we performed RNA-seq analysis on collected samples. Following a similar experimental design to previous studies, we selected four organoids (SK74, SK75, SK76, and SK77) and conducted two independent experiments, with the second experiment involving two sets of parallel samples, resulting in three replicates for each treatment condition. Principal component analysis (PCA) revealed a higher degree of sample consistency compared to the drug treatment results (Fig. 5a), while gene expression clustering analysis further confirmed inter-sample heterogeneity (Fig. 5b). Subsequent Weighted gene co-expression network analysis (WGCNA) aimed to identify shared changes following drug treatment, disregarding inter-organoid heterogeneity. We categorized downstream pathway changes into six distinct modules, and the results indicated that Imatinib treatment exhibited closer resemblance to the control group, whereas metformin treatment led to relatively substantial alterations in gene expression compared to the control and Imatinib treatment groups (Fig. 5c). Following metformin treatment, three modules (yellow, blue, and green) exhibited marked upregulation, with KEGG/GO analysis revealing enrichment of pathways related to cell cycle, phagocytosis, B cell activation, P53 signaling, immune system development, and ERK1/ERK2 cascade (Fig. 5d). Concurrently, three modules (red, turquoise, and brown) displayed significant downregulation following metformin treatment, with KEGG/GO analysis indicating pronounced downregulation of genes associated with pathways such as DNA transcription, apoptotic pathway, Innate-immune response, Wnt signaling, T cell differentiation, DNA replication, and TOR signaling (Fig. 5e). We suggested that the upregulated immune system development and downregulated innate-immune response after metformin treatment may be a response by the immune cells maintained in our cultured organoids (Figs. 3c and 3g).

Discussion

In contrast to previously reported tumor organoids derived from dissociated tumor cells, devoid of red blood cells, our skin tumor organoids maintain the native cell microenvironment and original tissue structure. Unlike the complex procedures involving Matrigel for organoid establishment, our culture system requires only 30 min to 1 h, based on a robust culture medium and mechanical dissociation. The skin tumor organoids demonstrate consistency with clinical tissues, as evidenced by histological analyses revealing similar tissue architecture and cellular morphologies, whole-exome sequencing confirming the preservation of somatic variants at comparable frequencies, and single-cell sequencing revealing the maintenance of multiple cell populations. Furthermore, heterogeneity between patients is evident, as observed through single-cell RNA-seq, which identifies different dominant cell types, and RNA-seq, which demonstrates diverse cell distributions in DFSP organoids. Additionally, we employed DFSP organoids to investigate the functional effects and genetic mechanisms of imatinib and metformin. Imatinib, a U.S. Food & Drug Administration (FDA)-approved drug, acts as an antagonist to inhibit tyrosine kinase, effectively suppressing the growth of DFSP organoids without modulating the expression of other genes. Conversely, metformin depresses the proliferation of DFSP organoids by modulating immune signaling pathways. Our practical and rapid method for culturing skin tumor organoids holds promise for advancing disease drug development.

The generation of traditional cancer organoid models typically involves the use of enzymatic digestion to dissociate clinical tissues into single cells, followed by the formation of 3D spheres with the aid of Matrigel or other biomaterials, resembling the primary culture method[17]. However, recent studies have proposed the establishment of tumor organoids using mechanical methods to preserve the optimal tumor microenvironment and cell–cell interactions by separating clinical tissues into small pieces without enzymatic treatment[32–35]. For instance, the glioma organoid (GBO) initiative has successfully created a live biobank of GBOs from 53 patients with diverse mutational profiles, serving as a valuable resource for future biological studies and therapeutic testing[32]. Given the rarity of DFSP, sample collection poses a significant challenge. In our study, we utilized samples from 10 skin tumor patients, including 6 DFSP patients. The limited number of available samples underscores the need to establish a larger biobank and information repository to comprehensively capture underlying patterns. This approach is crucial for advancing our understanding of DFSP and facilitating future research and therapeutic development.

When establishing a disease organoid model, it is essential to consider the tissue' s spatiotemporal specificity. Several studies have highlighted the spatiotemporal specificity of cancer tissue. For example, the Marco group has utilized bulk and single-cell genomic approaches to characterize genetic and transcriptional heterogeneity in glioblastoma (GBM), patient-derived explants (PDEs), and gliomasphere (GS) lines[33]. Given the distinct distribution of DFSP tumor tissue, the generation of singular tumor-specific organoids from the central part of the tumor is insufficient for accurately depicting the complete landscape of disease initiation and recurrence. There is a critical need for more sophisticated organ models to comprehensively investigate tumor regions and their surrounding areas. This approach is essential for gaining a deeper understanding of disease progression and developing more effective therapeutic strategies.

It is evident that organoids present challenges in terms of culture periods and consistency maintenance as comparing to two-dimensional (2D) primary culture methods and mouse models. However, organoids can better mimic the cellular microenvironment of tissues compared to 2D cell culture systems, and they more accurately represent tissue physiology[36]. They

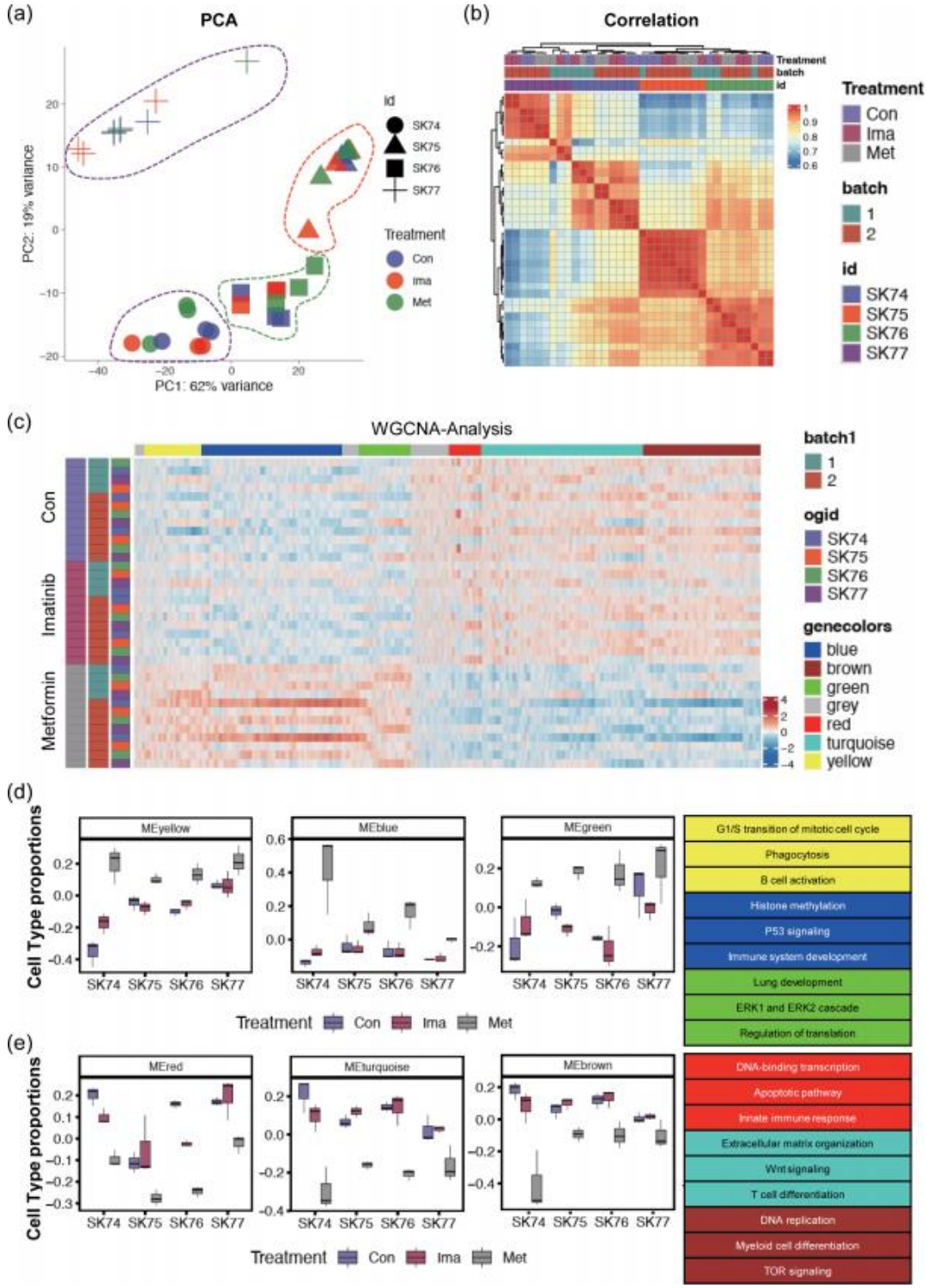

Figure 5. Downstream pathways and gene changes in organoids after treatment with imatinib and metformin. (a) PCA plot of RNA–seq data from four organoid samples after drug treatment. (b) Clustering plot of gene expression in three replicates of the four organoid samples. (c) WGCNA analysis conducted to identify gene expression differences among the four organ types after treatment with the two drugs. (d) Display of relevant signaling pathways within three upregulated modules after metformin treatment. (e) Display of relevant signaling pathways within three downregulated modules after metformin treatment.

exhibit higher cellular heterogeneity, organization, and tissue-like structures, making them a more relevant *in vitro* model for functional analyses and personalized therapies[37]. On the other hand, mouse models, being the closest to recapitulating human tissue functions and cellular interactions, can predict the development of treatments or diseases. However, they are limited by differences in species biology, sensitivity variations, high maintenance costs, and limited throughput. In contrast, 2D monolayer cell cultures, while more basic than animal models, provide insight into complex diseases with low cost, time efficiency, and high reproducibility. Nevertheless, they fail to recapitulate the complexity of the *in vivo* microenvironment due to the absence of an extracellular matrix (ECM), hindering the natural development of cells and tissues[38]. However, the choice of model often depends on the specific research question being addressed. Additionally, these models can be used complementarily in various research scenarios. In our study, we conducted single-cell RNA sequencing and bulk RNA sequencing when the cultured organoids reached a threshold volume of 2mm^3, which determined whether they would be subcultured to the next generation. Notably, each organoid reached this standard at different time points. However, based on our unpublished data, the differences in culture times within the same generation of organoids may not lead to genetic differences.

The single-cell sequencing results shown the skin tumor organoids have 11 distinct cell types including immune cells which indicating the possibility to use this culture method to test the drugs of immune therapy. Metformin, a common drug used for diabetes, has been found to have multiple anti-cancer effects. It can downregulate ACSL4 expression in early stages of colorectal cancer[39], improve the fitness of CD8 T cells in hypoxic conditions[40], and inhibit the Wnt signaling pathway, which is involved in cell proliferation and survival[41]. Further, metformin activates AMPK, enhances the anti-cancer activity of γδ T cells, providing a potential new approach for cancer immunotherapy[42]. Our RNA-seq analysis of DFSP organoids treated with metformin confirmed these genetic modulations. KEGG analysis indicated that metformin could inhibit the growth of DFSP organoids through immune signaling pathways. This suggests the potential for metformin to be repurposed as a therapeutic agent for DFSP, particularly in the context of immune modulation.

Based on the above experimental results, we believe that organoids have potential in the field of research and treatment of DFSP. Detailed genotyping is indeed crucial for the selection of drugs in personalized treatment. It allows for a better understanding of the genetic makeup of an individual's disease, which can guide the choice of therapeutic strategies. When combined with WES and RNA-seq data, it can help identify population heterogeneity, which is key to understanding the diverse responses to treatment observed among patients. Organoid databases and samples offer numerous advantages in the context of drug testing. They mimic the cellular microenvironment of tissues better than 2D cell culture systems and represent the tissue physiology. This makes them more physiologically relevant, providing a more accurate model for drug testing. Organoids capture the cellular composition and pharmaco-typic signatures ofthe parental tumor. This allows for a better understanding of how drugs might interact with different cell types within a tumor. Organoids have been applied in drug screening to demonstrate the correlation between genetic mutations and sensitivity to targeted therapy. This can help predict how a patient's tumor might respond to a particular drug. PDOs can provide clinicians with a model system to choose the most effective treatment options for individual patients. This is a significant step towards personalized medicine. Organoids offer reproducibility, which is crucial in drug testing. Biobanks can be generated for repeat study. Organoids hold great promise for toxicological drug and compound screening and could potentially reduce the use of non-human animals for the same purpose. Experiments on the effects of imatinib and metformin on DFSP organoids provide valuable information. Treatment of the organoids individually with Imatinib revealed inhibition of organoid sphere enlargement in SK74/SK75 compared to the control group. Notably, distinct phenotypic variations were observed under drug inhibition. Treatment of the SK77 organoids with Metformin resulted in effective inhibition of organoid sphere volume from the sixth day to the thirteenth day. This was accompanied by a decrease in cell numbers, along with notable changes in cell morphology and size. Subsequent testing on additional organoids confirmed the therapeutic efficacy of both drugs after 13 days of treatment, as evidenced by DAPI staining data of the adherent cells. These findings suggest that DFSP organoids can serve as a valuable method for drug sensitivity testing and new drug screening.

Methods and materials

Tissue collection

The clinical tissue sample collection methodology adhered to strict ethical guidelines and standard operating procedures to ensure the integrity and quality of the collected samples. Key steps in the methodology included patient identification, informed consent, sample collection, processing, storage, and documentation. The collection of clinical tissue samples was conducted by trained medical personnel, following established protocols to minimize contamination and ensure the preservation of sample viability for downstream analysis. Additionally, stringent record-keeping and labeling practices were implemented to maintain traceability and facilitate accurate data management. All the clinical samples were collected under the Shanghai Ninth People's Hospital ethical guidelines and were assigned the ethical code 2017125.T321.

Organoid culture

The tissue specimens were soaked in a washing solution (LSNO00100201; Shanghai LiSheng Biotech, China) for 3 min and then transferred to a 50 mL centrifuge tube for 3 rounds of washing using washing solution. Each wash involved the addition of 5 mL of washing solution and gentle agitation to cleanse the tissue surface. After decanting the supernatant, the tissue blocks were transferred to a 10 cm culture dish, where 100–200 μL of culture medium (LSTO015004; Shanghai LiSheng Biotech, China) was added. The tissue blocks were then cut into approximately 1 mm^3 microtissue blocks and transferred to a new 50 mL tube. Following the addition of 1 mL of culture medium to resuspend the microtissue blocks, they were transferred to a new 10 cm culture dish. The remaining tissue was collected and transferred to a new dish after rinsing with 1 mL of culture medium. Finally, 15 mL of culture medium were added to maintain the organoids

culture.

During the organoid culture process, a partial medium change should be performed every 5-7 days, or as needed based on changes in the color and turbidity of the medium, to ensure an adequate supply of nutrients for organoid growth. The specific steps for partial medium change involve opening the top cover of the culture container, tilting the container to allow the organoids to settle, and then using a 1 mL regular pipette tip to slowly remove the culture medium from the upper layer of the liquid surface. After removing half of the volume of the old medium, new culture medium should be added using a 3 mL pipette (Bart's Pipette), with an additional 1-2 mL as needed to compensate for potential volume reduction due to evaporation in the culture system. These steps ensure the proper maintenance of the organoid culture system and support the healthy growth of the organoids.

To subculture the organoids, the mechanical digestion method is employed without the use of digestive enzymes. Following the standard protocol for partial medium change as described above, 10 mL of the old medium is discarded. Subsequently, a 1 mL regular pipette tip (reference QSP Cat: T112NXLRS–Q) is used to gently detach the organoids adhering to the container walls. Then, the same pipette tip is used to draw small, intersecting lines at the bottom of the culture container to facilitate the separation of the adherent cells in the microenvironment, after which a cell scraper is used to gently lift all the cells from the bottom. The organoids and microenvironment cell suspension are then transferred to a 15 mL tube, centrifuged at 300× *g* for 3 min, and the supernatant is discarded. Subsequently, the organoids and microenvironment cells are resuspended in preheated fresh organoid culture medium using a dedicated organoid pipette tip and seeded into a new culture container at a 5:1 split ratio for passaging.

In advance of the cryopreservation process, the organoid cryopreservation medium is prepared by combining 10 mL of the organoid cryopreservation solution (LSNO00100701; Shanghai LiSheng Biotech, China) with 0.8 mL of cryopreservation additive (LSOR00400101; Shanghai LiSheng Biotech, China). The organoids and microenvironment cells are then resuspended in the organoid cryopreservation medium using a dedicated organoid pipette tip and evenly distributed into pre–labeled cryovials, with each cryovial containing 1-1.5 mL of the cryopreservation medium. Subsequently, the cryovials are placed in a controlled–rate freezing container and stored at -80 °C in a freezer. Within one week, the cryovials can be transferred to a liquid nitrogen tank for long–term storage.

Organoids size calculation and analysis

The organoids are imaged daily, and their size is quantified using the ImageJ software. Firstly, we organize the set of photos into one file and compile them into a single image. Then, we open the file in ImageJ and use the "Polygon selections" tool to outline the outer edge of the organoids. Next, we click on "Measure" under the "Analyze" menu to calculate the area of the organoid. To assess the growth capacity of the organoid, we divide the total area by the initial area on Day 0 to obtain a relative organoid size.

Organoids drug treatments

DFSP organoids of ~ 500 μm in diameter were selected from a 10 cm dish and seeded at a density of one spheroid per well in a 24–well cell culture plate, with each well containing 1 mL of organoid culture medium. The optimal concentrations of the drugs, namely 10 μmol/L imatinib and 2.5 mmol/L metformin, were determined based on a thorough literature review and added to the respective wells containing the spheroids. Daily photographic documentation of the spheroids was performed following the addition of the drugs, and at the final time point, a detailed observation of the cellular phenotype of the spheroids was conducted.

H&E staining

Tissues and organoids were fixed in 4% paraformaldehyde (PFA) (BL539A, Biosharp) for 30 min, dehydrated with sucrose, and embedded in 7.5% gelatin. Frozen sections of 10 μm thickness were obtained using citric acid (pH 6.0). Adherent cells were fixed using 4% PFA for 20 min. For H&E staining, the sections were washed twice and stained using a H&E Stain Kit (G1120, Solarbio, China) according to the manufacturer's instructions.

Whole exon sequencing (WES)

Clinical tissues and organoids were used to isolate DNA with the Gentra Puregene Blood Kit (QIAGEN, Hilden, Germany). Each sample underwent processing with 200 ng of genomic DNA, which was fragmented into 150-200 bp fragments for library construction. The AIExome® Human Exome Panel V3 and TargetSeq One® Hyb & Wash Kit v2.0 from iGeneTech Co., Ltd, Beijing, China was employed for whole exome capture, followed by sequencing on the DNBSEQ–T7 platform with 150–bp reads. Raw reads were filtered using FastQC to eliminate low–quality reads. Subsequently, the clean reads were mapped to the reference genome GRCh37. Quality control metrics included an average read length of > 100×, accurate mapping rate of > 98%, bases capture rate of > 55%, 20× mean depth coverage rate of > 96%, duplication rate of < 25%, and accurate mapping rate of < 96%. Single nucleotide variants (SNVs) were annotated and filtered using TGex (tgex.genecards.org). This optimized approach aimed to reduce redundancy and enhance the precision of the sequencing data analysis process.

Singe cell RNA-sequencing

Skin organoids were dissociated into single cells using the Organoid Dissociation Kit (LSTO01500501; Shanghai LiSheng Biotech, China). Following the removal of erythrocytes (Solarbio R1010), cell count and viability were assessed using a fluorescence Cell Analyzer (Countstar® Rigel S2) with AO/PI reagent. Subsequently, a decision was made on whether to remove debris and dead cells using Miltenyi 130–109–398/130–090–101. The fresh cells were then washed twice in RPMI1640, re–suspended at 1 × 10^6 cells/mL in 1× phosphate buffered saline (PBS), and 0.04% bovine serum albumin was added.

For single–cell RNA–Seq library preparation, the SeekOne® Digital Droplet Single Cell' library preparation kit (SeekGene Catalog No. K00202) was utilized. Initially, the appropriate number of cells was mixed with reverse transcription reagent and added to the sample well in the SeekOne® chip. Barcoded hydrogel beads (BHBs) and partitioning oil were dispensed into corresponding wells on the chip to generate emulsion droplets. Reverse transcription was carried out at 42 °C for 90 min, followed by inactivation at 80 °C for 15 min. Subsequently, cDNA was purified, amplified in a PCR reaction, cleaned, fragmented, end repaired, A–tailed, and ligated to sequencing adaptors. Indexed PCR was then performed to amplify the DNA representing the 3' polyA part of expressing genes, which also contained Cell Barcode and Unique Molecular Index. The

indexed sequencing libraries were cleaned up with solid-phase reversible immobilization (SPRI) beads and quantified using quantitative PCR (KAPA Biosystems KK4824).

Libraries were sequenced on the Illumina Hiseq 4000 with PE-150 bp reads for subsequent analysis. Raw data from the single-cell RNA sequencing (scRNA-seq) was processed using Cell Ranger, and downstream analyses were conducted using Seurat.

Cell type identification

We utilized the publicly available dataset GSE163973, which originally identified 10 major cell types in fibrotic skin diseases. However, we encountered some cells that were unassigned or incorrectly identified. To refine the classification, we divided the "Glandular" category into "Glandular" and "T cells" due to the expression of CD3E and PTPRC (CD45) in a subset of "Glandular" cells. Additionally, we relabeled the "unknown" category as "Mast cells" based on the presence of CPA3 and PTPRC. This approach helped us construct our reference dataset[43]. Given that cell states can change during *ex vivo* culturing, harmonizing single-cell RNA sequencing (scRNA-seq) data between our organoids and the reference proved challenging. Therefore, we adopted a strategy of forced mapping of our organoid scRNA-seq data onto the reference dataset based on the Pearson correlation between the two datasets. For each cell in our organoid data, we identified the 50 most similar cells from the reference dataset. A cell was then classified based on the predominant label of these 50 cells if the same label was present in at least 40 of them; otherwise, the cell was categorized as unknown.

RNA-sequencing

mRNA was isolated from organoids using the RNA Isolation Kit (DP451, TIANGEN, China). Each group of organoids, consisting of 4–6 organoids with diameter of 2 mm, was used as input for the extraction. The concentration of RNA was measured with a Qubit4 fluorometer. Subsequently, reverse transcription was carried out using the RT Kit (KR118, TIANGEN, China), and library preparation was performed using the RNA Library Prep Kit (E7530L, NEB, USA). For bulk RNA-seq analysis, RNA expression levels were quantified using fragments per kilobase transcript mapped reads per million (FPKM), and differentially expressed genes were identified using the Morpheus online software.

Statistical analysis

The data were collected from three or more replicates, and quantitative results are expressed as mean ± standard deviation. Statistical analysis was conducted using GraphPad Prism 7.0 (GraphPad Software, USA). Student's t-test was used for multiple comparisons to assess significance. A p value less than 0.05 was considered statistically significant. The p values were calculated from a minimum of 3 independent experiments. Statistical significance is indicated as: $*p < 0.05$, $**p < 0.01$, and $***p < 0.001$. Error bars represent the standard deviation of the mean.

Research ethics and patient consent

The collection of clinical samples followed the ethical guidelines established by Shanghai Ninth People's Hospital, with the study assigned the ethical approval No. 2017125.T321. Prior to providing samples, all participants signed informed consent forms, clearly indicating the planned utilization of their samples for future research. Their voluntary involvement and comprehension of the study's goals were crucial for maintaining ethical standards throughout this research.

Availability of data and material

The data and materials that support the findings of this study are available from the corresponding author upon reasonable request.

Declaration of conflicting interests

This work was sponsored by Shanghai Lisheng Biotech Ltd (Lisheng). The manuscript was written in a responsible and ethical manner. X.X.H. is a shareholder of Lisheng, as a founder. Y.H.S., L.Y.L., C.W., J.Z., M.J.R., J.P.L and C.H.C. are senior scientists of Lisheng. A patent on A skin fibrosarcoma like organoid model and its construction and application method has been applied (No. 2023118261310). All authors declare no competing financial interests.

X.X.H. and C.H.C. are the Editorial Board members of *Cell Organoid*. They were not involved in the journal's review of, or decisions related to, this manuscript.

Funding

The work was supported by the National Natural Science Foundation of China (Nos. 82373719, 82173662, and 32200581), Natural Science Foundation of Shanghai (No. 21ZR1436800), and Clinical Research Project of Multi-Disciplinary Team, Shanghai Ninth People's Hospital, Shanghai Jiao Tong University School of Medicine (No. 201901).

Author contributions

J.C., C.H.C., and X.X.H. conceived and designed the study. Y.H.S., L.Y.L., C.W., J.Z., and M.J.R. collected the samples, performed the experiments, and analyzed the data. J.P.L., J.C., C.H.C., and X.X.H. analyzed the data. Y.H.S., J.P.L., J.C., C.H.C., and X.X.H. wrote the manuscript. All the authors read and approved the final version of the manuscript.

Electronic Supplementary Material: Supplementary material (information of skin tumor samples and WGCNA and KEGG/GO analysis of DFSP organoids) is available in the online version of this article at https://doi.org/10.26599/CO.2024.9410001.

References

[1] Tay, S. S., Roediger, B., Tong, P. L., Tikoo, S., Weninger, W. The skin-resident immune network. *Current Dermatology Reports*, **2014**, 3(1): 13–22. https://doi.org/10.1007/s13671-013-0063-9

[2] Mestrallet, G., Rouas-Freiss, N., LeMaoult, J., Fortunel, N. O., Martin, M. T. Skin immunity and tolerance: Focus on epidermal keratinocytes expressing HLA-G. *Frontiers in Immunology*, **2021**, 12: 772516. https://doi.org/10.3389/fimmu.2021.772516

[3] Trompette, A., Ubags, N. D. Skin barrier immunology from early life to adulthood. *Mucosal Immunology*, **2023**, 16(2): 194–207. https://doi.org/10.1016/j.mucimm.2023.02.005

[4] Nestle, F. O., Di Meglio, P., Qin, J. Z., Nickoloff, B. J. Skin immune sentinels in health and disease. *Nature Reviews Immunology*, **2009**, 9(10): 679–691. https://doi.org/10.1038/nri2622

[5] Wang, T., Li, K., Xiao, S. X., Xia, Y. M. A plausible role for collectins in skin immune homeostasis. *Frontiers in Immunology*, **2021**, 12: 594858. https://doi.org/10.3389/fimmu.2021.594858

[6] Pasparakis, M., Haase, I., Nestle, F. O. Mechanisms regulating skin immunity and inflammation. *Nature Reviews Immunology*, **2014**, 14(5): 289–301. https://doi.org/10.1038/nri3646

[7] Johnson-Huang, L. M., McNutt, N. S., Krueger, J. G., Lowes, M. A. Cytokine-producing dendritic cells in the pathogenesis of inflammatory skin diseases. *Journal of Clinical Immunology*, **2009**, 29(3): 247–256. https://doi.org/10.1007/s10875-009-9278-8

[8] Turchin, I., Bourcier, M. The role of interleukins in the pathogenesis of dermatological immune-mediated diseases. *Advances in Therapy*, **2022**, 39(10): 4474–4508. https://doi.org/10.1007/s12325-022-02241-y

[9] Fetter, T., Niebel, D., Braegelmann, C., Wenzel, J. Skin-associated B cells in the pathogenesis of cutaneous autoimmune diseases—Implicationsfortherapeuticapproaches. *Cells*,**2020**,9(12):2627.https://doi.org/10.3390/cells9122627

[10] Xiong, D. D., Bordeaux, J. S. Incidence and survival outcomes of dermatofibrosarcoma protuberans from 2000 to 2020: A population-based retrospective cohort analysis. *Dermatologic Surgery*, **2023**, 49(12): 1096–1103. https://doi.org/10.1097/dss.0000000000004018

[11] Roh, M. R., Bae, B., Chung, K. Y. Mohs' micrographic surgery for dermatofibrosarcoma protuberans. *Clinical and Experimental Dermatology*, **2010**, 35(8): 849–852. https://doi.org/10.1111/j.1365-2230.2010.03819.x

[12] Doufekas, K., Duncan, T. J., Williamson, K. M., Varma, S., Nunns, D. Mohs micrographic surgery for dermatofibrosarcoma protuberans of the vulva. *Obstetrics and Gynecology International*, **2009**, 2009: 547672. https://doi.org/10.1155/2009/547672

[13] Zwald, F. O. Underuse of mohs micrographic surgery for the treatment of dermatofibrosarcoma protuberans. *Archives of Dermatology*, **2012**, 148(9): 1064. https://doi.org/10.1001/archdermatol.2012.2685

[14] Zeitouni, N., Cavanaugh, K., DuPont, J. Dermatofibrosarcoma protuberans: An update and review. *Current Dermatology Reports*, **2015**, 4(4): 195–204. https://doi.org/10.1007/s13671-015-0120-7

[15] Oyama, R., Kito, F., Qiao, Z. W., Sakumoto, M., Shiozawa, K., Toki, S., Yoshida, A., Kawai, A., Kondo, T. Establishment of novel patient-derived models of dermatofibrosarcoma protuberans: Two cell lines, NCC-DFSP1-C1 and NCC-DFSP2-C1. *In Vitro Cellular & Developmental Biology - Animal*, **2019**, 55(1): 62–73. https://doi.org/10.1007/s11626-018-0305-z

[16] Tang, X. Y., Wu, S., Wang, D., Chu, C., Hong, Y., Tao, M., Hu, H., Xu, M., Guo, X., Liu, Y. Human organoids in basic research and clinical applications. *Signal Transduction and Targeted Therapy*, **2022**, 7: 168. https://doi.org/10.1038/s41392-022-01024-9

[17] Xu, H. X., Jiao, D. C., Liu, A. G., Wu, K. M. Tumor organoids: Applications in cancer modeling and potentials in precision medicine. *Journal ofHematology & Oncology*, **2022**, 15(1): 58. https://doi.org/10.1186/s13045-022-01278-4

[18] Zhou, Z., Cong, L., Cong, X. Patient-derived organoids in precision medicine: Drug screening, organoid-on-a-chip and living organoid biobank. *Frontiers in Oncology*, **2021**, 11: 762184. https://doi.org/10.3389/fonc.2021.762184

[19] Forsythe, S. D., Sivakumar, H., Erali, R. A., Wajih, N., Li, W. C., Shen, P., Levine, E. A., Miller, K. E., Skardal, A., Votanopoulos, K. I. Patient-specific sarcoma organoids for personalized translational research: Unification of the operating room with rare cancer research and clinical implications. *Annals of Surgical Oncology*, **2022**, 29(12): 7354–7367. https://doi.org/10.1245/s10434-022- 12086-y

[20] Lei, M. X., Schumacher, L. J., Lai, Y. C., Juan, W. T., Yeh, C. Y., Wu, P., Jiang, T. X., Baker, R. E., Widelitz, R. B., Yang, L. et al. Self-organization process in newborn skin organoid formation inspires strategy to restore hair regeneration of adult cells. *Proceedings of the National Academy of Sciences of the United States ofAmerica*, **2017**, 114(34): E7101–E7110. https://doi.org/10.1073/pnas.1700475114

[21] Hong, Z. X., Zhu, S. T., Li, H., Luo, J. Z., Yang, Y., An, Y., Wang, X., Wang, K. Bioengineered skin organoids: From development to applications. *Military Medical Research*, **2023**, 10(1): 40. https://doi.org/10.1186/s40779-023-00475-7

[22] Navarrete-Dechent, C., Mori, S., Barker, C. A., Dickson, M. A., Nehal, K. S. Imatinib treatment for locally advanced or metastatic dermatofibrosarcoma protuberans: A systematic review. *JAMA Dermatology*, **2019**, 155(3): 361–369. https://doi.org/10.1001/jamadermatol.2018.4940

[23] Johnson-Jahangir, H., Sherman, W., Ratner, D. Using imatinib as neoadjuvant therapy in dermatofibrosarcoma protuberans: Potential pluses and minuses. *Journal of the National Comprehensive Cancer Network*, **2010**, 8(8): 881–885. https://doi.org/10.6004/jnccn.2010.0065

[24] Rutkowski, P., Wozniak, A., Switaj, T. Advances in molecular characterization and targeted therapy in dermatofibrosarcoma protuberans. *Sarcoma*, **2011**, 2011: 959132. https://doi.org/10.1155/2011/959132

[25] Peng, C., Jian, X. X., Xie, Y., Li, L. F., Ouyang, J., Tang, L., Zhang, X., Su, J., Zhao, S., Liu, H. et al. Genomic alterations of dermatofibrosarcoma protuberans revealed by whole-genome sequencing. *British Journal of Dermatology*, **2022**, 186(6): 997–1009. https://doi.org/10.1111/bjd.20976

[26] Deng, C. C., Hu, Y. F., Zhu, D. H., Cheng, Q., Gu, J. J., Feng, Q. L., Zhang, L. X., Xu, Y. P., Wang, D., Rong, Z. L. et al. Single-cell RNA-seq reveals fibroblast heterogeneity and increased mesenchymal fibroblasts in human fibrotic skin diseases. *Nature Communications*, **2021**, 12: 3709. https://doi.org/10.1038/s41467-021-24110-y

[27] Ge, L. L., Wang, Z. C., Wei, C. J., Huang, J. X., Liu, J., Gu, Y. H., Wang, W., Li, Q. F. Unraveling intratumoral complexity in metastatic dermatofibrosarcoma protuberans through single-cell RNA sequencing analysis. *Cancer Immunology, Immunotherapy*, **2023**, 72(12): 4415–4429. https://doi.org/10.1007/s00262-023-03577-2

[28] Kemper, K., Krijgsman, O., Cornelissen-Steijger, P., Shahrabi, A., Weeber, F., Song, J. Y., Kuilman, T., Vis, D. J., Wessels, L. F., Voest, E. E. et al. Intra- and inter-tumor heterogeneity in a vemurafenib-resistant melanoma patient and derived xenografts. *EMBO Molecular Medicine*, **2015**, 7(9): 1104–1118. https://doi.org/10.15252/emmm.201404914

[29] Kerkour, T., Zhou, C., Hollestein, L., Mooyaart, A. Genetic concordance in primary cutaneous melanoma and matched metastasis: A systematic review and meta-analysis. *International Journal ofMolecular Sciences*, **2023**, 24(22): 16281. https://doi.org/10.3390/ijms242216281

[30] Skuli, S. J., Alomari, S., Gaitsch, H., Bakayoko, A., Skuli, N., Tyler, B. Metformin and cancer, an ambiguanidous relationship. *Phamaceuticals*, **2022**, 15(5): 626. https://doi.org/10.3390/ph15050626

[31] Hua, Y., Zheng, Y., Yao, Y. R., Jia, R. B., Ge, S. F., Zhuang, A. Metformin and cancer hallmarks: Shedding new lights on therapeutic repurposing. *Journal of Translational Medicine*, **2023**, 21(1): 403. https://doi.org/10.1186/s12967-023-04263-8

[32] Jacob, F., Salinas, R. D., Zhang, D. Y., Nguyen, P. T. T., Schnoll, J. G., Wong, S. Z. H., Thokala, R., Sheikh, S., Saxena, D., Prokop, S. et al. A patient-derived glioblastoma organoid model and biobank recapitulates inter- and intra-tumoral heterogeneity. *Cell*, **2020**, 180(1): 188–204.e22. https://doi.org/10.1016/j.cell.2019.11.036

[33] LeBlanc, V. G., Trinh, D. L., Aslanpour, S., Hughes, M., Livingstone, D., Jin, D., Ahn, B. Y., Blough, M. D., Cairncross, J. G., Chan, J. A. et al. Single-cell landscapes of primary glioblastomas and matched explants and cell lines show variable retention of inter- and intratumor heterogeneity. *Cancer Cell*, **2022**, 40(4): 379–392.e9.

https://doi.org/10.1016/j.ccell.2022.02.016

[34] Choe, M. S., Kim, S. J., Oh, S. T., Bae, C. M., Choi, W. Y., Baek, K. M., Kim, J. S., Lee, M. Y. A simple method to improve the quality and yield of human pluripotent stem cell-derived cerebral organoids. *Heliyon*, **2021**, 7(6): e07350. https://doi.org/10.1016/j.heliyon.2021.e07350

[35] Hu, Y. W., Sui, X. Z., Song, F., Li, Y. Q., Li, K. Y., Chen, Z. Y., Yang, F., Chen, X. Y., Zhang, Y. H., Wang, X. N. et al. Lung cancer organoids analyzed on microwell arrays predict drug responses of patients within a week. *Nature Communications*, **2021**, 12: 2581. https://doi.org/10.1038/s41467-021-22676- 1

[36] Shankaran, A., Prasad, K., Chaudhari, S., Brand, A., Satyamoorthy, K. Advances in development and application of human organoids. *3 Biotech*, **2021**, 11(6): 257. https://doi.org/10.1007/s13205-021-02815-7

[37] Calà, G., Sina, B., De Coppi, P., Giobbe, G. G., Gerli, M. F. M. Primary human organoids models: Current progress and key milestones. *Frontiers in Bioengineering and Biotechnology*, **2023**, 11: 1058970. https://doi.org/10.3389/fbioe.2023.1058970

[38] Suarez-Martinez, E., Suazo-Sanchez, I., Celis-Romero, M., Carnero, A. 3D and organoid culture in research: Physiology, hereditary genetic diseases and cancer. *Cell & Bioscience*, **2022**, 12(1): 39. https://doi.org/10.1186/s13578-022-00775-w

[39] Cruz-Gil, S., Sánchez-Martínez, R., Wagner-Reguero, S., Stange, D., Schölch, S., Pape, K., Ramírez de Molina, A. A more physiological approach to lipid metabolism alterations in cancer: CRC-like organoids assessment. *PLoS One*, **2019**, 14(7): e0219944. https://doi.org/10.1371/journal.pone.0219944

[40] Finisguerra, V., Dvorakova, T., Formenti, M., Van Meerbeeck, P., Mignion, L., Gallez, B., Van den Eynde, B. J. Metformin improves cancer immunotherapy by directly rescuing tumor-infiltrating CD8 T lymphocytes from hypoxia-induced immunosuppression. *Journal for ImmunoTherapy of Cancer*, **2023**, 11(5): e005719. https://doi.org/10.1136/jitc-2022-005719

[41] Conza, D., Mirra, P., Fiory, F., Insabato, L., Nicolò, A., Beguinot, F., Ulianich, L. Metformin: A new inhibitor of the Wnt signaling pathway in cancer. *Cells*, **2023**, 12(17): 2182. https://doi.org/10.3390/cells12172182

[42] Mamedov, M. R., Vedova, S., Freimer, J. W., Das Sahu, A., Ramesh, A., Arce, M. M., Meringa, A. D., Ota, M., Chen, P. A., Hanspers, K. et al. CRISPR screens decode cancer cell pathways that trigger γδ T cell detection. *Nature*, **2023**, 621(7977): 188–195. https://doi.org/10.1038/s41586-023-06482-x

[43] Menden, K., Marouf, M., Oller, S., Dalmia, A., Magruder, D. S., Kloiber, K., Heutink, P., Bonn, S. Deep learning–based cell composition analysis from tissue expression profiles. *Science Advances*, **2020**, 6(30): eaba2619. https://doi.org/10.1126/sciadv.aba2619

Cell Organoid

Article

https://doi.org/10.26599/CO.2024.9410005

Crossroad of ovarian cancer organoid culture: Single cell suspension and mechanically sheared fragment

Authors

Lanyang Li, Jiping Liu, Qi Cao, Yuqing Zhao, Yanghua Shi, ..., Wei Deng*, Chunhui Cai*, Xinxin Han*

Correspondence

Xinxin Han, xxhan@sibs.ac.cn; Chunhui Cai, caichunhui@lishengbiotech.com; Wei Deng, dengwei@shsmu.edu.cn

Graphical abstract

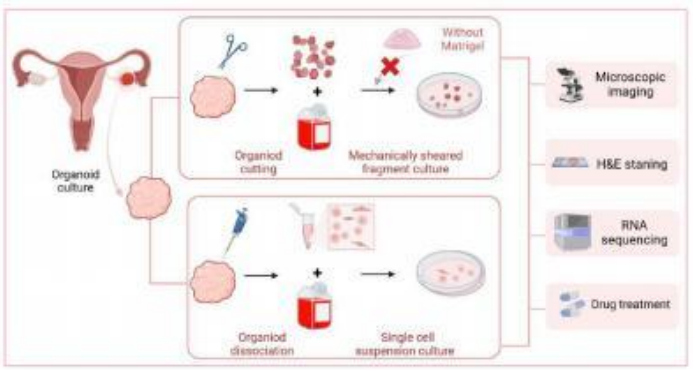

In Brief

This study explores the cultivation of uniformly-sized ovarian cancer organoids from single-cell suspensions, addressing challenges in high-throughput drug screening and providing insights into personalized treatment strategies against chemotherapy resistance.

Highlights

- Rapid and efficient generation of uniformly-sized organoids from single cell suspensions
- Consistent gene expression in two high-fidelity ovarian cancer organoid models
- Uniformly-sized ovarian cancer organoids show consistent, reliable drug responses for personalized chemotherapy resistance tests

Cell Organoid
Article
https://doi.org/10.26599/CO.2024.9410005

Crossroad of ovarian cancer organoid culture: Single cell suspension and mechanically sheared fragment

Lanyang Li[1,§], Jiping Liu[1,§], Qi Cao[2,§], Yuqing Zhao[2], Yanghua Shi[1], Chen Wang[1], Jian Zhang[1], Mingjie Rong[1], Xiang Tao[2], Wei Deng[3,4,*], Chunhui Cai[1,*], and Xinxin Han[1,5,*]

[1] *Shanghai Lisheng Biotech, Shanghai 200092, China*
[2] *Obstetrics and Gynecology Hospital of Fudan University, Shanghai, China*
[3] *LongHua Hospital, Shanghai University of Traditional Chinese Medicine, Shanghai 200032, China*
[4] *Department of Oncology, Shanghai Ninth People's Hospital, Shanghai Jiao Tong University School of Medicine, Shanghai 200125, China*
[5] *Organ Regeneration X Lab, LiSheng East China Institute of Biotechnology, Peking University, Nantong 226299, China*
[§] *Lanyang Li, Jiping Liu, and Qi Cao contributed equally to this work.*

Received: 6 February 2024 / **Revised:** 26 March 2024 / **Accepted:** 12 May 2024

ABSTRACT

Ovarian cancer, a common gynecologic tumor, is associated with a high mortality, due to challenges in early detection within the reproductive system. According to our previous research, cultivating patient-specific organoids from mechanically sheared tissues can be utilized for drug response evaluation but has limitations for high-throughput screening efficiency due to their inconsistent size. In this research, we focused on organoids developed from single-cell suspensions to address the critical requirement for uniformity in organoid size. By the day 3 of culture, single-cell suspensions rapidly and spontaneously aggregated into spherical structures with a more consistent size. Notably, the organoids of sample OVA-37 were ten times larger after 8 days of culture. Transcriptomic analysis was used to compare the two organoid culture techniques, demonstrating that the variations between different organoid culture methods were minimal, with higher variability observed among patients. Gene set enrichment analysis (GSEA) revealed only minor discrepancies in specific pathways, such as TGF-β and tight junctions. Furthermore, treatment with carboplatin in a 96-well plate setup resulted in reproducible drug responses, as evidenced by coefficients of variation lower than 40%. This finding suggests that single-cell suspension-cultured organoids can be employed for reproducible high-throughput drug screening. This approach holds potential for personalized drug screening in ovarian cancer and may contribute to the development of novel therapeutic strategies.

KEYWORDS

ovarian cancer, organoid, drug sensitive, personalized medicine

Introduction

Ovarian carcinoma represents a significant fraction of female reproductive system malignancies, posing a global health hazard. Its early detection remains elusive, chiefly due to the indistinct nature of early symptoms, thus complicating the diagnostic process [1]. The disease exhibits a heterogeneity marked by varied histological subtypes and a wide range of molecular expression patterns, which contributes to disparate drug responses and the emergence of drug resistance [2]. The intricate genetic mutation landscape in ovarian cancer presents formidable challenges to efficacious treatments [3]. Personalized treatment strategies, pivotal for enhancing patient outcomes, rely on advanced laboratory techniques that accurately predict individual drug responses [4]. Progress in organoid technology, particularly the development of self-organizing, three-dimensional tissue cultures that emulate the complexity and functionality of *in vivo* tissues, has become indispensable in drug response evaluation. Exploiting patient-derived tumor organoids for identifying potent chemotherapy agents enables personalized medicine to devise treatment regimens congruent with unique genetic and physiological profiles of individuals, potentially augmenting therapeutic efficacy and diminishing adverse effects [5]. Our research, focusing on ovarian cancer within our organoid-based drug screening model, addresses the imperative for more nuanced, precise, and effective treatment methodologies. We have pioneered novel techniques in establishing ovarian cancer organoids, thereby enhancing the relevance of organoid models and facilitating the establishment of high-throughput screening platforms. This approach heralds a promising avenue for personalized oncology treatment.

*Address correspondence to Wei Deng, xxhan@sibs.ac.cn; Chunhui Cai, caichunhui@lishengbiotech.com; Xinxin Han, dengwei@shsmu.edu.cn

Cite this article as Li, L. Y., et al. *Cell Organoid*, **2024**, 1: 9410005.

The generation of patient-specific organoids from tissue fragments is a crucial advancement in personalized healthcare, primarily due to its efficacy in evaluating drug responses [6]. However, this technique faces challenges related to the inconsistent sizes of organoids, which impairs their applicability in high-throughput drug screening [7,8]. Variations in organoid size can lead to inconsistent drug penetration and response, affecting the robustness of results [9]. Phenotypic evaluation of models is complicated by intra- and inter-patient differences in organoid size, cellular heterogeneity, and dynamic responses [10]. Our previous methods, utilizing tissue fragments to cultivate organoids, encountered limitations due to these size inconsistencies, complicating the observation of clear drug responses [6]. The importance of uniform organoid size is underscored, as it ensures consistent drug exposure and more clinically relevant results [9,11,12].

In our research, we have pioneered a novel approach for the cultivation of uniform-sized organoids from single-cell suspensions, a technique particularly advantageous for high-throughput drug screening in ovarian cancer models. This process involves the generation of single-cell suspensions from digested cultured organoids, which subsequently self-organize into organoids of uniform size. We conducted meticulous assessments of their growth and histological attributes, confirming the retention of tissue characteristics similar to those derived from tissue fragment cultures. Notably, these organoids displayed significant responsiveness to drug treatments, as evidenced by comprehensive cell viability assays. Furthermore, when embedded into a matrix gel, these organoids maintained sustained growth and preserved their distinctive features, highlighting the adaptability of our cultivation method, especially for matrix gel-requiring experiments. This approach significantly enhances reproducibility and robustness in chemotherapy drug screening, while also showing immense potential in revolutionizing personalized drug screening for ovarian cancer. It opens a promising path for developing tailored therapeutic strategies, specifically tailored to the nuances of ovarian cancer treatment in the realm of oncological research.

Methods and materials

Tissue collection

The ovarian cancer tissues were obtained after patients' post-surgery. None of the patients underwent chemical therapy prior to surgery. Samples from four patients were utilized for the study. Subsequent to surgery, the ovarian cancer tissues were promptly transported under cryogenic conditions to LiSheng Biotech Co., Ltd., and stored at 4 °C until processing, typically within 3 days.

Mechanically sheared fragment culture

The cancer tissue samples were initially washed in washing solution (LSNO00100201; Shanghai LiSheng Biotech, China) to remove any adherent blood or mucus, with this process repeated three times. Subsequently, the samples were cut into fragments of no more than 3 mm using ophthalmic surgical scissors and cultured in ovarian cancer culture medium (LSTO001004; Shanghai LiSheng Biotech, China) in a 10 cm culture dish. The culture medium was replaced every five days, with half of the medium aspirated and an equivalent volume of fresh culture medium added and mixed by pipetting. For passaging, the organoids and adherent cells were collected using cell scrapers, the supernatant was removed by centrifugation, and the collected organoids were fragmented with scissors to a size of no more than 3 mm. They were then cultured in fresh culture medium and mixed by pipetting. Irregular edges became rounded were saw as a criterion for successful organoid culture. The growth and morphological changes of the organoids were regularly observed using an inverted microscope (DMi1, Leica, USA), and the organoid size and area were measured using Image J software.

Single-cell suspension culture

After successfully culturing organoids from tissue fragments, we aimed to expand the application field of our culture method for high-throughput drug screening by digesting the organoids into single cell suspensions. Then the organoids obtained from fragment organoid culture were collected using cell scrapers and centrifuged to obtain all organoids. The collected organoids were then incubated with Organoid Dissociation Reagent I (LSNO00100501; Shanghai LiSheng Biotech, China) at 37 °C for 15 min. The digested liquid was aspirated repeatedly through 1 mL pipette tips. Digestion was terminated if smooth aspiration was achieved; otherwise, digestion was continued for an additional 10 minutes if there was a noticeable blockage during aspiration. The digested liquid was passed through a cell strainer (352340, Corning, USA) and collected. Any undigested organoids on the cell strainer underwent a second round of digestion for 10 minutes. Subsequently, the liquid from the second digestion was passed through a cell strainer again and centrifuged together with the suspension collected from the first round at 600 g for 10 min. The supernatant was removed, and 2 mL of ovarian cancer culture medium was added and mixed. The mixture was then centrifuged at 600 g for 10 min to completely remove residual digestion solution. Next, 2 mL of ovarian cancer culture medium was added and mixed to prepare the single-cell suspension. 1 ml of the suspension was used for culturing single-cell organoid spheres in a 6-well Clear TC-treated Multiple Well Plates (3516, Corning Incorporated, USA). The remaining 1 mL was added to 3 mL of ovarian cancer culture medium, mixed, and evenly distributed into 96-well Clear Round Bottom Ultra-Low Attachment Microplate (7007; Corning Incorporated, USA) for single cell automatically assembly observation experiments. The growth and morphological changes of the organoids in 96-well microplate were regularly observed through a stereo microscope (YZ39; ShanghaiYuehe, China).

Embedding organoidsin matrigel

The Matrigel Matrix (354263, Corning, China) was placed on ice and liquefied by incubating at 4 °C for 1 h. The organoid suspension was mixed with the liquefied Matrigel at a 3:2 ratio. The mixture was placed in a 10 cm culture dish and allowed to solidify in a 37 °C incubator, then supplemented with culture medium for continued cultivation. The growth and morphological changes of the organoids were regularly observed using an inverted microscope (DMi1, Leica, USA).

Hematoxylin and eosin (H&E) staining

Organoids were fixed in 4% formaldehyde (BL539A, Biosharp, China) for 24 h and embedding with Tissue-Tek O.C.T. compound (4583, Sakura Finetek, USA). 10 μm thick sections were then obtained using a cryostat microtome (CM 1950, Leica,

USA) and stained with hematoxylin solution (BL700A, Biosharp, China) for 5 min. Excess stain was removed by washing with distilled water, and the sections were differentiated in a H&E differentiate solution (G1862, Solarbio, China) for 10 s, followed by a 2-min rinse in running tap water. Eosin staining solution (BL700B, Biosharp, China) was then added for react 30 s. Finally, the sections were mounted with neutral balsam (G8593, Solarbio, China) and subjected to image acquisition through upright microscope (YI21, ShanghaiYuehe, China).

RNA sequencing

Organoid samples were collected and immediately submerged in TRIzol Reagent (15596018, ThermoFisher, USA) for RNA stabilization. The samples were then stored at – 80 °C until further processing. The samples were then sent to Honsun, a sequencing company, in dry ice for RNA extraction and sequencing. Honsun performed the RNA extraction and subsequent RNA sequencing using their established protocols and equipment. The raw sequencing data obtained from Honsun was further analyzed. RNA expression levels were quantified using fragments per kilobase transcript mapped reads per million (FPKM). The data was processed using R and Morpheus online software to perform differential gene expression analysis and other relevant analyses.

Drug treatment

The organoids cultured in a 96-well plate were used to drug treatment. Organoids were treated with different concentrations (0, 5, 25, and 50 μmol/L) of paclitaxel injection (H20067345; Taxus Pharma, China) and carboplatin injection (HJ20171063, Corden Pharma Latin a S.P.A., Italy), with each treatment group having 4 replicates to reduce random error. On Day 8, additional drug was added to maintain continuous treatment. Regular monitoring was conducted to record organoid growth and morphological changes. CellTiter-Glo®3D Cell Viability Assay (G9683, Promega, USA), as per the manufacturer's instructions, was used to assess cell viability to evaluate the efficacy of drug treatment.

Statistical analysis

The data were collected from three or more replicates, and data are presented as mean ± standard deviation from independent experiments. Statistical analysis was performed using GraphPad 8.

Results

Organoids derived from mechanically sheared tissue fragments and single-cell suspensions exhibit comparable characteristics

In our preceding study, we established that organoids derived from small tissue fragments closely resemble native tissues.[6] However, the significant size variability of these organoids, often exceeding 3mm in diameter, presented challenges for high-throughput drug screening in standard 96 or 384 well plates. To overcome this, we refined our culture technique to produce organoids suitable for high-throughput applications (Fig. 1a). This refinement involved enzymatically digesting organoids from tissue fragments to create single-cell suspensions for subsequent organoid cultures. Regular monitoring showed consistent organoid growth, and their structural integrity was verified via H&E staining. Remarkably, we observed that within 8 days, single cells in the culture medium spontaneously formed compact organoids (Figs. 1b and 1c), indicating the success of our modified method in maintaining key organoid characteristics suitable for high-throughput analysis. Over time, we observed increased adhesion among organoids from sample OG-OVA-37 through our microscopic observations of brightfield images. H&E staining corroborated that both the original and modified methods yield organoids with comparable histological structures (Fig. 1d)

The RNA-seq sequencing results, analyzed through principal component analysis (PCA) and correlation studies, distinctly highlight that inter-patient sample variability supersedes the differences attributable to the organoid culture methods (Figs 2.a and 2b). Particularly, the OG-OVA-39 and OG-OVA-40 samples displayed notable similarities. Our in-depth heatmap analysis of gene expression profiles across both single-cell suspension and mechanically sheared fragment methods revealed remarkable transcriptional congruence, particularly in genes with high and low expression levels (Fig. 2c). This striking similarity underscores the effectiveness of both methodologies in preserving the heterogeneity inherent in ovarian cancer tissue, a critical aspect for realistic disease modeling. Differential gene expression analysis further supported this, as no significant variations were observed in key pathways between the two methods. This is particularly evident in cell cycle pathways, pivotal in the tumorigenesis and progression of ovarian cancer. The lack of significant fold change differences (Fig. 2d) between the two methods not only affirms their individual efficacy but also suggests that organoids derived from single-cell suspensions are equally capable of simulating the authentic pathological state of ovarian cancer, akin to the previously validated minced tissue method. Our further gene set enrichment analysis (GSEA) transcriptome pathway analysis suggested enhanced TGF-β signaling and tight junction pathways in organoids derived from minced tissue compared to single-cell suspensions. This can be attributed to the preserved tissue architecture and cellular dynamics in minced tissue-derived organoids, which likely support more robust cell-cell and cell-matrix interactions, essential for pathways such as TGF-β and tight junctions. TGF-β signaling, vital for cell differentiation, proliferation, and apoptosis, is influenced by the structural integrity of the microenvironment [13,14]. Similarly, tight junction pathways, crucial for maintaining cellular polarity and barrier functions, depend on the physical organization of cells [15]. Conversely, organoids from single-cell suspensions, lacking this initial complex structure, rely on the self-organizing capacity of individual cells, potentially leading to less pronounced TGF-β and tight junction signaling. Thus, the stronger signals in minced tissue-derived organoids underscore the significant influence of tissue architecture and cellular interactions on these pathways, highlighting the importance of the organoid derivation method in accurately modeling disease pathology and cellular behavior (Fig. 2e).

Optimizing uniform organoid formation from single-cell suspensions for high-throughput screening

In high-throughput drug screening, the use of 96- or 384-well plates is crucial for testing multiple drugs across varied concentrations. Assessing whether single-cell suspensions could form organoids within 96-well plates was essential for integrating this method into high-throughput screening. Upon seeding single-

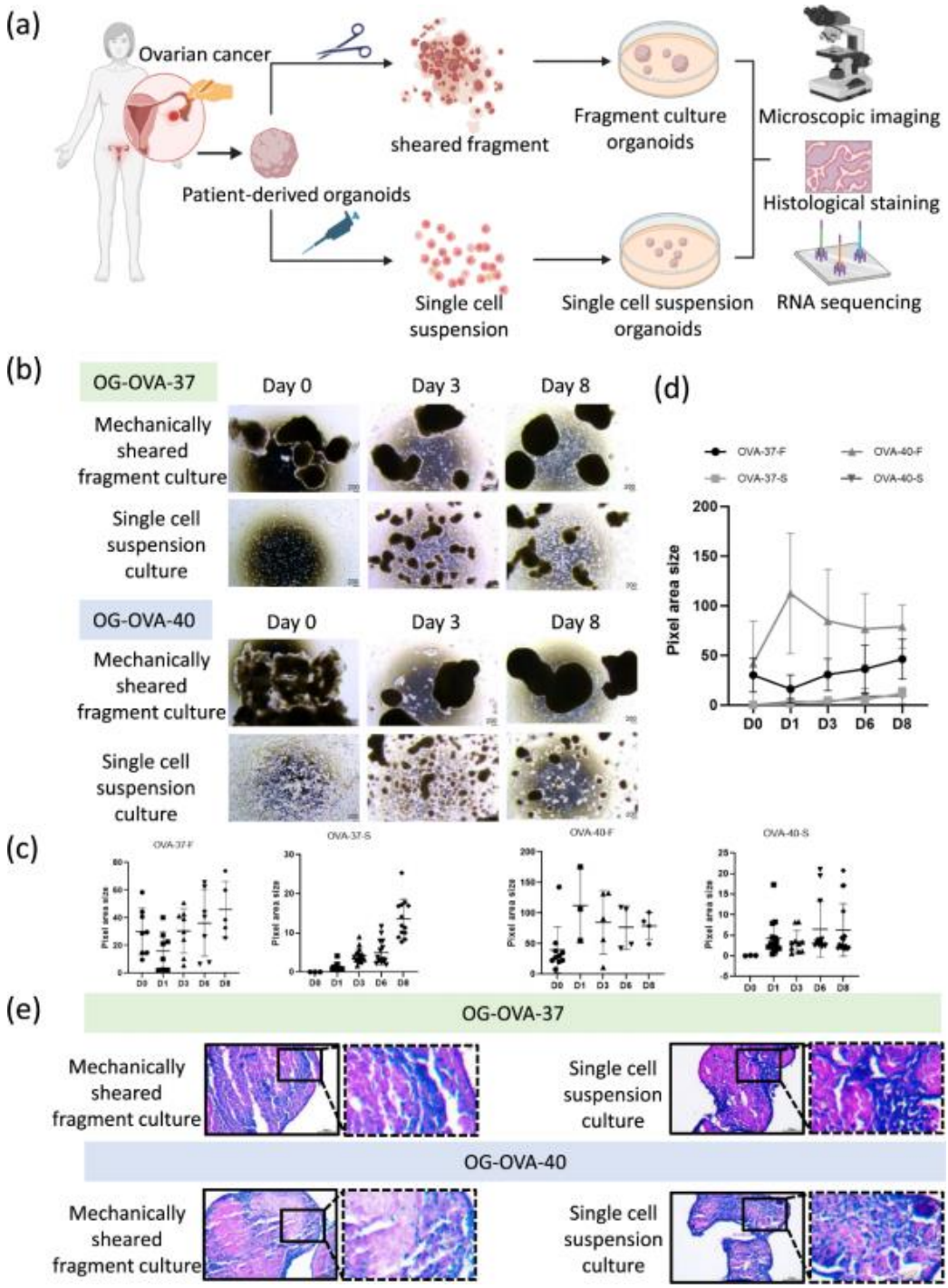

Figure 1. Comparative analysis of ovarian cancer organoid cultivation methods. (a) Diagram illustrating the methodology for generating organoids from single-cell suspensions versus mechanically sheared fragments, highlighting procedural differences. (b) Brightfield microscopy visualization of ovarian cancer organoids 8 days post-culture, with scale bars for size reference. (c) Quantitative results of organoid size evolution over time, utilizing brightfield imaging to document growth dynamics across culture methods. The *y*-axis represents the pixel area size calculated from ImageJ, while the *x*-axis indicates the number of days in culture. The F denotes the fragment culture method, while S represents the single cell suspension culture method. (d) Quantitative comparison of organoid size evolution over time, utilizing brightfield imaging to document growth dynamics across culture methods. (e) Histological comparison via H&E staining of organoids derived from each method, demonstrating morphological consistency with scale bars provided.

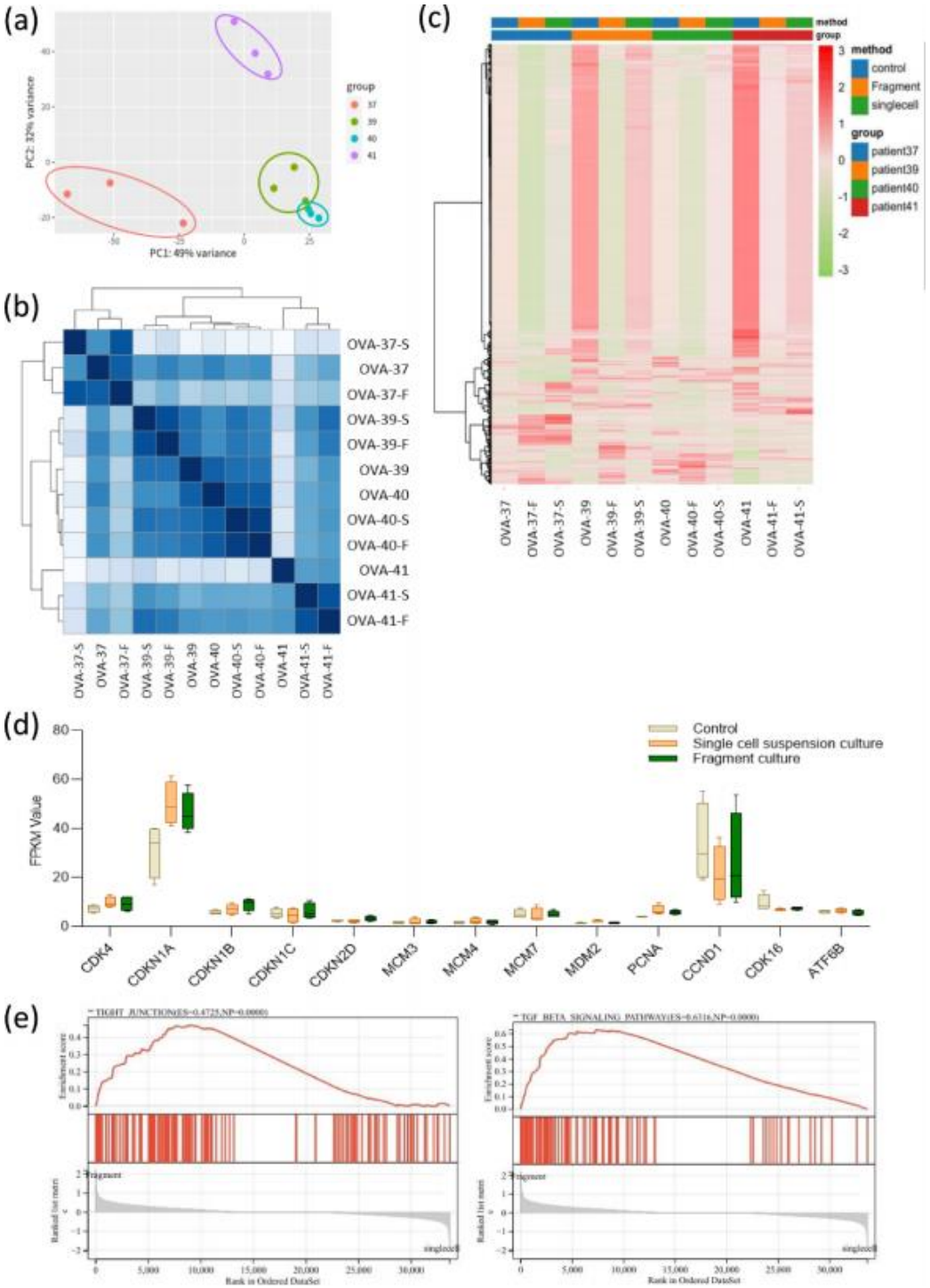

Figure 2. Transcriptomic profiling of ovarian cancer organoids cultured by different methods. (a) PCA showcasing the distinct genomic landscapes of organoids derived from single-cell suspensions and mechanically sheared fragments, with clustering by patient sample origin. (b) Sample correlation matrix highlighting the relationship between organoid culture methods, where intensity of color correlates with the degree of transcriptomic similarity. (c) Heatmap displaying differential gene expression patterns across samples, with normalization of raw counts to TPM and subsequent Z-score transformation for direct comparison. (d) Expression analysis of pivotal genes within cell cycle pathways, comparing their relative expression levels across the two organoid culture techniques. (e) GSEA revealing pathway variances between organoids derived via single-cell suspension and mechanical shearing, underscoring methodological impact on cellular function.

cell suspensions, derived from digested organoids, into 96-well plates (Fig. 3a), our daily monitoring identified that cells settled at the well bottoms and spontaneously formed spherical structures with defined boundaries (Figs.3d and 3e). Comparatively, mechanical shearing of OVA-41 organoids into fragments followed by seeding in 96-well plates resulted in uneven organoid formation and size distribution. In stark contrast, single-cell suspension-derived organoids demonstrated superior uniformity in size, although initial seeding density influenced some variation (Fig. 3b). Quantitative analysis of organoid sizes further validated that single-cell derived organoids maintained a more consistent size profile than those from pre-formed fragments (Fig. 3c).

Evaluating carboplatin efficacy on ovarian cancer organoids within a high-throughput screening framework

Investigating carboplatin efficacy on ovarian cancer organoids, derived from single-cell suspensions, we conducted a meticulous evaluation within a 96-well plate framework. Organoids were exposed to carboplatin concentrations reflective of clinical application. Due to the CellTiter-Glo® 3D Cell Viability Assay's reliance on consistent input amounts across different wells for reliable results, the size variability of the minced tissue culture method in input material precludes its reliable use for drug testing. Over 14 days, organoid morphology was closely monitored, revealing no significant alterations within the initial six-day period. Subsequently, a discernible onset of peripheral disintegration was observed, intensifying by day 14, particularly at 50 μmol/L carboplatin concentration (Fig. 4b). This structural degradation contrasted markedly with the untreated controls. Intriguingly, a concentration-dependent biphasic response was noted. At 5μM, an unexpected augmentation in metabolic activity suggested a stimulatory carboplatin effect, which subsided with increasing concentrations, yielding to a predominant cytotoxic impact (Figs.4c and 4d). Crucially, the reproducibility of these findings was affirmed across organoids derived from individual patients. Consistent drug-response patterns were observed in quadruplicate wells at each concentration, with coefficient of variation (CV) values aligning with the standards for high-throughput screening (Fig. 4c). This consistency demonstrates the robustness of these patient-specific organoids as a viable platform for high-throughput pharmacological screening.

Synergizing single-cell suspension cultivation with Matrigel embedding for enhanced organoid growth and analysis

Next, we explored the growth dynamics of organoids derived from single-cell suspensions in matrix gels, particularly focusing on Matrigel, a composite of extracellular matrix components like laminin and collagen IV, enriched with growth factors. Traditional organoid cultivation often employs Matrigel embedding of stem cells, which, while facilitating detailed longitudinal observations, might limit cellular heterogeneity compared to self-assembling organoids from single-cell suspensions. To optimize this process, we developed a novel hybrid technique. Initially, organoids are cultivated from single-cell suspensions to promote diverse cellular representation. Subsequently, these organoids are embedded in Matrigel,enabling their sustained growth and detailed monitoring (Fig. 5a). This approach has the potential to synergize the cellular diversity of self-assembly with the observational advantages of Matrigel embedding.

To assess the influence of Matrigel on organoid morphology, we performed histological analyses on organoids post-15 days of Matrigel embedding compared to those maintained in suspension (Figs.5b and 5c). Our results indicated no significant morphological differences between the two conditions, suggesting that Matrigel embedding does not compromise the intrinsic structural integrity of the organoids.

Discussion

In this study, we have not only optimized single-cell derived organoid technology for high-throughput screening applications but also bridged this approach with conventional matrix gel-based organoid culture methods. This integration facilitates the amalgamation of various technical advantages, offering an optimized strategy for personalized therapeutic screening in ovarian cancer.

Our findings underscore the importance of adapting 96-well and 384-well plate formats for drug testing, given their suitability for high-throughput applications. The ability of single-cell suspensions to form uniformly sized organoids in these plates and their responsiveness to drug treatment is a critical advancement in organoid-based drug screening methodologies. Moreover, the uniform size and consistent growth patterns of these organoids address previous limitations in organoid cultivation, enhancing the reliability of drug response assessments.

While our RNA-seq analysis indicates that mechanically fragmented tissue-derived organoids exhibit higher TGF-β pathway expression, suggesting a closer mimicry of the original tissue' s microenvironment, this does not diminish the value of single-cell suspension-derived organoids. The latter's utility in representing a physiologically relevant model for drug discovery, especially in the realm of immunotherapy, is noteworthy. Further investigations are needed to explore the potential benefits of mechanically fragmented organoids in immune-related drug screening.

Overall, this research paves the way for personalized medicine in ovarian cancer treatment, potentially improving patient outcomes. By offering a physiologically relevant platform for drug discovery and development, this approach could lead to the identification of novel therapeutic targets, customization of therapy, and reduction of adverse effects, thereby enhancing treatment efficacy for ovarian cancer and other diseases.

Research ethics and patient consent

This study adhered to the ethical standards set forth by the Obstetrics and Gynecology Hospital of Fudan University. Informed consent was obtained from all patients prior to collecting their samples, and they were made aware of the intention to use their samples for future research. Participants were enrolled in the study only after providing their informed consent, thereby ensuring voluntary involvement. The research was granted ethical approval under the number kyy2023-06.

Availability of data and material

The data and materials that support the findings of this study are available upon request from the corresponding author.

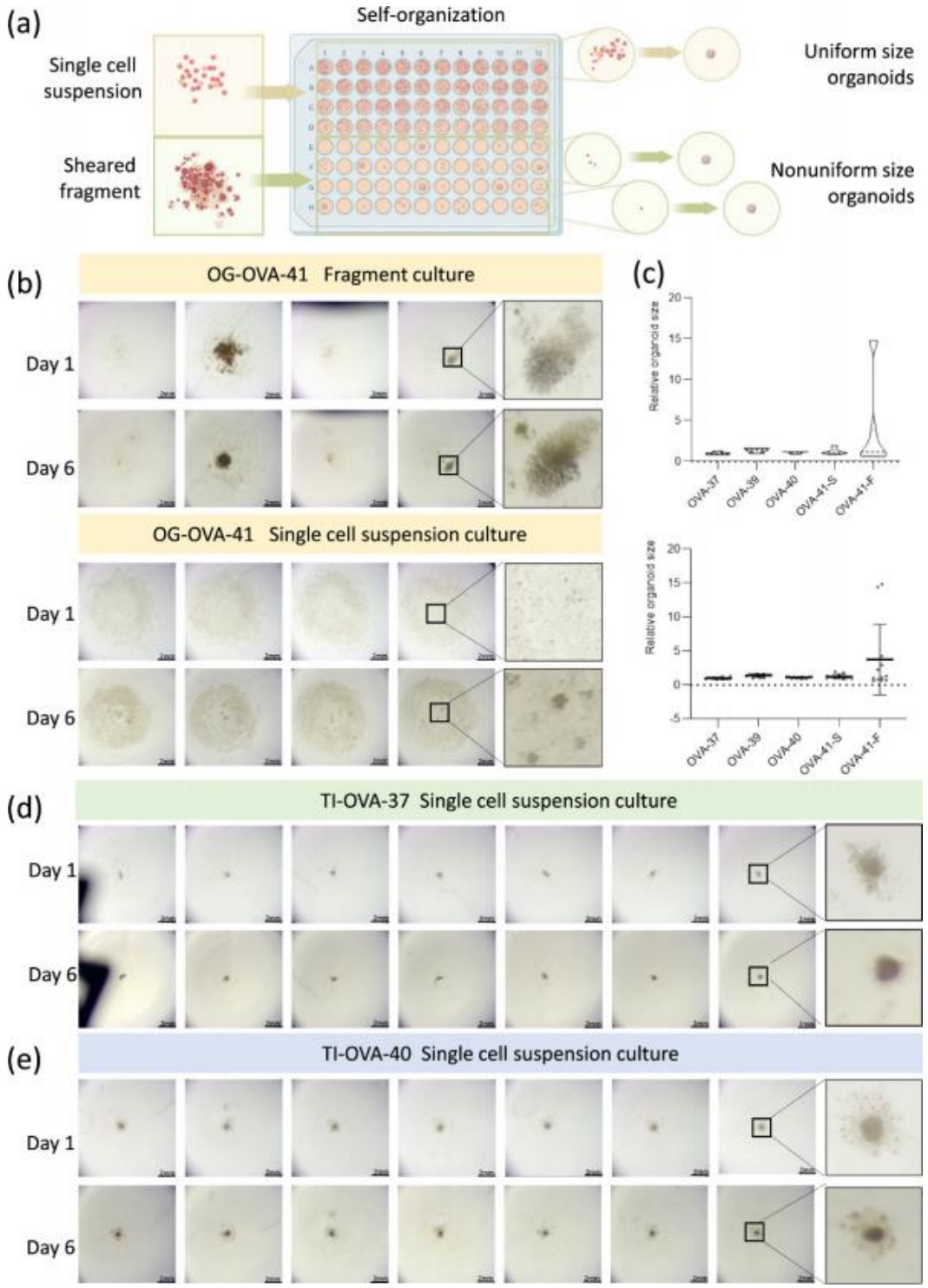

Figure 3. Establishment and growth dynamics of ovarian cancer organoids in 96-well plates. (a) Detailed schematic showcasing the formation process of organoids from single-cell suspensions within the microenvironments of 96-well plates, emphasizing the self-aggregation mechanism. (b) High-resolution brightfield microscopy images displaying the comparative growth patterns of ovarian cancer organoids, cultured from single-cell suspensions and tissue fragmentation methods, at day 6, with the OG-OVA-41 sample serving as a case study. (c) Quantitative image analysis to evaluate the size uniformity of organoids developed from single-cell suspensions, underscoring the methodological advantages in promoting consistent organoid formation.

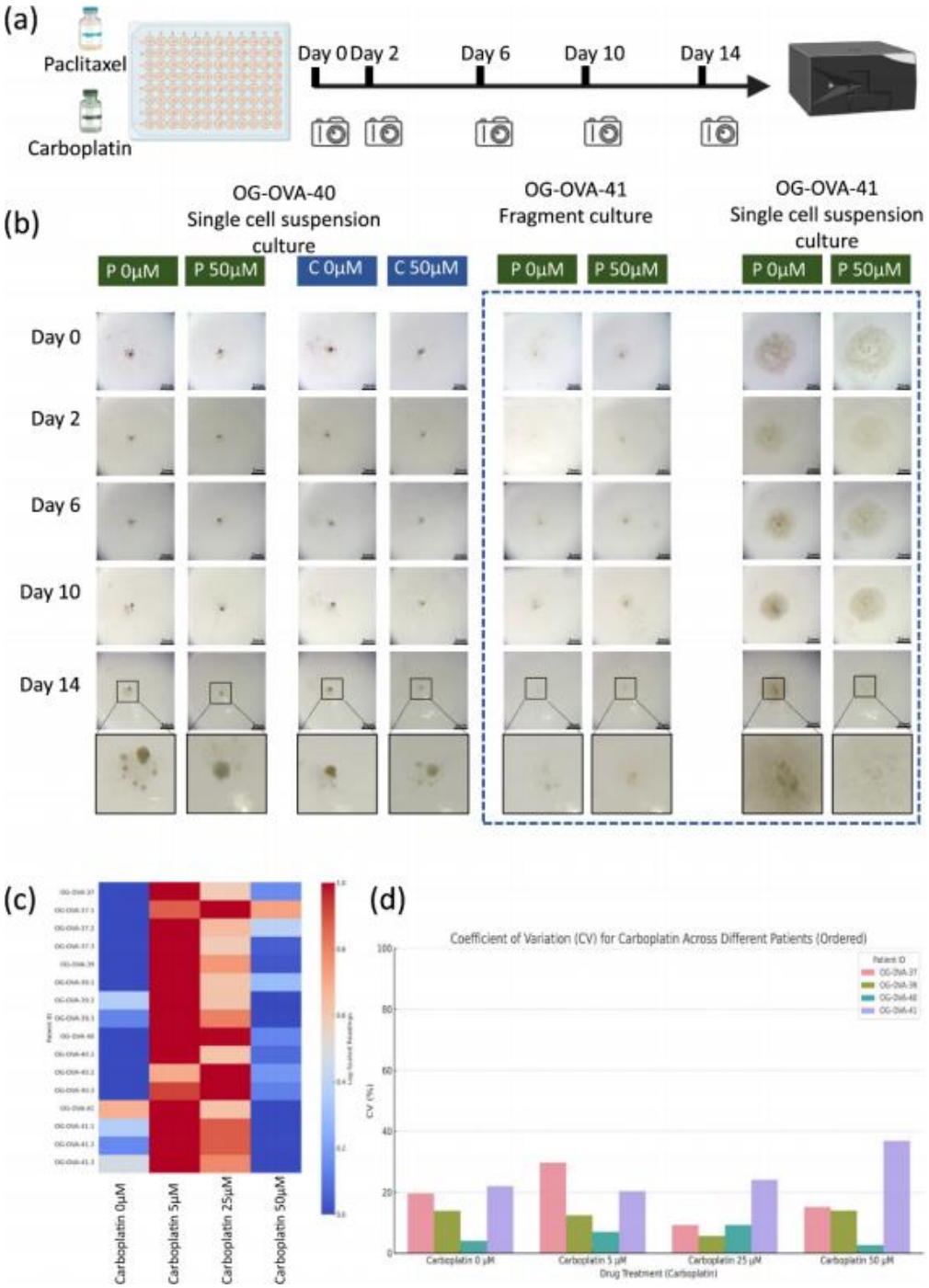

Figure 4. Organoid responses to chemotherapeutic treatment. (a) Detailed schematic outlining the protocol for administering drug treatment to organoids, highlighting key observation intervals for assessing cellular health and viability. (b) Comparative brightfield microscopy visuals of ovarian cancer organoids post-chemotherapy, emphasizing the differential impact of treatment on organoids cultured via single-cell suspensions and those from tissue fragments. (c) A heatmap illustrating the quantitative cell viability, as indicated by log-transformed luminescence intensities, across varying concentrations of carboplatin, with data from quadruplicate samples underlining the consistency of response. (d) Analysis of variability in carboplatin response, presented as CV, across organoids derived from different patient samples, demonstrating the assay's reliability for drug sensitivity testing.

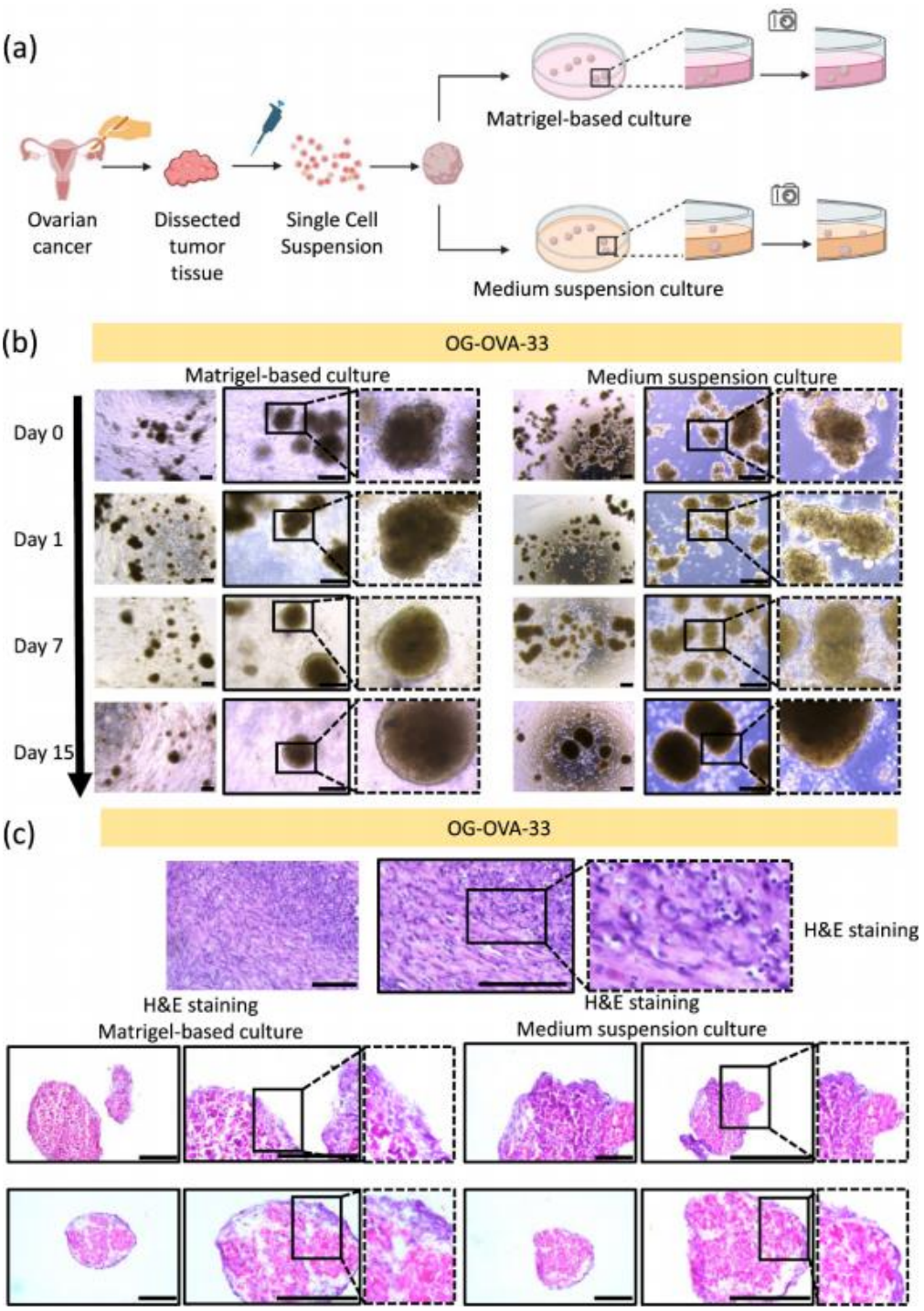

Figure 5. Cultivation dynamics of single cell suspension-derived organoids in varied environments. (a) Detailed schematic showcasing the methodology for continued cultivation of single-cell derived organoids, comparing suspension cultures against matrix gel environments. (b) Brightfield microscopy provides a visual comparison of organoid growth and morphology in suspension versus matrix gel conditions, with precise scale measurement for accurate size assessment. (c) Comparative histological analysis using H&E staining highlights the structural integrity and cellular detail of organoids cultivated under both conditions, with scale bars ensuring consistent magnification across samples.

Declaration of conflicting interests

This work was sponsored by Shanghai Lisheng Biotech Ltd (Lisheng). The manuscript was written in a responsible and ethical manner. X.X.H. is a shareholder of Lisheng, as a founder. Y.H.S., L.Y.L., C.W., J.Z., M.J.R., J.P.L and C.H.C. are senior scientists of Lisheng. All authors declare no competing financial interests.

X.X.H. and C.H.C., both members of the Editorial Board for Cell Organoid, have abstained from any roles in the journal's evaluation, review, or decision-making processes regarding this manuscript to ensure impartiality.

Funding

The work was supported by the National Natural Science Foundation of China (Nos. 82374506 and 32200581)

Author contributions

C.H.C. and X.X.H. conceived and designed the study. L.Y.L. Q.C., Y.Q.Z., X.T., C.W., J.Z., Y.H.S., and M.J.R. were responsible for sample collection and experimental procedures. J.P.L. conducted the analysis of the RNA sequencing data. L.Y.L., Q.C., D.W., C.H.C. and X.X.H. wrote the manuscript. All authors reviewed and approved the final version of the manuscript.

References

[1] Forstner, R. Early detection of ovarian cancer. *European Radiology*, **2020**, 30(10): 5370–5373. https://doi.org/10.1007/s00330-020-06937-z

[2] Xie, W. W., Sun, H. Z., Li, X. D., Lin, F. K., Wang, Z. L., Wang, X. P. Ovarian cancer: Epigenetics, drug resistance, and progression. *Cancer Cell International*, **2021**, 21(1): 434. https://doi.org/10.1186/s12935-021-02136-y

[3] Konstantinopoulos, P. A., Matulonis, U. A. Clinical and translational advances in ovarian cancer therapy. *Nature Cancer*, **2023**, 4(9): 1239–1257. https://doi.org/10.1038/s43018-023-00617-9

[4] Matsui, T., Shinozawa, T. Human organoids for predictive toxicology research and drug development. *Frontiers in Genetics*, **2021**, 12: 767621. https://doi.org/10.3389/fgene.2021.767621

[5] Granat, L. M., Kambhampati, O., Klosek, S., Niedzwecki, B., Parsa, K., Zhang, D. The promises and challenges of patient-derived tumor organoids in drug development and precision oncology. *Animal Models and Experimental Medicine*, **2019**, 2(3): 150–161. https://doi.org/10.1002/ame2.12077

[6] Cao, Q., Li, L. Y., Zhao, Y. Q., Wang, C., Shi, Y. H., Tao, X., Cai, C. H., Han, X. X. PARPi decreased primary ovarian cancer organoid growth through early apoptosis and base excision repair pathway. *Cell Transplantation*, **2023**, 32. https://doi.org/10.1177/09636897231187996

[7] Kondo, J., Inoue, M. Application of cancer organoid model for drug screening and personalized therapy. *Cells*, **2019**, 8(5): 470. https://doi.org/10.3390/cells8050470

[8] Jung, Y. H., Park, K., Kim, M., Oh, H., Choi, D. H., Ahn, J., Lee, S. B., Na, K., Min, B. S., Kim, J. A. et al. Development of an extracellular matrix plate for drug screening using patient-derived tumor organoids. *BioChip Journal*, **2023**, 17(2): 284–292. https://doi.org/10.1007/s13206-023-00099-y

[9] Mahbubi, R., Yousefi, N., Hamidieh, A., Gholizadeh, F., Sisakht, M. M. Tumor organoid as a drug screening platform for cancer research. *Current Stem Cell Research & Therapy*, **2023**, 19(9): 1210–1250. https://doi.org/10.2174/011574888X268366230922080423

[10] Spiller, E. R., Ung, N., Kim, S., Patsch, K., Lau, R., Strelez, C., Doshi, C., Choung, S., Choi, B., Juarez Rosales, E. F. et al. Imaging-based machine learning analysis of patient-derived tumor organoid drug response. *Frontiers in Oncology*, **2021**, 11: 771173. https://doi.org/10.3389/fonc.2021.771173

[11] Zhou, Z. L., Cong, L. L., Cong, X. L. Patient-derived organoids in precision medicine: Drug screening, organoid-on-a-chip and living organoid biobank. *Frontiers in Oncology*, **2021**, 11: 762184. https://doi.org/10.3389/fonc.2021.762184

[12] Wijler, L., Mateos, J. G., Nguyen, M., Staes, A. A. L., van Seters, L., Hasan, L. A., Tiroille, V., Herpers, B., Price, L., Madej, M. et al. Abstract 198: Pan-cancer assay-ready organoid drug screening with robust, reproducible and clinically-relevant output. *Cancer Research*, **2023**, 83(7_Supplement): 198. https://doi.org/10.1158/1538-7445.AM2023- 198

[13] Yan, Y. T., Liu, J. L., Lawrence, A., Dykstra, M. J., Fannin, R., Gerrish, K., Tucker, C. J., Scappini, E., Dixon, D. Prolonged cadmium exposure alters benign uterine fibroid cell behavior, extracellular matrix components, and TGFB signaling. *The FASEB Journal*, **2021**, 35(8): e21738. https://doi.org/10.1096/fj.202100354r

[14] Pickup, M. W., Owens, P., Moses, H. L. TGF-β, bone morphogenetic protein, and activin signaling and the tumor microenvironment. *Cold Spring Harbor Perspectives in Biology*, **2017**, 9(5): a022285. https://doi.org/10.1101/cshperspect.a022285

[15] Nehme, Z., Roehlen, N., Dhawan, P., Baumert, T. F. Tight junction protein signaling and cancer biology. *Cells*, **2023**, 12(2): 243. https://doi.org/10.3390/cells12020243

Cell Organoid
Article
https://doi.org/10.26599/CO.2024.9410003

An advanced culture methodology suitable for the self-assemble and tissue-fragment derived intrahepatic cholangiocarcinoma organoids

Authors

Chen Wang, Ao Huang, Yanghua Shi, Jiping Liu, Lanyang Li, ..., Xin Zhang*, Chunhui Cai*, Xinxin Han*

Correspondence

Xin Zhang, zhang.xin3@zs-hospital.sh.cn;
Chunhui Cai, caichunhui@lishengbiotech.com;
Xinxin Han, xxhan@sibs.ac.cn

In Brief

We have established an efficient and rapid ICC organoid model that recapitulates and maintains the disease characteristics of ICC *in vitro*. Bulk RNA–seq revealed the presence of viable immune cells in this organoid model, which was not observed in previous established ICC organoid models. Our work provides a novel model for studying immunotherapeutic approaches in ICC.

Graphical abstract

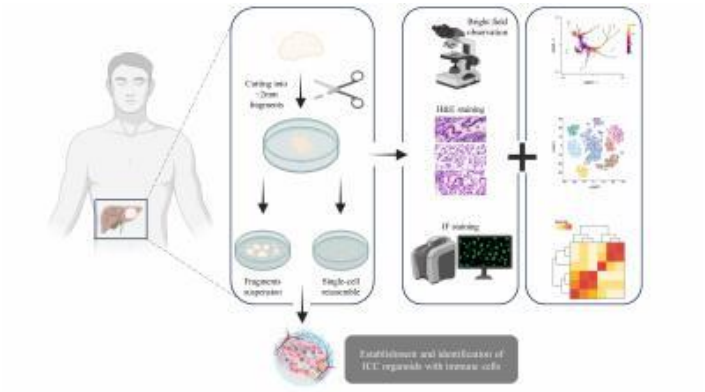

Highlights

- An advanced and user–friendly organoid culture methodology
- Consistent genome stability and gene expression profiles throughout the culture process
- Potential for high–throughput drug screening without reliance on matrigel

LISHENG 上海礼升生物 Shanghai Lisheng Biotech

Cell Organoid

Article

https://doi.org/10.26599/CO.2024.9410003

An advanced culture methodology suitable for the self-assemble and tissue-fragment derived intrahepatic cholangiocarcinoma organoids

Chen Wang[1,§], Ao Huang[2,3,§], Yanghua Shi[1], Jiping Liu[1], Lanyang Li[1], Jian Zhang[1], Mingjie Rong[1], Xin Zhang[2,3,*], Chunhui Cai[1,*], and Xinxin Han[1,4,*]

[1] Shanghai Lisheng Biotech, Shanghai 200092, China
[2] Department of Liver Surgery and Transplantation, Liver Cancer Institute, Zhongshan Hospital, Fudan University; Key Laboratory of Carcinogenesis and Cancer Invasion of Ministry of Education, Shanghai 200032, China
[3] Research Unit of Liver cancer Recurrence and Metastasis, Chinese Academy of Medical Sciences, Beijing 100010, China
[4] Organ Regeneration X Lab, LiSheng East China Institute of Biotechnology, Peking University, Nantong 226299, China
[§] Chen Wang and Ao Huang contributed equally to this work.

Received: 2 February 2024 / **Revised:** 3 April 2023 / **Accepted:** 12 May 2024

ABSTRACT

Intrahepatic cholangiocarcinoma (ICC) is a highly lethal malignancy associated with significant morbidity, necessitating the urgent development of an effective chemotherapeutic assay for ICC patients. In this study, we have successfully established an advanced culture method for ICC organoids that can be utilized with both single-cell assembly and tissue fragmentation initiation techniques. These ICC organoids maintain the morphological characteristics, including mutation profiles and frequency (46.9% in organoid and 48.5% in tumor tissue) of *IDH1* genes, and 1733 high-frequent overlapped mutated genes (94.2%). Additionally, ICC biomarkers such as CK7 and CK19 also maintain a similar pattern compared with the original tissue. Furthermore, RNA-seq analysis reveals upregulation of immune-related genes in single-cell assembly organoids. The significantly changed genes including *IL9R* (4.4-fold), *IL2RB* (3.2-fold), *CCR4* (3.5-fold), *TESPA1* (4.4-fold), *ZAP70* (4.3-fold) and *CD6* (4.3-fold) in log scale. These evidence both indicating the presence of viable and active immune cells. Overall, our findings present an advanced and user-friendly culture approach for generating ICC organoids adaptable to diverse experimental objectives.

KEYWORDS

intrahepatic cholangiocarcinoma, organoid, culture methodology

Introduction

ICC (intrahepatic cholangiocarcinoma) is one of the most lethal liver cancers, and the overall 5-year survival rate for patients after surgery is only around 9%[1]. Moreover, the incidence and mortality of ICC are increasing rapidly, endangering the lives and health of patients[2]. The most efficient therapy for ICC patients is curative-intent surgical resection; however, the 5-year overall survival rate after surgery is only 20%–35%[3]. Because of this, chemotherapy plays a critical role in ICC treatment, but the efficacy of drugs such as gemcitabine and oxaliplatin varies among different patients[4–8]. Therefore, it is important to establish a fast and precise drug testing method for clinical treatment.

Unfortunately, analysis of drug response features and biomarker investigation for precision therapy in patients with ICC is still lacking. Patient-derived organoids (PDOs) have been established and utilized in research related to clinical cancer treatment in recent studies, including liver, colon, and pancreas cancers[9–11]. However, these matrigel-based organoid culture methods are relatively difficult to handle for beginners, limiting their application in clinical therapy. While matrigel-based organoids can reflect molecular features of origin tissues, the small volume of single-cell derived organoids makes it difficult to reflect millimeter-scale morphological features accurately. Therefore, a more advanced culture method is needed for clinical treatment and scientific research purposes.

Here, we present an advanced robust ICC organoid culture method that is compatible with both single-cell derived and tissue-fragment derived organoids. Tissue-fragment derived organoids maintain morphology features due to their relatively large volume (millimeter scale). Both types of organoids maintain gene

*Address correspondence to Xin Zhang, zhang.xin3@zs-hospital.sh.cn; Chunhui Cai, caichunhui@lishengbiotech.com; Xinxin Han, xxhan@sibs.ac.cn

Cite this article as Wang, C., et al. *Cell Organoid*, **2024**, 1: 9410003.

expression profiles compared with public ICC data, suggesting their high–throughput drug screening potential.

Methods and materials

Tissue collection

The ICC tumor tissues were obtained from patients undergoing clinical surgery. Samples from four patients were utilized for this study. If necessary, samples were temporarily stored at 4 °C until processed.

Microscopy observing

Daily observations were performed using an inverted microscope (DMi1, Leica, USA), and immunofluorescence was observed with a fluorescence microscope (K5, Leica, USA).

Culture of tissue-fragment derived organoids

ICC tumor tissues were washed at least 3 times with a washing solution (LSNO00100201, Shanghai LiSheng Biotech, China), then fragmented into diameters of 0.5–2 mm using scissors. Tissue–fragment derived organoids were collected and resuspended in medium (LSTO01000403, Shanghai LiSheng Biotech, China), then transferred into 10 cm dishes. The medium was semi–replaced every week. The information of washing solution and medium can be found on the website: http://www.sh–lise.com

Culture of single-cell derived organoids

Tissue–fragment derived ICC organoids were collected after 7–14 days and then digested into single cells using Organoid Dissociation Reagent I (LSNO00100501, Shanghai LiSheng Biotech, China) at 37 °C for 15–45 min. When the volume of organoids decreased by half, the digestion liquid was filtered with a 40 μm cell strainer (352340, Corning, USA) and centrifuged at 600× *g* for 10 min. The supernatant was removed and 2 mL of medium was added to resuspend the cells. The cells were centrifuged again at 600× *g* for 10 min and then resuspended in 1 mL of medium. Finally, the cells were cultured in Clear TC–treated Multiple Well Plates (3516, Corning Incorporated, USA).

Hematoxylin and Eosin (H&E) staining

Organoids were fixed with 4% formaldehyde (BL539A, Biosharp, China) for at least 24 h and embedded in Tissue–Tek O.C.T. compound (4583, Sakura Finetek, USA). Samples were sectioned into 10 μm slices using a cryostat microtome (CM 1950, Leica, USA). The sections were stained with hematoxylin solution (BL700A, Biosharp, China) for 5 min and eosin staining solution (BL700B, Biosharp, China) for 30 s. Finally, the sections were mounted with neutral balsam (G8593, Solarbio, China) and observed under a microscope (YI21, Shanghai Yuehe, China).

Immunofluorescence

Sections were permeabilized with PBS+0.25% TritonX–100 buffer for 20 min at room temperature, followed by blocking with a blocking buffer (E674004, BBI Life Science, China). Rabbit anti–CK7 (ab68459, Abcam, USA) and CK19 (ab76539, Abcam, USA) primary antibodies were diluted at a ratio of 1:200 and incubated with the sections overnight at 4 °C. The sections were then washed five times using 0.125% phosphate buffered saline with Tween 20 (PBST) and incubated with a secondary Cy3 antibody (711–165–152, Jackson ImmunoResearch Laboratories Inc., USA) diluted at a ratio of 1:500. Nuclei were stained with DAPI (diluted at a ratio of 1:1000). Fluorescence images were acquired using a Leica K5 microscope.

Whole exome sequencing

For each sample, 200 ng of genomic DNA was shared with 150–200 bp fragments to construct libraries. The whole exome was captured using AIExome® Human Exome Panel V3 with TargetSeq One® Hyb & Wash Kit v2.0 (iGeneTech Co., Ltd, Beijing, China) and sequenced on DNBSEQ–T7 with 150–bp reads.

RNA sequencing

RNA Isolation Kit (DP451, TIANGEN, China) was used to isolate cellular mRNA. The RNA concentration was measured using a Qubit4 fluorometer. Reverse transcription was performed using an RT Kit (KR118, TIANGEN, China) and libraries were generated using an RNA Library Prep Kit (E7530L, NEB, USA). Both libraries were sequenced on DNBSEQ–T7 with PE–150 bp reads for subsequent analysis.

Statistical analysis

Angle degree and size of organoids were measured with ImageJ and data analysis was performed using Prism software. All data are expressed as mean ± standard deviation. Expression level of immune genes was measured with TPM value, and visualized with Omicshare website tool. Mutations from WES were annotated with ANNOVAR. TPM value was generated with Salmon, and clustered with factoextra package, and DEGs were found with DESeq2. GO analysis were performed with ClusterProfiler website tool.

Results

Establishment and identification of tissue-fragment derived ICC organoids

We obtained primary tumor tissue from patients with intrahepatic cholangiocarcinoma (ICC) and generated ICC organoids using two distinct methodologies: single–cell isolation and tissue fragmentation (Fig. 1a). For the generation of tissue–fragment derived organoids, patient tissues were mechanically dissected into fragments measuring approximately 0.5–2 mm in diameter using surgical scissors, followed by suspension culture in a specialized medium. In contrast, for the production of single–cell derived organoids, patient tissues were enzymatically digested to obtain individual cells which were subsequently cultured under suspension conditions.

The mechanical fragmentation method used for organoid generation results in tissue–fragment derived ICC organoids exhibiting jagged edges at the beginning of the culture period. However, over time, these organoids acquire a smoother edge, indicating their growth and self–repair capabilities (Fig. 1b). We took the minimum angle degree to measure the growth of organoids. During the culture, the minimum angle degree of organoids increase to 180° (spherical), indicate that ICC organoids could repair and regenerate.

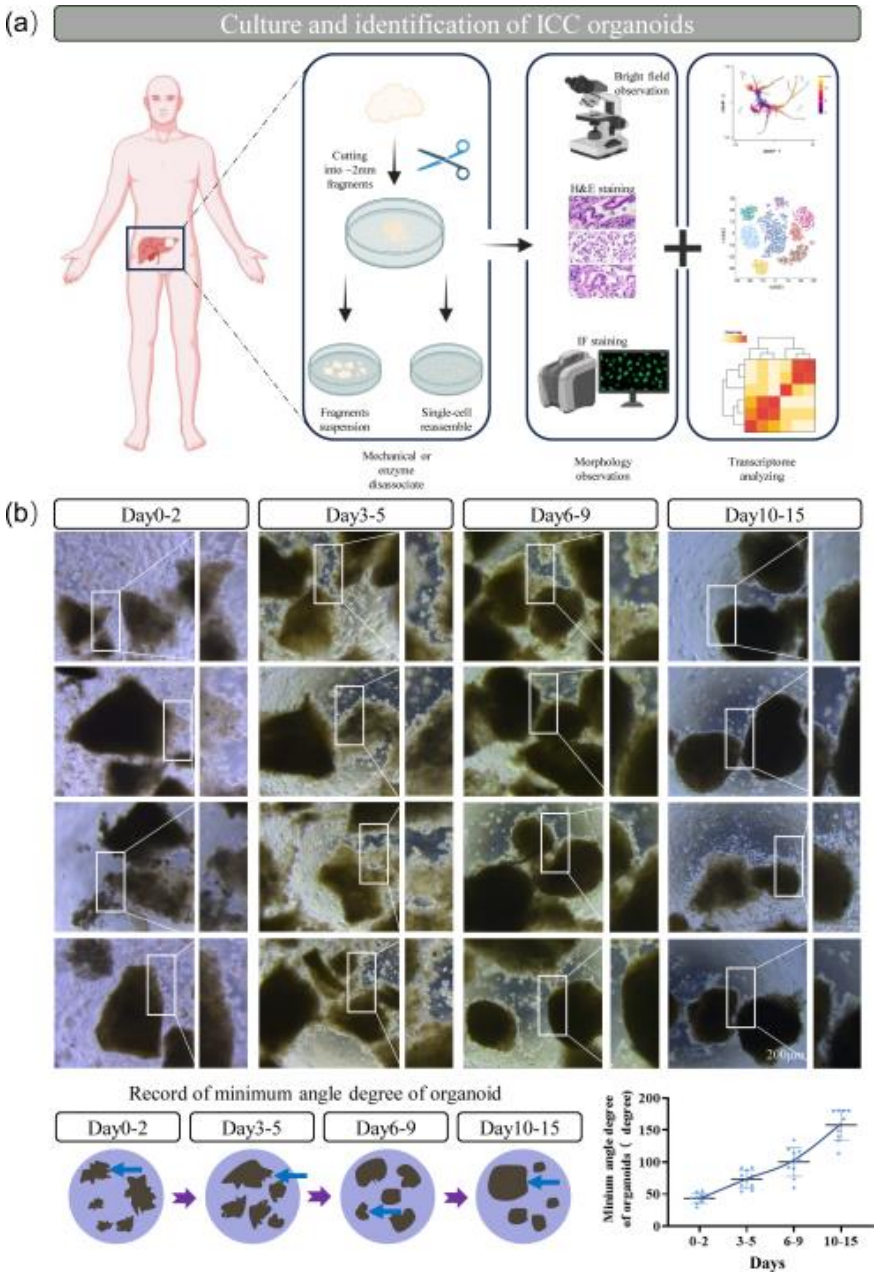

Figure 1. Refined establishment protocol for the culture of organoids: (a) Schematic illustration of this study; (b) development of tissue-fragment derived ICC organoids. During the culture period, the organoid edges exhibited a smooth appearance, indicating growth and self-repair. Top: microscopy observation of ICC organoids. Bottom: the degree of minimum angle of organoids (left), measurements ofthe growth of organoids (right). The scale bar represents 200 μm.

Morphology and molecular features of tissue-fragment derived ICC organoids

One of the key features of organoids is their ability to recapitulate characteristics of their tissue of origin. Therefore, we conducted immunocytochemistry experiments on ICC organoids derived from tissue fragments and compared them with the corresponding tissue source. CK7 and CK19 are biomarkers for biliary epithelial cells, which were found to be significantly upregulated in ICC tumor tissues[12]. The expression patterns of CK7, CK19, and CD45 in organoids and tissue were found to be similar, indicating that organoids maintain the pathological features of their origin tissue at a millimeter scale, and maintain immune microenvironment (Fig. 2a). Additionally, H&E staining of ICC organoids demonstrated the resemblance between ICC organoids and tissue (Fig. 2b).

To further validate the stability of organoids, whole exome sequencing (WES) was conducted to investigate the mutation

profile. The analysis revealed that the number and type of mutations in organoids remained consistent (1733 mutations affecting 94.2% genes, as shown in Fig. 2c), indicating the robustness of our culture method and medium. Additionally, we identified a mutation in *IDH1* (exon6:c.G532A:p.V178I), a key gene involved in intrahepatic cholangiocarcinoma (ICC) development, which was also maintained in the organoids (Fig. 2c). Therefore, both morphological characteristics and

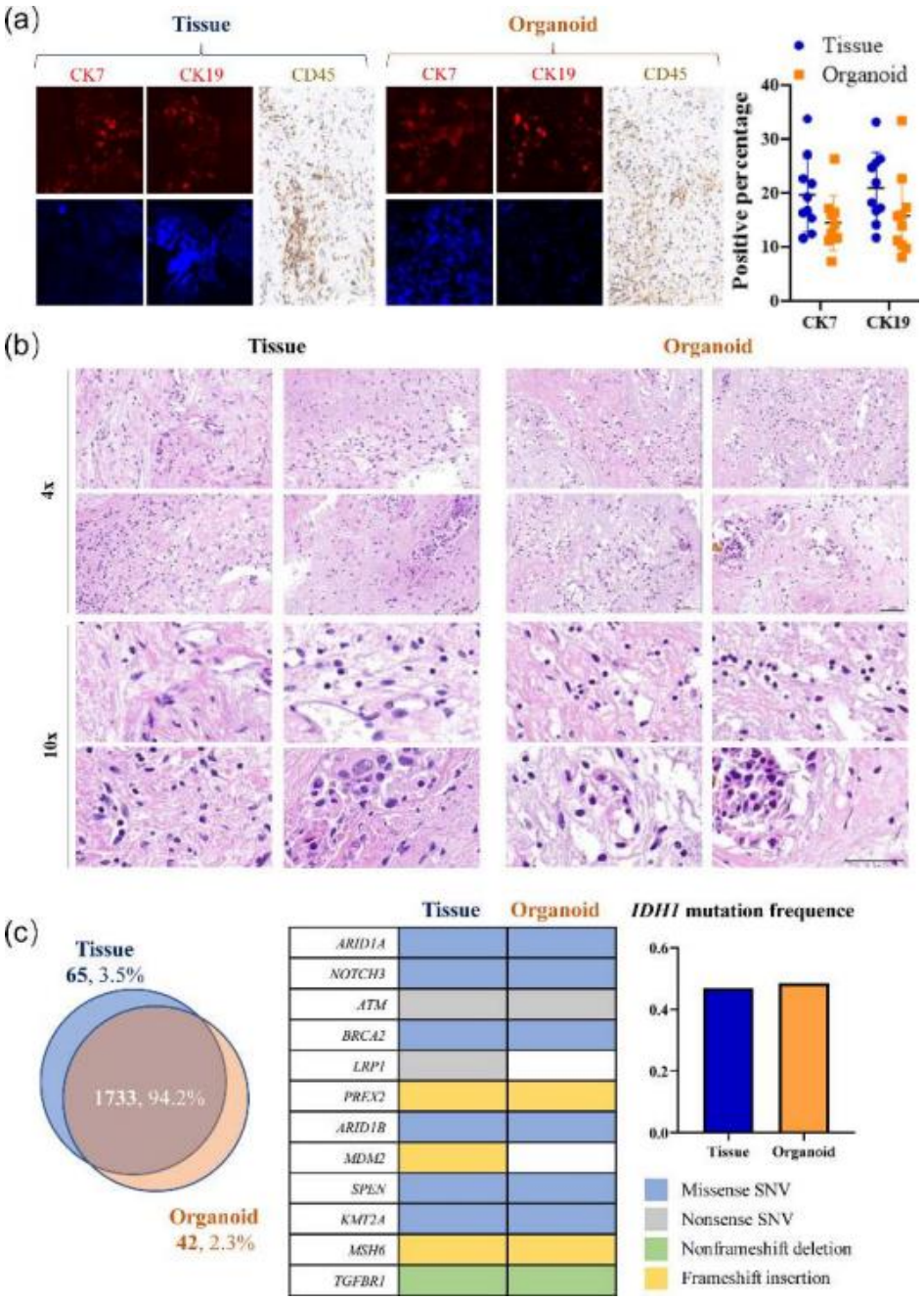

Figure 2. Identification of tissue-fragment derived ICC organoids: (a) Expression patterns of CK7 and CK19 in ICC tumor tissue and organoids were found to be similar, with a consistent pattern observed in both tissue samples and organoids. The scale bar represents 200 μm. (b) H&E staining revealed that the cancer region was preserved in the organoids compared to its original tissue. The scale bar represents 200 μm. (c) Comparison of gene mutation numbers between tumor tissue and organoids showed that mutations with an allele frequency > 0.25 were selected for analysis. Both tissue samples and organoids exhibited IDH1 exon6:c.G532A:p.V178I mutation, which remained stable even after 14 days of culture.

genomic features were preserved in tissue–fragment derived ICC organoids, demonstrating the feasibility of our advanced culture approach.

Establishment of single-cell derived ICC organoids

Although tissue–fragment derived ICC organoids can capture the diverse characteristics of ICC tumor tissue, their application potential in the industry field, such as high–throughput drug screening, is limited due to their relatively large volume and low throughput. In the matrigel–based organoid culture method, matrigel serves as a scaffold for single cells, facilitating the generation of self–proliferating organoids. However, handling matrigel can be challenging for beginners and both time and financial resources required are substantial. Therefore, we investigated the potential of ICC cells to form organoids in suspension culture without the use of matrigel. Intriguingly, after only 20 h of suspension culture in medium, the cells self–organized into organoids (Fig. 3a). These organoids exhibited growth and proliferation throughout the culture period, indicating their suitability for high–throughput screening applications (Fig. 3b). However, due to their small size and suspended state, obtaining sections of these compact organoids was challenging.

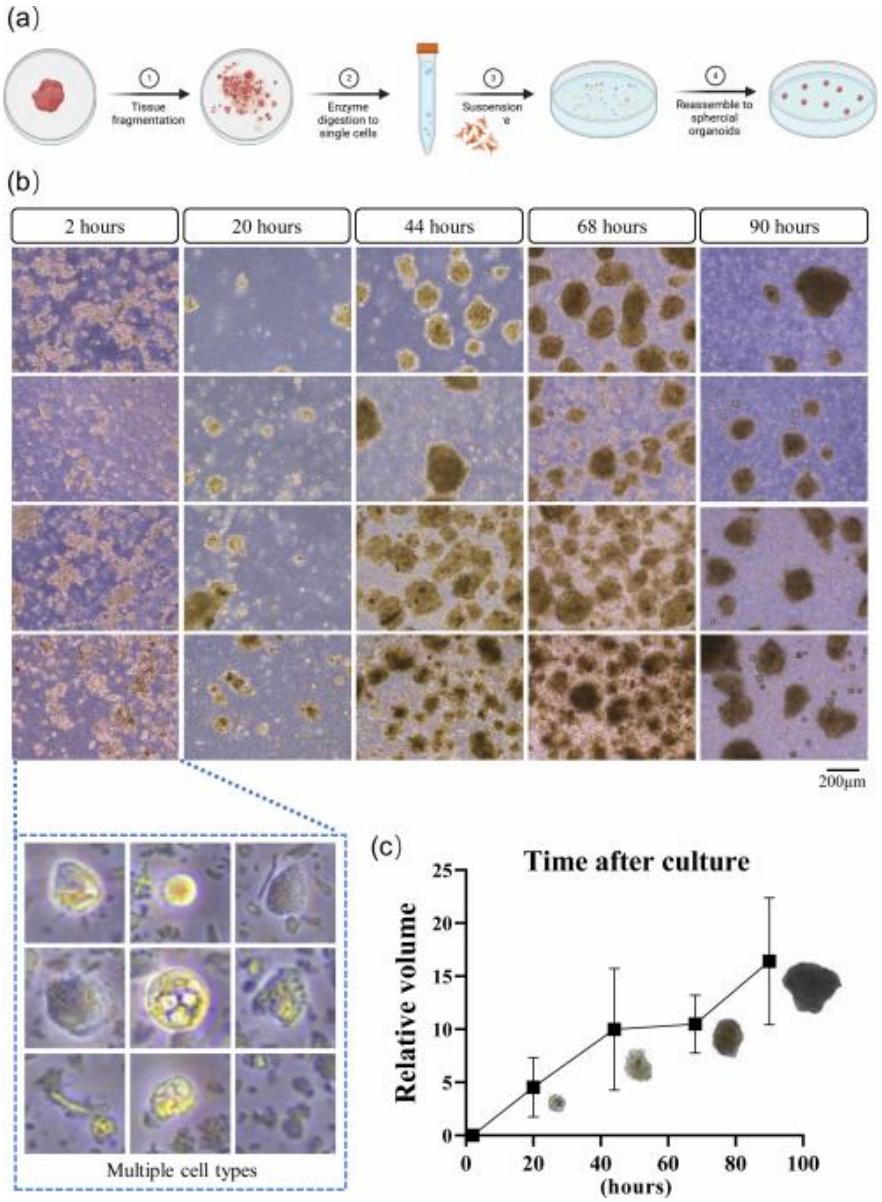

Figure 3. Observation of single-cell derived ICC organoids: (a) Schematic diagram of generation of single–cell derived ICC organoids. (b) Development and growth of single–cell–derived ICC organoids. The organoids exhibiting increased volume during culture after 20 h. Scale bar represents 200 μm. (c) The change of relative volume of organoids during culture.

Gene expression profile of ICC organoids and clinic tissues

To gain a comprehensive understanding of ICC organoids using our advanced methodology, we conducted RNA–seq analysis at day 3, day 6, and day 9. Furthermore, we also examined publicly available ICC tissue and organoid datasets, GSE107943[13,14] and GSE215997[15]. The cluster dendrogram reveals that large duct type ICC organoids (SRR21949015–21949019) are grouped together in a distinct branch. Interestingly, our organoids exhibit proximity to ICC tumor tissues (SRR6373759–6373787), as supported by the correlation heatmap analysis (Figs 4.a and 4b). This suggests that

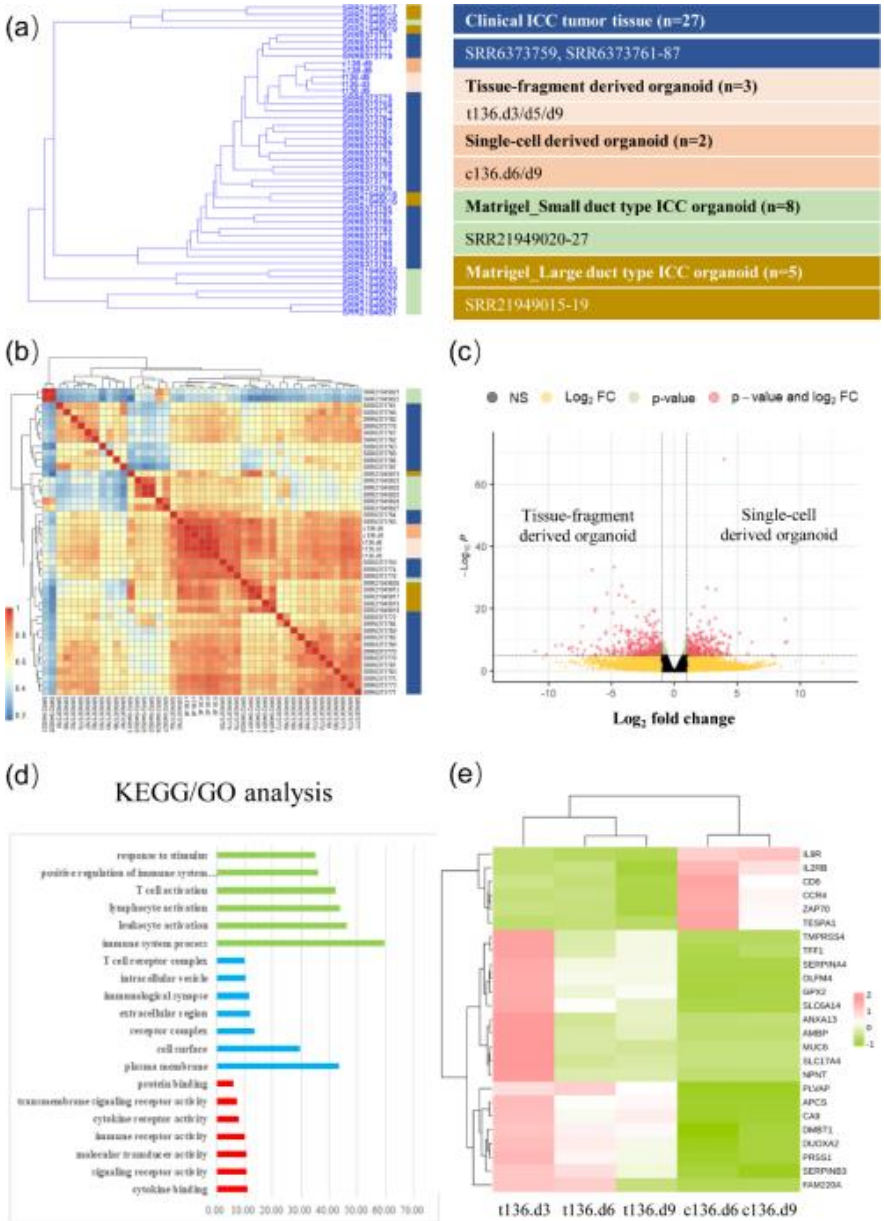

Figure 4. Gene expression profile of organoids: Cluster dendrogram illustrating the grouping of our samples and public data, with the red branch indicating the presence of large duct type ICC organoids. Our organoids clustered closely with clinical ICC tissues. (b) Correlation heatmap depicting the strong correlation between ICC tissues and both single–cell and tissue–fragment derived organoids, highlighting the robustness of our culture method. (c) Volcano map displaying differentially expressed genes (DEGs) between single–cell and tissue–fragment derived organoids. While most genes maintained stable expression levels, DEGs were still observed due to variations in culture protocols. (d) Gene Ontology (GO) analysis revealed up–regulated immune pathways in single–cell derived organoids. (e) Heatmap of DEGs express in tissue and single–cell–derived organoids, suggesting that different pathways were activate, and immune cells persisted within the organoid environment despite being under abnormal activation states.

our organoids share similarities with clinical ICC tumor tissues. However, it is worth noting that single–cell and tissue–fragment organoids are clustered into separate branches, indicating inherent differences between these two types. To quantify the impact of these dissimilarities, we examined differentially expressed genes (DEGs) between the two types of organoids. A total of 1638 genes (5.9%) were found to be up–regulated, while 2132 genes (7.7%) were down–regulated in single–cell derived organoids (Fig. 4c). Gene Ontology analysis revealed distinct alterations in pathways between the two types of organoids. Notably, immune–related pathways exhibited upregulation in single–cell derived organoids (Fig. 4d). Further investigation into these pathways identified several immune–related genes that were upregulated, including *IL9R*, *CCR4* and *IL2RB* etc. (Fig. 4e). This observation may be attributed to the stimulation caused by enzyme digestion; however, it was also confirmed that the presence of immune cells within the culture environment is crucial for immune drug testing.

Discussion

Although the rapid development of the organoid field has provided researchers with a novel model, certain limitations still persist. The widely–used matrigel–based organoid culture method poses challenges for beginners and is time–consuming, rendering it unsuitable for clinical practitioners. In this study, we present an advanced ICC organoid culture method that eliminates the need for matrigel, making it accessible to both single–cell and tissue–fragment derived ICC organoids. Our developed method ensures the preservation of molecular and morphological features such as CK7 and CK19 expression in these organoids, while exhibiting a gene expression profile similar to that of public ICC tumor tissue data. Additionally, the data from whole–exome sequencing indicate that organoids exhibit similarity in mutation sites and the number of genes compared to the tissue of origin. This suggests that organoids maintain genomic stability at the chromosomal level. These compelling findings validate the usability and robustness of our advanced ICC culture method.

Our future research will focus on investigating the microenvironment of organoids in greater detail. The fragmentation culture method we have employed has shown promise in preserving the tissue microenvironment and organization pattern, albeit temporarily (Fig. 5). However, there is still much to learn about how this preservation can be optimized and extended. One significant advantage of our tissue–fragment derived ICC organoids is their ability to retain the local tumor immune microenvironment that is lacking in matrigel–based organoid culture methods. This opens up new possibilities for studying the interactions between cancer cells and immune cells within a more physiologically relevant context. In particular, we are interested in determining whether this preserved microenvironment can maintain its biological function over time. Understanding how these organoids respond to various stimuli and treatments will provide valuable insights into the mechanisms underlying tumor–immune cell interactions. It is worth noting that immune drugs such as pembrolizumab have already demonstrated success in clinical therapy for ICC cancer patients. By utilizing our advanced organoid culture method, we hope to contribute significantly to drug screening efforts aimed at identifying novel immunotherapies or optimizing existing ones for a larger patient population. Furthermore, by studying the microenvironment of these organoids, we may uncover potential biomarkers or therapeutic targets specific to ICC cancers. This knowledge could lead to personalized treatment strategies tailored specifically for individual patients based on their unique tumor characteristics.

Research ethics and patient consent

The study was approved by the Ethics Committee of Zhongshan Hospital, Fudan University (B2018–018(2)). Patient gave informed consent to this study.

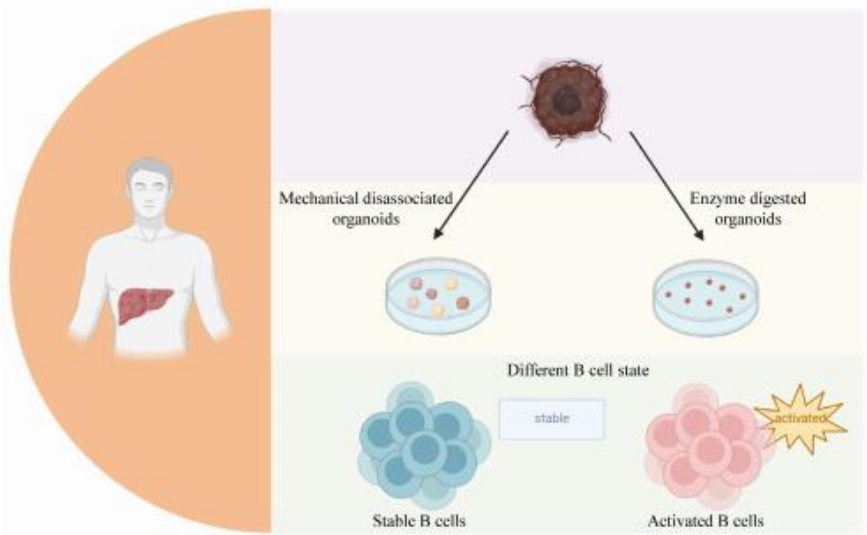

Figure 5. Different B cell state in two different protocols: Different organoid construction methods can lead to varying states of B cells. In organoids derived from single cells, B cells are activated, possibly due to the exposure of new antigenic epitopes during the enzymatic digestion process, which stimulates the immune cells. In contrast, in organoids from tissue fragments, B cells remain in a stable state.

Declaration of conflicting interests

This work was sponsored by Shanghai Lisheng Biotech Ltd (Lisheng). X.X.H. is a shareholder of Lisheng, as a founder. C.W., Y.H.S., J.P.L., L.Y.L., J.Z., M.J.R., and C.H.C. are senior scientists of Lisheng. X.X.H. and C.H.C. are members of the Editorial Board for *Cell Organoid*. They were not involved in the journal's review of, or decisions related to, this manuscript. All authors declare no competing financial interests.

Availability of data and material

The data and materials that support the findings of this study are available from the corresponding author upon reasonable request.

Acknowledgements

None.

Funding

No funding for this research.

Author contributions

X.Z, C.H.C. and X.X.H conceived and designed the study. C.W, Y.H.S, L.Y.L, J.Z, M.J.R and A.H were responsible for sample collection and experimental procedures. J.P.L conducted the analysis of the RNA sequencing data. C.W, C.H.C and X.X.H. wrote the manuscript. All authors reviewed and approved the final version of the manuscript.

References

[1] Yao, K. J., Jabbour, S., Parekh, N., Lin, Y., Moss, R. A. Increasing mortality in the United States from cholangiocarcinoma: An analysis of the National Center for Health Statistics Database. *BMC Gastroenterology*, **2016**, 16(1): 117. https://doi.org/10.1186/s12876-016-0527-z

[2] Valle, J. W., Kelley, R. K., Nervi, B., Oh, D. Y., Zhu, A. X. Biliary tract cancer. *The Lancet*, **2021**, 397(10272): 428–444. https://doi.org/10.1016/s0140-6736(21)00153-7

[3] El-Diwany, R., Pawlik, T. M., Ejaz, A. Intrahepatic cholangiocarcinoma. *Surgical Oncology Clinics of North America*, **2019**, 28(4): 587–599. https://doi.org/10.1016/j.soc.2019.06.002

[4] Benson, A. B., D'Angelica, M. I., Abrams, T. A., Are, C., Bloomston, P. M., Chang, D. T., Clary, B. M., Covey, A. M., Ensminger, W. D., Iyer, R. et al. Hepatobiliary cancers, version 2.*2014*. *Official Journal of the National Comprehensive Cancer Network*, **2014**, 12(8): 1152–1182. https://doi.org/10.6004/jnccn.2014.0112

[5] Rizzo, A., Ricci, A. D., Brandi, G. Durvalumab: An investigational anti-PD-L1 antibody for the treatment of biliary tract cancer. *Expert Opinion on Investigational Drugs*, **2021**, 30(4): 343–350. https://doi.org/10.1080/13543784.2021.1897102

[6] Ricci, A. D., Rizzo, A., Brandi, G. The DNA damage repair (DDR) pathway in biliary tract cancer (BTC): A new Pandora's box? *ESMO Open*, **2020**, 5(5): e001042. https://doi.org/10.1136/esmoopen-2020-001042

[7] Oh, D. Y., Lee, K. H., Lee, D. W., Yoon, J., Kim, T. Y., Bang, J. H., Nam, A. R., Oh, K. S., Kim, J. M., Lee, Y. et al. Gemcitabine and cisplatin plus durvalumab with or without tremelimumab in chemotherapy-naive patients with advanced biliary tract cancer: An open-label, single-centre, phase 2 study. *The Lancet Gastroenterology & Hepatology*, **2022**, 7(6): 522–532. https://doi.org/10.1016/s2468- 1253(22)00043-7

[8] Vogel, A., Bridgewater, J., Edeline, J., Kelley, R. K., Klümpen, H. J., Malka, D., Primrose, J. N., Rimassa, L., Stenzinger, A., Valle, J. W. et al. Biliary tract cancer: ESMO Clinical Practice Guideline for diagnosis, treatment and follow-up. *Annals of Oncology*, **2023**, 34(2): 127–140. https://doi.org/10.1016/j.annonc.2022.10.506

[9] Wang, Z. W., Jin, Y., Guo, Y. H., Tan, Z. H., Zhang, X. X., Ye, D., Yu, Y. Q., Peng, S. Y., Zheng, L., Li, J. T. Conversion therapy of intrahepatic cholangiocarcinoma is associated with improved prognosis and verified by a case of patient-derived organoid. *Cancers*, **2021**, 13(5): 1179. https://doi.org/10.3390/cancers13051179

[10] Wang, Z. W., Guo, Y. H., Jin, Y., Zhang, X. X., Geng, H., Xie, G. Y., Ye, D., Yu, Y. Q., Liu, D. R., Zhou, D. E. et al. Establishment and drug screening of patient-derived extrahepatic biliary tract carcinoma organoids. *Cancer Cell International*, **2021**, 21(1): 519. https://doi.org/10.1186/s12935-021-02219-w

[11] Broutier, L., Mastrogiovanni, G., Verstegen, M. M., Francies, H. E., Gavarró, L. M., Bradshaw, C. R., Allen, G. E., Arnes-Benito, R., Sidorova, O., Gaspersz, M. P. et al. Human primary liver cancer–derived organoid cultures for disease modeling and drug screening. *Nature Medicine*, **2017**, 23(12): 1424–1435. https://doi.org/10.1038/nm.4438

[12] Liu, L. Z., Yang, L. X., Zheng, B. H., Dong, P. P., Liu, X. Y., Wang, Z. C., Zhou, J., Fan, J., Wang, X. Y., Gao, Q. CK7/CK19 index: A potential prognostic factor for postoperative intrahepatic cholangiocarcinoma patients. *Journal of Surgical Oncology*, **2018**, 117(7): 1531–1539. https://doi.org/10.1002/jso.25027

[13] Ahn, K. S., Kang, K. J., Kim, Y. H., Kim, T. S., Song, B. I., Kim, H. W., O'Brien, D., Roberts, L. R., Lee, J. W., Won, K. S. Genetic features associated with ^{18}F-FDG uptake in intrahepatic cholangiocarcinoma. *Annals of Surgical Treatment and Research*, **2019**, 96(4): 153. https://doi.org/10.4174/astr.2019.96.4.153

[14] Ahn, K. S., O'Brien, D., Kang, Y. N., Mounajjed, T., Kim, Y. H., Kim, T. S., Kocher, J. P A., Allotey, L. K., Borad, M. J., Roberts, L. R. et al. Prognostic subclass of intrahepatic cholangiocarcinoma by integrative molecular–clinical analysis and potential targeted approach. *Hepatology International*, **2019**, 13(4): 490–500. https://doi.org/10.1007/s12072-019-09954-3

[15] Lee, H. S., Han, D. H., Cho, K., Park, S. B., Kim, C., Leem, G., Jung, D. E., Kwon, S. S., Kim, C. H., Jo, J. H. et al. Integrative analysis of multiple genomic data from intrahepatic cholangiocarcinoma organoids enables tumor subtyping. *Nature Communications*, **2023**, 14: 237. https://doi.org/10.1038/s41467-023-35896-4

Cell Organoid

Article

https://doi.org/10.26599/CO.2024.9410004

Generation of patient-derived glioblastoma organoids: a comparative study of enzymatic digestion and mechanical fragmentation methods

Authors

Jian Zhang, Jiping Liu, Yanghua Shi, Lanyang Li, Chen Wang, ..., Chunhui Cai*, Xinxin Han*

Correspondence

Chunhui Cai, caichunhui@lishengbiotech.com; Xinxin Han, xxhan@sibs.ac.cn

Graphical abstract

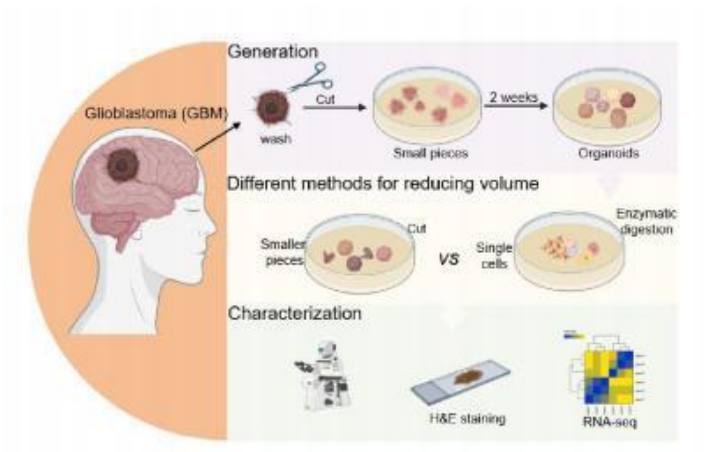

In Brief

In this study, we employed enzymatic digestion and mechanical fragmentation to generate Glioblastoma (GBM) organoids.Utilizing photography, RNA sequencing (RNA-seq), and histological staining, we meticulously documented and compared the morphological and molecular features ofthe organoids derived from both methods.Our findings underscore the preservation of GBM' s key characteristics, including its unique tissue architecture and gene expression patterns.

Highlights

- Successfully generated four patient-derived organoids.
- RNA-seq was used to monitor gene expression changes at various stages of organoid growth.
- Both propagation methods successfully maintain the typical characteristics and immune microenvironment of glioblastoma (GBM) organoids.
- The GBM organoids prepared by mechanical fragmentation retained vascular architecture.

Cell Organoid
Article
https://doi.org/10.26599/CO.2024.9410004

Generation of patient-derived glioblastoma organoids: a comparative study of enzymatic digestion and mechanical fragmentation methods

Jian Zhang[1], Jiping Liu[1], Yanghua Shi[1], Lanyang Li[1], Chen Wang[1], Mingjie Rong[1], Bangbao Tao[2], Hong Tan[3], Wei Deng[4], Chunhui Cai[1,*], and Xinxin Han[1,5,*]

[1] *Shanghai Lisheng Biotech, Shanghai 200092, China*
[2] *Department of Neurosurgery, Xinhua Hospital, School of Medicine, Shanghai Jiao Tong University, Shanghai 200092, China*
[3] *Department of Anesthesiology, Huashan Hospital, Fudan University, Shanghai, China*
[4] *LongHua Hospital, Shanghai University of Traditional Chinese Medicine, Shanghai 200032, China*
[5] *Organ Regeneration X Lab, LiSheng East China Institute of Biotechnology, Peking University, Nantong 226299, China*

Received: 2 February 2024 / **Revised:** 29 April 2024 / **Accepted:** 12 May 2024

ABSTRACT

Glioblastoma (GBM) is a highly aggressive brain tumor characterized by rapid growth and high heterogeneity, posing challenges for fundamental research and personalized drug screening due to the lack of suitable models. GBM organoids serve as an innovative research tool, providing a valuable model for studying the biological characteristics of GBM. In this study, we successfully generated 4 GBM organoids and employed enzymatic digestion and mechanical fragmentation techniques for subsequent cultivation. Through continuous observation, pathological assessment, and RNA sequencing (RNA-seq), we observed that all the organoids generated through both methods demonstrated good growth characteristics. The organoids derived from mechanical fragmentation not only achieved a two-dimensional (2D) area of ~ 1.5 mm^2 but also exhibited distinct vascular structures. The organoids derived from enzymatic digestion achieved a 2D area of approximately 0.8 mm^2. Furthermore, RNA-seq analysis has revealed that organoids cultured using two distinct methods exhibit a heterogeneous cellular composition, comprising a total of 20 cell types (endothelial, immune cells ...). Our studies show that both methods successfully maintained the essential characteristics of GBM, encompassing its distinctive tissue structure and gene expression patterns. Each method exhibits its own attributes, contributing to the understanding of GBM organoids.

KEYWORDS

glioblastoma (GBM), organoids, patient-derived models, RNA sequencing, heterogeneity

Introduction

Glioblastoma (GBM) is the most common high-grade primary malignant brain tumor in adults. This tumor is characterized by its highly invasive nature, widespread heterogeneity, and has a poor prognosis, with a median survival period typically not exceeding two years[1]. Despite recent progress in GBM research, there is still no curative treatment. Comprehensive therapeutic approaches such as surgical resection, radiotherapy, and chemotherapy can only marginally prolong patients' survival times[2,3]. Therefore, GBM remains a significant challenge in the field of neuro-oncology.

Traditional two-dimensional (2D) cell lines hold substantial value for disease research[4,5]. However, these models are constrained by their inability to fully replicate the complexity and three-dimensional architecture of *in vivo* tissues. They may not accurately reflect the dynamic and spatially organized microenvironments found in real tissues, potentially leading to a reduced predictive accuracy of therapeutic responses. In recent years, organoid research has received widespread attention and development, and organoids have significant advantages over traditional 2D cell lines in retaining complexity and heterogeneity of the original tumor[6–8]. Many studies have shown that organoid models exhibit sensitivities to targeted therapies or radiation that are similar to those of tumors in the body[9,10], demonstrating significant potential in drug screening[11,12]. For instance, the breast cancer organoids established by Norman Sachs and colleagues have successfully retained the histological and genetic

*Address correspondence to Chunhui Cai, caichunhui@lishengbiotech.com; Xinxin Han, xxhan@sibs.ac.cn

Cite this article as Zhang, J., et al. *Cell Organoid*, **2024**, 1: 9410004.

characteristics of the original tumors[13]. The observation that the organoids' drug responses corresponded with the patients' responses underscores the potential of organoids as predictive in vitro models. Currently, an increasing number of organoid models are being developed to simulate various tumors, such as ovarian, pancreatic, and liver tumors[14–16]. These organoid models provide more reliable experimental evidence for studying the occurrence, development, and treatment of tumor. With the continuous development and optimization of organoid technology, more breakthroughs in the field of biomedicine are expected in the future.

GBM exhibits extensive inter- and intratumor heterogeneity, which hinders in-depth investigations into the pathogenesis of GBM and impacts the development of effective treatment strategies[17]. Existing models often struggle to capture the intricacies of GBM. Consequently, there is a pressing need for the development of more sophisticated models that can better reflect these complexities. GBM organoids can better simulate the heterogeneity and complexity of GBM[18–21]. For example, Jeremy Rich derived organoids from patient GBM tissue and characterized the stem cell heterogeneity and hypoxia gradients[18]; Fadi Jacob and colleagues have developed an innovative method to quickly establish GBM organoids from tumor tissue without dissociating the tumor tissue into single cells. The organoids derived from this method retain a significant degree of heterogeneity, gene expression profiles, and mutational characteristics of the original tumor cells[19]. These organoids are expected to provide powerful tools for in-depth study of GBM pathogenesis, drug responses, and treatment strategies. Despite recent significant progress in the development of GBM organoid, there are still some limitations that need to be resolved. Such as immune response deficiencies and the absence of a vascular system, as well as debates regarding structural and genetic fidelity[22,23]. Consequently, the development of novel GBM organoids is crucial for a deeper understanding of the biological characteristics of this disease.

In this study, we generated organoid using surgical samples from four patients with GBM. This method does not require the dissociation of tissue into single cells, nor the addition of matrix gel. To avoid necrosis in the core of the organoids, we adopted two methods to reduce the size of the organoids: One is to mechanically fragment the organoids, resulting in smaller pieces, and the other is enzymatic digestion of the organoids into single cells. To enhance our understanding of the characteristics of each method, we conducted photography, pathological staining, and RNA-seq analysis. Our results demonstrated that the organoids could preserve the key features of GBM and a portion of the tumor microenvironment. Furthermore, we observed heterogeneity among organoids derived from different patients. In summary, both methods provide insights for organoid research.

Results

Generation of GBM organoids without Matrigel and enzymes

With the full informed consent of the patients, we processed fresh surgically resected GBM tissue samples from four patients. In contrast to the conventional method of digesting tissue into single cells for organoid generation, we adopted a simplified method: Initially, the GBM tissue was meticulously washed with a tissue irrigation buffer to eliminate contaminants, ensuring the sterility of subsequent experiments. Subsequently, the tissue was manually cut into small pieces approximately 1 mm^3 in size using ophthalmic scissors. These pieces were directly mixed into organoid medium (without Matrigel) to facilitate in vitro growth. This simplified method is designed to promote organoid formation more efficiently. Typically, these small tissue pieces can generate organoids within approximately 2 weeks. To avoid necrosis in the core of the organoids, we adopted 2 methods to reduce the size of the organoids. As shown in Fig. 1a, we first treated the surgical tissue from four patients using the method and successfully generated GBM organoids. Subsequently, we subjected some of these organoids to RNA-seq analysis and divided the remaining organoids into 2 groups: one group underwent mechanical fragmentation into smaller pieces (Group 1), while the other was enzymatically digested to obtain a single-cell suspension (Group 2). Both groups were seeded into low attachment six-well plates (with three replicate wells each) and continued to be cultured. On the third post-inoculation (Day 2), we observed the formation of GBM organoids with a diameter of approximately 200 μm in Group 2, partial organoid samples from all groups were collected simultaneously for RNA-seq analysis. After 14 days, we collected all groups of organoids, with some used for pathological staining and others for RNA-seq.

The growth of GBMorganoids

To monitor the development of the organoids, we performed serial photography. Organoids generated from tissue pieces demonstrated favorable growth characteristics. Initially, the edges of these small pieces were distinct. After 2 weeks in culture, the organoids' edges became smooth and even, with cells observed to proliferate outward (Fig. 1b). On the third day post-inoculation (Day 2), cells from Group 2 had formed numerous small organoids. Over time, these organoids increased in size and began to merge with adjacent organoids, resulting in larger, diversely shaped organoids (Figs.2a and 2c). It is worth noting that the organoids within this group exhibited a small volume difference, with a relative increase in volume ranging from 2 to 5 times (Fig. 3a). However, Group 2-2, after forming organoids with a diameter of approximately 200 mm, did not exhibit significant growth changes during subsequent cultivation, and the specific reasons for this observation are yet to be elucidated. In contrast, the organoids from Group 1, which started with larger volumes, showed a relatively mild growth trend. These organoids gradually proliferate and grow, and have undergone fusion, resulting in the formation of organoids with diverse shapes. (Figs 2.a and 2b). It was encouraging to observe that some Group 1 organoids displayed clear vascular structures (Fig. 1c), although there was a significant variation in the volume of organoids within the group (Fig. 3a). To better summarize the growth characteristics of organoids, we conducted a detailed statistical analysis of the number of organoids (Fig. 3b), the maximum volume of organoids in each group (Fig. 3c), and the number of organoids exceeding a volume of 200,000 $μm^2$ (Fig. 3d). The results show that, during the early stages of organoid cultivation, there was a higher abundance of organoids with relatively smaller volumes. As the cultivation period progressed, the total number of organoids decreased, while the volume of organoids increased, and the count of larger organoids also rose.

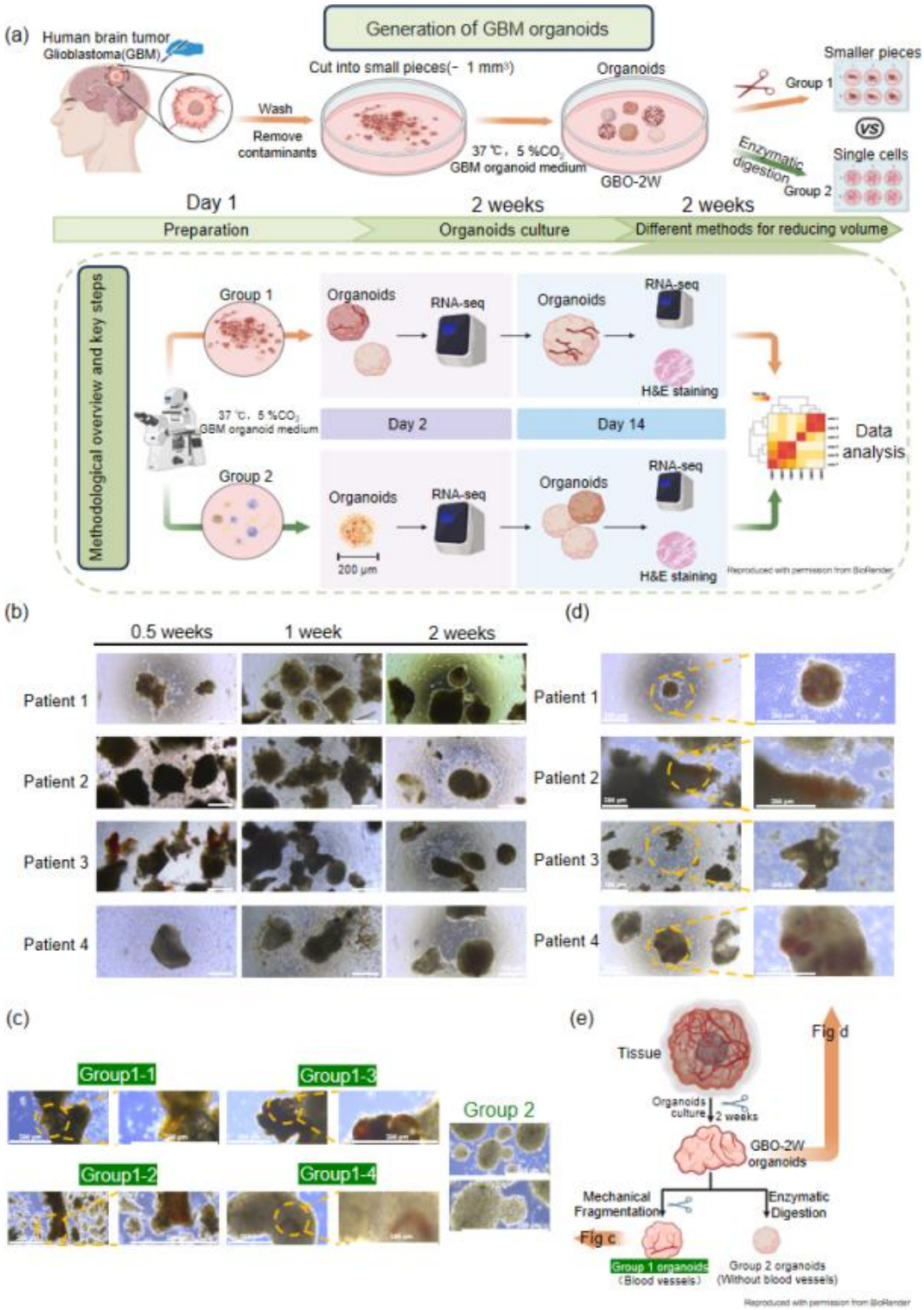

Figure 1. Generation of GBM organoids. (a) Methodological overview and key steps. (b) Brightfield microscopy images of organoid GBO-2W (organoids generated after 2 weeks of tissue culture) derived from tissue; scale bar = 500 μm. (c) Organoids with vascular structures (Group 1); Scale bar = 500 μm. (d) Organoids with vascular structures (GBO-2W); scale bar = 500 μm. (e) Schematic diagram of organoid characteristics across groups.

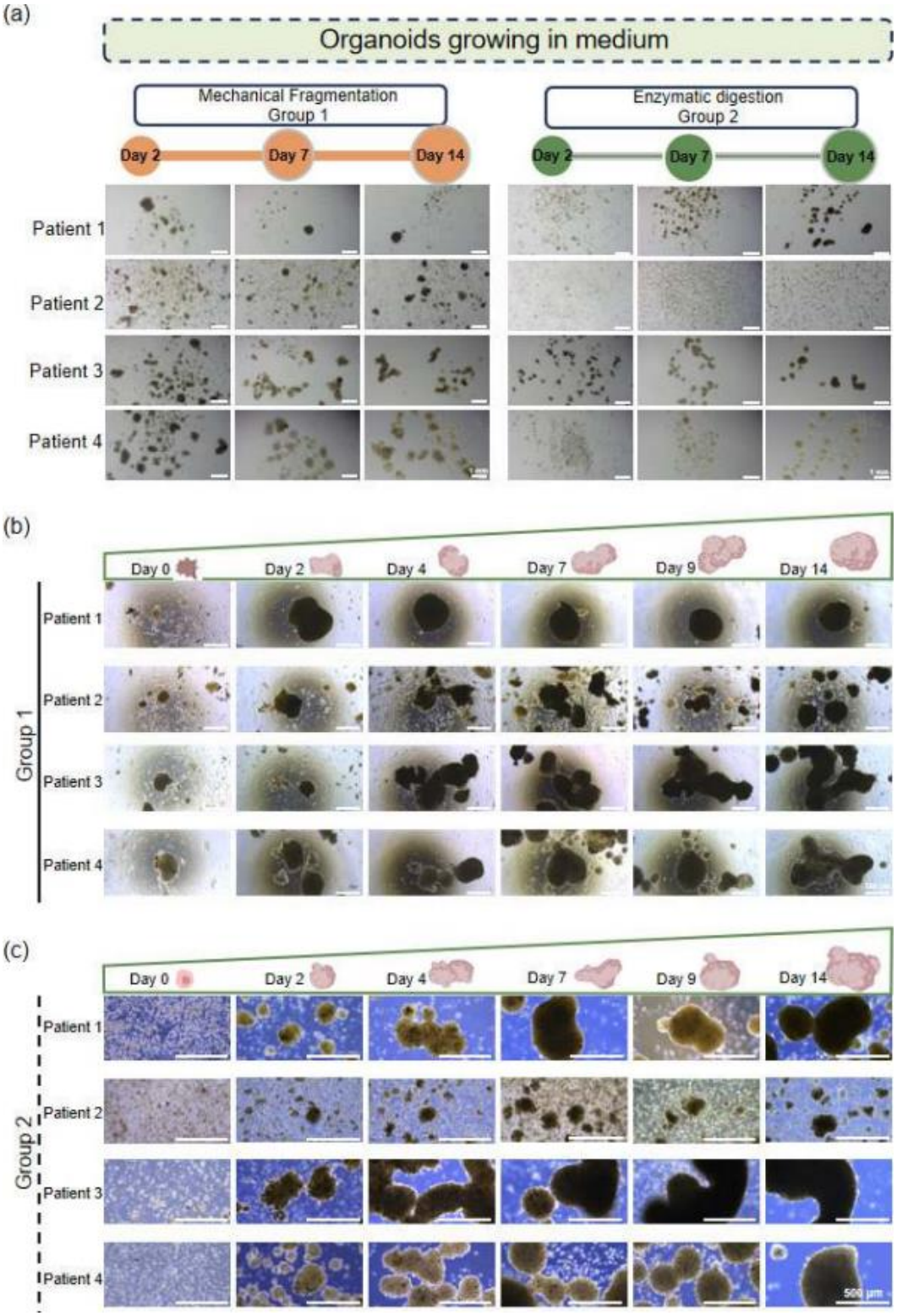

Figure 2. Growth record of organoids. (a) Organoid growth panorama; scale bar = 500 μm. (b) Brightfield microscopy images of Group 1; Scale bar = 500 μm. (c) Brightfield microscopy images of Group 2; scale bar = 500 μm.

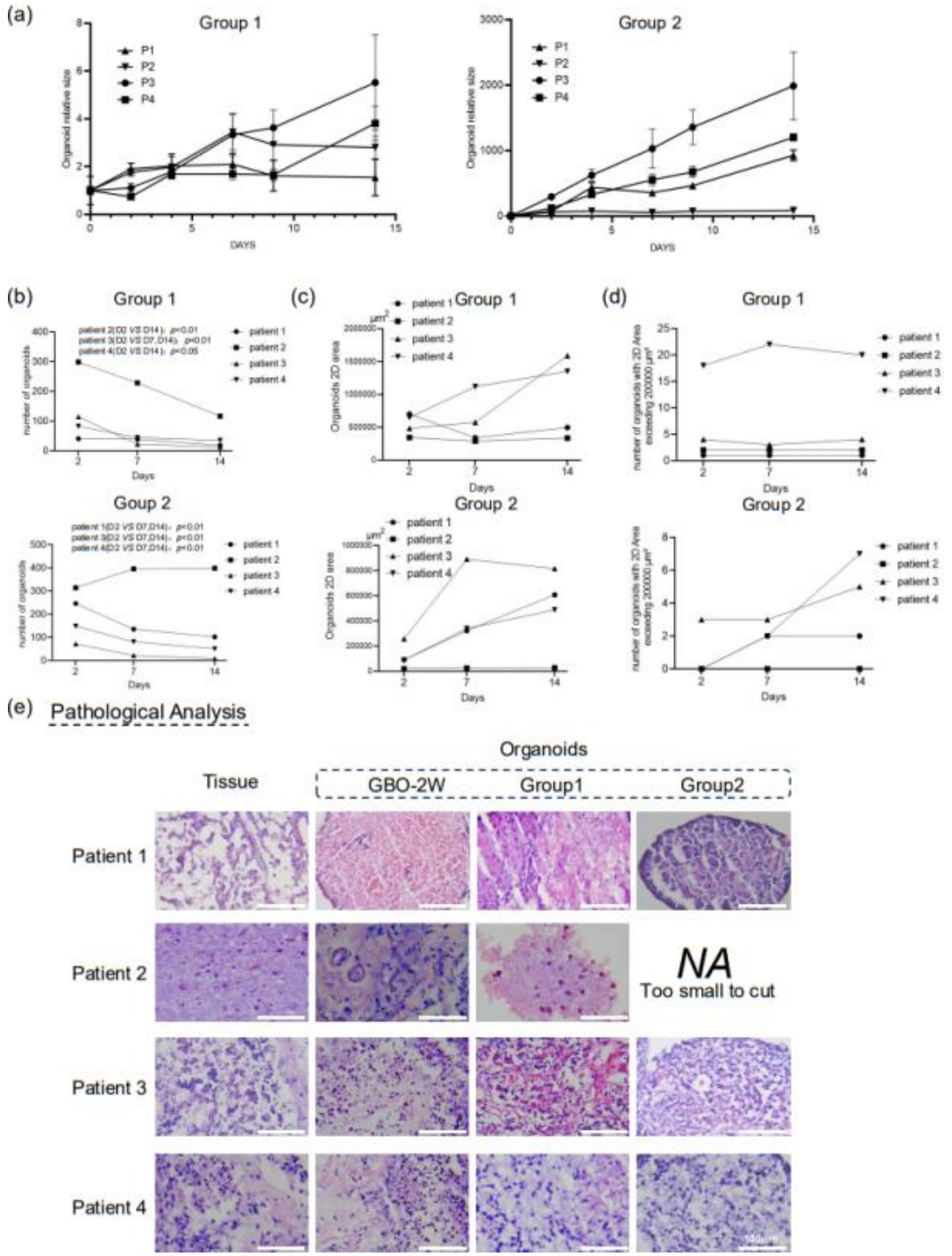

Figure 3. Growth record statistics chart and H&E staining results. (a) The statistics chart of organoid relative size. (b) The quantitative statistics chart of organoids. (c) The 2D area statistics chart of the largest organoids per group. (d) The statistical chart of the number of organoids with 2D area exceeding 200,000 μm^2. (e) Pathological analysis (H&E staining); Scale bar = 100 μm.

Histological characterization of GBM organoids

Hematoxylin and Eosin (H&E) staining is a commonly used histological technique that clearly reveals the morphological structure of tissues and cells. Analysis of the organoids and their matched tissues after H&E staining revealed that our organoids

closely resembled their parental tumors in tissue morphology and exhibited typical features of GBM. In the organoid sections, dense clusters of tumor cells with irregular shapes and varying sizes were observed. The nuclei were enlarged, irregular in shape, and exhibited uneven chromatin distribution. Binucleation or multinucleation was also observed. Additionally, necrotic features characteristic of GBM, such as pseudopalisading, were observed in the organoids from patients 3 and 4, designated as GBO-2W (Fig. 3c).

Transcriptome Characterization of GBM Organoids

RNA sequencing (RNA-seq) technology was employed to elucidate the dynamics of gene expression during disease progression. To confirm whether organoids retained key characteristics of GBM, bulk RNA-seq analysis was conducted on organoids from Groups 1 and 2, encompassing two time points (Days 2 and 14), as well as organoids at the GBO-2W (Organoids generated after 2 weeks of tissue culture) stage (Fig. 4a). Utilizing a panel of cell markers to distinguish various cell populations within the neural tissue (Fig. 5a), our results showed that organoids derived from Patient 1 exhibited pronounced expression of genes related to the immune and vascular systems. In contrast, organoids from Patient 3 showed significant expression of genes associated with astrocytes and cell proliferation. Organoids from Patients 2 and 4 displayed elevated expression of genes related to astrocytes, immune cells, oligodendrocyte precursor cells, angiogenesis, and cell cycle regulation. The organoids from the four patients exhibited a rich diversity of cell types, including tumor cells, immune cells, and vascular-related cells (Fig. 4c). Moreover, the organoids from different patients exhibited significant transcriptional differences, which were further confirmed by principal component analysis (PCA) (Fig. 4d). Notably, organoids from the same patient source in Groups 1 and 2 at the two time points (Days 2 and 14) demonstrated a high degree of similarity in cell composition to the GBO-2W organoids, with the proportion of various cell types remaining relatively stable over time (Fig. 5b). Correlation analysis further indicated a high level of transcriptional consistency among organoids from different groups of the same patient source (Fig. 4b).

The tumor immune microenvironment plays a crucial role in tumor growth and progression. To investigate the dynamic changes in the immune microenvironment within organoids, we analyzed the RNA-seq data. The results showed that the proportions of various immune cells in Groups 1 and 2 remained strikingly similar across different time points (Fig. 5b), with monocytes consistently maintaining a high proportion. Further analysis of the proportion of each immune cell type revealed that the immune cell composition in Groups 1 and 2 did not undergo significant changes over time (Fig. 5d). Additionally, it was observed that the endothelial cell population in both Groups 1 and 2 did not exhibit significant changes over time (Fig. 5c).

Discussion

Traditional GBM cell lines, including U87, U251, and GL261, have played a pivotal role in medical research, providing a foundational experimental platform for elucidating disease mechanisms, and conducting drug screening[24,25]. However, these cell lines are limited by their inability to accurately replicate the three-dimensional architecture and heterogeneity of tumors[26,27]. In contrast, GBM organoid models offer a more authentic representation of tumors, providing a more precise experimental platform for studying cellular interactions, immune cell dynamics, and drug responses[18,19,28].

In this study, we successfully generated organoids from GBM tissue resected from patients. HE staining showed that these organoids retained the typical histological features of GBM. RNA-seq confirmed that the organoids maintained GBM-specific gene expression profiles. cell type analysis demonstrated the diversity of cells within the organoids. Previous studies have shown significant heterogeneity among GBM patients[29], a characteristic that was reflected in our organoids, The organoids derived from tumor tissues of various patients demonstrated a notable diversity in their transcriptional profiles. Unlike other methods for generating organoids from patient-derived tissues, our methods circumvent the need for dissociating tumor tissue into single cells and does not employ the use of Matrigel.

The generation of organoids from tissue pieces typically takes about two weeks. As organoids increase in size, larger ones may experience hypoxia and nutrient deprivation in their central regions, leading to cell apoptosis and necrosis. To overcome this limitation, we adopted two methods—enzymatic digestion and mechanical fragmentation—to reduce the organoids' size. Encouragingly, after enzymatic digestion, the dissociated single cells exhibited the capacity to self-assemble into new organoids without the supplementation of any extracellular matrigel. Both H&E staining and RNA sequencing analysis showed that organoids treated with enzymatic digestion (Group 1) and mechanical fragmentation (Group 2) successfully retained the typical histological features and gene expression profiles of GBM. Additionally, organoids from both treatment methods showed a significant similarity in transcriptome and cell diversity to the GBO-2W organoids. Photography records indicated that the mechanical fragmentation tended to preserve some of the original tissue's architecture, while the enzymatic digestion required cells to re-establish interactions during the cultivation process, which might have resulted in the loss of the original tissue structure. However, enzymatic digestion leads to the formation of uniformly sized organoids. Both methods have their advantages in the cultivation of patient-derived organoids mechanical fragmentation may be suitable for experiments requiring the preservation of the original tissue structure, while enzymatic digestion may be more appropriate for studying the process of cellular tissue remodeling.

Tumors are complex ecosystems composed of various cell types, not just tumor cells, but also including multiple non-tumor cell types[30]. Our organoids also contained other non-tumor cell types, such as endothelial cells, mural cell and immune cells. Significantly, the relative proportions of these cell types remained stable throughout the cultivation process. The tumor immune microenvironment plays a pivotal role in tumor development, and researchers are continuously optimizing organoid culture techniques to mimic the immune response more accurately within tumors[31–33]. Currently, two main strategies are employed: one involves retaining and expanding the original immune cells within the organoids, and the other involves introducing new immune cells into the organoid culture system[34]. We have paid particular attention to the retention of immune cells during the organoid culture process and found that our culture system effectively maintained the immune microenvironment in both Groups 1 and 2.

Although we successfully generated organoids that reflect

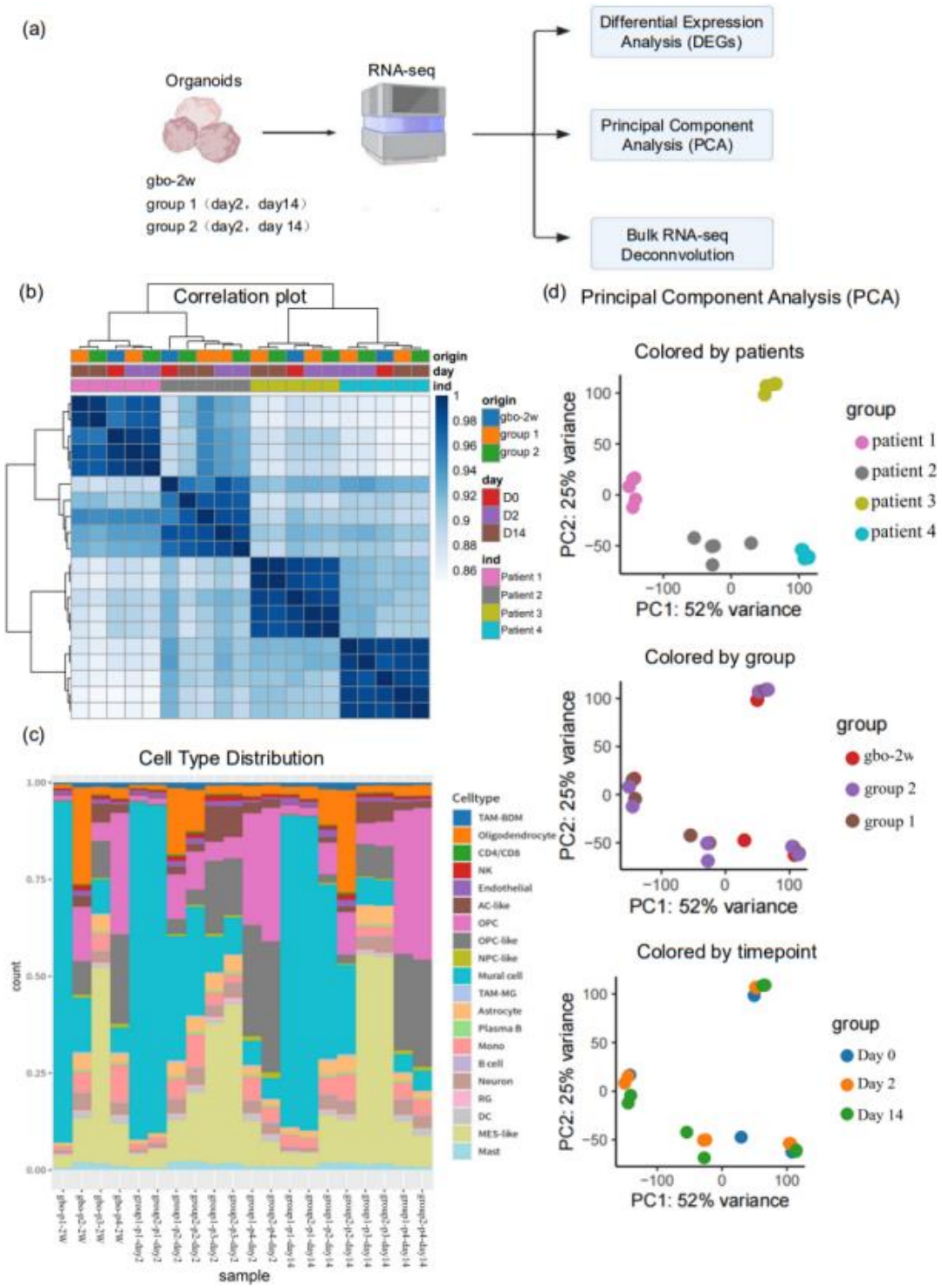

Figure 4. Bulk RNA-Seq analysis of organoids. (a) The workflow for Bulk RNA-Seq analysis. (b) Correlation analysis. (c) Cell type distribution. (d) Principal component analysis.

typical GBM features and partially retain the immune microenvironment, our study still faces some limitations. The scarcity of GBM patient tissue, coupled with their small volume, limits the number of organoids we can generate. In this

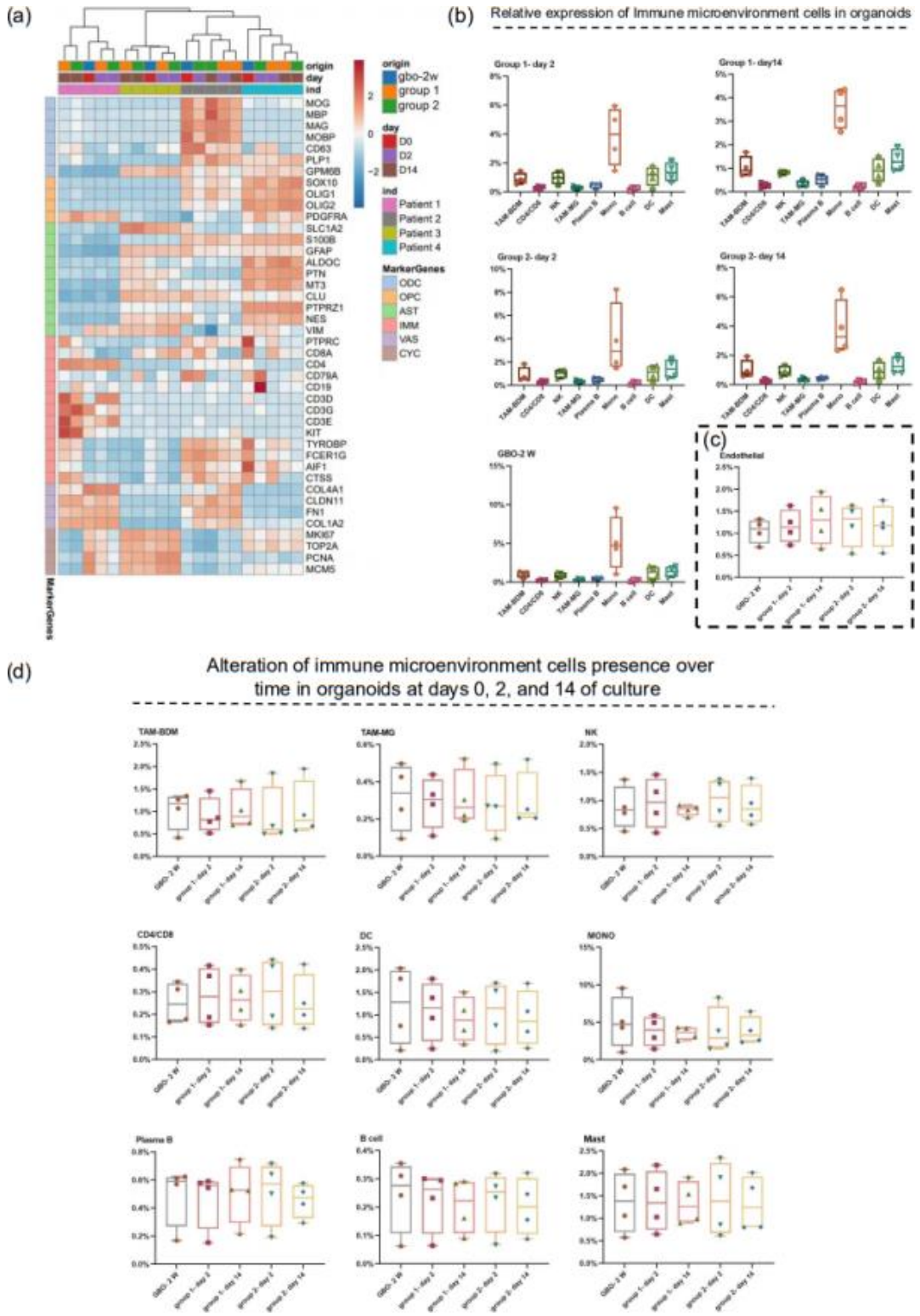

Figure 5. Cell type-specific molecular markers in organoids and RNA-Seq analysis of the immune microenvironment. (a) Cell type-specific molecular marker expression analysis. (b) Relative expression of immune microenvironment cells in organoids. (c) Alteration of immune microenvironment cells presence over time in organoids at Days 0, 2, and 14 of culture.

experiment, we generated organoids from GBM tissue of only four patients. Moreover, despite adopting some histological staining and RNA-seq analysis, the limited number of organoid samples may not fully reveal the characteristics of our GBM organoids. Therefore, enhancing the efficiency of organoid generation and delving into a more comprehensive analysis of their characteristics will be central to our upcoming research endeavors.

In summary, our study shows the characteristics of mechanical fragmentation and enzymatic digestion within the organoid cultivation process, which may offer a preliminary reference for future research in this area. Furthermore, it is advisable for researchers to take into account their research objectives and specific needs when choosing a suitable cultivation method.

Methods and materials

Tissue collection

We strictly adhere to ethical norms and standard operating procedures in the collection of clinical tissue samples, ensuring the integrity and quality of the samples. The main steps include: identifying patients, obtaining informed consent, collecting samples, processing samples, storage, and documentation. All sample collection work is carried out by professionally trained medical personnel following prescribed procedures to reduce the risk of sample contamination, ensure the viability of the samples, and facilitate subsequent analysis. At the same time, we also implement strict record-keeping and label management systems to ensure the traceability of samples and facilitate accurate data management. In the collection of all clinical samples, we strictly adhered to the ethical guidelines of the Xinhua Hospital Affiliated to Shanghai Jiao Tong University School of Medicine and the ethical codeXHEC-D-2024-019.

Organoid culture

In this study, we employed a standardized protocol for processing fresh GBM tissue samples to generate organoids. First, freshly obtained GBM tissue samples were immersed in a tissue irrigation buffer (LSNO00100201; Shanghai Lisheng Biotech, China) for 3 min to eliminate potential contaminants and non-cellular debris. The tissue samples were then transferred to a 50 mL centrifuge tube and washed 3–5 times with fresh tissue irrigation buffer, each time adding 5–10 mL and gently agitating to ensure thorough cleansing. Following the washing steps, the tissue samples were placed into a 10 cm dish and infused with 100 µL of medium (LSTO015004; Shanghai Lisheng Biotech, China). Utilizing ophthalmic scissors, the tissue samples were cut into micro-tissue pieces approximately 1 mm^3 in size. After resuspending the micro-tissue pieces in 1 mL of medium, they were transferred to a new 10 cm dish for observation and further cultivation. Finally, 15 mL of medium was added, and the dish was incubated in an incubator at 37 °C with 5% CO_2 to facilitate growth.

During the organoid cultivation process, we replaced part of the medium every 5–7 days, or adjusted it in time according to the color and turbidity of the medium to ensure sufficient nutrition for the growth of organoids. We meticulously monitored and regulated the cultivation conditions throughout the process to guarantee the precision and reliability of our experimental outcomes.

Group 1: A portion of the GBO-2W organoids were aspirated and transferred to a new 10 cm dish, with a minimal volume of liquid retained to preserve organoid hydration while excess medium was removed. The organoids were cut into smaller pieces using ophthalmic scissors. Subsequently, 6 mL of medium was added, and the organoid-laden medium was evenly distributed into low-adhesion 6-well plates. Throughout the cultivation process, the medium was consistently replenished every 5–7 days, and its composition was promptly adjusted based on its color and turbidity to ensure an optimal environment for organoid growth.

Enzymatic digestion

Group 2: An appropriate number of organoids was carefully taken, transferred to a 6-well plate, and allowed to settle at the bottom, with any excess supernatant being removed. Subsequently, 200 µL of organoid dissociation reagent (LSNO00100501; Shanghai Lisheng Biotech, China) was added, and the organoids were cut into small pieces with ophthalmic scissors to facilitate enzymatic digestion. After adding 1 mL of organoid dissociation reagent and thoroughly mixing, the mixture was placed in an incubator and shaken for 20 min to complete the digestion process. The mixture was repeatedly aspirated with a 1 mL pipette to break up any visible clumps. If a noticeable resistance due to clogged particles was felt, the digestion was continued for an additional 10 min. The mixture was filtered through a 70 µm cell strainer, and the strainer was rinsed with 2 mL of medium to collect a single-cell suspension. This suspension was then centrifuged (600 r/min, 10 min). After centrifugation, the supernatant was carefully removed, and the cells were resuspended in 2 mL of medium. This suspension underwent a second centrifugation at 600 r/min for 10 min. Following the second spin, the supernatant was again removed, and the cells were resuspended in 6 mL of fresh medium. This cell suspension was then evenly distributed into three replicate wells in a 6-well plate. The medium was routinely replenished every 5–7 days, with adjustments made as necessary based on the medium's color and turbidity to ensure a conducive culture environment.

Organoids growth analysis

In this study, we used ImageJ software to quantitatively analyze the size of the organoids, measuring the changes in size at different time points and continuously monitoring the growth and morphological changes of the organoids. These data provided important information for assessing the impact of experimental methods on organoid growth.

H&E staining

Tissue and organoids were fixed in 4% paraformaldehyde (PFA, BL539A, Biosharp) for 48 h, followed by gradient dehydration (1 h in 10%, 2 h in 20%, and overnight in 30% sucrose), then embedded in tissue-freezing medium (OCT) and rapidly frozen with liquid nitrogen. Section 10 micrometers thick were prepared using a microtome. Subsequently, H&E staining was performed according to the instructions provided with the H&E staining kit (G1120) from Solarbio (China).

RNA sequencing

After the collection of organoids, the samples were immediately placed on ice and treated with an adequate amount of TRIzol reagent for tissue lysis. The samples were then thoroughly homogenized using a disposable pestle to ensure complete

disruption of the tissue cells. The homogenate was carefully stored at –80 °C in a low-temperature freezer to maintain sample integrity. Subsequently, the samples were sent to Shanghai HonSun Biological Technology Co., Ltd. for professional sequencing services to ensure the accuracy and quality of the analysis.The bulk RNA-seq data were processed using the kb Python package, a wrapper around kallisto and bustools. The reference genome and gene annotation files were sourced from 10× Genomics. A kallisto index was created for efficient transcript-to-gene mapping. The resulting count matrices were imported into R for normalization and differential gene expression analysis using the DESeq2 R package. PCA was performed on the variable gene matrix, selecting the top 50 components for further analysis. To correct for batch effects from different organoids, the harmony algorithm was employed. Cell clusters were defined using the Leiden algorithm on nearest neighbor graphs based on harmonized embedding. UMAP was used for visualization. Marker genes were identified using Scanpy's `rank_genes_groups` function with logistic regression (method='logreg') for up to 200 genes. Cluster markers were interpreted, and cluster identities were assigned based on known cell type annotations from literature, such as Astrocyte (SLC1A2, S100B GFAP, ALDOC, PTN...), Cell Cycle (MKI67, TPO2A, PCNA, MCM5), Immune cell (PTPRC, CD8A, CD4, CD79A, CD19...), Oligodendrocyte/OPC(MOG, MBP, MAG, MOBP, SOX10, OLIG1, OLIG2, PDGFRA...), Vasculature (COL4A1, CLDN11, FN1, COL1A2).

Statistical analysis

Data were gathered from a minimum of three replicates, with the quantitative outcomes presented as the mean value accompanied by the standard deviation. The statistical analysis was executed utilizing GraphPad Prism 8.0.

Research ethics and patient consent

Clinical samples were collected in accordance with the ethical guidelines set forth by the Ethics Committee of Xinhua Hospital Affiliated with Shanghai Jiao Tong University School of Medicine. The study was granted ethical Approval No. XHEC-D-2024-019. Before donating samples, all participants provided informed consent, explicitly stating the intended use of their samples for future research. The voluntary participation and understanding of the study's objectives by the participants played a vital role in upholding ethical standards throughout the course of this research.

Availability of data and material

The data and materials that support the findings of this study are available from the corresponding author upon reasonable request.

Declaration of conflicting interests

This work was sponsored by Shanghai Lisheng Biotech Ltd (Lisheng). The manuscript was written in a responsible and ethical manner. X.X.H. is a shareholder of Lisheng, as a founder. Y.H.S., L.Y.L., C.W., J.Z., M.J.R., J.P.L and C.H.C. are senior scientists of Lisheng.

X.X.H. and C.H.C. are members of the Editorial Board for Cell Organoid. They were not involved in the journal's review of, or decisions related to, this manuscript.

Author contributions

X.X.H., C.H.C. and J.Z. conceived and designed the study. Y.H.S., L.Y.L., C.W., M.J.R.,B.B.T., H.T. and J. Z. collected the samples, and performed the experiments. J.P.L., C.H.C, X.X.H. and J.Z. analyzed the data. C.H.C., X.X.H., W.D. and J.Z. wrote the manuscript. All the authors read and approved the final version of the manuscript.

References

[1] Schaff, L. R., Mellinghoff, I. K. Glioblastoma and other primary brain malignancies in adults: a review. *JAMA*, **2023**, 329(7): 574–587. https://doi.org/10.1001/jama.2023.0023

[2] Ahluwalia, M. S., Reardon, D. A., Abad, A. P., Curry, W. T., Wong, E. T., Figel, S. A., Mechtler, L. L., Peereboom, D. M., Hutson, A. D., Withers, H. G. et al. Phase IIa study of SurVaxM plus adjuvant temozolomide for newly diagnosed glioblastoma. *Journal of Clinical Oncology*, **2023**, 41(7): 1453–1465. https://doi.org/10.1200/jco.22.00996

[3] Tsien, C. I., Pugh, S. L., Dicker, A. P., Raizer, J. J., Matuszak, M. M., Lallana, E. C., Huang, J. Y., Algan, O., Deb, N., Portelance, L. et al. NRG oncology/RTOG1205: A randomized phase II trial of concurrent bevacizumab and reirradiation versus bevacizumab alone as treatment for recurrent glioblastoma. *Journal of Clinical Oncology*, **2023**, 41(6): 1285–1295. https://doi.org/10.1200/jco.22.00164

[4] Gonçalves, E., Poulos, R. C., Cai, Z., Barthorpe, S., Manda, S. S., Lucas, N., Beck, A., Bucio-Noble, D., Dausmann, M., Hall, C., et al. Pan-cancer proteomic map of 949 human cell lines. *Cancer Cell*, **2022**, 40(8): 835–849. https://doi.org/10.1016/j.ccell.2022.06.010

[5] Barretina, J., Caponigro, G., Stransky, N., Venkatesan, K., Margolin, A. A., Kim, S., J Wilson, C., Lehár, J., Kryukov, G. V., Sonkin, D. et al. Addendum: The Cancer Cell Line Encyclopedia enables predictive modelling of anticancer drug sensitivity. *Nature*, **2012**, 492(7428): 290. https://doi.org/10.1038/nature11735

[6] Cowan, C. S., Renner, M., De Gennaro, M., Gross-Scherf, B., Goldblum, D., Hou, Y. Y., Munz, M., Rodrigues, T. M., Krol, J., Szikra, T., et al. Cell types of the human retina and its organoids at single-cell resolution. *Cell*, **2020**, 182(6): 1623–1640. https://doi.org/10.1016/j.cell.2020.08.013

[7] Mo, S. B., Tang, P. Y., Luo, W. Q., Zhang, L., Li, Y. Q., Hu, X., Ma, X. J., Chen, Y. K., Bao, Y. C., He, X. F. et al. Patient-derived organoids from colorectal cancer with paired liver metastasis reveal tumor heterogeneity and predict response to chemotherapy. *Advanced Science*, **2022**, 9(31): e2204097. https://doi.org/10.1002/advs.202204097

[8] Han, X. X., Cai, C. H., Deng, W., Shi, Y. H., Li, L. Y., Wang, C., Zhang, J., Rong, M. J., Liu, J. P., Fang, B. J. et al. Landscape of human organoids: Ideal model in clinics and research. *The Innovation*, **2024**, 5(3): 100620. https://doi.org/10.1016/j.xinn.2024.100620

[9] Bian, S., Repic, M., Guo, Z. M., Kavirayani, A., Burkard, T., Bagley, J. A., Krauditsch, C., Knoblich, J. A. Genetically engineered cerebral organoids model brain tumor formation. *Nature Methods*, **2018**, 15(8): 631–639. https://doi.org/10.1038/s41592-018-0070-7

[10] Gao, D., Vela, I., Sboner, A., Iaquinta, P. J., Karthaus, W. R., Gopalan, A., Dowling, C., Wanjala, J. N., Undvall, E. A., Arora, V. K. et al. Organoid cultures derived from patients with advanced prostate cancer. *Cell*, **2014**, 159(1): 176–187. https://doi.org/10.1016/j.cell.2014.08.016

[11] Drost, J., van Jaarsveld, R. H., Ponsioen, B., Zimberlin, C., van Boxtel, R., Buijs, A., Sachs, N., Overmeer, R. M., Offerhaus, G. J., Begthel, H. et al. Sequential cancer mutations in cultured human intestinal stem cells. *Nature*, **2015**, 521(7550): 43–47. https://doi.org/10.1038/nature14415

[12] Broutier, L., Mastrogiovanni, G., Verstegen, M. M., Francies, H. E., Gavarró, L. M., Bradshaw, C. R., Allen, G. E., Arnes-Benito, R., Sidorova, O., Gaspersz, M. P. et al. Human primary liver cancer-derived organoid cultures for disease modeling and drug screening. *Nature Medicine*, **2017**, 23(12): 1424–1435. https://doi.org/10.1038/nm.4438

[13] Sachs, N., de Ligt, J., Kopper, O., Gogola, E., Bounova, G., Weeber, F., Balgobind, A. V., Wind, K., Gracanin, A., Begthel, H. et al. A living biobank of breast cancer organoids captures disease heterogeneity. *Cell*, 2018, 172(1–2): 373–386.e10. https://doi.org/10.1016/j.cell.2017.11.010

[14] Kopper, O., de Witte, C. J., Lõhmussaar, K., Valle-Inclan, J. E., Hami, N., Kester, L., Balgobind, A. V., Korving, J., Proost, N., Begthel, H. et al. An organoid platform for ovarian cancer captures intra- and interpatient heterogeneity. *Nature Medicine*, **2019**, 25(5): 838–849. https://doi.org/10.1038/s41591-019-0422-6

[15] Boj, S. F., Hwang, C. I., Baker, L. A., Chio, I. I., Engle, D. D., Corbo, V., Jager, M., Ponz-Sarvise, M., Tiriac, H., Spector, M. S. et al. Organoid models of human and mouse ductal pancreatic cancer. *Cell*, **2015**, 160(1–2): 324–338. https://doi.org/10.1016/j.cell.2014.12.021

[16] Mun, S. J., Ryu, J. S., Lee, M. O., Son, Y. S., Oh, S. J., Cho, H. S., Son, M. Y., Kim, D. S., Kim, S. J., Yoo, H. J. et al. Generation of expandable human pluripotent stem cell-derived hepatocyte-like liver organoids. *Journal of Hepatology*, **2019**, 71(5): 970–985. https://doi.org/10.1016/j.jhep.2019.06.030

[17] Andersen, B. M., Faust, A. C., Wheeler, M. A., Chiocca, E. A., Reardon D. A., Quintana, F. J. Glial and myeloid heterogeneity in the brain tumour microenvironment. *Nature Review Cancer*, **2021**, 21(12): 786–802. https://doi.org/10.1038/s41568-021-00397-3

[18] Hubert, C. G., Rivera, M., Spangler, L. C., Wu, Q. L., Mack, S. C., Prager, B. C., Couce, M., McLendon, R. E., Sloan, A. E., Rich, J. N. A three-dimensional organoid culture system derived from human glioblastomas recapitulates the hypoxic gradients and cancer stem cell heterogeneity of tumors found *in vivo*. *Cancer Research*, **2016**, 76(8): 2465–2477. https://doi.org/10.1158/0008-5472.can- 15-2402

[19] Jacob, F., Salinas, R. D., Zhang, D. Y., Nguyen, P. T. T., Schnoll, J. G., Wong, S. Z. H., Thokala, R., Sheikh, S., Saxena, D., Prokop, S. et al. A patient-derived glioblastoma organoid model and biobank recapitulates inter- and intra-tumoral heterogeneity. *Cell*, **2020**, 180(1): 188–204.e22. https://doi.org/10.1016/j.cell.2019.11.036

[20] Ogawa, J., Pao, G., Shokhirev, M., Verma, I. Glioblastoma model using human cerebral organoids. *Cell Reports*, **2018**, 23(4): 1220–1229. https://doi.org/10.1016/j.celrep.2018.03.105

[21] Ratliff, M., Kim, H., Qi, H., Kim, M., Ku, B., Azorin, D. D., Hausmann, D., Khajuria, R. K., Patel, A., Maier, E., et al. Patient-derived tumor organoids for guidance of personalized drug therapies in recurrent glioblastoma. *International Journal of Molecular Sciences*, **2022**, 23(12): 6572. https://doi.org/10.3390/ijms23126572

[22] Silvia, V., Kedaigle Amanda, J., Simmons Sean, K., Allison, N., Marina, R., Giorgia, Q., Bruna, P., Lan, N., Xian, A., Aviv, R. et al. Individual brain organoids reproducibly form cell diversity of the human cerebral cortex. *Nature*, **2019**, 570(7762): 523–527. https://doi.org/10.1038/s41586-019- 1289-x

[23] Zhang, C. C., Jin, M. Z., Zhao, J. N., Chen, J. X., Jin, W. L. Organoid models of glioblastoma: Advances, applications and challenges. *American Journal of Cancer Research*, **2020**, 10(8): 2242–2257.

[24] Qiu, G.-Z., Mao, X.-Y., Ma, Y., Gao, X.-C., Wang, Z., Jin, M.-Z., Sun, W., Zou, Y.-X., Lin, J., Fu, H.-L., et al. Ubiquitin-specific protease 22 acts as an oncoprotein to maintain glioma malignancy through deubiquitinating b cell-specific moloney murine leukemia virus integration site 1 for stabilization. *Cancer Science*, **2018**, 109(7): 2199–2210. https://doi.org/10.1111/cas.13646

[25] Li, H., Chen, L., Li, J. J., Zhou, Q., Huang, A. N., Liu, W. W., Wang, K., Gao, L., Qi, S. T., Lu, Y. T. MiR-519a enhances chemosensitivity and promotes autophagy in glioblastoma by targeting STAT3/Bcl2 signaling pathway. *Journal ofHematology & Oncology*, **2018**, 11(1): 70. https://doi.org/10.1186/s13045-018-0618-0

[26] Allen, M., Bjerke, M., Edlund, H., Nelander, S., Westermark, B. Origin of the u87mg glioma cell line: good news and bad news. *Science Translation Medicine*, **2016**, 8(354): 354re3. https://doi.org/10.1126/scitranslmed.aaf685

[27] Da Hora, C. C., Schweiger, M. W., Wurdinger, T., Tannous, B. A. Patient-derived glioma models: from patients to dish to animals. *Cells*, **2019**, 8(10): 1177. https://doi.org/10.3390/cells8101177

[28] Krieger, T., Tirier, S., Park, J., Eisemann, T., Peterziel, H., Angel, P., Eils, R., Conrad, C. Modeling glioblastoma invasion using human brain organoids and single-cell transcriptomics. *Neuro-Oncology*, **2020**, 22(8): 1138–1149. https://doi.org/10.1093/neuonc/noaa091

[29] Neftel, C., Laffy, J., Filbin, M. G., Hara, T., Shore, M., Shore, M., Rahme, G., Rahme, G., Richman, A. R., Richman, A. R. et al. An integrative model of cellular states, plasticity, and genetics for glioblastoma. *Cell*, **2019**, 178(4): 835–849. https://doi.org/10.1016/j.cell.2019.06.024

[30] Pitt, J. M., Marabelle, A., Eggermont, A., Soria, J. C., Kroemer, G., Zitvogel, L. Targeting the tumor microenvironment: Removing obstruction to anticancer immune responses and immunotherapy. *Annals of Oncology*, **2016**, 27(8): 1482–1492. https://doi.org/10.1093/annonc/mdw168

[31] Jin, M. Z., Jin, W. L. The updated landscape of tumor microenvironment and drug repurposing. *Signal Transduction and Targeted Therapy*, **2020**, 5: 166. https://doi.org/10.1038/s41392-020-00280-x

[32] Tang, H. D., Qiao, J., Fu, Y.-X. Immunotherapy and tumor microenvironment. *Cancer Letters*, **2016**, 370(1): 85–90. https://doi.org/10.1016/j.canlet.2015.10.009

[33] Fu, T., Dai, L. J., Wu, S. Y., Xiao, Y., Ma, D., Jiang, Y. Z., Shao, Z. M. Spatial architecture of the immune microenvironment orchestrates tumor immunity and therapeutic response. *Journal of Hematology & Oncology*, **2021**, 14(1): 98. https://doi.org/10.1186/s13045-021-01103-4

[34] Grönholm, M., Feodoroff, M., Antignani, G., Martins, B., Hamdan, F., Cerullo, V. Patient-derived organoids for precision cancer immunotherapy. *Cancer Research*, **2021**, 81(12): 3149–3155. https://doi.org/10.1158/0008-5472.CAN-20-4026

Received: 8 November 2023 | Revised: 15 June 2024 | Accepted: 28 June 2024

DOI: 10.1002/mco2.697

MedComm WILEY

ORIGINAL ARTICLE

Patient-derived ovarian cancer organoid carries immune microenvironment and bloodvessel keeping high response to cisplatin

Yuqing Zhao[1,#] | Chen Wang[2,#] | Wei Deng[3,4,#] | Lanyang Li[2,#] | Jiping Liu[2] | Yanghua Shi[2] | Xiang Tao[1] | Jian Zhang[2] | Qi Cao[1,*] | Chunhui Cai[2,*] | Xinxin Han[2,5,*]

[1] Obstetrics & Gynecology Hospital, Fudan University, Shanghai, China

[2] Department of Research, Shanghai LiSheng Biotech, Shanghai, China

[3] LongHua Hospital, Shanghai University of Traditional Chinese Medicine, Shanghai, China

[4] Department of Oncology, Shanghai Ninth People's Hospital, Shanghai Jiao Tong University School of Medicine, Shanghai, China

[5] Organ Regeneration X Lab, LiSheng East China Institute of Biotechnology, Peking University, Jiangsu, China

[*] **Correspondence**

Xinxin Han, Organ Regeneration X Lab, LiSheng East China Institute of Biotechnology, Peking University, Jiangsu 226299, China.

Email: xxhan@sibs.ac.cn

Chunhui Cai, Department of Research, Shanghai LiSheng Biotech, Shanghai, China.

Email: caichunhui@lishengbiotech.com

Qi Cao, Obstetrics & Gynecology Hospital, Fudan University, Shanghai, China.

Email: qicao@fudan.edu.cn

Funding information

National Natural Science Foundation of China, Grant/Award Numbers: 82374506, 32200581

Abstract

Ovarian cancer is high recurrence and mortality malignant tumor. The most common ovarian cancer was High-Grade Serous Ovarian Cancer. However, High-Grade Serous Ovarian Cancer organoid is rare, which organoid with patient immune microenvironment and blood vessels even absence. Here, we report a novel High-Grade Serous Ovarian Cancer organoid system derived from patient ovarian cancer samples. These organoids recapitulate High-Grade Serous Ovarian Cancer organoids' histological and molecular heterogeneity while preserving the critical immune microenvironment and blood vessels, as evidenced by the presence of *CD34+* endothelial cells. Whole exome sequencing identifies key mutations (*CSMD3*, *TP53*, *GABRA6*). Organoids show promise in testing cisplatin sensitivity for patients resistant to carboplatin and paclitaxel, with notable responses in cancer proteoglycans and *p53* (*TP53*) signaling, like *ACTG*/*ACTB1*/*AKT2* genes and *BBC3*/*MDM2*/*PERP*. Integration of immune microenvironment and blood vessels enhances potential for novel therapies like immunotherapies and angiogenesis inhibitors. Our work may provide a new detection system and theoretical basis for ovarian cancer research and individual therapy.

[#] Yuqing Zhao, Chen Wang, Wei Deng and Lanyang Li contributed equally to this work.

KEYWORDS
cisplatin, organoid, ovarian cancer, tumor microenvironment (TME), vascularization

1 | INTRODUCTION

Ovarian cancer, a complex and multifaceted disease, remains a formidable challenge in oncology, with High-Grade Serous Ovarian Cancer (HGSOC) being the most aggressive and prevalent form.[1,2] Despite advances in detection and treatment, HGSOC is characterized by high recurrence, incidence, and mortality rates that underscore the urgent need for more effective therapeutic strategies.[3–5] The 5-year relative survival rate for all types of ovarian cancer is approximately 50%, with significant variation depending on factors such as the stage at diagnosis, age, and health of the patient, and the efficacy of the treatment plan.[6–8]The standard first-line treatment for ovarian cancer postsurgery has been a regimen of platinum-based chemotherapy, such as carboplatin or cisplatin, combined with paclitaxel or similar drugs.[9,10] While this approach can be initially effective, approximately 70% of HGSOC patients experience a recurrence, highlighting the limitations of current therapies and the critical need for alternative strategies.[11–14] In cases of platinum-resistant ovarian cancer, a variety of treatments are considered, including targeted therapy with Bevacizumab, which inhibits angiogenesis by blocking VEGF-A, and PARP inhibitors like Niraparib and Olaparib that interfere with DNA repair mechanisms in cancer cells.[11,15,16] Additionally, the integration of chemotherapy with immunotherapies, such as checkpoint inhibitors Nivolumab and Pembrolizumab, represents a promising avenue of exploration.[17]

HGSOC, characterized by its aggressive nature and high relapse rate, exemplifies the limitations of a one-size-fits-all treatment approach. This situation highlights a profound need for personalized treatment plans, driven by a deep understanding of individual tumor biology and patient-specific response patterns to various therapies.[18,19] The intricate interplay of genetic, molecular, and environmental factors influencing tumor behavior necessitates a departure from traditional treatment modalities towards more individualized strategies.[1,20–22] The advent of organoid technology, which allows for the cultivation of patient-derived tumor cells in three-dimensional structures that closely replicate the cellular heterogeneity, genomic characteristics, and microenvironment of the original tumor, offers a groundbreaking approach to precision medicine.[23–26] By enabling high-fidelity disease modeling and drug response testing, organoids hold the potential to transform the landscape of ovarian cancer treatment, paving the way for highly individualized and effective therapeutic strategies. This approach not only enhances the efficacy of treatment but also minimizes the risk of adverse effects and the development of resistance.[27–31]

In the evolving landscape of ovarian cancer research, the development of models that accurately reflect the complex biology of HGSOC remains a critical challenge.[32] Herein, we introduce a meticulously developed method for the swift creation of ovarian cancer organoids from freshly procured tumor samples, employing a defined culture medium without necessitating single-cell dissociation. Our initiative has led to the establishment of a little biobank of ovarian cancer organoids, alongside thorough histological, molecular, and genomic evaluations demonstrating that these organoids closely mirror the heterogeneity observed both between and within tumors. These organoids faithfully preserve key features of their parental tumors, including specific immune cell markers and vascular endothelial markers, thus demonstrating the advanced methodological design and biological fidelity of the organoid platform.

Our organoids have been meticulously engineered to encapsulate a wide array of cellular markers identified through single-cell RNA sequencing (scRNA-seq), providing insight into the cellular heterogeneity inherent to HGSOC. This includes the identification of specific immune cell markers and vascular endothelial markers, crucial for understanding the interactions within the tumor microenvironment. For instance, the presence of *CD4*, *CD8A*, and *CD8B* for T cells, and *PECAM1*, *CD34*, and *CDH5* for endothelial cells within our organoids offers a nuanced view of the tumor's immune landscape and vascular network. This comprehensive characterization exemplifies our dedication to developing a model that closely mimics the complex biological landscape of ovarian malignancies. A cornerstone of our research has been the application of these organoids in assessing the responsiveness to cisplatin, particularly for patients who have previously undergone treatment with carboplatin and paclitaxel. This approach yielded insights that are closely aligned with the patients' individual reactions, thereby offering a predictive framework for addressing resistance to standard chemotherapy regimens. It is a testament to our organoids' utility in facilitating personalized treatment strategies, marking a stride towards precision oncology.

2 | RESULTS

2.1 | Culture and characterization of ovarian cancer organoids from patient-derived tumors

In an effort to closely emulate the intricate morphological characteristics and crucial cell–cell interactions present in original ovarian tumors, we devised a novel organoid culture protocol. This method circumvents the enzymatic dissociation of tumors into single cells, thereby preserving the structural integrity and cellular heterogeneity of the original tumor tissue. We totally established 7 organoids in this research, including OV004 (61 years old, HGSOC), OV014 (68 years old, HGSOC), OV015 (52 years old, HGSOC), OV016 (69 years old, HGSOC), OV076 (59 years old, right-sided fallopian tube mass), OV077 (96 years old, unknown) and OV078 (67 years old, unknown). Utilizing precision-cutting techniques, we sectioned patient-derived ovarian tumors into fragments approximately 1 mm in size. These fragments were sourced from various regions within the tumors to encompass a broad representation of the tumor's cellular composition (Figure 1A). Notably, our protocol deliberately abstained from removing red blood cells and tissue debris, a step we hypothesized would aid in maintaining the organoid's fidelity to the tumor's microenvironment.

Upon incubation at standard culture conditions, we observed the formation of three distinct ovarian cancer organoids. Each organoid exhibited successful culture establishment and, within approximately 2 weeks, demonstrated spherical growth, indicative of their proliferative capacity. Histological examination of the organoids revealed the preservation of key features characteristic of ovarian tumors, including the presence of intra-organoid vascular structures. Interestingly, despite our method not incorporating a red blood cell removal step, the vascular features within the ovarian cancer organoids were distinctly observable, with blood vessels persisting for up to 18 days in culture (Figure 1B). Immunohistochemical analysis further substantiated the presence of vascular structures, with CD31 expression delineating a tubular vascular pattern within the organoids (Figure 1B). Moreover, our culture conditions facilitated the preservation of diverse cell types, suggesting the retention of the cellular diversity within the organoids, especially CD4+ and CD8+ T cells (Figure 1C).

The ovarian cancer organoids' capacity for subculture was also evaluated. Following a 28-day incubation period, the organoids were mechanically divided and redistributed across new culture vessels. Remarkably, these secondary organoids mirrored the initial spherical morphology observed in their predecessors, although they lacked vascular components, likely attributable to the absence of hematopoietic functionality (Figure 1D).

Our study demonstrates the successful establishment of ovarian cancer organoids that not only maintain growth ability but also show potential in preserving the native immune microenvironment and blood vessel. This advancement represents a significant step forward in the development of biologically relevant in vitro models for ovarian cancer, offering promising avenues for future therapeutic research and personalized medicine approaches.

2.2 | Preservation of tumor molecular characteristics in ovarian cancer organoids

Addressing the inherent challenge of replicating the complex heterogeneity of ovarian tumors, our study focuses on the capacity of ovarian cancer organoids to mirror the diverse cellular makeup of the parent tumors accurately. Employing scRNA-seq at day 14 postformation, we identified distinct cell clusters within the ovarian cancer organoids. Cross-referencing with recent single-cell sequencing datasets from ovarian cancer tissues, the cellular composition of our organoids is largely similar to that of public data (Figure 2A and B). These included T cells (positive for *CD3* and *CD8*), endothelial cells (positive for *CD34* and *FLT1*), smooth muscle cells (*DCN* and *ACTA2* positive), monocytes and macrophages (*LYZ* and *CD163* positive), and B cells (*CD79A* positive). This evidence confirms the existence of equivalent cell populations within the ovarian cancer organoids, validating the capacity of our organoid model to faithfully recapitulate the cellular diversity inherent to ovarian tumors (Figure 2B).[33]

Focusing on the organoids' microenvironment, particularly the vascular and immune components, we analyzed the expression of key marker genes. Notably, the presence of vascular endothelial markers, such as *FLT1*, *CD34*, and *KDR*, underscores the organoids' capability to maintain blood vessel-like structures. Simultaneously, the detection of T-cell markers, including *CD3* and *CD8*, highlights the preservation of immune cell subsets within the ovarian cancer organoids. This cellular composition, closely mirroring that of the original ovarian tissues, emphasizes the ovarian cancer organoids' utility as a robust model for studying ovarian cancer in a physiologically relevant context (Figure 2C and D).

To assess the genetic stability of ovarian cancer organoids over the culture period, whole exome sequencing (WES) was performed, revealing the preservation of key ovarian cancer-related mutations, including *CSMD3*, *TP53*, and *GABRA6*. Comparative analysis between the

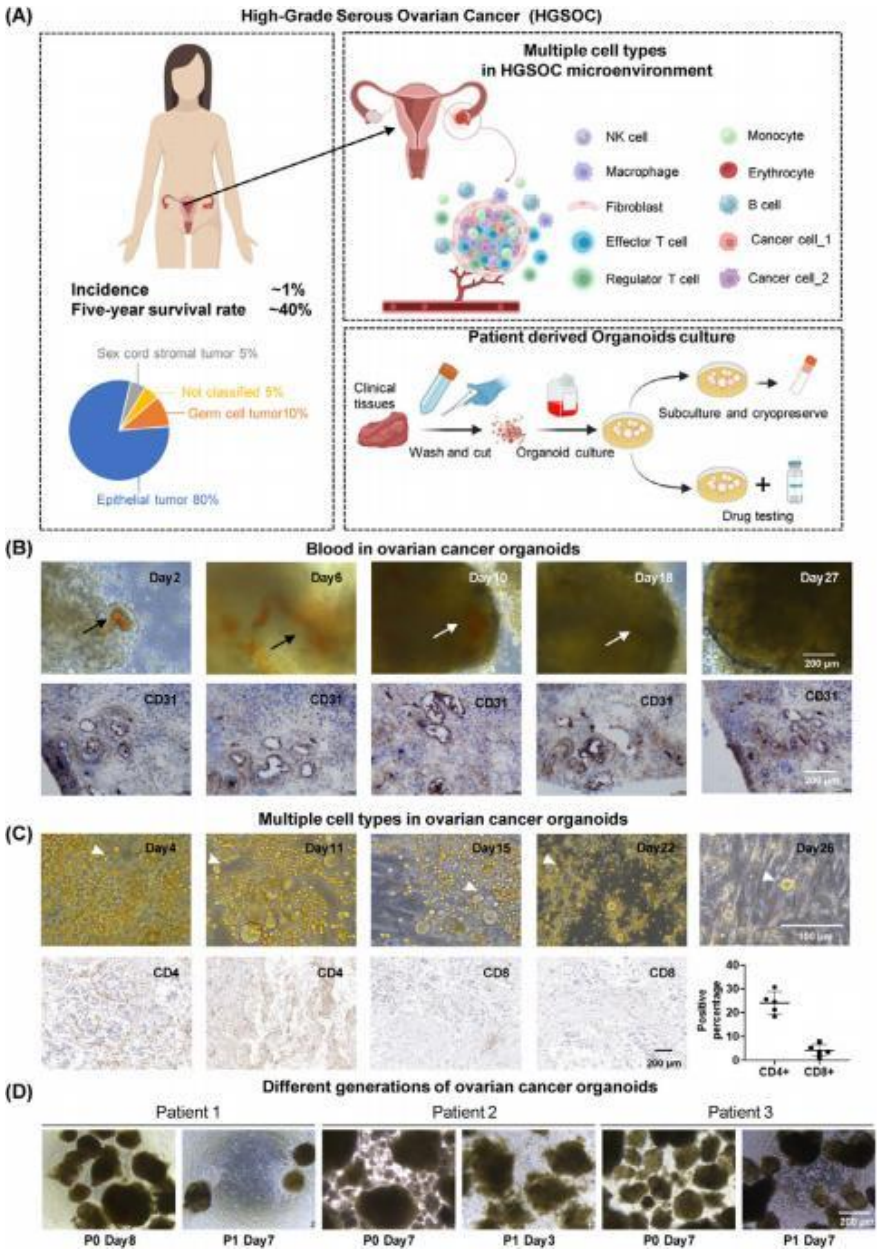

FIGURE 1 Establishment of reproducible ovarian cancer organoid model. The tumor tissue obtained from the patient was washed and minced into pieces of less than 2 mm in diameter using dissecting scissors. The minced tissue was then resuspended in culture medium and culture in Petri dish. (A) Left: Overview of HGSOC. Right: Cell types in HGSOC and schematic diagram of establishment of ovarian cancer organoids. Throughout the culture process, neither enzymatic digestion nor matrigel were employed. (B) Top: Morphology of P0 ovarian cancer organoids. Blood vessels were visible until day 18. Arrows indicate blood vessels in ovarian cancer organoids. Bottom: Distribution of CD31 positive cells in organoids. The tubular distribution indicated existence of blood vessels. Different images originate from different sections of the same organoid. (C) Cells in P0 ovarian cancer organoids. Top: In addition to cells evolved in organoids, suspension cells with diversity morphology were maintained in culture system. Tips point to different cell types in dish. Bottom: The presence of $CD4^+$ and $CD8^+$ T cells within the organoids, as demonstrated by IHC staining. (D) Subculture of ovarian cancer organoids. Ovarian cancer organoids maintained growth ability from P0 to P1.

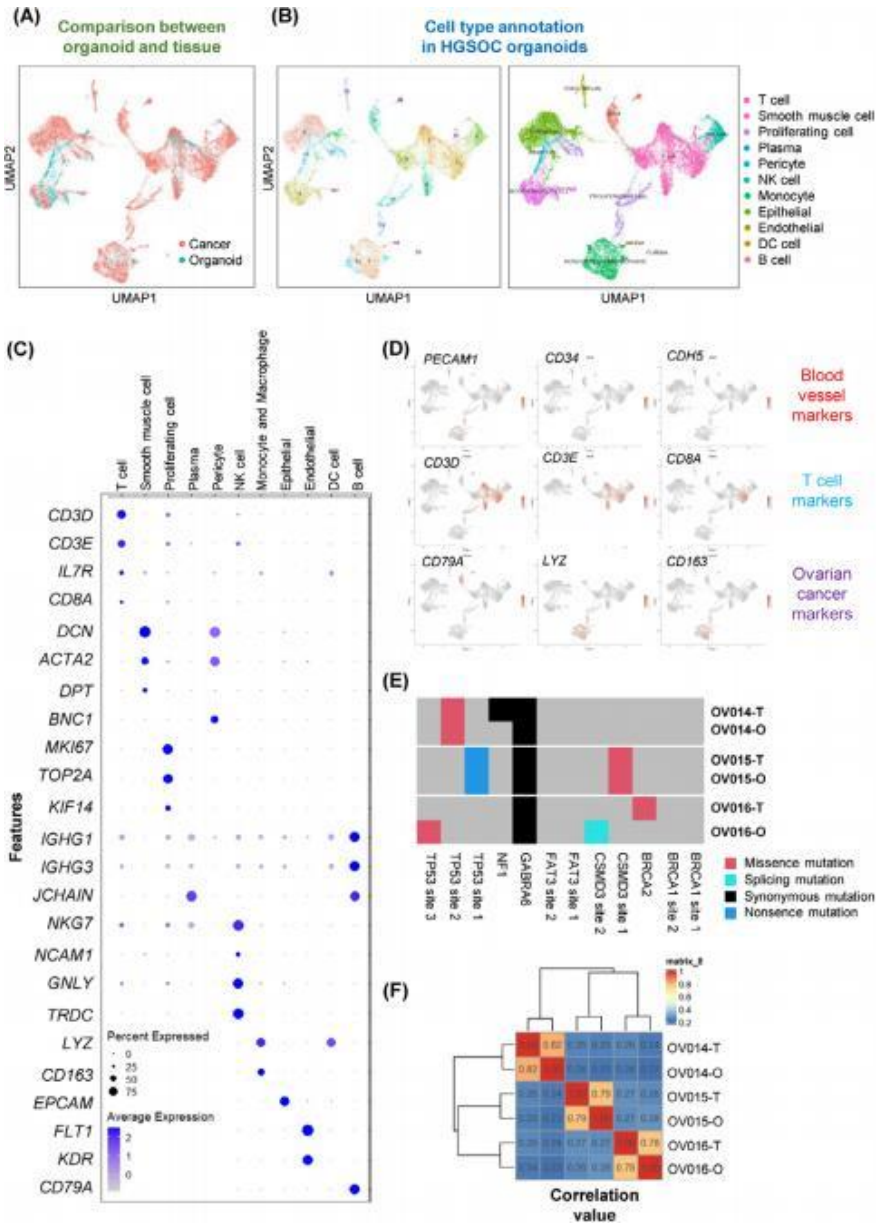

FIGURE 2 Results ofscRNA-seq and WES of ovarian organoids. (A) UMAP visualization of single-cell RNA-seq results compared with public dataset. The distribution patterns of UMAP of organoids and tissues exhibit similarity. (B) Annotation of organoids and ovarian cancers regarding the composition of cell types. All 11 cell types were identified in both organoids and tissues, demonstrating the similarity between ovarian cancer organoids and tissues. (C) Expression profiles of different cell type marker genes in organoids and cancer tissues. (D) Marker genes of blood vessel cells, T cells, and other immune cells. Top: Blood vessel cell marker genes *PECAM1*, *CD34*, and *CDH5* expressed in endothelial cells, indicating the presence of vascular endothelial cells. Middle: Three clusters ofT cells were annotated into $CD3^+$ and $CD8^+$ T cells. Bottom: Marker genes of B cells (*CD79A*), macrophages (*CD163*), and monocytes (*LYZ*). (E) Mutation types of critical cancer genes in tissue and organoids, including *BRCA1/2*, *TP53*, and *CSMD3*. (F) Correlation value between samples, including tissues and organoids. Organoids and its parent tissues maintain high correlation value compared with other groups.

organoids and their tissue of origin demonstrated a high correlation, affirming that ovarian cancer organoids maintain the genetic landscape of the parent tumors throughout the culture process (Figure 2E and F).

Our findings underscore the ovarian cancer organoids' remarkable ability to preserve the complex cellular and molecular landscape of ovarian tumors, offering a promising platform for in-depth studies on tumor biology, drug testing, and personalized medicine approaches in ovarian cancer.

2.3 | Preservation of tumor pathological phenotypes in ovarian cancer organoids

The criticality of maintaining not only cellular types but also their inherent organizational architecture to emulate biological function is paramount in our study. Our assessment of the organoids' pathological features elucidates this cellular organization and the expression profiles of pivotal biomarkers. Utilizing hematoxylin and eosin (H&E) staining, we established a clear parallelism in the tissue architecture between the organoids and their clinical counterparts (Figure 3A), affirming the organoids' capability to conserve the structural integrity observed in vivo. Additionally, the nuclear-to-cytoplasmic (N/C) ratio, a metric indicative of malignancy, was closely studied. The comparative N/C ratios, 1.056 in tissue versus 0.901 in organoids for one patient pair and 0.524 versus 0.578 for another, demonstrate the organoids' proficiency in mirroring the cytological features pertinent to cancer assessment (Figure 3B).

In the clinical setting, Ki67 serves as a prognostic marker for ovarian cancer, reflecting cellular proliferation rates, while PAX8 identifies the gynecological origin of the malignancy, correlating with patient outcomes. Our meticulous immunohistochemical (IHC) evaluation demonstrated analogous expression and localization patterns for Ki67 and PAX8 across organoids and tissue samples (Figure 3C). Despite some quantitative differences—38.8–42.1% for Ki67 and 41.2–51.3% for PAX8 in organoids versus 70.5–72.2% and 56.5–60.1% in tissues, respectively (Figure 3D)—these variations provide insights into the microenvironmental adaptation within the organoid culture.

Collectively, these findings substantiate the organoids' utility in preserving and reflecting the pathological nuances of ovarian cancer, showcasing their potential as an instrumental model for the pathological study and therapeutic assessment of this disease. Through these organoid models, we can achieve a more nuanced understanding of ovarian cancer's pathology, facilitating advanced research and personalized treatment approaches.

2.4 | Enhanced cisplatin sensitivity assessment through patient-derived ovarian cancer organoid models

Central to our investigation has been the application of patient-derived ovarian cancer organoids for evaluating cisplatin responsiveness, particularly in the context of patients previously treated with carboplatin and paclitaxel. To establish a rapid screening method for drug sensitivity, we assessed the impact of cisplatin on ovarian cancer organoids. Notably, after a 3-day exposure to 16.7 μM of cisplatin, the treated organoids exhibited a marked structural collapse compared to the untreated control group, suggesting significant sensitivity to cisplatin at this concentration (Figure 4A). Further elucidation of cisplatin's effect was obtained through flow cytometry analysis of cell apoptosis. This revealed a substantial increase in the fraction of early-stage apoptotic cells (PI-/Annexin V+) posttreatment, with the extent of early-stage apoptosis amplifying in response to higher cisplatin concentrations. Conversely, the proportion of cells in late-stage apoptosis remained unchanged, underscoring cisplatin's mechanism of action through the induction of early apoptosis (Figures 4B and C). Corroborating this, caspase-3 levels, indicative of early-stage apoptosis, were significantly elevated in cisplatin-treated cells (Figure 4D). This dose-dependent effect highlights the ineffectiveness of low cisplatin concentrations in suppressing ovarian cancer organoids' activity, emphasizing the drug's cytotoxic efficacy at higher doses. Indeed, different concentrations of cisplatin have different inhibitory effects on organoids (Figure 4E). Immunocytochemistry (ICC) analysis further demonstrated a diminished proliferation capacity within the organoids following cisplatin treatment, as evidenced by a significant reduction in Ki67 expression. In contrast, PAX8 expression remained unaffected, indicating the specificity of cisplatin's action on proliferative markers (Figure 4F).

Collectively, our findings affirm that cisplatin significantly curtails the proliferative capabilities of ovarian cancer organoids, aligning with clinical observations and underscoring the utility of ovarian cancer organoids in devising personalized treatment plans. This study also reinforces the predictive value of organoids in fast-assessing drug sensitivity.

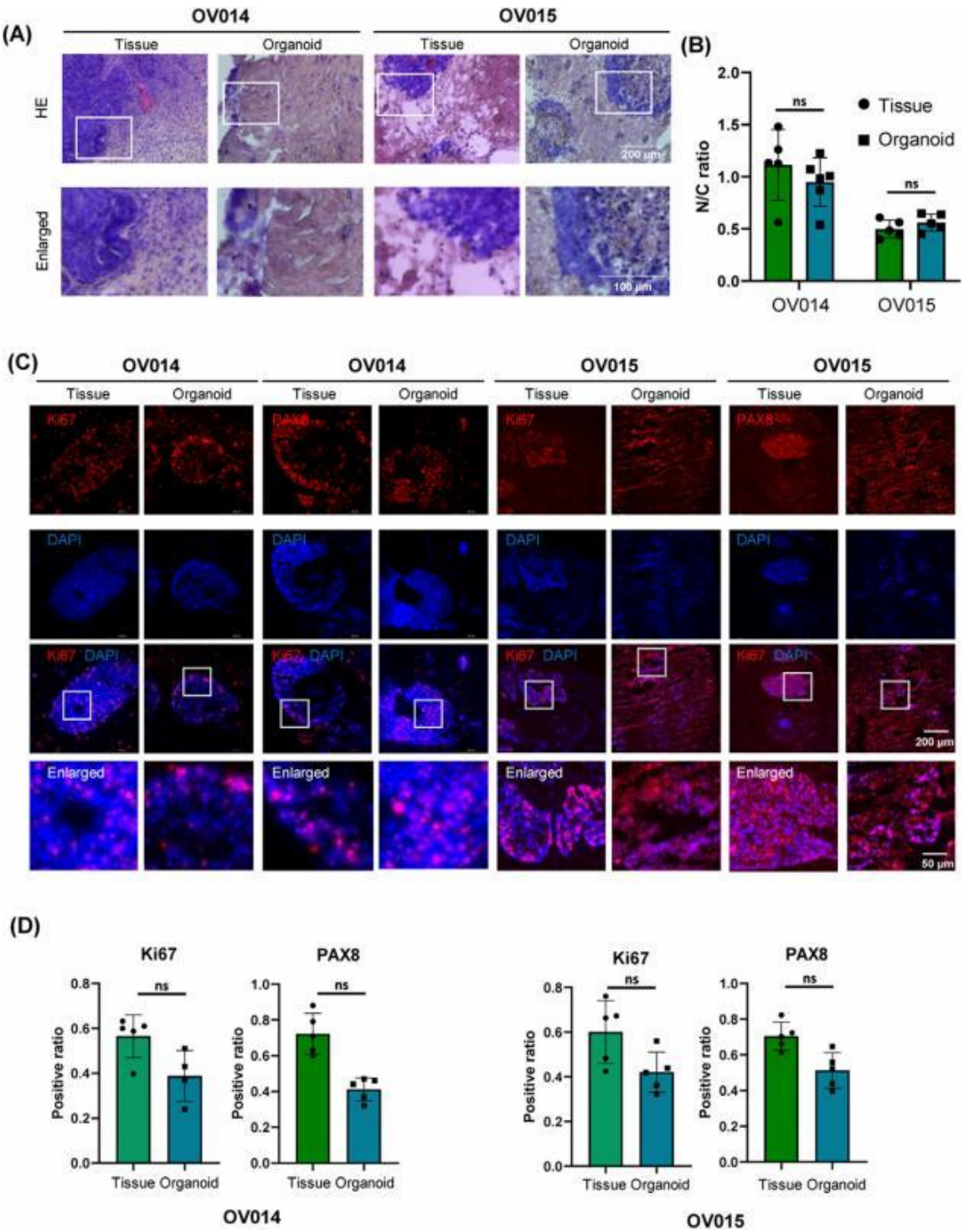

FIGURE 3 Resemblance of histopathological characteristics and biomarker expression patterns between ovarian cancer organoids and primary tissues. All image data were derived from P0 organoids. (A) Similar structures between tissues and organoids stained with H&E. (B) Organoids maintained similar N/C ratio compared with tissues, indicated its cancerous characteristic. The ratio of nuclei and cytoplasm were defined by H&E staining area. (C) ICC results of ovarian cancer organoids and tissues indicated similar distribution patterns of Ki67 and PAX8 in organoids and tissues. (D) Expression level of cell markers PAX8 and Ki67. Expression level of Ki67 was similar between organoids and tissues. However, expression of PAX8 decreased in organoids, possibly due to in vitro culture environment. ns, no significance.

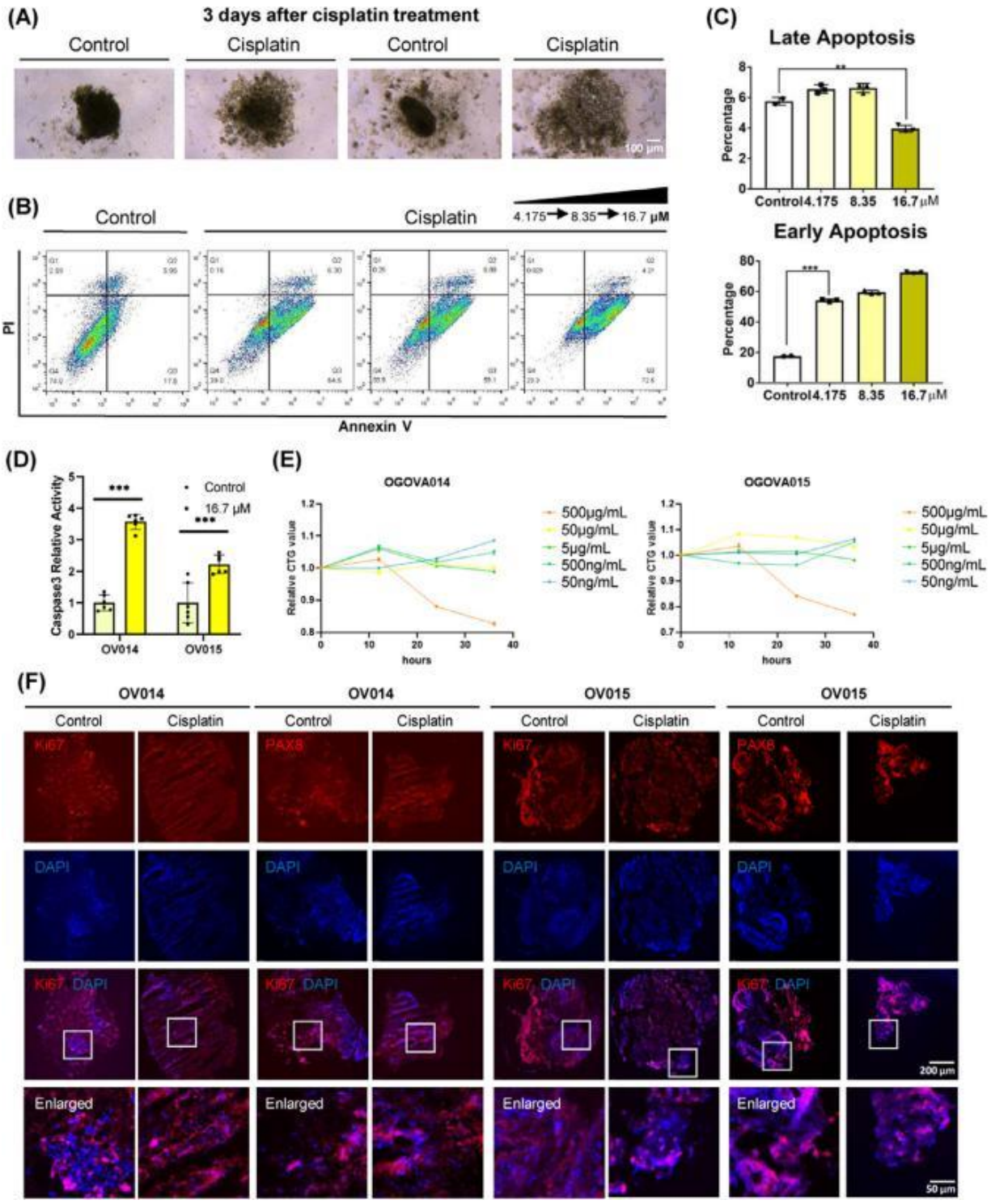

FIGURE 4 Cisplatin sensitivity test using ovarian cancer organoids. (A) Morphology changes between control and cisplatin-treated organoids. After cisplatin treatment, ovarian cancer organoids became obvious collapse. (B, C) Early-stage apoptosis was induced by cisplatin treatment validated with flow cytometry. (D) Caspase3, a biomarker of early-stage apoptosis, increased after cisplatin treatment, validating that early-stage apoptosis occurs. (E) CTG assay results of organoids under different concentration cisplatin treatment. (F) Expression level of Ki67 decreased after cisplatin treatment, but PAX8 maintained a stable level. $^{**}p < 0.01$; $^{***}p < 0.001$.

2.5 | Deepened molecular understanding ofcisplatin responsiveness through patient-derived ovarian cancer organoid models

In order to study the intricacies of cisplatin's impact on ovarian cancer at the molecular level, we conducted RNA-seq analysis on two sets of patient-derived ovarian cancer organoids subjected to cisplatin treatment. The analysis revealed significant alterations in the gene expression profiles under the influence of cisplatin, demonstrating the drug's pervasive action across various patient-derived models (Figure 5A). Among the top 1000 genes modulated by cisplatin treatment, there was a substantial overlap, with 339 genes upregulated and 346 genes downregulated in both sets of organoids (Figure 5B). This overlap highlights the consistent and broad-spectrum efficacy of cisplatin across different ovarian cancer backgrounds.

Further exploration of these changes through Gene Ontology (GO) and Kyoto Encyclopedia of Genes and Genomes (KEGG) pathway analyses pinpointed specific clusters of genes that were differentially regulated by cisplatin treatment. Notably, there was an enhanced expression of genes associated with apoptosis in the cisplatin-treated organoids, in contrast to the control group, which showed elevated expression of genes involved in cell division (Figure 5C). This differential gene expression pattern aligns with our understanding that cisplatin exerts its anticancer effects primarily through the induction of apoptosis.

Particularly, the analysis shed light on the differential pathway activation between the control and cisplatin-treated groups (Figure 5D). Control organoids demonstrated heightened activity of genes related to cancer proteoglycans, indicating an active metabolic state conducive to cancer progression. Conversely, the cisplatin-treated organoids exhibited a marked upregulation of genes within the p53 signaling pathway, suggesting that cisplatin's mechanism of inhibiting cancer cell proliferation is mediated through apoptosis, triggered by the activation of the p53 pathway. This observation is in harmony with previous study,[34,35] underscoring the pivotal role of the p53 pathway in cisplatin-induced apoptosis mechanisms. Moreover, our RNA-seq analysis unveiled a notable reduction in the expression of genes crucial for cell proliferation and tumor genesis, such as *Ki67* and *BRCA1/2*, following cisplatin administration. This finding substantiates the drug's efficacy in curtailing oncogenic processes within the organoids.

In summary, notwithstanding the interpatient heterogeneity, the organoid models consistently recapitulated the clinical efficacy of cisplatin, corroborating the notion that these organoids retain patient-specific biological features and substantiating their value in drug sensitivity testing. This convergence of clinical and organoid-based responses to cisplatin underscores the potential of organoid models in facilitating personalized oncology, particularly in predicting and understanding patient-specific responses to chemotherapy.

3 | DISCUSSION

This study introduces a novel organoid model derived from patient ovarian tumors, encapsulating the complex heterogeneity and microenvironmental intricacies of HGSOC. Our findings underscore the organoids' remarkable fidelity in replicating the histological and molecular landscapes of the originating tumors, alongside preserving key components of the immune system and vascular structures. This mirrors the methodological advancements and contributions to the field of cancer research akin to those detailed in our reference document, emphasizing the organoid model's potential in translational research.

Ovarian cancer is characterized by its significant heterogeneity and a commonality of late-stage diagnosis, presenting substantial challenges in both understanding and treating this malignancy effectively.[36] Despite huge advancements,[2–4] the field of ovarian cancer organoid modeling still faces considerable hurdles, particularly in the accurate simulation of tumor markers and the cancer's inherent heterogeneity.[37] These aspects are crucial for a realistic representation of the disease, yet existing models often fall short in capturing this complexity fully. A more nuanced organoid model that endeavors to closely approximate the tumor markers and heterogeneity inherent in ovarian cancer could potentially facilitate advancementsin critical areas of research.

A principal advantage of our approach lies in the maintenance of the immune microenvironment and vasculature within the organoids, alongside the rapid assessment of drug responses. This integration of immune and vascular markers signifies a critical methodological progression, enabling a more detailed evaluation of therapeutic effectiveness and the mechanisms of resistance. These advancements also deepen our comprehension of the biological intricacies of HGSOC.

While our study represents a significant step forward in ovarian cancer research, it is not without limitations. The scalability of organoid models and the potential for selection bias in tumor sample procurement necessitate cautious interpretation of our results. However, the strengths of our study, particularly the methodological innovations in organoid development and the comprehensive analysis of chemotherapy responsiveness, provide a solid foundation for future research. Our previous research has demonstrated that our organoid model also responds to PARP inhibitors, suggesting the potential of

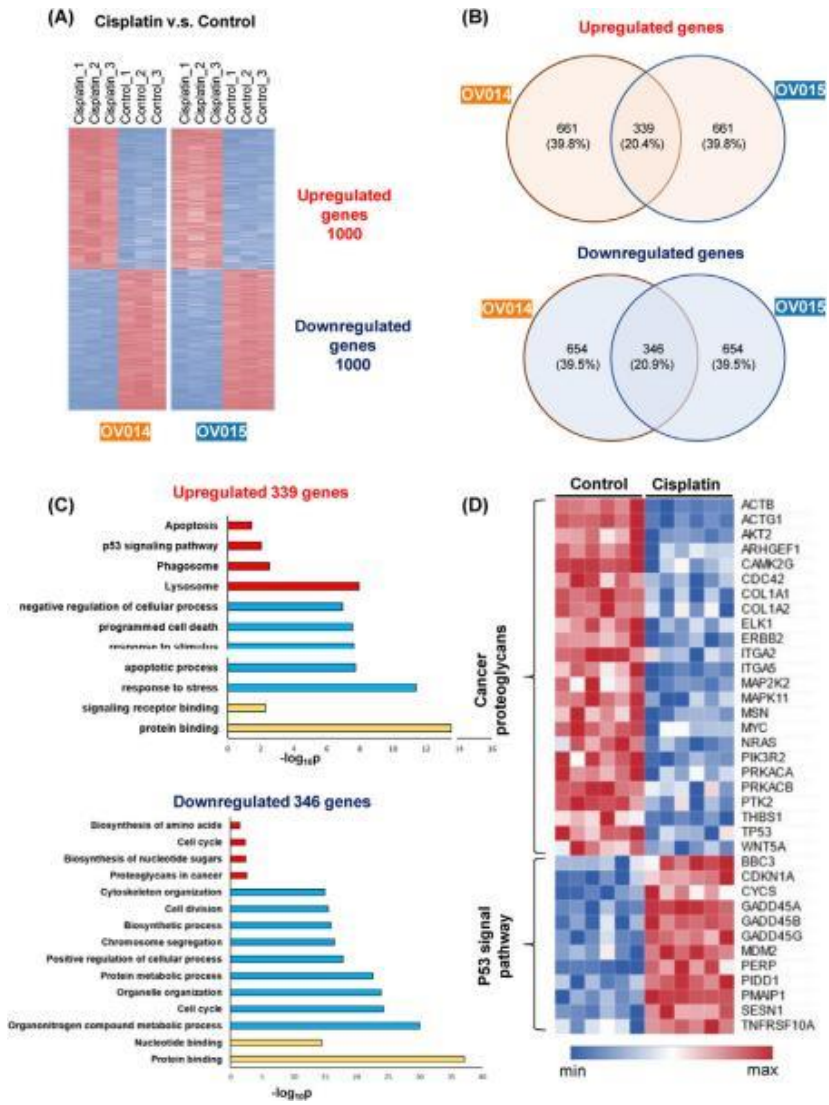

FIGURE 5 Transcriptome analysis ofcisplatin-treated ovarian cancer organoids. (A) Obvious changes in gene expression profiles between control and cisplatin-treated organoids. Only top 1000 genes that were up- or downregulated are shown. (B) Organoids derived from two individual patients showed an overlap of regulated genes. Despite heterogeneity between patients, similar response occurred in two organoid lines. (C) GO and KEGG analysis of regulated genes in two organoid lines. Consistent with previous studies, p53 pathway was upregulated under cisplatin treatment. (D) Heatmap of genes in p53 pathway and cancer proteoglycans synthesis.

this model in drug sensitivity testing for various types of medications.[38]

Looking ahead, the potential applications of our organoid model extend beyond the scope of this study. Using the aforementioned experimental methods, we have established organoid models including dermatofibrosarcoma protuberans (DFSP), intrahepatic cholangiocarcinoma (ICC), and glioblastoma.[39–43] Future research should explore the organoids' utility in screening a broader range of therapeutic agents, including immunotherapies and targeted therapies, to further tailor treatment plans to individual patient profiles. Additionally, expanding the organoid model to encompass other cancer types could offer new avenues for understanding and treating cancer at a personalized level.[44]

4 | METHODS

4.1 | Patient information

Ovarian cancer tissues were collected from 7 individual patients (OV004(61 years old, HGSOC), OV014(68 years old, HGSOC), OV015(52 years old, HGSOC), OV016(69

years old, HGSOC), OV076(59 years old, Right-sided fallopian tube mass), OV077(96 years old, unknown) and OV078(67 years old, unknown)) with ovarian cancer at Obstetrics and Gynecology Hospital of Fudan University in 2022, after obtaining informed consent of the patient before surgery. OV004 was used for scRNA-seq. OV014, OV015, and OV016 were used for living microscopy observe and subsequent experiments. OV014 and OV015 were used for cisplatin treatment, ICC staining and RNA-seq. OV076, OV077, and OV078 were utilized for live microscopic observation. These patients underwent a laparotomy primary debulking surgery with optimal cytoreduction. Our study was approved by the Ethics Committee of the Obstetrics and Gynecology Hospital ofFudan University.

4.2 | Organoids formation, culture, and subculture

Patient-derived OC tissues were washed 4−6 times with organoid washing buffer (LSTO00100201, Shanghai Lisheng Biotech, China) and then dissociated to about 1 mm diameter pieces with surgical scissors, no collagenase, trypsin or dispase needed. Tumor pieces were resuspended ovarian cancer organoid medium (LSTO00100501, Shanghai Lisheng Biotech, China) and transferred into new dishes. The ovarian organoids were maintained with at 37◦C, 5% CO_2, and medium was semichanged per week. When the diameter of organoids reached 2 to 4 mm (about 4 weeks), the organoids were collected and mechanically dissociated, then subcultured as described above.

4.3 | Whole exome sequencing

For each sample, 200 ng genomic DNA was sheared to 150−200 bp fragments to construct libraries. The whole exome was captured using AIExome® Human Exome Panel V3 with TargetSeq One® Hyb & Wash Kit v2.0 (iGeneTech Co., Ltd, Beijing, China) and sequenced on DNBSEQ-T7 with 150-bp reads.

4.4 | Immunofluorescence and immunohistochemistry

Tissue or organoids were first fixed with 4% PFA (BL539A, Biosharp, China), then dehydrated with 10%, 20% and 30% sucrose solution sequentially. Embedding medium with samples (7.5% gelatin and 10% sucrose in 1× PBS) was cooled at 4◦C for 10 min and quickly frozen on dry ice for 10 min, then stored at −80◦C. Materials were sectioned using Leica CM 1950. On-plate adherent cells were fixed with 4% PFA for 20 min at room temperature. Permeabilization of cells and sections was performed with PBS+0.25% TritonX-100 for 18 min at room temperature, followed by blocking with 3% BSA.

For immunofluorescence, rabbit anti-Ki67 (1:1000; MA5-14520, ThermoFisher, England) and anti-PAX8 (1:1000; 10336-1-AP, Proteintech, China) were used as primary antibodies to stain proteins overnight at 4◦C. Samples were then washed 5 times with 0.125% PBST and incubated with the CY3-anti-rabbit secondary antibody (1:1000) for 3 h at room temperature. Nuclei were stained by DAPI (1:1000).

For immunohistochemistry, mouse anti-CD31 (1:250; ab9498, Abcam, USA) were used as primary antibodies to stain CD31 positive cells. Samples were incubated overnight at 4◦C then washed 5 times with 0.125% PBST and incubated with the HRP-anti-mouse secondary antibody (1:500; ab6789, Abcam, USA) for 3 h at room temperature. Recolor the slices using DAB substrate kit (ab64328, Abcam, USA).

4.5 | RNA sequencing

For bulk RNA, RNA Isolation Kit (DP451, TIANGEN, China) was used to isolate cell mRNA. Four to six 2-mm-diameter organoids were collected as input for each group of organoids. Concentration of RNA was measured using Qubit4 fluorometer. Reverse transcription was performed with RT Kit (KR118, TIANGEN, China) and libraries were generated with RNA Library Prep Kit (E7530L, NEB, USA).

For single cell RNA, libraries were generated with 10× genomics protocol using 15,000 cells as input. Both libraries were sequenced on the Illumina Hiseq 4000 with PE-150 bp reads for subsequent analysis.

4.6 | Bioinformatics analysis

For RNA-seq, the kallisto software was utilized to quantify transcript abundance, employing Fragments Per Kilobase of transcript per Million mapped reads to estimate RNA expression levels. Differentially expressed genes were identified using the Morpheus online platform. In the case of scRNA-seq, the raw data were processed using Cell Ranger, with subsequent analyses conducted via the Seurat package. For WES, the BWA-MEM algorithm facilitated alignment of raw sequence data to the reference human genome (hg38). Downstream analyses, including variant calling, were performed using the Genome Analysis Toolkit and Mutect2.

4.7 | Cisplatin sensitivity test

Organoids were cultured in 6-well plates as mentioned above, and cisplatin was added into medium at 8/48 h after the initial time point at final concentrations of 4.175, 8.35, and 16.7 μM. At 168 h, the organoids were collected and sectioned as described above.

4.8 | Microscopy observing

All bright-field images were taken using Leica Ti-1 microscope. Fluorescence images were taken using Leica K5 microscope.

4.9 | Caspase3 activity assay

Organoids cultured with protocols described above were dissociated with 0.25% trypsin and then cultured in 96-well ultralow attachment plates at 10,000 to 20,000 cells per well. Cisplatin was added to concentration of 16.7 μM, and caspase3 activity assay was performed using Promega G8091 kit after 3 days treatment.

4.10 | CTG assay

Organoids were cultured in 6-well plates as mentioned above, and cisplatin was added into medium at the beginning of culture. At 0, 12, 24, and 36 h respectively, same amount of organoids were collected and performed CTG assay with CellTiter-Glo Luminescent Cell Viability Assay Kit (G7572, Promega).

4.11 | Cell cytometry

Organoids were dissociated with collagenase NB 4 in 0.25% trypsin, then collect 1×10^6 cells in 1.5 mL EP tube and centrifuge at 250 × *g* for 3 min. Cells were suspended in 1× PBS and stained with PI (0.01 mg/mL) and annexin V (1:100) for 15 min. Cells were then centrifuged at 250 × *g* for 3 min and collected. The cell flow cytometry was performed with a BD FACS Verse kit (Franklin Lakes, NJ, USA) following standard procedures.

4.12 | Statistical analysis

In ICC assay and qPCR, data analysis was performed using Prism software. p Value < 0.05 was considered statistically significant. All data are expressed as mean ± standard deviation.

AUTH OR CONTRIBUTIONS

HXX, CCH, and CQ conceived and designed the experiments; ZYQ, WC, LLY, SYH, and ZJ performed the experiments; ZYQ, WC, JPL, and CCH analyzed the data; TX gave pathology analysis of ovarian cancer; ZYQ, WC, DW, CCH, and HXX wrote the manuscript. All the authors approved the final manuscript.

ACKNOWLEDGMENTS

We would like to thank all the colleges in our lab. This work was supported by the National Natural Science Foundation of China (grant numbers: 82374506 and 32200581). Diagrams were created with BioRender.com.

CONFLICT OF INTEREST STATEMENT

Author Chen Wang, Xinxin Han, Jian Zhang, Chunhui Cai are the employees in Shanghai LiSheng Biotech, but has no potential relevant financial or non-financial interests to disclose. The other authors have no conflicts of interest to declare.

DATA AVAILABILITY STATEMENT

The raw sequence data reported in this paper, including Bulk-RNAseq, sc-RNAseq, and WES, have been deposited in the Genome Sequence Archive (GSA) at the National Genomics Data Center, Beijing Institute of Genomics, Chinese Academy of Sciences. The data are publicly accessible at https://ngdc.cncb.ac.cn/gsa-human with the accession number PRJCA027584.

ETH ICS STATEMENT

This study was approved by the Ethics Committee of the Obstetrics and Gynecology Hospital of Fudan University (kyy2023-06). Written informed consent was obtained from all participants. All human specimens were performed according to the Declaration of Helsinki and the Chinese guidelines of GB/T4352.1-2021 and GB/T38736-2020. Approved by the Ethics Committee of the Obstetrics and Gynecology Hospital of Fudan University, patients/subjects signed a written informed consent. All human tissues were collected with patient consent according to clinical SOPs.

REFERENCES

1. Lisio MA, Fu L, Goyeneche A, Gao ZH, Telleria C. High-Grade Serous Ovarian Cancer: basic sciences, clinical and therapeutic standpoints. *Int J Mol Sci*. 2019;20(4):952. doi:10.3390/ijms20040952
2. Grabska K, Pilarska I, Magdalena Fudalej M, Deptała A, Badowska-Kozakiewicz A. What is new about ovarian malignancies? *Współczesna Onkol*. 2021;25(4):225-231. doi:10.5114/wo.2021.112037
3. Nero C, Vizzielli G, Lorusso D, et al. Patient-derived organoids and high grade serous ovarian cancer: from disease modeling

to personalized medicine. *J Exp Clin Canc Res*. 2021;40(1):116. doi:10.1186/s13046-021-01917-7

4. Webb PM, Jordan SJ. Epidemiology of epithelial ovarian cancer. *Best Practice & Research Clinical Obstetrics & Gynaecology*. 2017;41:3-14. doi:10.1016/j.bpobgyn.2016.08.006
5. Lheureux S, Braunstein M, Oza AM. Epithelial ovarian cancer: evolution of management in the era of precision medicine. *CA Cancer J Clin*. 2019;69(4):280-304. doi:10.3322/caac.21559
6. Veneziani AC, Gonzalez-Ochoa E, Alqaisi H, et al. Heterogeneity and treatment landscape of ovarian carcinoma. *Nat Rev Clin Oncol*. 2023;20(12):820-842. doi:10.1038/s41571-023-00819-1
7. Gaitskell K, Hermon C, Barnes I, et al. Ovarian cancer survival by stage, histotype, and pre-diagnostic lifestyle factors, in the prospective UK Million Women Study. *Cancer Epidemiol*. 2022;76:102074. doi:10.1016/j.canep.2021.102074
8. Torre LA, Trabert B, DeSantis CE, et al. Ovarian cancer statistics, 2018. *CA Cancer JClin*. 2018;68(4):284-296. doi:10.3322/caac.21456
9. Ledermann JA. First-line treatment of ovarian cancer: questions and controversies to address. *Ther Adv Med Oncol*. 2018;10:175883591876823. doi:10.1177/1758835918768232
10. Vergote I, Denys H, Greve JD, et al. Treatment algorithm in patients with ovarian cancer. *Facts Views Vis ObGyn*. 2020;12(3):227.
11. Chandra A, Pius C, Nabeel M, et al. Ovarian cancer: current status and strategies for improving therapeutic outcomes. *Cancer Med*. 2019;8(16):7018-7031. doi:10.1002/cam4.2560
12. Falzone L, Bordonaro R, Libra M. SnapShot: cancer chemotherapy. *Cell*. 2023;186(8):1816-1816. doi:10.1016/j.cell.2023.02.038e1
13. Havasi A, Cainap SS, Havasi AT, Cainap C. Ovarian cancer—insights into platinum resistance and overcoming it. *Medicina (Mex)*. 2023;59(3):544. doi:10.3390/medicina59030544
14. Leung D, Price ZK, Lokman NA, et al. Platinum-resistance in epithelial ovarian cancer: an interplay of epithelial–mesenchymal transition interlinked with reprogrammed metabolism. *J Transl Med*. 2022;20(1):556. doi:10.1186/s12967-022-03776-y
15. Konstantinopoulos PA, Matulonis UA. Clinical and translational advances in ovarian cancer therapy. *Nat Cancer*. 2023;4(9):1239-1257. doi:10.1038/s43018-023-00617-9
16. Harter P, Sehouli J, Vergote I, et al. Randomized trial of cytoreductive surgery for relapsed ovarian cancer. *N Engl J Med*. 2021;385(23):2123-2131. doi:10.1056/NEJMoa2103294
17. Leary A, Tan D, Ledermann J. Immune checkpoint inhibitors in ovarian cancer: where do we stand? *Ther Adv Med Oncol*. 2021;13:175883592110398. doi:10.1177/17588359211039899
18. Kotnik EN, Mullen MM, Spies NC, et al. Genetic characterization of primary and metastatic High-Grade Serous Ovarian Cancer tumors reveals distinct features associated with survival. *Commun Biol*. 2023;6(1):688. doi:10.1038/s42003-023-05026-3
19. Kandalaft LE, Dangaj Laniti D, Coukos G. Immunobiology of High-Grade Serous Ovarian Cancer: lessons for clinical translation. *Nat Rev Cancer*. 2022;22(11):640-656. doi:10.1038/s41568-022-00503-z
20. Voutsadakis IA. Further understanding of high-grade serous ovarian carcinogenesis: potential therapeutic targets. *Cancer Manag Res*. 2020;12:10423-10437. doi:10.2147/CMAR.S249540
21. Sun J, Yan C, Xu D, et al. Immuno-genomic characterisation of High-Grade Serous Ovarian Cancer reveals immune evasion mechanisms and identifies an immunological subtype with a favourable prognosis and improved therapeutic efficacy. *Br J Cancer*. 2022;126(11):1570-1580. doi:10.1038/s41416-021-01692-4
22. Neal JT, Li X, Zhu J, et al. Organoid modeling of the tumor immune microenvironment. *Cell*. 2018;175(7):1972-1988. doi:10.1016/j.cell.2018.11.021 e16
23. Bose S, Clevers H, Shen X. Promises and challenges of organoid-guided precision medicine. *Med*. 2021;2(9):1011-1026. doi:10.1016/j.medj.2021.08.005
24. Zhou Z, Cong L, Cong X. Patient-derived organoids in precision medicine: drug screening, organoid-on-a-chip and living organoid biobank. *Front Oncol*. 2021;11:762184. doi:10.3389/fonc.2021.762184
25. Sun XY, Ju XC, Li Y, et al. Generation of vascularized brain organoids to study neurovascular interactions. *eLife*. 2022;11:e76707. doi:10.7554/eLife.76707
26. Mansour AA, Gonçalves JT, Bloyd CW, et al. An in vivo model of functional and vascularized human brain organoids. *Nat Biotechnol*. 2018;36(5):432-441. doi:10.1038/nbt.4127
27. Seidlitz T, Stange DE. Gastrointestinal cancer organoids—applications in basic and translational cancer research. *Exp Mol Med*. 2021;53(10):1459-1470. doi:10.1038/S12276-021-00654-3
28. Lo YH, Karlsson K, Kuo CJ. Applications of organoids for cancer biology and precision medicine. *Nat Cancer*. 2020;1(8):761-773. doi:10.1038/s43018-020-0102-y
29. Kopper O, de Witte CJ, Lohmussaar K, et al. An organoid platform for ovarian cancer captures intra- and interpatient heterogeneity. *Nat Med*. 2019;25(5):838-849. doi:10.1038/s41591- 019-0422-6
30. Nanki Y, Chiyoda T, Hirasawa A, et al. Patient-derived ovarian cancer organoids capture the genomic profiles of primary tumours applicable for drug sensitivity and resistance testing. *Sci Rep*. 2020;10(1):12581. doi:10.1038/s41598-020-69488-9
31. Senkowski W, Gall-Mas L, Falco MM, et al. A platform for efficient establishment and drug-response profiling of High-Grade Serous Ovarian Cancer organoids. *Dev Cell*. 2023;58(12):1106-1121. doi:10.1016/j.devcel.2023.04.012e7
32. Liu HD, Xia BR, Jin MZ, Lou G. Organoid of ovarian cancer: genomic analysis and drug screening. *Clin Transl Oncol*. 2020;22(8):1240-1251. doi:10.1007/s12094-019-02276-8
33. Xu J, Fang Y, Chen K, et al. Single-cell RNA sequencing reveals the tissue architecture in human High-Grade Serous Ovarian Cancer. *Clin Cancer Res*. 2022;28(16):3590-3602. doi:10.1158/1078-0432.CCR-22-0296
34. Kong Q, Yan X, Cheng M, et al. p62 promotes the mitochondrial localization of p53 through its UBA domain and participates in regulating the sensitivity of ovarian cancer cells to cisplatin. *Int JMol Sci*. 2022;23(6):3290. doi:10.3390/ijms23063290
35. Tchounwou PB, Dasari S, Noubissi FK, Ray P, Kumar S. Advances in our understanding of the molecular mechanisms of action of cisplatin in cancer therapy. *J Exp Pharmacol*. 2021;13:303-328. doi:10.2147/JEP.S267383
36. Pectasides D, Fountzilas G, Aravantinos G, et al. Advanced stage clear-cell epithelial ovarian cancer: the Hellenic Cooperative Oncology Group experience. *Gynecol Oncol*. 2006;102(2):285-291. doi:10.1016/j.ygyno.2005.12.038
37. Kopper O, De Witte CJ, Lõhmussaar K, et al. An organoid platform for ovarian cancer captures intra- and interpatient heterogeneity. *Nat Med*. 2019;25(5):838-849. doi:10.1038/s41591-019-0422-6

38. Cao Q, Li L, Zhao Y, et al. PARPi decreased primary ovarian cancer organoid growth through early apoptosis and base excision repair pathway. *Cell Transplant*. 2023;32:9636897231187996. doi:10.1177/09636897231187996

39. Lou L, Wang K, Leng L, et al. Unveiling cell organoid: a vanguard in organoid research. *Cell Organoid*. 2024. doi:10.26599/CO.2024.9410000

40. Fang Y, Akhtar H, Wang J. The application of organoids in toxicity test of environmental pollutants. *Cell Organoid*. 2024. doi:10.26599/CO.2024.9410002

41. Shi Y, Liu J, Li L, et al. Patient-derived skin tumor organoids with immune cells respond to metformin. *Cell Organoid*. 2024. doi:10.26599/CO.2024.9410001

42. Wang C, Huang A, Shi Y, et al. An advanced culture methodology suitable for the self-assemble and tissue-fragment derived intrahepatic cholangiocarcinoma organoids. *Cell Organoid*. doi:10.26599/CO.2024.9410003

43. Zhang J, Liu J, Shi Y, et al. Generation of patient-derived glioblastoma organoids: a comparative study of enzymatic digestion and mechanical fragmentation methods. *Cell Organoid*. doi:10.26599/CO.2024.9410004

44. Han X, Cai C, Deng W, et al. Landscape of human organoids: ideal model in clinics and research. *Innovation (Camb)*. 2024;5(3):100620. doi:10.1016/j.xinn.2024.100620

How to cite this article: Zhao Y, Wang C, Deng W, et al. Patient-derived ovarian cancer organoid carries immune microenvironment and blood vessel keeping high response to cisplatin. *MedComm*. 2024;5:e697.
https://doi.org/10.1002/mco2.697

Phytomedicine 141 (2025) 156721

Contents lists available at ScienceDirect

Phytomedicine

journal homepage: www.elsevier.com/locate/phymed

Original Article

Zengmian Yiliu formula suppresses cell cycle in immune-rich ovarian cancer patient-derived organoids

Qi Cao [a,1], Chunhui Cai [b,1], Chen Wang [b], Lanyang Li [b], Jiping Liu [b], Jian Zhang [b], Mingjie Rong [b], Jiaqi Ren [b], Yanyan Han [b], Jie Zhang [c,*], Xinxin Han [b,d,**]

[a] Obstetrics & Gynecology Hospital of Fudan University, Shanghai, China

[b] Shanghai LiSheng Biotech, Shanghai, China

[c] LongHua Hospital, Shanghai University of Traditional Chinese Medicine, 725 Wanping South Road, Xuhui District, Shanghai, China

[d] Organ Regeneration X Lab, LiSheng East China Institute of Biotechnology, Peking University, Jiangsu, China

ARTICLE INFO

Keywords:
Ovarian cancer
Cancer organoid
Zengmian Yiliu formula
Immune response gene
Cell cycle
Immune therapy

ABSTRACT

Background: Ovarian cancer, often diagnosed at advanced stages, has a 5-year survival rate below 50%, indicating a critical need for innovative treatments. The Zengmian Yiliu (ZMYL) formula, a Traditional Chinese Medicine (TCM) prescription, has shown potential in enhancing chemotherapy efficacy and improving patients' quality of life,

Purpose: To investigate the effects of the ZMYL formula on ovarian cancer organoids, focusing on its impact on organoid phenotypes and underlying mechanisms, and to explore its potential as an immunotherapeutic agent.

Methods: Ovarian cancer organoids were established from surgical tissues and treated with the ZMYL formula at varying concentrations. Network pharmacology was utilized to predict the formula's therapeutic targets and pathways, and molecular docking was conducted to validate ingredient-target interactions. Phenotypic changes were monitored, and RNA sequencing was performed post-treatment to analyze gene expression alterations.

Results: A total of 34 overlapping targets of 10 compounds in the ZMYL formula and ovarian cancer were predicted by Network pharmacology analysis. The ZMYL formula induced dose-dependent morphological changes in organoids, including a reduction in size and structural sparsity at higher concentrations. RNA sequencing revealed significant modulation of cell cycle and immune response pathways, with a particular focus on immunomodulatory effects. The formula's treatment targeted key genes involved in these processes, reshaping the tumor's molecular landscape.

Conclusions: This study establishes ZMYL's capacity to simultaneously target oncogenic drivers (e.g., cell cycle regulators) and immune checkpoints (e.g., CXCL10-mediated T cell recruitment) in ovarian cancer organoids. Unlike conventional monotherapy-focused approaches, ZMYL's multi-component mechanism offers a synergistic framework for integrating TCM with modern immunotherapies. These findings provide a foundation for future clinical evaluation of ZMYL as a precision medicine strategy to enhance treatment efficacy and mitigate chemoresistance in ovarian cancer.

Introduction

Ovarian cancer is a diverse disease with distinct histologic subtypes, each with unique risk factors and treatments; global estimates for 2020 identify over 133,000 new serous cases, highlighting the need for targeted prevention strategies (Wang et al., 2024a). Typically diagnosed at advanced stages due to late detection and chemotherapy resistance, it has a disheartening 5-year survival rate of less than 50%, emphasizing the pressing need for innovative therapeutic strategies (Bray et al., 2024). Recent research has begun to unravel the complex tumor microenvironment in ovarian cancer, revealing a landscape ripe for immunotherapeutic intervention (Luo et al., 2024). With the identification of key immunological markers and the role of homologous recombination deficiency in shaping the tumor microenvironment

* Corresponding author.
** Corresponding author at: Shanghai LiSheng Biotech, Shanghai, China.
E-mail addresses: zhangjie1122@shutcm.edu.cn (J. Zhang), xxhan@sibs.ac.cn (X. Han).
[1] These authors contributed equally to this work.

https://doi.org/10.1016/j.phymed.2025.156721
Received 10 October 2024; Received in revised form 18 March 2025; Accepted 1 April 2025
Available online 3 April 2025

(Vazquez-Garcia et al., 2022), the path forward includes the development of targeted therapies that harness the immune system to combat this deadly disease.

Building on the quest for innovative therapeutic approaches for ovarian cancer, Traditional Chinese Medicine (TCM) offers a promising avenue. The Zengmian Yiliu (ZMYL) formula, an empirical prescription adapted from the ancient Baozhen Decotion, has demonstrated potential in complementing conventional treatments (Gong et al., 2015a; Qi et al., 2012). Comprising 10 herbs with properties that nourish Qi and Yin, as well as clear heat and detoxify, the ZMYL formula has been clinically shown to enhance chemotherapy efficacy, mitigate its side effects, and notably improve the quality of life for patients. Notably, studies have reported a higher survival rate and better Karnofsky Performance Status (KPS) in patients administered the ZMYL formula compared to chemotherapy alone (Gong et al., 2015b; Zhang et al., 2015). The formula's multifaceted action on tumor cell apoptosis suggests a role in regulating cellular death mechanisms (Qi et al., 2012). Despite these promising findings, the intricate "multi-components and multi-targets" nature of TCM like the ZMYL formula necessitates further exploration to elucidate its precise mechanisms, especially in the context of immunotherapy, offering a bridge between traditional practices and modern medical advancements.

Given the intricate and prolonged clinical effects of Traditional Chinese Medicine (TCM), such as the ZMYL formula, and the challenges in deciphering their downstream mechanisms, an *in vitro* model that replicates the human tumor microenvironment is essential. Ovarian cancer organoids fulfill this need, providing a controlled model that can respond to TCM treatments and offer insights into their complex therapeutic dynamics (Kopper et al., 2019; Maenhoudt et al., 2020). These organoids have surpassed traditional models by accurately simulating the tumor's microenvironment, including the preservation of genomic and histological tumor features, which is vital for personalized medicine (de Witte et al., 2020; Senkowski et al., 2023; Zhang et al., 2021). Our previously research has highlighted the organoids' ability to maintain a rich immune context and vasculature, crucial for studying the formula's impact on cisplatin sensitivity (Zhao et al., 2024). By avoiding enzymatic digestion and Matrigel, these organoids offer a more authentic *in vivo*-like model, making them ideal for exploring TCM's role in immunotherapy and serving as a bridge between traditional and modern treatment strategies.

In this study, we validated the therapeutic effects of the ZMYL formula on ovarian cancer organoids based on our network pharmacology predictions. The organoids demonstrated a dose-dependent response, exhibiting morphological changes and alterations in cellular architecture, particularly a reduction in size and structural sparsity at higher concentrations of the ZMYL formula. RNA sequencing analysis post-treatment revealed significant modulation of key pathways, highlighting the formula's ability to reshape the tumor's molecular landscape. Importantly, the treatment primarily targeted cell cycle signaling and immune response cells, indicating a focused immunomodulatory effect. These findings not only confirm our computational predictions but also emphasize the potential of the ZMYL formula to specifically influence critical immune cell populations, paving the way for enhanced immunotherapeutic strategies in ovarian cancer.

Materials and methods

Ovarian cancer tissue collection

Our study encompassed a total of 21 ovarian cancer tissue (Table 1) samples collected post-surgically from patients at the Obstetrics and Gynecology Hospital of Fudan University. All samples were handled with the utmost care to preserve their integrity for research purposes. This study was conducted in compliance with the ethical guidelines and received approval from the Ethics Committee of the Obstetrics and Gynecology Hospital of Fudan University (Approval Number: kyy2023-06; Approval Date: 2023.2.27). All patients provided written informed consent to participate in the study, and they were aware that the data would be published in accordance with ethical standards.

Table 1
The patients' information.

Patient number	Age	Diseases	Tumor location
OV023	72	High-grade serous carcinoma of the fallopian tube	NA
OV043	45	Ovarian clear cell carcinoma	NA
OV045	60	High-grade serous carcinoma of the fallopian tube and ovary	Peritoneum
OV049	55	High-grade serous carcinoma of the fallopian tube	Left ovary
OV054	60	High-grade serous carcinoma of the fallopian tube	Omentum
OV055	57	ovarian endometrioid carcinoma	Right ovary
OV063	70	High-grade serous carcinoma of the fallopian tube	NA
OV064	52	High-grade serous carcinoma of the fallopian tube	Left adnexa
OV069	71	High-grade serous carcinoma of the fallopian tube	Primary adnexal mass
OV075	55	High-grade serous carcinoma of the ovary	NA
OV076	59	High-grade serous carcinoma of the fallopian tube	Right tubal mass
OV077	65	High-grade serous carcinoma of the ovary	NA
OV078	67	High-grade serous carcinoma of the fallopian tube	NA
OV080	60	High-grade serous carcinoma of the fallopian tube	Left adnexal mass
OV081	50	High-grade serous carcinoma of the fallopian tube	NA
OV082	55	High-grade serous carcinoma of the fallopian tube	NA
OV083	46	High-grade serous carcinoma of the fallopian tube and ovary	Left and right adnexal masses
OV084	64	High-grade serous carcinoma of the fallopian tube and ovary	right adnexal mass
OV086	66	Ovarian clear cell carcinoma	Pelvis, right adnexa
OV087	69	High-grade serous carcinoma of the fallopian tube	Right adnexal mass
OV088	42	Ovarian clear cell carcinoma	Pelvis, right adnexa

Ovarian cancer organoids culture

Ovarian cancer tissues were collected and processed for organoid culture using organoid washing buffer (LSTO00100201; Shanghai LiSheng Biotech, China). Tissues were sheared into 3mm fragments and cultured in ovarian cancer culture medium (LSTO001004; Shanghai LiSheng Biotech, China) at 37°C and 5% CO2, with medium changes every seven days (Cao et al., 2023; Zhao et al., 2024). Organoids were passaged by harvesting with cell scrapers, centrifuging to remove supernatant, and fragmenting to 3mm before transfer to fresh medium. Successful culture was confirmed by the rounding of organoid edges, with growth monitored using an inverted microscope (DMi1, Leica, USA).

HE and IHC staining

Paraffin-embedded ovarian cancer tissue sections and ovarian cancer organoids sections were processed for both hematoxylin and eosin (H&E) staining and immunohistochemical (IHC) analysis. For H&E staining, sections were deparaffinized and stained with hematoxylin (WAS30011, Wasci) and eosin (WAS30012, Wasci) to visualize cellular structures, followed by dehydration, clearing, and mounting with neutral balsam (National Medicine 10004160). For IHC, after deparaffinization and antigen retrieval, the sections were incubated with

primary antibodies against Ki67 (MA5-14520, ThermoFisher) and PAX8 (10336-1-AP, Proteintech) at a dilution of 1:1000 overnight at 4°C. This was followed by incubation with a biotinylated secondary antibody and an avidin-biotin-peroxidase complex, with immune complexes visualized using a DAB substrate kit (ab64328, Abcam). The slides were then counterstained, dehydrated, and mounted for examination under a light microscope, enabling the assessment of cellular morphology and protein expression patterns within the ovarian cancer tissues.

Single cell RNA sequencing and annotation

Single-cell RNA sequencing was applied to two patient-derived tissue samples and three organoid samples to explore cellular heterogeneity. Utilizing a specific organoid dissociation kit from Shanghai LiSheng Biotech, individual cells were isolated, erythrocytes removed, and cell viability assessed with Solarbio lysis solution and a Countstar® Rigel S2 analyzer. Libraries for sequencing were prepared with the SeekOne® kit, followed by cDNA synthesis, purification, and amplification with unique molecular identifiers. The libraries were cleaned, quantified with KAPA Biosystems qPCR, and sequenced on the Illumina HiSeq 4000 platform. Data analysis with Cell Ranger and Seurat software elucidated the cellular landscape within the ovarian cancer samples and organoids. The expression matrix was generated using Cell Ranger v8.0.0 and SeekoulTools v1.2.1, depending on the type of single-cell sequencing kit used. Different samples were integrated using Canonical Correlation Analysis (CCA) in Seurat v5.1.0. The annotation was generated manually based on marker genes.

Preparation of ZMYL extracts and UHPLC/Q-TOF/MS

The ZMYL formula (provided by Longhua Hospital, Shanghai University of Traditional Chinese Medicine, China) contains ten species of herbal medicines (Table 2). The ten component species were identified by the Department of Pharmacy of Longhua Hospital. Add 10 times the amount of water and soak for 30 min. After boiling, simmer for 30 min. Strain the residue, add 8 times the amount of water to boil, simmer for half an hour. Strain, combine filtrate twice and concentrate under pressure to 850 ml. 2 ml of concentrated liquid was centrifuged in a centrifuge tube and centrifuged at 12,000 RPM for 5 min. The supernatant was obtained. Ultra-high-performance liquid chromatography-quadrupole time-of-flight mass spectrometry (UHPLC/Q-TOF/MS) was used to analyse the samples. Chromatographic separation was achieved on anAgilent SB C18 analytical HPLC column (2.1 × 150 mm, 1.8 μm).

ZMYL formula ingredients collection and target screening

The ZMYL formula, comprised of 10 TCM extracts, was evaluated for its component compounds' potential targets. Databases including TCMSP (Ru et al., 2014), HERB (Fang et al., 2021), TCM-ID (Chen et al., 2006), and BATMA-TCM (Liu et al., 2016) were searched to identify these targets. The selection of active compounds was based on oral bioavailability (OB) ≥30% and drug likeness (DL) ≥0.18. DrugBank (Knox et al., 2024) was then used to associate targets with these active compounds.

Table 2
The composition of ZMYL.

Pharmaceutical	Chinese name	Part used	Ratio
Radix Astragali	Huangqi	Root	15
Codonopsis pilosula	Dangshen	Root	15
Lycium barbarum	Gouqizi	Fruit	15
Scutellariae Barbatae	Banzhilian	Aerial part	18
Akebia trifoliata Koidz	Bayuezha	Fruit	18
Asparagus cochinchinensis	Tiandong	Root and Rhizome	12
Paeonia lactiflora pallas	Baishao	Root	15
Rhizoma Atractylodis Macrocephalae	Baizhu	Root and Rhizome	9
Aucklandia lappa Decne	Muxiang	Root	9
Rehmannia glutinosa Libosch	Shengdihuang	Root and Rhizome	12

Ovarian cancer-related targets collection and differential gene expression analysis

Ovarian cancer-related targets were identified from GeneCards (Stelzer et al., 2016), DisGeNET (Pinero et al., 2020), DrugBank (Knox et al., 2024), TTD (Wang et al., 2020), and OMIM (Amberger et al., 2015) using "ovarian cancer" as the search term. Visualization of the targets was facilitated by the R package UpSetR. The GEO database was also mined for DEGs from the GES26712 dataset, contrasting 10 normal samples with 185 ovarian cancer samples. DEGs were identified using the R Limma package with the criteria of |log2FC| >1 and Padjust <0.05. Visualization of these DEGs was achieved using ggplot2 for volcanic maps and pheatmap for heatmaps.

Network construction, PPI network, and molecular docking

The intersection of targets associated with the ZMYL formula, ovarian cancer-related targets, and DEGs was determined using the R package VennDiagram (version 1.7.1). Networks illustrating the relationships among disease, drugs, compounds, targets, and biological processes were constructed in Cytoscape (version 3.8.2). The STRING database was utilized to build a PPI network for the key targets, applying a confidence threshold of 0.4 and hiding disconnected nodes. Molecular docking was performed to validate the interactions between active ingredients of the ZMYL formula and key targets. The three-dimensional (3D) structures of the selected targets were downloaded from the RSCB PDB (Burley et al., 2021). AutoDock Tools (version 1.5.6) was used to remove water molecules, isolate proteins, add nonpolar hydrogen, and calculate Gasteiger charges for the target structures, which were then saved in PDBQT format. The two-dimensional (2D) structures of the common active ingredients were downloaded from the PubChem (Kim et al., 2019). The 2D structure was processed and transformed into PDB format through Chem3D, and were saved in PDBQT format as docking ligand in AutoDock (version 1.5.6). The selected target proteins were used as receptors, and the active ingredient quercetin was used as ligand. The active site of the molecular docking was determined by the ligand coordinate in the target protein complex. AutoDock vina (version 1.1.2) was used for molecular docking simulation, setting energy <-5 kcal/mol as strong. A total of 20 conformations were generated for each docking result, and the conformation with the best affinity was chosen as the final docking conformation and was visualized using PyMol (version 2.4.1).

Functional detection of ZMYL formula in ovarian cancer organoids

In the investigation of ZMYL formula's impact on ovarian cancer organoids, the formula's lyophilized powder was dissolved in water and filtered, then applied to organoids at concentrations of 25 ng/mL, 2.5 μg/mL, 250 μg/mL, and 25 mg/mL. Organoids were observed and photographed at set time points to assess their response to treatment. For the OV081 organoids, histological assessment was performed on Day 14 post-treatment through paraffin embedding and section staining to examine cellular morphology. Meanwhile, RNA from OV087 and OV088 organoids was collected 48 h after treatment for subsequent transcriptomic analysis, aiming to explore the molecular effects of the ZMYL formula.

RNA-sequencing and analysis

For the RNA sequencing component of our study, organoids were collected and preserved in TRIzol Reagent (15596018, ThermoFisher,

USA) for RNA stabilization before being stored at -80°C. Total RNA was isolated using the RNA Easy Fast Tissue/Cell Kit (4992732, Tiangen, China), and RNA quality was assessed with a Qubit 3.0 Fluorometer (ThermoFisher, Waltham, England). Reverse transcription and library preparation were performed using the RT Kit (KR118, TIANGEN, China) and the RNA Library Prep Kit (E7530L, NEB, USA), respectively. Sequencing was conducted on an Illumina HiSeq 4000 platform, yielding data analyzed based on fragments per kilobase of transcript per million mapped reads (FPKM). Differential gene expression analysis was carried out using R and Morpheus online software, with functional and pathway enrichment analyses performed via the g:Profiler database.

Statistical analysis

Data, derived from a minimum of three replicates, are expressed as the mean ± standard deviation across separate experiments. Statistical evaluations were conducted utilizing GraphPad Prism version 8.

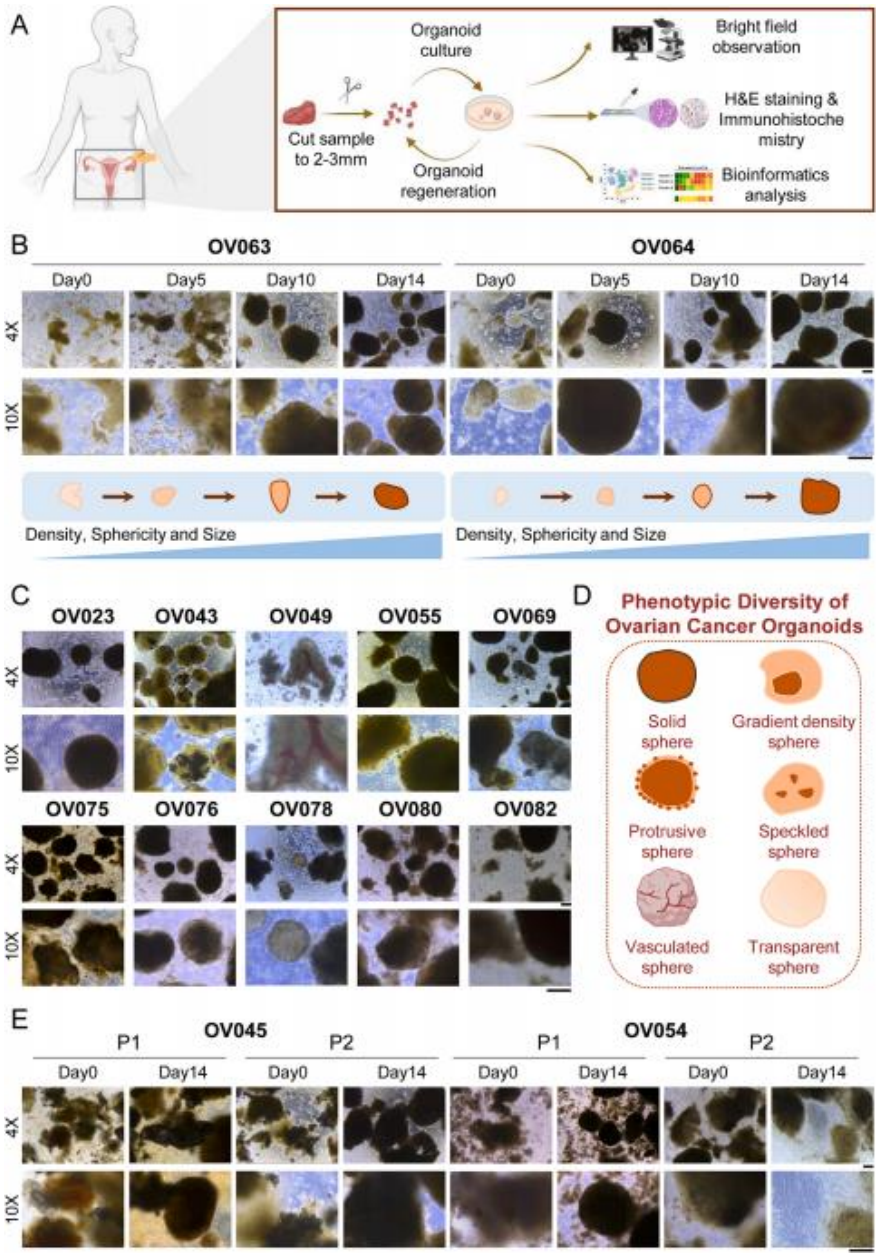

Fig. 1. Establishment of ovarian cancer organoids. (A) Workflow diagram outlining the process of establishing ovarian cancer organoids, from initiation to analysis. (B) Growth progression of OV063 and OV064 organoids captured by bright-field images at Days 0, 5, 10, and 14. Accompanying schematics indicate the increase in density, sphericity, and size over time. (C) Varied phenotypes of organoids from 10 distinct patient samples on Day 14, illustrating the phenotypic diversity. (D) Summary of organoid phenotypes, categorized as Solid, Gradient Density, Protrusive, Speckled, Vasculated, and Transparent. (E) Growth comparison of OV045 and OV054 organoids at Passage 0 (P0) and Passage 1 (P1), indicating their growth kinetics. Scale Bar: 200 μm.

Results

Establishment and morphological tracking of ovarian cancer organoids

To preserve the native microenvironment of ovarian tumor tissues and prevent clonal selection, we established ovarian cancer organoids without enzymatic dissociation or the use of Matrigel, as outlined in the workflow diagram (Fig. 1A). This approach facilitated the maintenance of tissue architecture and cellular interactions, critical for reflecting the *in vivo* tumor ecosystem. The organoids were cultured from mechanically sheared tissue fragments and monitored for growth and morphological changes using bright-field imaging, which captured the increase in density, sphericity, and size over time (Fig. 1B). On Day 14, the organoids exhibited a spectrum of phenotypes, underscoring the heterogeneity of ovarian cancer and the representativeness of our model system (Fig. 1C). Phenotypes were systematically categorized into six distinct groups, aiding in the comparative analysis of organoid characteristics (Fig. 1D). A growth kinetics comparison between passages demonstrated the adaptability and growth potential of these organoids, highlighting the importance of passaging in organoid culture (Fig. 1E). These results pave the way for our upcoming investigations into the organoids' internal structure and cellular makeup, which are expected to yield additional understanding of their biological characteristics and their value as research models for ovarian cancer.

Comprehensive characterization of ovarian cancer organoids and cellular heterogeneity

Our ovarian cancer organoid system, designed to closely mimic native tumor characteristics, was validated through comprehensive histological and cellular analyses. H&E staining (Fig. 2A) revealed well-preserved tissue architecture across organoids from six patients, while PAX8 staining confirmed their epithelial origin (Fig. 2B). Ki67 staining indicated active proliferation, demonstrating the organoids' viability (Fig. 2C).

The single-cell RNA sequencing analysis of ovarian cancer tissues and organoids has revealed a complex cellular landscape that mirrors the heterogeneity of the original tumors, with a high degree of overlap in cellular distributions observed between organoids and their corresponding tissues (Fig. 3A, B). This suggests that the organoid system can replicate a broad range of cell types and proportions, preserving the sample-specific heterogeneity. The annotated cluster map categorizes the cells into thirteen distinct groups, including various immune cells such as B cells, marcrophages, proliferating T cells and other T cells, indicating the organoid culture system's potential for studying immune-related therapies and drug responses (Fig. 3C). The marker genes for each cluster, displayed in (Fig. 3D), further highlight the molecular diversity of the cell types present. A detailed analysis of different types ofT cells, as shown in (Fig. 3E, F), reveals the expression patterns of genes associated with distinct T cell states, including activation, exhaustion, and cytotoxicity, providing crucial insights into the impact of TCM

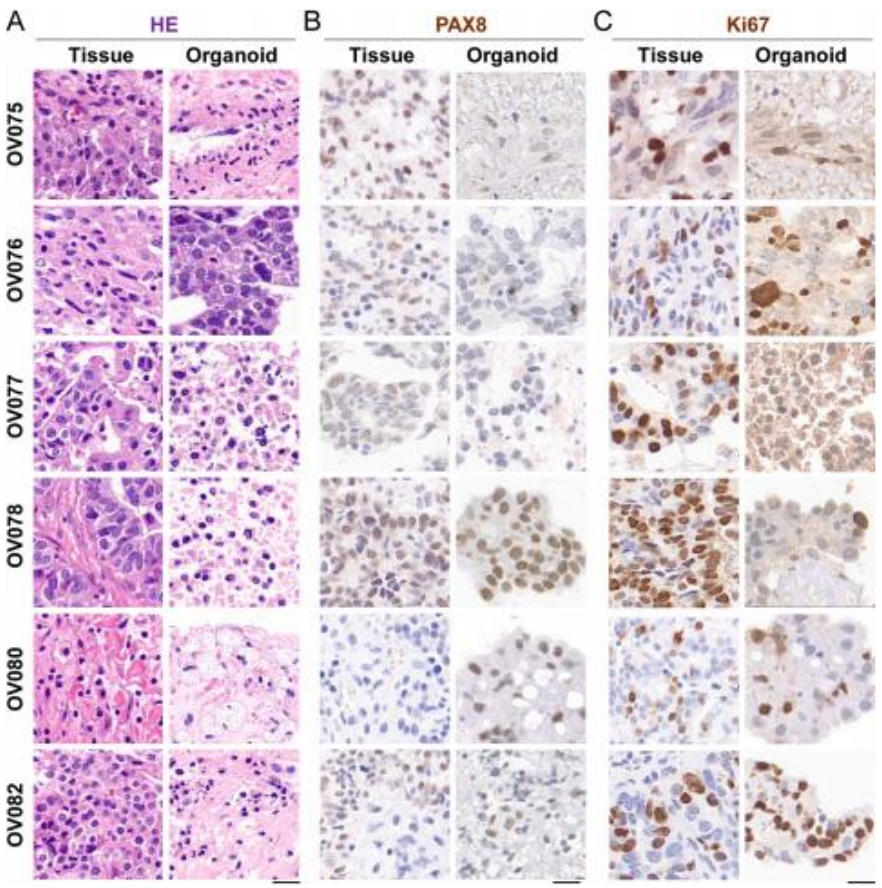

Fig. 2. Ovarian cancer organoid characterization. (A) H&E staining of organoids from six patients (OV075, OV076, OV077, OV078, OV080, and OV082), showcasing cellular arrangement and tissue structure. (B) PAX8 staining confirms the organoids' ovarian epithelial origin. (C) Ki67 staining assesses the organoids' proliferative activity. Scale Bar: 20 μm.

Phytomedicine 141 (2025) 156721

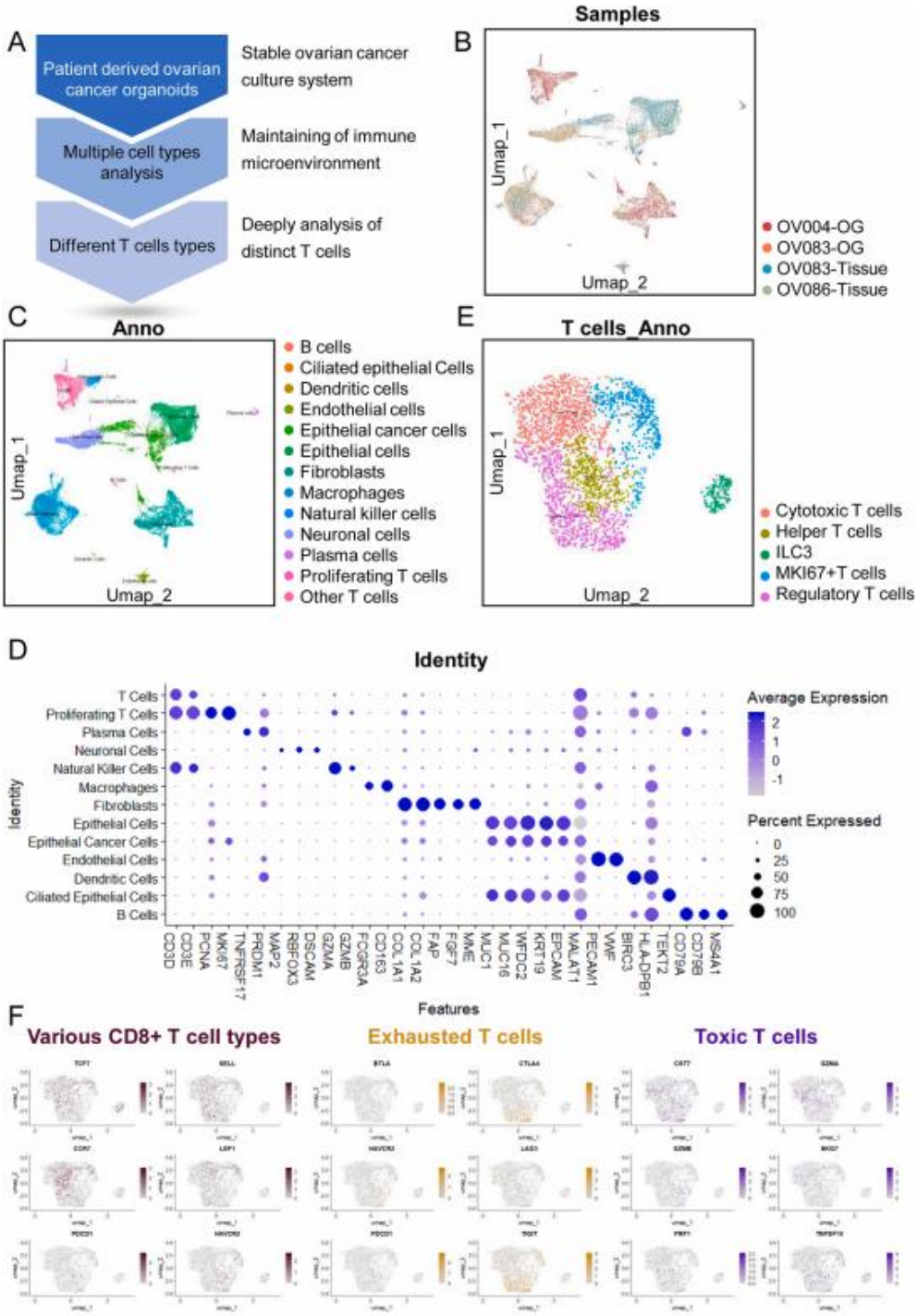

Fig. 3. Single-cell RNA sequencing of ovarian cancer tissues and organoids. (A) The overview of the single-cell RNA sequencing approach. (B) Distribution plots of ovarian cancer tissues (OV083, OV086) and organoids (OV004, OV0083) reveal the cellular heterogeneity within the samples. (C) The annotated cluster map delineates thirteen distinct cell populations, including B cells, ciliated epithelial cells, dendritic cells, endothelial cells, epithelial cancer cells, epithelial cells, fibroblasts, macrophages, natural killer cells, neuronal cells, plasma cells, proliferating T cells and other T cells, providing a comprehensive view of the cellular composition. (D) The marker genes characteristic of each cell cluster, providing a molecular overview. (E) The annotated cluster map delineates five different types of T cells, including cytotoxic T cells, helper T cells, ILC3, MKI67+ T cells and regulatory T cells. (F) Subgroup analysis of CD8-positive T cells, differentiated by gene expression profiles, distinguishes among various T cell states, including activated, exhausted, and toxic phenotypes.

treatments like the ZMYL formula on the tumor's immune microenvironment. These results underscore the organoid model's potential in advancing research into immunotherapeutic strategies for ovarian cancer.

Network pharmacology-driven identification of ZMYL formula 's therapeutic targets and pathways in ovarian cancer

Following the establishment of an organoid system that recapitulates the immune microenvironment of ovarian cancer, we delved into the therapeutic effects and underlying mechanisms of the Zengmian Yiliu (ZMYL) formula (Figs. 4 and 5A) using a network pharmacology approach. This analysis was crucial for identifying the active constituents and pathways that the ZMYL formula might target in ovarian cancer. Our analysis began with the identification of formula targets from OMIM (Amberger et al., 2015), TCMSP (Ru et al., 2014), HERB (Fang et al., 2021), TCM-ID (Ru et al., 2014) and BATMAN-TCM (Liu et al., 2016) (Table 3), and the collection of ovarian cancer therapeutic targets from GeneCards (Stelzer et al., 2016), DisGeNET (Pinero et al., 2020) and DrugBank (Knox et al., 2024) (Fig. 5B). We further examined the genomic data using the GES26712 dataset, revealing a total of 1768 DEGs in ovarian cancer, with distinct upregulation and downregulation patterns visualized in a volcanic map (Fig. 5C). Consolidating the overlapping targets from the formula, ovarian cancer, and DEGs, we pinpointed a core set of 34 targets that may be modulated by the ZMYL formula (Fig. 5D). A subsequent disease-drug-compound-target network construction revealed 18 bioactive compounds from eight herbs that potentially interact with these genes, forming a network with 221 edges indicative of the formula's therapeutic pathways (Fig. 5E). To elucidate the molecular interactions within this network, a PPI network was constructed, highlighting key regulatory genes that the ZMYL formula may target, as reflected by the nodes' size and darkness (Fig. 5F). Lastly, molecular docking analysis provided insights into the specific interactions between the formula's active ingredients, such as diosgenin, baicalein, and quercetin, with key targets like TP53, JUN, VEGFA, ERBB2, MMP2 and CAV1, as shown in the molecular docking patterns

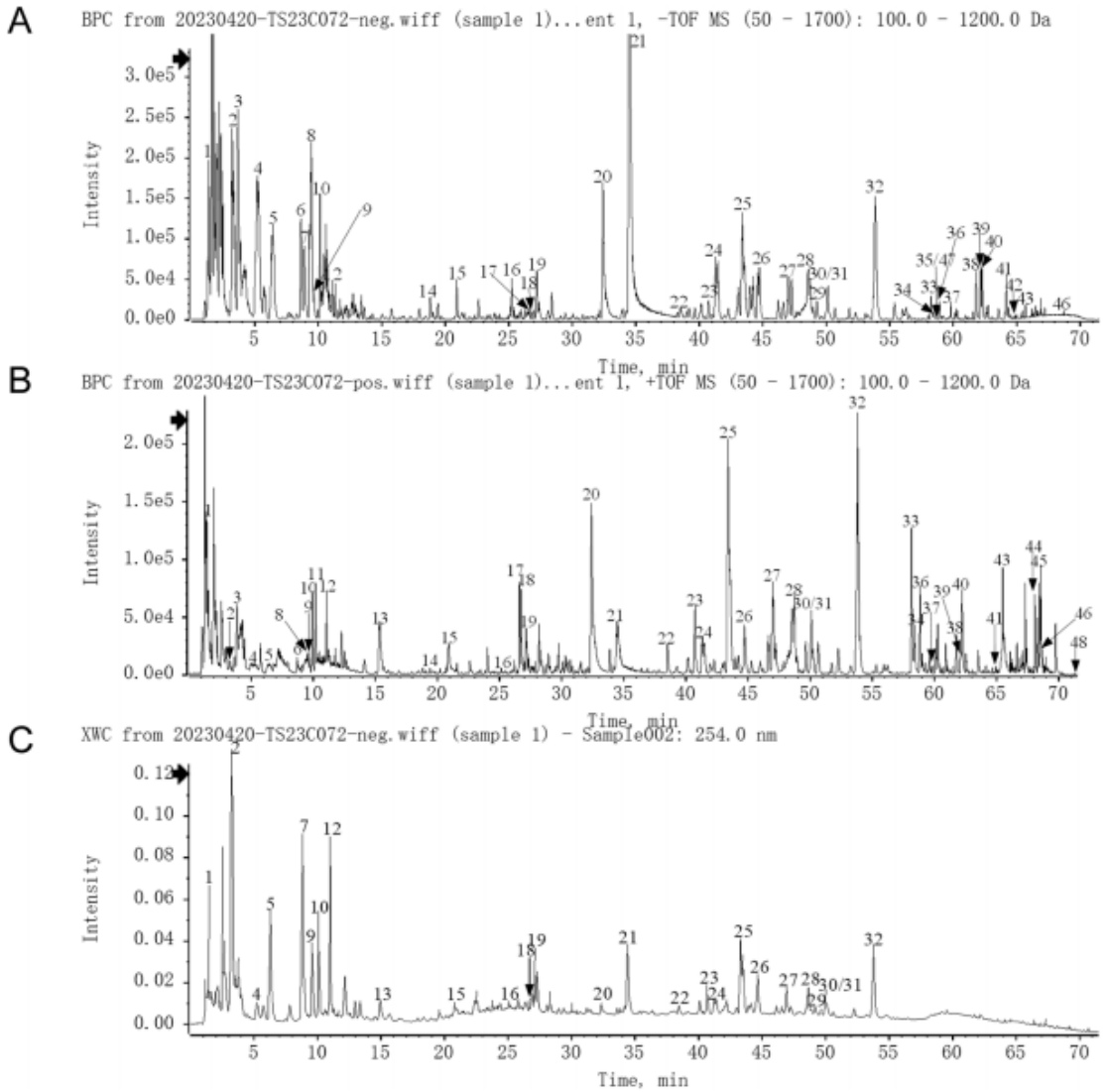

Fig. 4. UPLC-QTOF-MS analysis of ZMYL formula ingredients. (A) Representative ion chromatogram of ZMYL Formula in the negative mode. (B) Representative ion chromatogram of ZMYL Formula in the positive mode. (C) UPLC UV chromatogram of ZMYL compound sample -UV 254 nm.

Phytomedicine 141 (2025) 156721

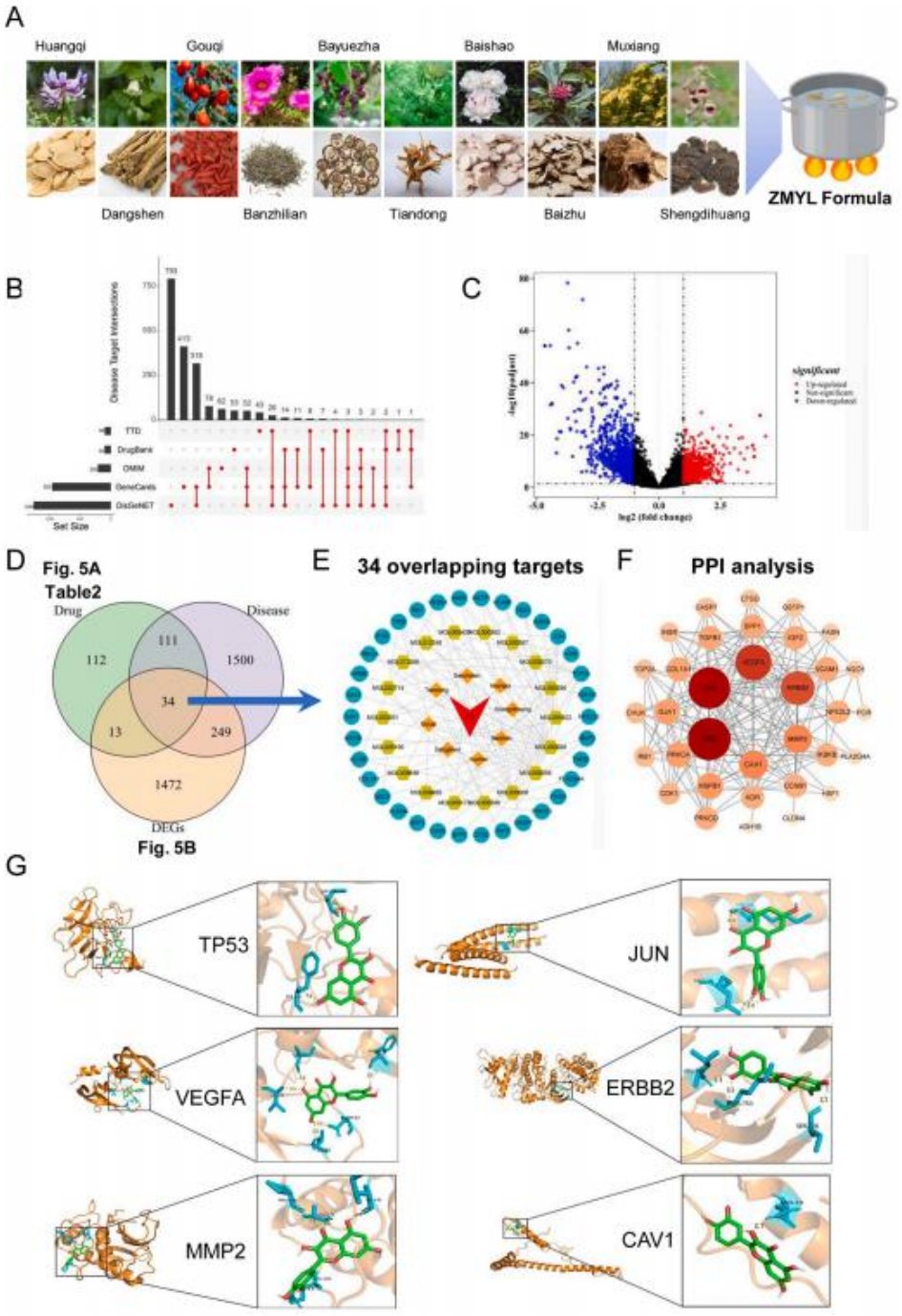

Fig. 5. Disease-drug-compound-target network construction of ZMYL formula. (A) Nature medical plants and traditional Chinese medicine for ZMYL formula. (B) The network construction begins with the identification of ovarian cancer targets from five databases: GeneCards, DisGeNET, DrugBank, TTD, and OMIM. A comparative bar chart details the number of unique and shared targets from each database, with a visual dot representation indicating the intersection of these datasets. (C) A volcanic map illustrates the differential gene expression in ovarian cancer, with red dots for up-regulated genes, blue for down-regulated, and black for non-significant genes, offering a snapshot of the genetic alterations associated with the disease. (D) The identification of overlapping targets between ovarian cancer and the ZMYL formula, along with DEGs, reveals 34 common candidate genes that may be key to the formula's therapeutic effects. (E) The Disease-Drug-Compound-Target network visually maps the interactions between 8 herbs and 18 bioactive compounds from the ZMYL formula and the 34 overlapping genes, highlighting 221 edges that represent potential therapeutic pathways. (F) The PPI network of these overlapping genes emphasizes the importance of specific genes in the treatment of ovarian cancer, with node size and darkness reflecting gene significance in the disease's molecular mechanisms. (G) Molecular docking patterns demonstrate the specific interactions between active ingredients like diosgenin, baicalein, and quercetin with key targets such as TP53, JUN, VEGFA, ERBB2, MMP2, and CAV1, suggesting the potential molecular mechanisms of the ZMYL formula's therapeutic action in ovarian cancer treatment.

Table 3
The compounds in ZMYL satisfying OB≥30% and DL≥0.18.

Molecule ID	Molecule name	OB %	DL	Herb name
MOL000211	Mairin	55.38	0.78	Huangqi/Muxiang/Baishao
MOL000239	Jaranol	50.83	0.29	Huangqi
MOL000296	hederagenin	36.9	0.75	Huangqi
MOL000033	(3S,8S,9S,10R,13R,14S,17R)-10,13-dimethyl-17-[(2R,5S)-5-propan-2-yloctan-2-yl]-2,3,4,7,8,9,11,12,14,15,16,17-dodecahydro-1H-cyclopenta[a]phenanthren-3-ol	36.23	0.78	Huangqi/Baizhu
MOL000354	isorhamnetin	49.6	0.31	Huangqi
MOL000371	3,9-di-O-methylnissolin	53.74	0.48	Huangqi
MOL000374	5,-hydroxyiso-muronulatol-2,,5,-di-O-glucoside	41.72	0.69	Huangqi
MOL000378	7-O-methylisomucronulatol	74.67	0.30	Huangqi
MOL000379	9,10-dimethoxypterocarpan-3-O-#-D-glucoside	36.74	0.92	Huangqi
MOL000380	(6aR,11aR)-9,10-dimethoxy-6a,11a-dihydro-6H-benzofurano[3,2-c]chromen-3-ol	64.26	0.42	Huangqi
MOL000387	Bifendate	31.10	0.67	Huangqi
MOL000392	formononetin	69.67	0.21	Huangqi
MOL000398	isoflavanone	109.99	0.30	Huangqi
MOL000417	Calycosin	47.75	0.24	Huangqi
MOL000422	kaempferol	41.88	0.24	Huangqi/Baishao
MOL000433	FA	68.96	0.71	Huangqi
MOL000438	(3R)-3-(2-hydroxy-3,4-dimethoxyphenyl)chroman-7-ol	67.67	0.26	Huangqi
MOL000439	isomucronulatol-7,2,-di-O-glucosiole	49.28	0.62	Huangqi
MOL000442	1,7-Dihydroxy-3,9-dimethoxy pterocarpene	39.05	0.48	Huangqi
MOL000098	quercetin	46.43	0.28	Huangqi/Banzhilian/Tiandong/Gouqi
MOL001006	poriferasta-7,22E-dien-3beta-ol	42.98	0.76	Dangshen
MOL002140	Perlolyrine	65.95	0.27	Dangshen
MOL002879	Diop	43.59	0.39	Dangshen
MOL003036	ZINC03978781	43.83	0.76	Dangshen
MOL000449	Stigmasterol	43.83	0.76	Dangshen/Banzhilian/Tiandong/Gouqi/Muxiang
MOL003896	7-Methoxy-2-methylisoflavone	42.56	0.20	Dangshen/Tiandong
MOL004355	Spinasterol	42.98	0.76	Dangshen
MOL004492	Chrysanthemaxanthin	38.72	0.58	Dangshen
MOL005321	Frutinone A	65.90	0.34	Dangshen
MOL000006	luteolin	36.16	0.25	Dangshen/Banzhilian
MOL006554	Taraxerol	38.40	0.77	Dangshen
MOL006774	stigmast-7-enol	37.42	0.75	Dangshen
MOL007059	3-beta-Hydroxymethyllenetanshiquinone	32.16	0.41	Dangshen
MOL007514	methyl icosa-11,14-dienoate	39.67	0.23	Dangshen
MOL008391	5alpha-Stigmastan-3,6-dione	33.12	0.79	Dangshen
MOL008393	7-(beta-Xylosyl)cephalomannine_qt	38.33	0.29	Dangshen
MOL008397	Daturilin	50.37	0.77	Dangshen
MOL008400	glycitein	50.48	0.24	Dangshen/Gouqi
MOL008406	Spinoside A	39.97	0.40	Dangshen
MOL008407	(8S,9S,10R,13R,14S,17R)-17-[(E,2R,5S)-5-ethyl-6-methylhept-3-en-2-yl]-10,13-dimethyl-1,2,4,7,8,9,11,12,14,15,16,17-dodecahydrocyclopenta[a]phenanthren-3-one	45.40	0.76	Dangshen
MOL008411	11-Hydroxyrankinidine	40.00	0.66	Dangshen
MOL001040	(2R)-5,7-dihydroxy-2-(4-hydroxyphenyl)chroman-4-one	42.36	0.21	Banzhilian
MOL012245	5,7,4,-trihydroxy-6-methoxyflavanone	36.63	0.27	Banzhilian
MOL012246	5,7,4,-trihydroxy-8-methoxyflavanone	74.24	0.26	Banzhilian
MOL012248	5-hydroxy-7,8-dimethoxy-2-(4-methoxyphenyl)chromone	65.82	0.33	Banzhilian
MOL012250	7-hydroxy-5,8-dimethoxy-2-phenyl-chromone	43.72	0.25	Banzhilian
MOL012251	Chrysin-5-methylether	37.27	0.20	Banzhilian
MOL012252	9,19-cyclolanost-24-en-3-ol	38.69	0.78	Banzhilian
MOL002776	Baicalin	40.12	0.75	Banzhilian
MOL012254	campesterol	37.58	0.71	Banzhilian/Shengdihuang
MOL000953	CLR	37.87	0.68	Banzhilian/Gouqi
MOL000358	beta-sitosterol	36.91	0.75	Banzhilian/Tiandong/Gouqi/Yuzhizi/Baishao/Shengdihuang
MOL012266	rivularin	37.94	0.3663	Banzhilian
MOL001973	Sitosteryl acetate	40.39	0.85	Banzhilian
MOL012269	Stigmasta-5,22-dien-3-ol-acetate	46.44	0.86	Banzhilian
MOL012270	Stigmastan-3,5,22-triene	45.03	0.71	Banzhilian
MOL000173	wogonin	30.68	0.23	Banzhilian
MOL001735	Dinatin	30.97	0.27	Banzhilian
MOL001755	24-Ethylcholest-4-en-3-one	36.08	0.76	Banzhilian
MOL002714	baicalein	33.52	0.21	Banzhilian
MOL002719	6-Hydroxynaringenin	33.23	0.24	Banzhilian
MOL002915	Salvigenin	49.07	0.33	Banzhilian
MOL000351	Rhamnazin	47.14	0.34	Banzhilian
MOL000359	sitosterol	36.91	0.75	Banzhilian/Tiandong/Yuzhizi/Muxiang/Baishao
MOL005190	eriodictyol	71.79	0.24	Banzhilian
MOL005869	daucostero_qt	36.91	0.75	Banzhilian
MOL008206	Moslosooflavone	44.09	0.25	Banzhilian

(*continued on nextpage*)

Table 3 (*continued*)

Molecule ID	Molecule name	OB %	DL	Herb name
MOL000020	12-senecioyl-2E,8E,10E-atractylentriol	62.40	0.22	Baizhu
MOL000021	14-acetyl-12-senecioyl-2E,8E,10E-atractylentriol	60.31	0.31	Baizhu
MOL000022	14-acetyl-12-senecioyl-2E,8Z,10E-atractylentriol	63.37	0.30	Baizhu
MOL000028	α-Amyrin	39.51	0.76	Baizhu
MOL000049	3#-acetoxyatractylone	54.07	0.22	Baizhu
MOL000072	8#-ethoxy atractylenolide III	35.95	0.21	Baizhu
MOL003889	methylprotodioscin_qt	35.12	0.86	Tiandong
MOL003891	pseudoprotodioscin_qt	37.93	0.87	Tiandong
MOL003901	Asparaside A_qt	30.60	0.86	Tiandong
MOL000546	diosgenin	80.88	0.81	Tiandong
MOL001323	Sitosterol alpha1	43.28	0.78	Gouqi
MOL003578	Cycloartenol	38.69	0.78	Gouqi
MOL001494	Mandenol	41.99	0.19	Gouqi
MOL001495	Ethyl linolenate	46.10	0.20	Gouqi
MOL001979	LAN	42.12	0.75	Gouqi
MOL005406	atropine	45.97	0.19	Gouqi
MOL005438	campesterol	37.58	0.71	Gouqi
MOL006209	cyanin	47.42	0.76	Gouqi
MOL007449	24-methylidenelophenol	44.19	0.75	Gouqi
MOL008173	daucosterol_qt	36.91	0.75	Gouqi
MOL010234	delta-Carotene	31.80	0.55	Gouqi
MOL009604	14b-pregnane	34.78	0.34	Gouqi
MOL009612	(24R)-4alpha-Methyl-24-ethylcholesta-7,25-dien-3beta-ylacetate	46.36	0.8398	Gouqi
MOL009615	24-Methylenecycloartan-3beta,21-diol	37.32	0.8	Gouqi
MOL009617	24-ethylcholest-22-enol	37.09	0.75	Gouqi
MOL009618	24-ethylcholesta-5,22-dienol	43.83	0.76	Gouqi
MOL009620	24-methyl-31-norlanost-9(11)-enol	38.00	0.75	Gouqi
MOL009621	24-methylenelanost-8-enol	42.37	0.77	Gouqi
MOL009622	Fucosterol	43.78	0.76	Gouqi
MOL009631	31-Norcyclolaudenol	38.68	0.81	Gouqi
MOL009633	31-norlanost-9(11)-enol	38.35	0.72	Gouqi
MOL009634	31-norlanosterol	42.20	0.73	Gouqi
MOL009635	4,24-methyllophenol	37.83	0.75	Gouqi
MOL009639	Lophenol	38.13	0.71	Gouqi
MOL009640	4alpha,14alpha,24-trimethylcholesta-8,24-dienol	38.91	0.76	Gouqi
MOL009641	4alpha,24-dimethylcholesta-7,24-dienol	42.65	0.75	Gouqi
MOL009642	4alpha-methyl-24-ethylcholesta-7,24-dienol	42.30	0.78	Gouqi
MOL009644	6-Fluoroindole-7-Dehydrocholesterol	43.73	0.72	Gouqi
MOL009646	7-O-Methylluteolin-6-C-beta-glucoside_qt	40.77	0.30	Gouqi
MOL009650	Atropine	42.16	0.19	Gouqi
MOL009651	Cryptoxanthin monoepoxide	46.95	0.56	Gouqi
MOL009653	Cycloeucalenol	39.73	0.79	Gouqi
MOL009656	(E,E)-1-ethyl octadeca-3,13-dienoate	42.00	0.19	Gouqi
MOL009660	methyl (1R,4aS,7R,7aS)-4a,7-dihydroxy-7-methyl-1-[(2S,3R,4S,5S,6R)-3,4,5-trihydroxy-6-(hydroxymethyl)oxan-2-yl]oxy-1,5,6,7a-tetrahydrocyclopenta[d]pyran-4-carboxylate	39.43	0.47	Gouqi
MOL009662	Lantadene A	38.68	0.57	Gouqi
MOL009664	Physalin A	91.71	0.27	Gouqi
MOL009665	Physcion-8-O-beta-D-gentiobioside	43.90	0.62	Gouqi
MOL009677	lanost-8-en-3beta-ol	34.23	0.74	Gouqi
MOL009678	lanost-8-enol	34.23	0.74	Gouqi
MOL009681	Obtusifoliol	42.55	0.76	Gouqi
MOL010929	glyceryl linolenate	38.14	0.31	Yuzhizi
MOL002882	[(2R)-2,3-dihydroxypropyl] (Z)-octadec-9-enoate	34.13	0.30	Yuzhizi
MOL008121	2-Monoolein	34.23	0.29	Yuzhizi
MOL008218	1-Monoolein	34.13	0.30	Yuzhizi
MOL010813	Benzo[a]carbazole	35.22	0.22	Muxiang
MOL010828	cynaropicrin	67.50	0.38	Muxiang
MOL010839	lappadilactone	38.56	0.73	Muxiang
MOL001910	11alpha,12alpha-epoxy-3beta-23-dihydroxy-30-norolean-20-en-28,12beta-olide	64.77	0.38	Baishao
MOL001918	paeoniflorgenone	87.59	0.37	Baishao
MOL001919	(3S,5R,8R,9R,10S,14S)-3,17-dihydroxy-4,4,8,10,14-pentamethyl-2,3,5,6,7,9-hexahydro-1H-cyclopenta[a]phenanthrene-15,16-dione	43.56	0.53	Baishao
MOL001921	Lactiflorin	49.12	0.80	Baishao
MOL001924	paeoniflorin	53.87	0.79	Baishao
MOL001925	paeoniflorin_qt	68.18	0.40	Baishao
MOL001928	albiflorin_qt	66.64	0.33	Baishao
MOL001930	benzoyl paeoniflorin	31.27	0.75	Baishao
MOL000492	(+)-catechin	54.83	0.24	Baishao

(Fig. 5G). In essence, our network pharmacology analysis has succinctly outlined the ZMYL formula's multi-targeted therapeutic strategy in ovarian cancer, laying the groundwork for subsequent organoid-based experiments and pharmacological inquiries.

Dose-dependent effects of ZMYL formula on ovarian cancer organoids

As a result of our network pharmacology predictions on the potential effects of the ZMYL formula in ovarian cancer, we sought to verify its therapeutic efficacy using a human ovarian organoids culture system

which has been proven to be a reliable platform for drug screening in ovarian cancer research (Cao et al., 2023; Zhao et al., 2024). The ZMYL formula's dose-dependent impact on ovarian cancer organoids is evident from the treatment efficacy flowchart (Fig. 6A), detailing the exposure of organoids from various patients to a gradient of formula concentrations. By Day 8, morphological changes were apparent, with (Fig. 6B) showing a reduction in size and shape alteration in organoids treated with higher concentrations. H&E staining by Day 14, as depicted in (Fig. 6C), revealed that escalating dosages of the ZMYL formula corresponded to a decrease in cellular density and an increase in structural

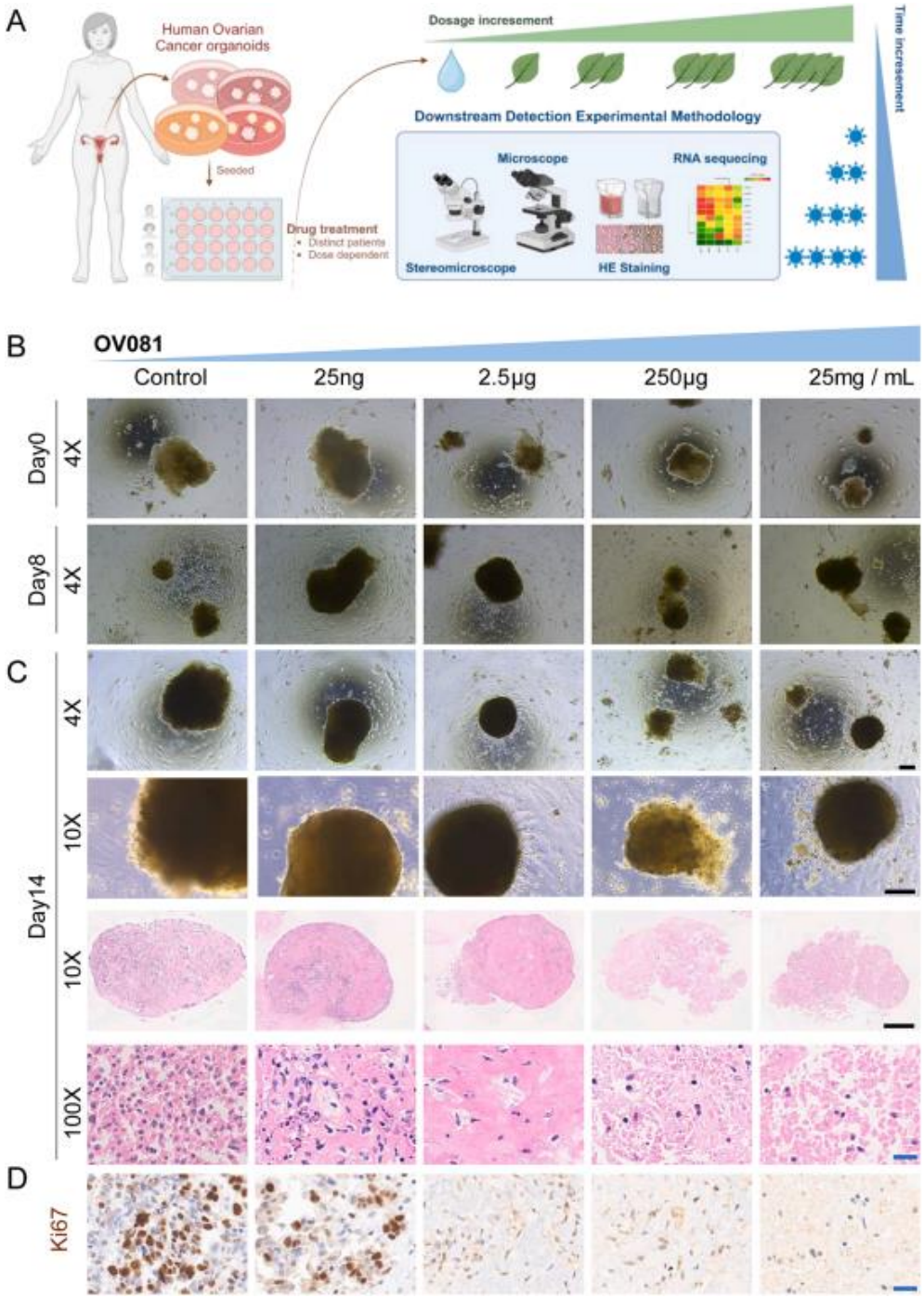

Fig. 6. Dose-dependent effects of ZMYL formula on ovarian cancer organoids. (A) Flowchart of the efficacy testing process of the ZMYL formula on organoids derived from different ovarian cancer patients. (B) Morphological comparison of organoids at Day 0 and Day 8 post-treatment with the ZMYL formula at various concentrations. (C) Day 14 organoid state and corresponding HE-stained sections, showcasing the dose-dependent effects on growth and morphology. (D) Ki67 immunohistochemical staining of organoids treated with different concentrations of ZMYL formula. Black scales: 200; Blue scale: 20 μm.

sparsity within the organoids. Furthermore, Ki67 immunohistochemical staining (Fig. 6D) demonstrated a significant reduction in Ki67-positive cells with increasing concentrations of ZMYL, indicating a decrease in cell proliferation. These findings indicate that the formula influences not only the growth but also the internal cellular architecture of ovarian cancer organoids, thereby substantiating its therapeutic potential as suggested by our initial computational analysis.

Modulation of cellular pathways by the ZMYL formula in ovarian cancer organoids

The time-lapse imaging of OV087 and OV088 organoids exposed to various concentrations of the ZMYL formula has captured the morphological changes over the course of 31 days, demonstrating the formula's impact on organoid growth and structure (Fig. 7A). The PCA analysis (Fig. 7B) reveals the transcriptional variance among the organoids, underscoring the diversity in their responses to the treatment. For the transcriptomic analysis, we used four different doses of ZMYL formula: 25 ng/mL, 2.5 μg/mL, 250 μg/mL, and 25 mg/mL. These doses were selected based on preliminary experiments to capture a range of pharmacological effects without complete cytotoxicity. The samples for RNA-seq were labeled as -1 (Control group), -3, -5, -7, and -9 (ZMYL treatment groups). The combined hierarchical clustering analysis (Fig. 7C) not only highlights the heterogeneity between patient samples but also distinguishes the treated groups from the controls, suggesting a clear effect of the ZMYL formula on gene expression patterns. Furthermore, the heatmaps correspond with the single-cell sequencing analysis, showcase the expression of T cell-related genes and the 34 target genes identified through network pharmacology (Fig. 7D, E). The significant binding interactions of six genes (*TP53, JUN, VEGFA, ERBB2, MMP2, CAV1*) marked with red arrows indicate their potential roles in mediating the formula's effects.

Trend analysis of OV087 and OV088 after ZMYL treatment revealed gene expression changes. In OV087, 5554 genes were downregulated and 1023 upregulated; in OV088, 4177 downregulated and 651 upregulated. Venn diagram analysis identified common genes affected in both organoids. This analysis pinpointed 853 downregulated and 68 upregulated genes in response to the ZMYL formula (Fig. 8A). The Gene Ontology (GO) analysis indicates that the formula's treatment leads to the suppression of cell cycle pathways and the activation of immune response pathways (Fig. 8B, C). Specifically, cell cycle-related genes such as *CCNB2, CDC20, CDC25A*, and *CDK10* are significantly downregulated, consistent with the reduced Ki67 staining observed in Fig. 6D. Additionally, immune-related genes like *CXCL10* are upregulated, suggesting the formula's potential to modulate the tumor's immune microenvironment. The heatmaps visually represent the expression changes of these cell cycle and immune response genes in OV087 and OV088 organoids (Fig. 8D, E), reinforcing the formula's potential to inhibit cancer cell proliferation while enhancing immune cell activity.

Discussion

Our study presents a cutting-edge approach to establishing ovarian cancer organoids, which is critical for advancing research in cancer therapeutics. By utilizing a method that avoids enzymatic dissociation and Matrigel, we have successfully maintained the native microenvironment of ovarian tumor tissues, as outlined in our methodology. This method, consistent with the sophisticated approaches reported in the literature, ensures the maintenance of diverse cellular components and their interactions, closely mirroring the complexity of the tumor's native environment (Kopper et al., 2019). The retention of patient-specific heterogeneity in our organoids is a significant advantage, as it ensures the potential for personalized medicine, a key aspect of modern cancer treatment strategies.

Network pharmacology is a powerful tool for understanding the complex mechanisms of multi-component therapies like the ZMYL formula. Our analysis identified 34 target genes, some significantly changed in RNA-seq data, confirming the reliability of network pharmacology in predicting therapeutic targets for TCM formulas. For instance, *CCNB1* and *CDK1* are well-known regulators of the cell cycle, and their dysregulation is linked to ovarian cancer progression (Kim et al., 2024; Yang et al., 2022). ZMYL's potential effect on these genes could be a mechanism through which it influences cell cycle arrest. Additionally, genes such as *VCAM1* is involved in immune cell recruitment and the formation of new blood vessels, respectively. *VCAM1* plays a crucial role in the adhesion and migration of immune cells to the tumor site (Samaha et al., 2018), while VEGFA is known for its role in angiogenesis and immune evasion. The impact of ZMYL on these genes might further explain its therapeutic effects on ovarian cancer. However, the six key targets from molecular docking (TP53, VEGFA, MMP2, JUN, ERBB2, and CAV1) showed no significant changes in RNA-seq. These genes might still influence the formula's effects through their downstream pathways, such as cell cycle regulation for TP53 (Qiu et al., 2022) and immune modulation for VEGFA (Wen et al., 2024). While molecular docking offers insights into drug-target interactions, further experimental validation is needed. Our study provides a foundation for understanding ZMYL's mechanisms, but more *in vitro* and *in vivo* experiments are required to fully explore its effects on these pathways. Compared to previous studies, our work innovatively combines network pharmacology with transcriptomic data to explore the multi-target effects of ZMYL on ovarian cancer. This integrative approach not only confirms known targets but also identifies novel potential targets, offering a more comprehensive understanding of the formula's therapeutic mechanisms. Our study offers fresh perspectives on TCM formula research in cancer treatment through two key innovations. First, we systematically investigated ZMYL's dual effects on cell cycle regulation and immune response modulation. Second, we used organoid models, the most realistic *in vitro* systems reflecting *in vivo* conditions, to observe TCM formulas' effects on cancer cell cycle and immune response. This approach enhances our understanding of TCM's role in cancer treatment.

The phenotypic responses of organoids to drug treatments can vary widely, as observed in our study and previously reported outcomes. While some organoids may exhibit shrinkage and edge disintegration (Zhao et al., 2024), others might show a reduction in migrating cells post-treatment (Cao et al., 2023). Interestingly, organoids treated with the ZMYL formula did not display drastic morphological changes but did exhibit internal structural disarray. This highlights the need for a multifaceted approach in assessing drug responses in organoids, including both morphological and molecular analyses.

Further, our study's gene expression analysis post-ZMYL formula treatment has provided valuable insights into the molecular changes within ovarian cancer organoids. The cell cycle-related genes *CCNB2, CDC20, CDC25A, CDK10*, and others, which we identified as being modulated by the ZMYL formula, are consistent with key regulators of cell division (Fig. 9). Notably, *CCNB2* has been reported to be involved in the G2/M transition of the cell cycle and is associated with poor prognosis in ovarian cancer (Ke et al., 2022). Similarly, *CDC20* and *CDC25A* are known to play crucial roles in cell cycle regulation and have been implicated in chemoresistance in ovarian cancer (Sun et al., 2021; Sun et al., 2019). The modulation of these genes by the ZMYL formula suggests a potential mechanism for its therapeutic effects. Immune-related genes such as *ABI3, ARHGDIB, CD1A*, and *CXCL10*, which were also found to be affected by the ZMYL formula, are known to play significant roles in immune cell function and tumor immunology. For instance, *CXCL10* is a chemokine that attracts immune cells to the tumor site and has been associated with improved survival in ovarian cancer patients (Bronger et al., 2016). The ability of the ZMYL formula to regulate these genes indicates its potential to modulate the tumor's immune microenvironment, which is a critical aspect of cancer immunotherapy. The differential gene expression we observed aligns with previous reports on the effects of traditional Chinese medicine in cancer

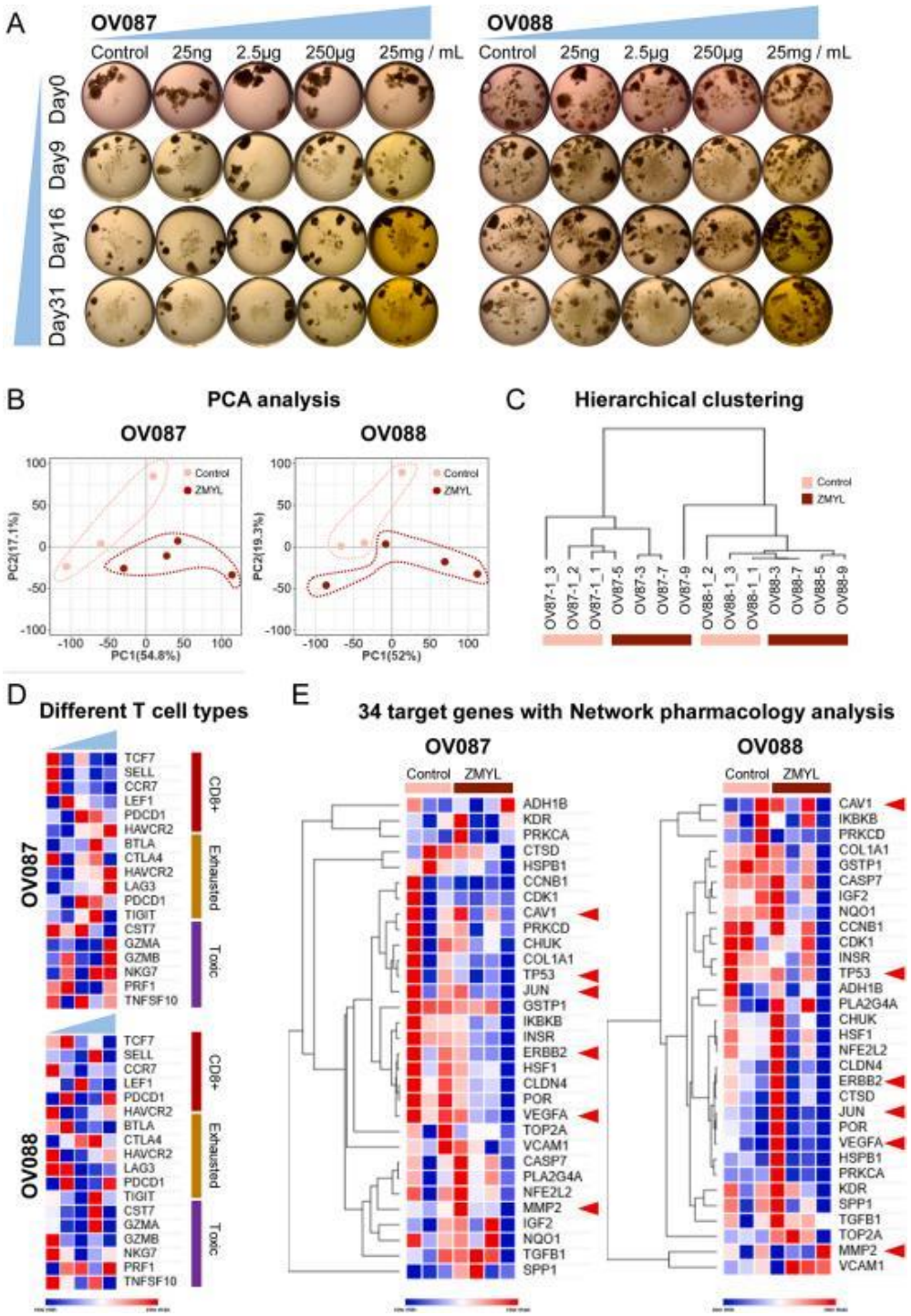

Fig. 7. Modulation of gene expression in ovarian cancer organoids by the ZMYL formula. (A) Time-lapse bright-field microscopy images of OV087 and OV088 organoids treated with the ZMYL formula at different concentrations (25 ng/mL, 2.5 μg/mL, 250 μg/mL, 25 mg/mL) and captured at various time points (Day 0, 9, 16, 31), illustrating the morphological changes. (B) PCA analysis of RNA-seq data from the treated organoids, highlighting the transcriptional variance and clustering. (C) Combined hierarchical clustering analysis of the two samples, revealing coordinated gene expression patterns. (D) Heatmap of 19 T cell related genes identified different types of T cells. (E) Heatmap of the 34 target genes identified from the network pharmacology analysis, with six genes (*TP53, JUN, VEGFA, ERBB2, MMP2, CAV1*) connected to the ZMYL formula and marked with red arrows for their significant binding interactions.

Phytomedicine 141 (2025) 156721

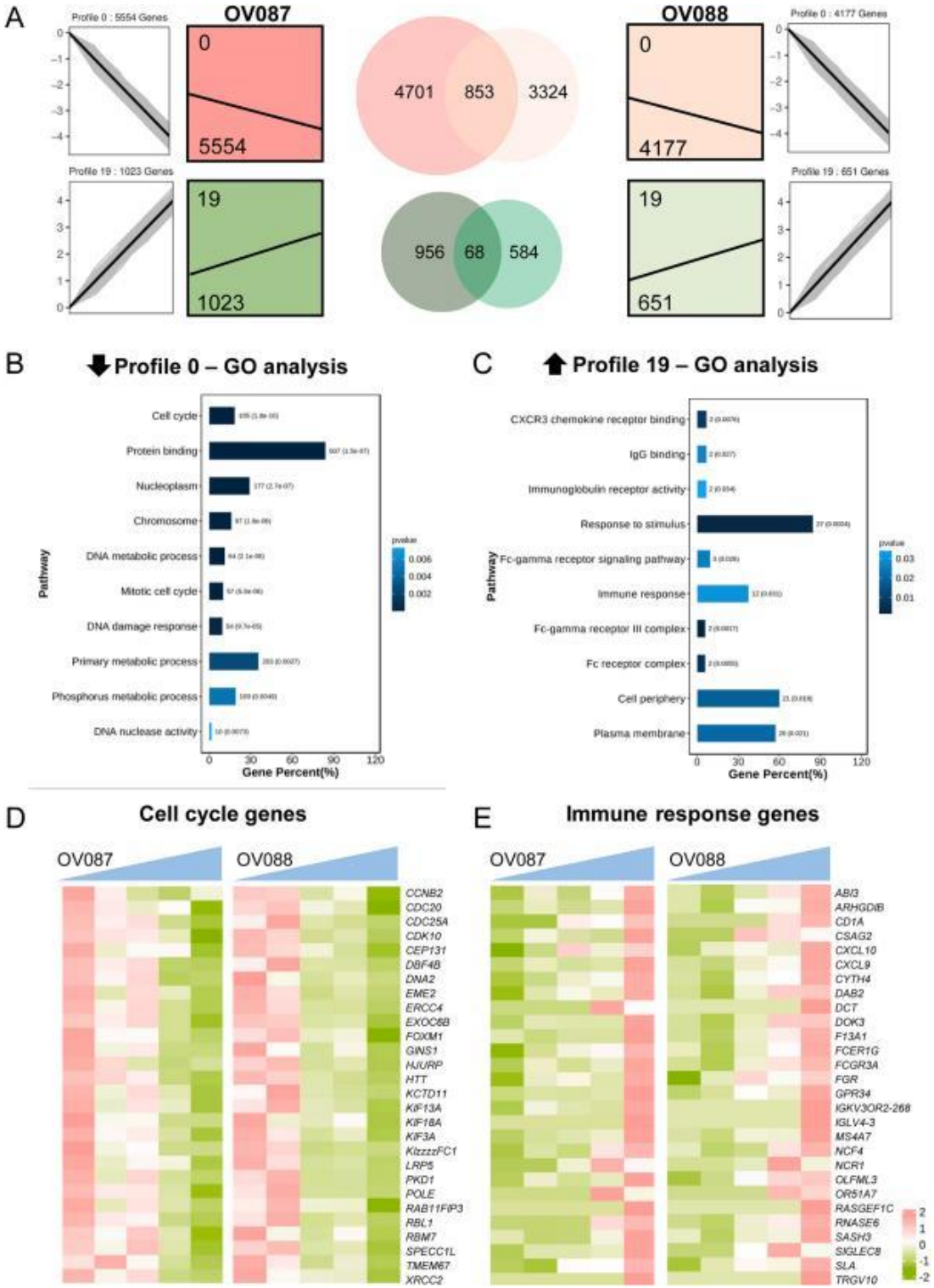

Fig. 8. Impact of ZMYL formula on immune response and cell cycle pathways in ovarian cancer organoids. (A) Trend analysis coupled with Venn diagram analysis identifies a set of 853 commonly downregulated genes and 68 commonly upregulated genes in response to increasing concentrations of the ZMYL formula. (B, C) GO analysis of the downregulated genes (profile0) suggests a suppression of cell cycle pathways, while the upregulated genes (profile19) indicate an activation of immune response pathways. (D, E) Heatmaps depict the expression of cell cycle and immune response genes in OV087 and OV088 organoids, respectively.

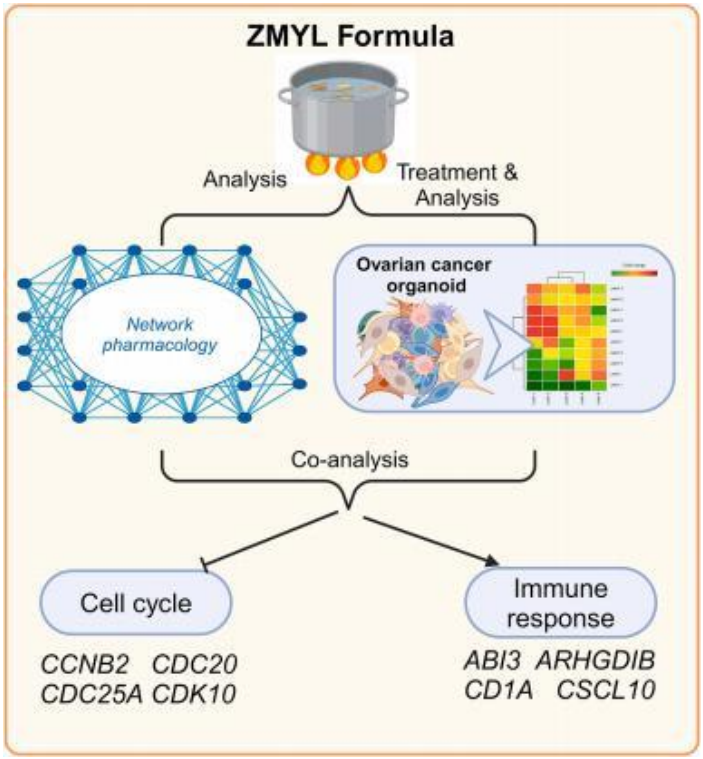

Fig. 9. Potential molecular mechanism of ZMYL formula in ovarian cancer organoids. This figure illustrates how the ZMYL formula affects ovarian cancer organoids by modulating genes in cell cycle regulation and immune response pathways, as identified through network pharmacology and transcriptomic analysis.

treatment. For example, a review of Chinese medicine's effectiveness against ovarian cancer highlights the multi-component, multi-target nature of such treatments, which is reflected in our findings (Wang et al., 2024b). The modulation of immune and cell cycle-related genes by the ZMYL formula could enhance the body's immune response against cancer cells while also targeting cell proliferation, offering a comprehensive approach to treatment.

While our study provides valuable insights into the potential of the ZMYL formula in ovarian cancer therapy, it is not without limitations. The complexity of TCM formulas and the variability in organoid responses across patients necessitate further research. Additionally, the translation of our *in vitro* findings to *in vivo* models and clinical settings is a critical next step. Despite these challenges, our work lays a solid foundation for the integration of TCM with modern oncological treatments.

Conclusion

In conclusion, our study demonstrates the potential of the ZMYL formula as a complementary therapy in ovarian cancer treatment, particularly in modulating immune responses and cell cycle progression. The integration of network pharmacology with *in vitro* organoid models offers a promising strategy for elucidating the mechanisms of action of TCM and informs future directions in cancer research and therapy.

CRediT authorship contribution statement

Qi Cao: Writing - review & editing, Writing - original draft, Methodology, Funding acquisition, Data curation, Conceptualization. **Chunhui Cai:** Writing - review & editing, Writing - original draft, Visualization, Supervision, Project administration, Methodology, Formal analysis, Data curation, Conceptualization. **Chen Wang:** Validation, Software, Methodology, Formal analysis, Data curation. **Lanyang Li:** Validation, Methodology, Data curation. **Jiping Liu:** Validation, Methodology, Investigation, Data curation. **Jian Zhang:** Visualization, Data curation. **Mingjie Rong:** Data curation. **Jiaqi Ren:** Resources. **Yanyan Han:** Resources, Data curation. **Jie Zhang:** Writing - review & editing, Writing - original draft, Visualization, Methodology, Funding acquisition, Data curation, Conceptualization. **Xinxin Han:** Writing - review & editing, Writing - original draft, Supervision, Project administration, Investigation, Conceptualization.

Declaration of competing interest

The authors declare that they have no known competing financial interests or personal relationships that could have appeared to influence the work reported in this paper.

Acknowledgments

We extend our sincere gratitude to all members of our laboratory for their invaluable contributions. This research was made possible by the generous support from the National Natural Science Foundation of China, with grant numbers 82374506 and 82174428. Additionally, we acknowledge the use of BioRender.com in crafting the diagrams for this study.

References

Amberger, J.S., Bocchini, C.A., Schiettecatte, F., Scott, A.F., Hamosh, A., 2015. OMIM.org: Online Mendelian Inheritance in Man (OMIM(R)), an online catalog of human genes and genetic disorders. Nucleic Acids Res. 43, D789-D798.

Bray, F., Laversanne, M., Sung, H., Ferlay, J., Siegel, R.L., Soerjomataram, I., Jemal, A., 2024. Global cancer statistics 2022: GLOBOCAN estimates of incidence and mortality worldwide for 36 cancers in 185 countries. CA Cancer J. Clin. 74, 229-263.

Bronger, H., Singer, J., Windmuller, C., Reuning, U., Zech, D., Delbridge, C., Dorn, J., Kiechle, M., Schmalfeldt, B., Schmitt, M., Avril, S., 2016. CXCL9 and CXCL10 predict survival and are regulated by cyclooxygenase inhibition in advanced serous ovarian cancer. Br. J. Cancer 115, 553-563.

Burley, S.K., Bhikadiya, C., Bi, C., Bittrich, S., Chen, L., Crichlow, G.V., Christie, C.H., Dalenberg, K., Di Costanzo, L., Duarte, J.M., Dutta, S., Feng, Z., Ganesan, S., Goodsell, D.S., Ghosh, S., Green, R.K., Guranovic, V., Guzenko, D., Hudson, B.P., Lawson, C.L., Liang, Y., Lowe, R., Namkoong, H., Peisach, E., Persikova, I., Randle, C., Rose, A., Rose, Y., Sali, A., Segura, J., Sekharan, M., Shao, C., Tao, Y.P., Voigt, M., Westbrook, J.D., Young, J.Y., Zardecki, C., Zhuravleva, M., 2021. RCSB Protein Data Bank: powerful new tools for exploring 3D structures of biological macromolecules for basic and applied research and education in fundamental biology, biomedicine, biotechnology, bioengineering and energy sciences. Nucleic Acids Res. 49, D437-D451.

Cao, Q., Li, L., Zhao, Y., Wang, C., Shi, Y., Tao, X., Cai, C., Han, X.X., 2023. PARPi decreased primary ovarian cancer organoid growth through early apoptosis and base excision repair pathway. Cell Transplant. 32, 9636897231187996.

Chen, X., Zhou, H., Liu, Y.B., Wang, J.F., Li, H., Ung, C.Y., Han, L.Y., Cao, Z.W., Chen, Y. Z., 2006. Database of traditional Chinese medicine and its application to studies of mechanism and to prescription validation. Br. J. Pharmacol. 149, 1092-1103.

de Witte, C.J., Espejo Valle-Inclan, J., Hami, N., Lohmussaar, K., Kopper, O., Vreuls, C.P. H., Jonges, G.N., van Diest, P., Nguyen, L., Clevers, H., Kloosterman, W.P., Cuppen, E., Snippert, H.J.G., Zweemer, R.P., Witteveen, P.O., Stelloo, E., 2020. Patient-derived ovarian cancer organoids mimic clinical response and exhibit heterogeneous inter- and intrapatient drug responses. Cell Rep. 31, 107762.

Fang, S., Dong, L., Liu, L., Guo, J., Zhao, L., Zhang, J., Bu, D., Liu, X., Huo, P., Cao, W., Dong, Q., Wu, J., Zeng, X., Wu, Y., Zhao, Y., 2021. HERB: a high-throughput experiment- and reference-guided database of traditional Chinese medicine. Nucleic Acids Res. 49, D1197-D1206.

Gong, C., Qian, L., Yang, H., Ji, L.L., Wei, H., Zhou, W.B., Qi, C., Wang, C.H., 2015a. Hepatotoxicity and pharmacokinetics of cisplatin in combination therapy with a traditional Chinese medicine compound of Zengmian Yiliu granules in ICR mice and SKOV-3-bearing nude mice. BMC Complement. Altern. Med. 15, 283.

Gong, C., Yang, H., Wei, H., Qi, C., Wang, C.H., 2015b. Pharmacokinetic comparisons by UPLC-MS/MS of isomer paeoniflorin and albiflorin after oral administration decoctions of single-herb Radix Paeoniae Alba and Zengmian Yiliu prescription to rats. Biomed. Chromatogr. 29, 416-424.

Ke, Y., Zhuang, X., You, L., 2022. Identification of core genes shared by endometrial cancer and ovarian cancer using an integrated approach. Cell Mol. Biol. 68, 140-145.

Kim, G., Jang, S.K., Ahn, S.H., Kim, S., Park, C.S., Seong, M.K., Kim, H.A., Bae, S., Lee, J. H., Kim, H., Jin, H.O., Park, I.C., 2024. Proapoptotic role of CDK1 in overcoming paclitaxel resistance in ovarian cancer cells in response to combined treatment with paclitaxel and duloxetine. Cancer Cell Int. 24, 409.

Kim, S., Chen, J., Cheng, T., Gindulyte, A., He, J., He, S., Li, Q., Shoemaker, B.A., Thiessen, P.A., Yu, B., Zaslavsky, L., Zhang, J., Bolton, E.E., 2019. PubChem 2019 update: improved access to chemical data. Nucleic Acids Res. 47, D1102-D1109.

Knox, C., Wilson, M., Klinger, C.M., Franklin, M., Oler, E., Wilson, A., Pon, A., Cox, J., Chin, N.E.L., Strawbridge, S.A., Garcia-Patino, M., Kruger, R., Sivakumaran, A., Sanford, S., Doshi, R., Khetarpal, N., Fatokun, O., Doucet, D., Zubkowski, A., Rayat, D.Y., Jackson, H., Harford, K., Anjum, A., Zakir, M., Wang, F., Tian, S., Lee, B., Liigand, J., Peters, H., Wang, R.Q.R., Nguyen, T., So, D., Sharp, M., da Silva, R., Gabriel, C., Scantlebury, J., Jasinski, M., Ackerman, D., Jewison, T., Sajed, T., Gautam, V., Wishart, D.S., 2024. DrugBank 6.0: the DrugBank Knowledgebase for 2024. Nucleic Acids Res. 52, D1265-D1275.

Kopper, O., de Witte, C.J., Lohmussaar, K., Valle-Inclan, J.E., Hami, N., Kester, L., Balgobind, A.V., Korving, J., Proost, N., Begthel, H., van Wijk, L.M., Revilla, S.A., Theeuwsen, R., van de Ven, M., van Roosmalen, M.J., Ponsioen, B., Ho, V.W.H., Neel, B.G., Bosse, T., Gaarenstroom, K.N., Vrieling, H., Vreeswijk, M.P.G., van Diest, P.J., Witteveen, P.O., Jonges, T., Bos, J.L., van Oudenaarden, A., Zweemer, R. P., Snippert, H.J.G., Kloosterman, W.P., Clevers, H., 2019. An organoid platform for ovarian cancer captures intra- and interpatient heterogeneity. Nat. Med. 25, 838-849.

Liu, Z., Guo, F., Wang, Y., Li, C., Zhang, X., Li, H., Diao, L., Gu, J., Wang, W., Li, D., He, F., 2016. BATMAN-TCM: a Bioinformatics Analysis Tool for Molecular mechANism of Traditional Chinese Medicine. Sci. Rep. 6, 21146.

Luo, Y., Xia, Y., Liu, D., Li, X., Li, H., Liu, J., Zhou, D., Dong, Y., Li, X., Qian, Y., Xu, C., Tao, K., Li, G., Pan, W., Zhong, Q., Liu, X., Xu, S., Wang, Z., Liu, R., Zhang, W., Shan, W., Fang, T., Wang, S., Peng, Z., Jin, P., Jin, N., Shi, S., Chen, Y., Wang, M., Jiao, X., Luo, M., Gong, W., Wang, Y., Yao, Y., Zhao, Y., Huang, X., Ji, X., He, Z., Zhao, G., Liu, R., Wu, M., Chen, G., Hong, L., Consortium, C., Ma, D., Fang, Y., Liang, H., Gao, Q., 2024. Neoadjuvant PARPi or chemotherapy in ovarian cancer informs targeting effector Treg cells for homologous-recombination-deficient tumors. Cell 187, 4905-4925 e4924.

Maenhoudt, N., Defraye, C., Boretto, M., Jan, Z., Heremans, R., Boeckx, B., Hermans, F., Arijs, I., Cox, B., Van Nieuwenhuysen, E., Vergote, I., Van Rompuy, A.S., Lambrechts, D., Timmerman, D., Vankelecom, H., 2020. Developing organoids from ovarian cancer as experimental and preclinical models. Stem Cell Rep. 14, 717-729.

Pinero, J., Ramirez-Anguita, J.M., Sauch-Pitarch, J., Ronzano, F., Centeno, E., Sanz, F., Furlong, L.I., 2020. The DisGeNET knowledge platform for disease genomics: 2019 update. Nucleic Acids Res. 48, D845-D855.

Qi, C., Zhang, Q.H., Li, J.X., 2012. [Effects of Zengmian Yiliu Recipe combined cisplatin on the tumor inhibition rate in platinum-resistant ovarian cancer]. Zhongguo Zhong Xi Yi Jie He Za Zhi 32, 817-821.

Qiu, P., Jie, Y., Ma, C., Chen, H., Qin, Y., Tu, K., Wang, L., Zhang, Z., 2022. Paired box 8 facilitates the c-MYC related cell cycle progress in TP53-mutation uterine corpus endometrial carcinoma through interaction with DDX5. Cell Death Discov. 8, 276.

Ru, J., Li, P., Wang, J., Zhou, W., Li, B., Huang, C., Li, P., Guo, Z., Tao, W., Yang, Y., Xu, X., Li, Y., Wang, Y., Yang, L., 2014. TCMSP: a database of systems pharmacology for drug discovery from herbal medicines. J. Cheminform. 6, 13.

Samaha, H., Pignata, A., Fousek, K., Ren, J., Lam, F.W., Stossi, F., Dubrulle, J., Salsman, V.S., Krishnan, S., Hong, S.H., Baker, M.L., Shree, A., Gad, A.Z., Shum, T., Fukumura, D., Byrd, T.T., Mukherjee, M., Marrelli, S.P., Orange, J.S., Joseph, S.K., Sorensen, P.H., Taylor, M.D., Hegde, M., Mamonkin, M., Jain, R.K., El-Naggar, S., Ahmed, N., 2018. A homing system targets therapeutic T cells to brain cancer. Nature 561, 331-337.

Senkowski, W., Gall-Mas, L., Falco, M.M., Li, Y., Lavikka, K., Kriegbaum, M.C., Oikkonen, J., Bulanova, D., Pietras, E.J., Vossgrone, K., Chen, Y.J., Erkan, E.P., Dai, J., Lundgren, A., Gronning Hog, M.K., Larsen, I.M., Lamminen, T., Kaipio, K., Huvila, J., Virtanen, A., Engelholm, L., Christiansen, P., Santoni-Rugiu, E., Huhtinen, K., Carpen, O., Hynninen, J., Hautaniemi, S., Vaharautio, A., Wennerberg, K., 2023. A platform for efficient establishment and drug-response profiling of high-grade serous ovarian cancer organoids. Dev. Cell 58, 1106-1121 e1107.

Stelzer, G., Rosen, N., Plaschkes, I., Zimmerman, S., Twik, M., Fishilevich, S., Stein, T.I., Nudel, R., Lieder, I., Mazor, Y., Kaplan, S., Dahary, D., Warshawsky, D., Guan-Golan, Y., Kohn, A., Rappaport, N., Safran, M., Lancet, D., 2016. The GeneCards Suite: from gene data mining to disease genome sequence analyses. Curr. Protoc. Bioinform. 54, 1 30 31-31 30 33.

Sun, X., Liu, Q., Huang, J., Diao, G., Liang, Z., 2021. Transcriptome-based stemness indices analysis reveals platinum-based chemo-theraputic response indicators in advanced-stage serous ovarian cancer. Bioengineered 12, 3753-3771.

Sun, Y., Li, S., Yang, L., Zhang, D., Zhao, Z., Gao, J., Liu, L., 2019. CDC25A facilitates chemo-resistance in ovarian cancer multicellular spheroids by promoting E-cadherin expression and arresting cell cycles. J. Cancer 10, 2874-2884.

Vazquez-Garcia, I., Uhlitz, F., Ceglia, N., Lim, J.L.P., Wu, M., Mohibullah, N., Niyazov, J., Ruiz, A.E.B., Boehm, K.M., Bojilova, V., Fong, C.J., Funnell, T., Grewal, D., Havasov, E., Leung, S., Pasha, A., Patel, D.M., Pourmaleki, M., Rusk, N., Shi, H., Vanguri, R., Williams, M.J., Zhang, A.W., Broach, V., Chi, D.S., Da Cruz Paula, A., Gardner, G.J., Kim, S.H., Lennon, M., Long Roche, K., Sonoda, Y., Zivanovic, O., Kundra, R., Viale, A., Derakhshan, F.N., Geneslaw, L., Issa Bhaloo, S., Maroldi, A., Nunez, R., Pareja, F., Stylianou, A., Vahdatinia, M., Bykov, Y., Grisham, R.N., Liu, Y. L., Lakhman, Y., Nikolovski, I., Kelly, D., Gao, J., Schietinger, A., Hollmann, T.J., Bakhoum, S.F., Soslow, R.A., Ellenson, L.H., Abu-Rustum, N.R., Aghajanian, C., Friedman, C.F., McPherson, A., Weigelt, B., Zamarin, D., Shah, S.P., 2022. Ovarian cancer mutational processes drive site-specific immune evasion. Nature 612, 778-786.

Wang, M., Bi, Y., Jin, Y., Zheng, Z.J., 2024a. Global incidence of ovarian cancer according to histologic subtype: a population-based cancer registry study. JCO Glob. Oncol. 10, e2300393.

Wang, Y., Xie, L., Liu, F., Ding, D., Wei, W., Han, F., 2024b. Research progress on traditional Chinese medicine-induced apoptosis signaling pathways in ovarian cancer cells. J. Ethnopharmacol. 319, 117299.

Wang, Y., Zhang, S., Li, F., Zhou, Y., Zhang, Y., Wang, Z., Zhang, R., Zhu, J., Ren, Y., Tan, Y., Qin, C., Li, Y., Li, X., Chen, Y., Zhu, F., 2020. Therapeutic target database 2020: enriched resource for facilitating research and early development of targeted therapeutics. Nucleic Acids Res. 48, D1031-D1041.

Wen, J., Xue, L., Wei, Y., Liang, J., Jia, W., Yong, T., Chu, L., Li, H., Han, S., Liao, J., Chen, Z., Liu, Y., Liu, Q., Ding, Z., Liang, H., Gan, L., Chen, X., Huang, Z., Zhang, B., 2024. YTHDF2 is a therapeutic target for HCC by suppressing immune evasion and angiogenesis through ETV5/PD-L1/VEGFA axis. Adv. Sci. 11, e2307242 (Weinh).

Yang, X., Zhou, S., Yang, C., Cao, C., He, M., Zi, S., 2022. CCNB1 negatively regulated by miR-559, promotes the proliferation, migration, and invasion of ovarian carcinoma cells. Mol. Biotechnol. 64, 958-969.

Zhang, Q.H., Gong, C., Yang, H., Wei, H., Zhou, W.B., Qi, C., Wang, C.H., 2015. Pharmacokinetics of cisplatin in the absence or presence of Zengmian Yiliu granules (a traditional Chinese medicine compound) in rats determined via ICP-MS: an investigation on drug-herb interactions. Pharm. Biol. 53, 159-166.

Zhang, S., Iyer, S., Ran, H., Dolgalev, I., Gu, S., Wei, W., Foster, C.J.R., Loomis, C.A., Olvera, N., Dao, F., Levine, D.A., Weinberg, R.A., Neel, B.G., 2021. Genetically defined, syngeneic organoid platform for developing combination therapies for ovarian cancer. Cancer Discov. 11, 362-383.

Zhao, Y., Wang, C., Deng, W., Li, L., Liu, J., Shi, Y., Tao, X., Zhang, J., Cao, Q., Cai, C., Han, X., 2024. Patient-derived ovarian cancer organoid carries immune microenvironment and blood vessel keeping high response to cisplatin. MedComm 5, e697 (2020).

Theranostics 2025, Vol. 15, Issue 17
9029

IVYSPRING INTERNATIONAL PUBLISHER

Theranostics

2025; 15(17): 9029-9046. doi: 10.7150/thno.118193

Research Paper

The first abdominal aortic aneurysm organoid model replicates complex microenvironment for *in vitro* disease study

Jiaxuan Feng[1#], Mingjie Rong[2#], Yudong Sun[1#], Guanglang Zhu[1#], Guangkuo Wang[3#], Jiping Liu[2], Chen Wang[2], Jian Zhang[2], Xiaochen Ma[1], Junyi Yan[1], Yaojie Wang[4], Youjin Li[4], Yu Ning[5], Chunhui Cai[2], Xinxin Han[2,6]

1. Department of Vascular Surgery, Department of General Surgery, Ruijin Hospital, Affiliated to Shanghai Jiao Tong University School of Medicine, Shanghai, 200025, China.
2. Shanghai Lisheng Biotech, Shanghai, 200092, China.
3. Department of Cardiovascular Surgery, Jiangmen Central Hospital, Guangdong, 529000, China.
4. Department of Cardiovascular Surgery, People's Hospital of Ningxia Hui Autonomous Region, Ningxia, 750002, China.
5. Department of Vascular Surgery, The First People's Hospital of Yulin, Guangxi, 537000, China.
6. LiSheng Organ Regeneration X Lab, East China Institute of Biotechnology, Peking University, Jiangsu, 226299, China.

#These authors made equal contributions to this work.

Corresponding authors: E-mail addresses: fengjiaxuan01@163.com (Jiaxuan Feng), sunyudong@smmu.edu.cn (Yudong Sun), caichunhui@lishengbiotech.com (Chunhui Cai), xxhan@sibs.ac.cn (Xinxin Han).

Received: 2025.05.24; Accepted: 2025.07.25; Published: 2025.08.16

Abstract

Background: Abdominal Aortic Aneurysm (AAA) is a critical global health issue, affecting an estimated up to 8% of men over 65, with a complex etiology involving smoking, age and gender. However, the lack of specific drug treatments underscores the need for a robust in vitro model to advance our comprehension of AAA pathophysiology and serve as an ex vivo surrogate for drug testing. **Methods:** This study introduces an innovative AAA patient-derived organoid (PDO) model using a non-enzymatic procedure, a Matrigel-free system, and specialized organoid culture medium, leveraging 3-dimensional (3D) cultures to replicate the disease's microenvironment. The stability of this culture system was assessed through microscopic observation, H&E staining, immunohistochemistry (IHC), viability assays, and whole-genome sequencing (WES). Additionally, we conducted pharmacological assessments to explore the effects of drug treatments on AAA PDO.

Results: Our model maintains aortic morphological integrity and pathological phenotypes, incorporates the immune microenvironment (validated by IHC markers for macrophages and lymphocytes), and adjacent tissues (loose connective tissue and vegetative blood vessels). The model demonstrates remarkable stability, confirmed by consistent genetic mutation sites throughout cultivation via WES, and cell survival after five weeks in vitro via live-cell staining. Preliminary pharmacological assessments show promising efficacy, with distinct responses to 1 μM metformin, 1 μM RU.521, or 1 μM STING-IN-2 treatments for 48 h via mass spectrometry.

Conclusions: The AAA organoid model, to the best of our knowledge, is the first reported abdominal aortic aneurysm PDO model, and signifies a promising step towards therapeutic treatment options for AAA, potentially complementing existing surgical approaches.

Keywords: Abdominal aortic aneurysm, Organoid, Patient-derived organoid, Immune microenvironment, *In vitro* disease model, Cardiovascular disease

Introduction

Abdominal aortic aneurysm (AAA) is a critical and prevalent vascular disorder characterized by the abnormal enlargement of the abdominal aorta to more than 3 cm in diameter, typically asymptomatic and potentially leading to rupture and life-threatening hemorrhage [1, 2]. The global impact of AAA is substantial, contributing to over 1% of all mortalities among men aged 65-85 in developed countries [1]. A

study of over 3 million individuals revealed that patients aged 55 and above accounted for a significant proportion (>95%) of AAA cases across various sizes (3-6 cm) [3]. A complex interplay of hereditary and environmental risk factors contributes to AAA, most notably older age, smoking, male sex, and a positive family history [2, 4-8].

The pathological basis of AAA lies in the loss of vascular structural integrity. This process includes the degradation of the extracellular matrix (ECM) and apoptosis of vascular smooth muscle cells (VSMCs) [9, 10]. Inflammation and the infiltration of inflammatory cells are key factors contributing to the disease's progression through the release of reactive oxygen species (ROS), which induce oxidative stress within the aortic wall [11-20]. Additionally, the secretion of pro-inflammatory cytokines such as tumor necrosis factor-alpha (TNF-α) and interleukin-6 (IL-6) further fuels inflammation and tissue damage. The action of proteolytic enzymes, such as matrix metalloproteinase-9 (MMP-9), secreted by inflammatory cells, weakens the structural integrity of the aortic wall and accelerates aneurysmal degeneration [11-13].

Current clinical management for high-risk AAA is primarily surgical, involving endovascular aortic repair and open surgical repair [13, 14]. Despite the prevalence of AAA, there is a significant lack of an effective model and no pharmacological treatments with proven enough efficacy, highlighting the need for a deeper understanding of the disease mechanisms and the development of novel treatment strategies [21, 22]. Human organoids, as innovative *in vitro* models, emulate the intricate microenvironment of human tissues and organs, offering a potential tool for studying organ development, function, disease mechanisms, modeling and drug screening [23, 24]. Furthermore, human organoids are recognized as an ideal model in clinical and research settings for their potential to bridge the gap between traditional *in vitro* models and *in vivo* systems, offering a more physiologically relevant context for investigation [25]. Their ability to recapitulate tissue-specific architecture and physiological conditions makes organoids a valuable tool for studying AAA pathogenesis and for identifying potential therapeutics.

In this study, we present a novel organoid model of AAA designed to emulate the *in vivo* 3D architecture and some functionalities of the abdominal aorta, serving as a biological ex vivo surrogate for drug testing and pathophysiological investigation. Previously, AAA models were mostly developed from traditional animal models by drug-induced vascular inflammatory responses [26-29]. Efforts to develop functional vascular organoids have involved differentiating induced pluripotent stem cells into endothelial and vascular wall cells. However, these models did not specifically target AAA [30, 31]. Some studies have utilized 3D printing technology to create cystic dilation structures of human vascularized tissue to simulate AAA, mainly focusing on biomechanical properties like hemodynamic effects on vascular dilation [32]. Additionally, dispersing smooth muscle cells (SMCs) from AAA patients onto electrospun poly-lactide-co-glycolide scaffolds has been explored for creating AAA models with certain mechanical and biological characteristics being demonstrated [33]. In contrast, our culture system encompasses a multifaceted microenvironment including elements of the immune microenvironment, *vasa vasorum,* perivascular connective tissue and the model's morphological consistency, preserved pathological phenotypes and genomic steadiness are well retained. Early pharmacological testing on the model has indicated its potential, with drug response data providing preliminary but positive indications. This makes it the first abdominal aortic aneurysm PDO model in the world. The innovative approach provides a potentially useful tool for advancing our understanding of AAA pathophysiology and facilitating the discovery of effective therapeutics.

Results

AAA PDO modeling and morphological consistency

To preserve the native microenvironment and anatomical structure of AAA tissues, we developed a method for generating AAA PDO without the need for enzymatic dissociation into single cells. Considering the substantial extracellular matrix of the aortic walls and the limited proliferative capacity, which poses challenges for enzymatic digestion and risks cell death with prolonged digestion times, enzymatic treatment was avoided. Furthermore, the AAA PDO models were established without the use of Matrigel or other biomaterials; they were cultured in a special medium without constraints. For details, AAA specimens were collected from patients post-surgery. Following thoroughly washing, the specimens were trimmed into rectangles measuring approximately 3-5 mm on each side using surgical scissors, and subsequently transferred to a 10 cm culture dish filled with 20 mL of culture medium (Figure 1A).

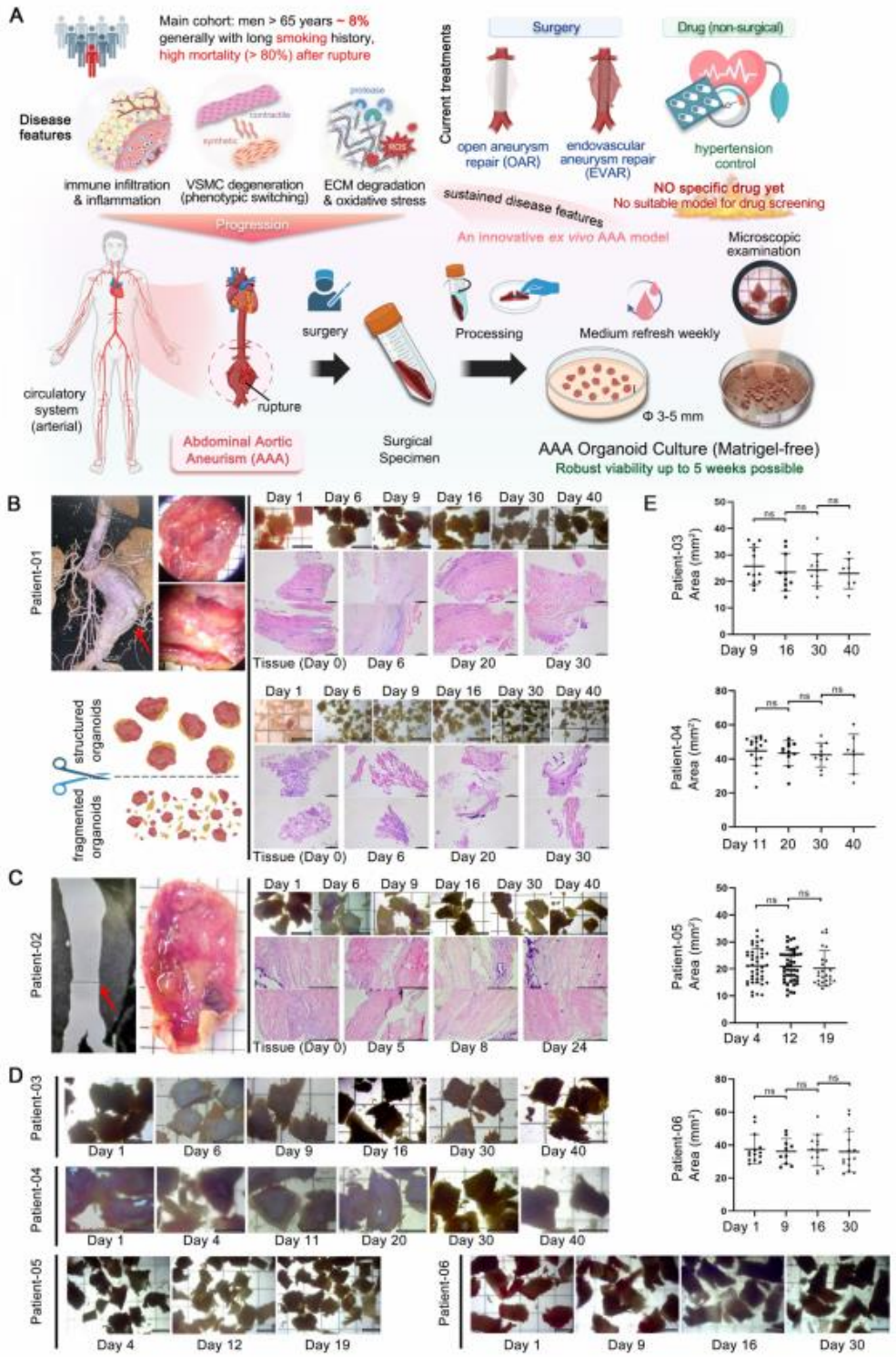

Figure 1. Modeling and Growth of AAA PDO. (A) Anatomical location of AAA, from clinical tissue specimens to organoid culture. (B) Tissue sampling location images for Patient 01, comparing two culture methods: preserved layered structure and minced (bright-field microscopy and H&E staining). (C) Tissue sampling location images for Patient 02. (D) Bright-field microscopy of the culture process for Patients 03-06. (E) Corresponding organoid size changes to Figure 1D, with size measurements completed using ImageJ. Variable sample size n = 7-44 due to sampling during cultivation. Bright-field imaging Scale Bar = 5 mm, H&E staining Scale Bar = 500 μm. Data are represented as the mean ± SEM, with individual data points displayed. Illustration and statistical analysis were performed using GraphPad 9.0.

Regular sampling was conducted to evaluate morphological changes. Medical imaging data and stereomicroscope observations, as well as bright-field and hematoxylin & eosin (H&E) staining images of samples with different culture durations from Patient 01 and 02, are demonstrated in (Figure 1B-C). Additionally, a series of bright-field images from PDO derived from Patient 03 to 06 across varying days in culture are presented (Figure 1D). The size changes of these PDO were statistically analyzed (Figure 1E). No significant variations were observed throughout the culture period. Altogether, the AAA PDO exhibited no notable morphological changes under bright-field microscopy, indicating that their structural integrity was well maintained.

The PDO model preserved AAA pathological phenotypes

To evaluate the similarity of AAA PDO to their native tissues, we performed histological analyses. The H&E staining indicated that sampling of fully minced organoid was non-systematic, potentially resulting in the acquisition of solely the loose connective tissue of the adventitia, and its structure appeared more dispersed relative to the intact tissue (Figure 1B). In contrast, the "rectangular" PDO were capable of preserving a dense, layered structure. Consequently, in subsequent culturing, all tissue processing ensured the preservation of the layered structure, avoiding fragmentation.

Detailed H&E staining data are organized into two principal sections (Figure 2A). The tissue and organoid samples from Patient 01, following cryosectioning and staining (Figure 2B), retained similarities with the tissue post 30 days in culture, exhibiting nuclei that were dispersed in a seemingly random pattern. The arrangement of the media, or luminal region, is denser and more uniformly structured than that of the adventitia. Additionally, loose connective tissues, including Perivascular Adipose Tissue (PVAT) and *vasa vasorum*, adjacent to the adventitia, are clearly discernible.

The tissue and organoid samples from Patient 07, following paraffin embedding, sectioning, staining (Figure 2C), and high-resolution scanning, produced results with enhanced clarity. The tissue morphology remained consistent throughout the culture process, with no notable loss of cells, particularly vascular smooth muscle cells, observed. According to the quantitative analysis (Figure 2D), the mean number of nuclei exhibited a slight decline with increasing culture duration up to Day 20. Furthermore, the adventitia, which is adjacent to loose connective tissue, contained a significantly higher cell count relative to the luminal side.

A key pathological feature of AAA is the degradation of the extracellular matrix (ECM), particularly characterized by the loss of elastic fibers, contributing to the risk of aneurysm dilation and rupture. Hence, it is essential to ascertain whether the culture system can preserve the native ECM structure of the tissue. Elastic staining, using the Verhoeff-van Gieson technique, was utilized (Figure S1A). The staining of cryosectioned samples (Figure S1B) demonstrated that elastic fibers in the tissue and PDO with diverse culture durations consistently presented a brief, filamentous (S-shaped) or truncated rod-like morphology, without any significant loss, even after a four-week culture period. By segmenting the stained images into distinct regions and conducting a quantitative analysis to determine the proportion of elastic fibers within the tissue, it was observed that the percentage of elastic fibers showed only a minimal reduction, if any, over extended culture periods (Figure S1C). Consequently, the culture system effectively maintains the physiological and pathological integrity of the elastic fibers.

The AAA PDO owned sustained microenvironment

In addition to ECM degradation, key pathological characteristics of AAA encompass extensive inflammatory infiltration by immune cells and the degeneration of smooth muscle. The effective preservation of the immune microenvironment is a critical benchmark for successful organoid culture, thereby enhancing the comprehension of the disease process and facilitating drug target assessment. Immunohistochemistry (IHC) is a technique that effectively and conveniently delineates the immune microenvironment. We selected a panel of immune cell markers, including CD3, CD38, CD45, CD68, F4/80, and MMP-9 for testing. Additionally, α-actin was utilized to assess the capacity of the culture system to preserve the native state of smooth muscle in tissue (Figure 3A).

The expression profiles of CD3, CD38, CD45, CD68, F4/80, MMP-9, and α-actin in both tissue and PDO are demonstrated, with specific staining for these markers showing moderate attenuation as the organoid culture period extends (Figure 3B, Figure S2). For a quantitative assessment of these results, the tissue sections were manually segmented into four distinct areas, ensuring minimal overlap and blank space, with both maintained below 20%. Subsequent quantitative analysis was conducted using the IHC profiler plugin in ImageJ, scoring the positive areas. Statistical analysis reveals no significant differences in the expression of CD3, CD45, CD68, MMP-9, F4/80 and α-actin between tissues and PDO across various

culture time points (Figure 3C). However, CD38 showed significant variation due to uneven distribution at different time points, as determined by one-way ANOVA analysis. From an overall trend perspective, the expression of the aforementioned markers in organoid cultures remains relatively stable within the first 12 days.

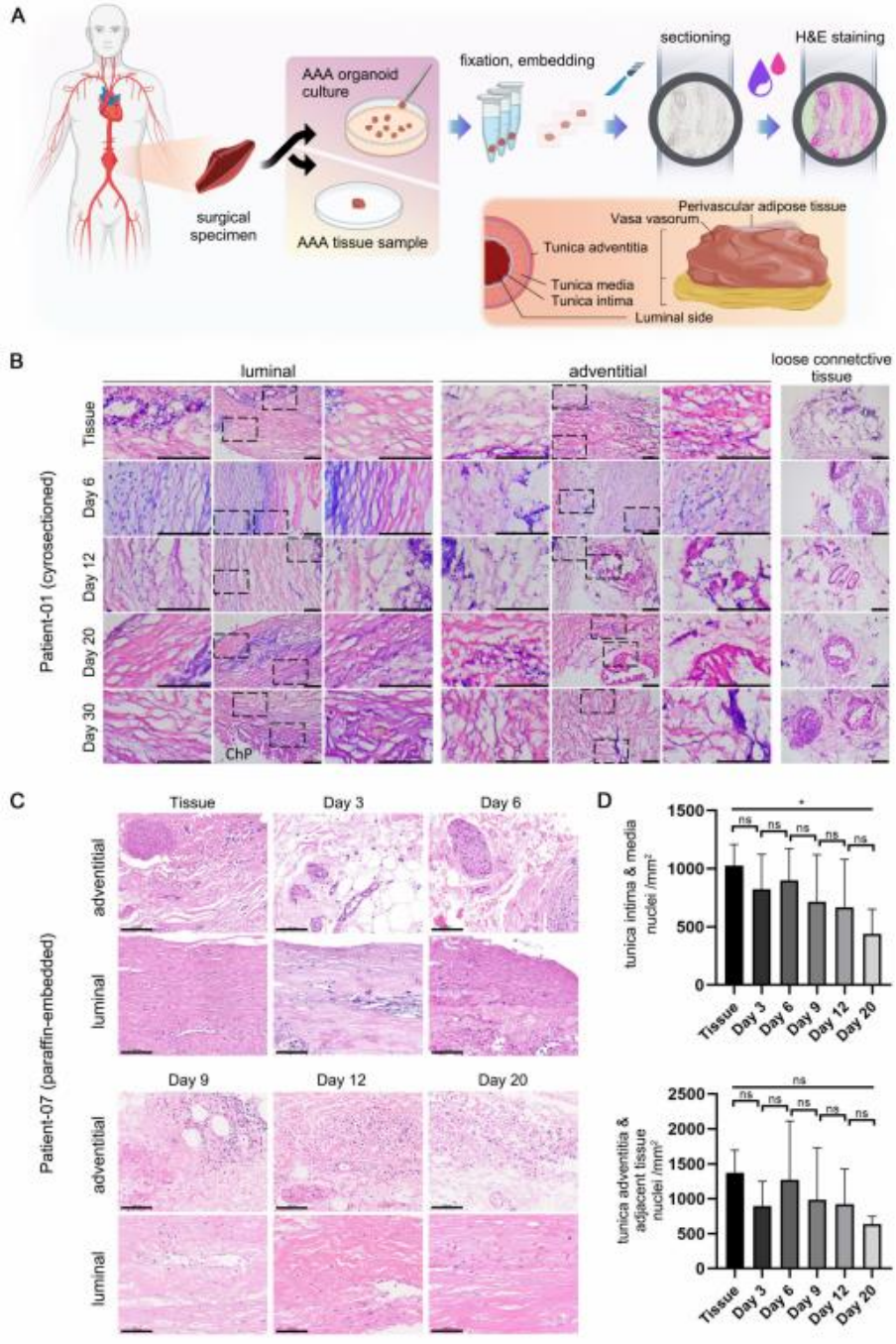

Figure 2. H&E Staining of AAA PDO. (A) Schematic diagram of the staining process and anatomical illustration of abdominal aortic tissue. (B) Cryosection H&E staining images from Patient 01. Scale Bar = 200 μm. ChP = Cholesterol Plaque (C) Paraffin section H&E staining images from Patient 07. Scale Bar = 100 μm (D) Quantitative analysis based on Figure 2C. Using ImageJ to calculate the number of cell nuclei per unit area (n = 6 ROIs). The Tunica intima & media area and the Tunica adventitia & adjacent tissue area were analyzed separately. Data are represented as the mean ± SEM. Illustration and statistical analysis were performed using GraphPad 9.0.

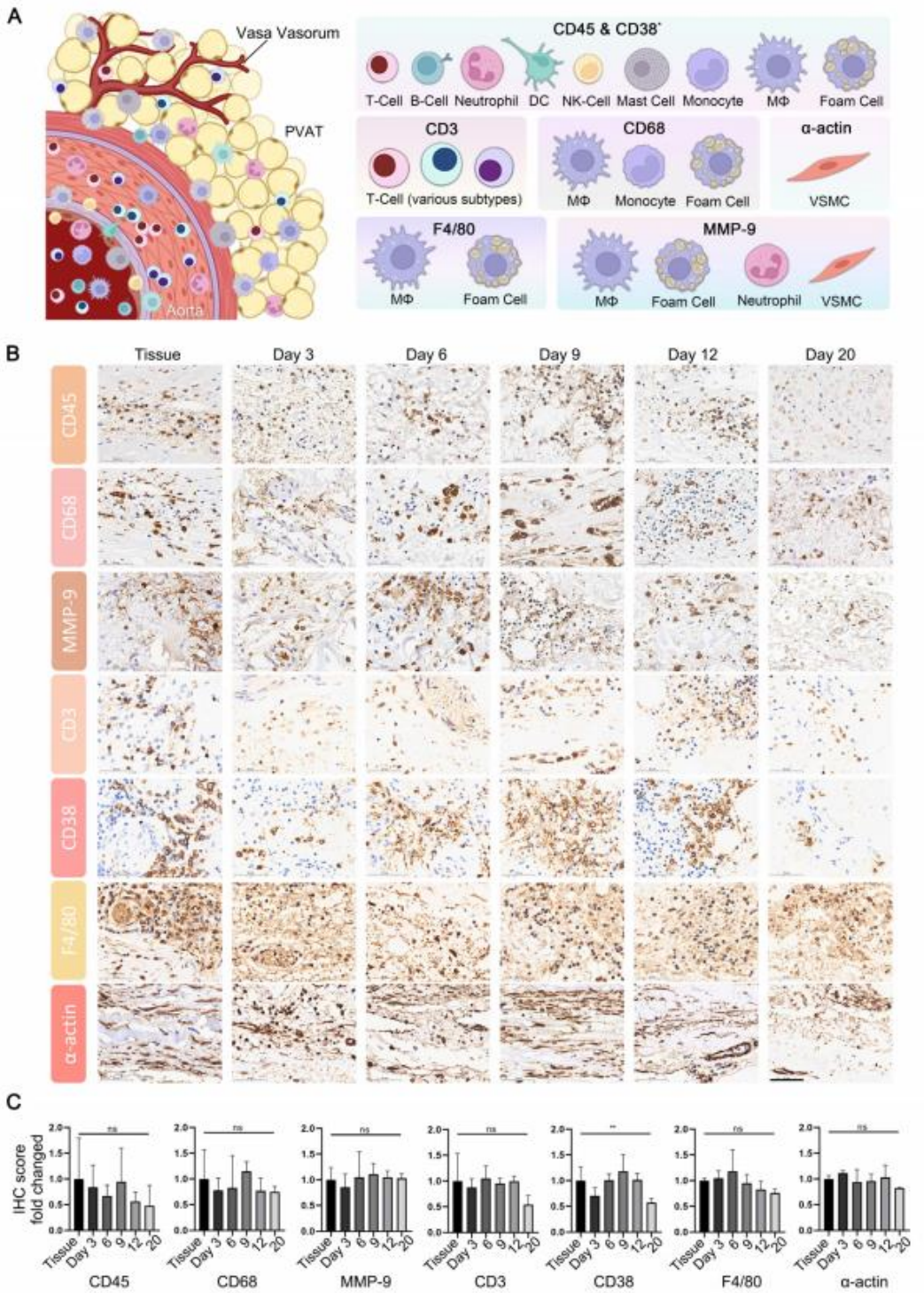

Figure 3. Characterization of Microenvironment in AAA PDO via Immunohistochemistry (IHC). (A) Schematic representation of the vascular immune microenvironment, along with the cells corresponding to various marker. DC = Dendritic Cell, NK = Natural Killer, MΦ = Macrophage, VSMC = Vascular Smooth Muscle Cell, PVAT = Perivascular Adipose Tissue. Created with BioRender.com and Adobe PhotoShop 2024. (B) IHC images of related markers. scale bar = 50 μm. (C) Quantitative analysis of IHC images: Original data were divided into four approximate equal parts with minimal overlap and blank space (< 20%). The ImageJ IHC profiler plugin was utilized to score the percentage of positive areas. The scores for high positive, positive, and low positive areas were multiplied by factors of 3, 2, and 1, respectively, and then summed. Data are represented as the mean ± SEM. Illustration and statistical analysis were performed using GraphPad 9.0.

The genomic steadiness of AAA organoid

Through WES, we confirmed the genomic stability of AAA organoids, showing high genetic similarity to source tissues (Figure 4A). The concordance in mutation profiles between tissue and organoid samples was notably high, exceeding 95% (Figure 4B). The proportions of insertions and deletions (InDels) and single nucleotide polymorphisms (SNPs) were highly consistent, further confirming the genetic stability of our culture system (Figure 4C).

Cross-sample analysis revealed many shared mutation sites. We identified 108 risk genes frequently mutated in AAA patients from literatures [34-38], 28 of which were confirmed by our samples, including notably recurrent genes such as ADAMTS8, CELSR2, CHRNA3, DAB2IP, GDF7, MYH7, and TTN (Figure 4D). The specific mutations are shown in Figure 4E.

WES also detected numerous previously unreported high-frequency mutation sites, enhancing our understanding of AAA's genetic basis. We found 496 mutated genes present in both tissues and organoids across all six patients. Some of these genes are strongly associated with cardiovascular diseases, such as the MUC family, COL18A1, and TNXB. Various mutation types and frequencies were observed within these genes (Figure 4E). Within each patient-matched sample group, the variant allele frequency between matched tissue and organoid was highly concordant (Figure 4F), indicating that the organoid model did not markedly alter the overall mutation burden within the analyzed exome.

The organoid viability maintenance during cultivation

Maintaining viability over a specified duration is a critical criterion for the successful establishment of AAA organoid models and essential for their subsequent application in drug testing. Following the initial development of the models, the PDO maintained roughly 50% of their initial viability after approximately 12 days in culture.

This study utilized two distinct fluorescence-based assays for the assessment of viability (Figure 5A). The alamarBlue™ HS assay, employing a non-fluorescent blue dye, offers an alternative approach. The dye is directly incorporated into the culture medium and subjected to a 20 h incubation period, during which it is converted to a strong red fluorescent product by viable cells. Owing to its low toxicity, this assay facilitates the continuous monitoring of viability changes within the same sample over time. PDO derived from Patient 05 were concurrently tested for viability using this assay (Figure 5B), exhibiting an average viability decline to 50% of the initial state after approximately 12 days of culture.

The Calcein AM/PI assay entails the direct fluorescent staining of viable cells, characterized by green fluorescence, in contrast to non-viable cells that exhibit red fluorescence. The staining patterns of fragmented PDO derived from two individual patients at multiple culture time points are illustrated in (Figure 5C-D). PDO derived from Patient 01 exhibited sustained robust viability even after 5 weeks, characterized by intense punctate green fluorescence upon enzymatic dissociation, signifying the presence of metabolically active cells. Nonetheless, the samples from the fourth week demonstrated a modest decrease in viability relative to the fifth week, possibly attributable to sampling variability, batch effects, or human error. The AAA PDO derived from Patient 07 underwent more frequent sampling and staining, initially showing high viability on Day 1 and 3, which subsequently gradually declined, as confirmed by quantitative analysis (Figure 5E). In addition, Calcein AM/PI staining effectively demonstrates the culture system's ability to maintain complex tissue structure including loose connective tissue, as seen in the green fluorescent stained *vaso vasorum* and the adipose tissue in (Figure 5F).

Organoid responses to drug treatments

The preliminary evaluation of pharmacological interventions within our AAA organoid model showcased its great potential as a therapeutic tool and approach for AAA treatment. Following the validation of the stability of this organoid culture system, we commenced pharmacological treatment of AAA PDO derived from samples of Patient 10 on the third day of cultivation with 1 μM RU.521 (RU), 1 μM STING-IN-2 (ST), accompanied by a solvent control and another control of 1 μM metformin (Met), which has the potential for the treatment of AAA [22, 39, 40]. After 48 h of incubation, the supernatants were subjected to mass spectrometry analysis. Conversely, the bright-field images were captured on days 0, 2, 7 and 14 post-treatments (Figure 6A). Bright-field imaging (Figure 6B) shows that after 14 days of drug treatment, the AAA PDO did not exhibit notable morphological changes. In the PCA analysis (Figure 6C), samples within each group were closely clustered, with distinct differences observed between the drug-treated groups and the control group, indicating satisfactory sample quality.

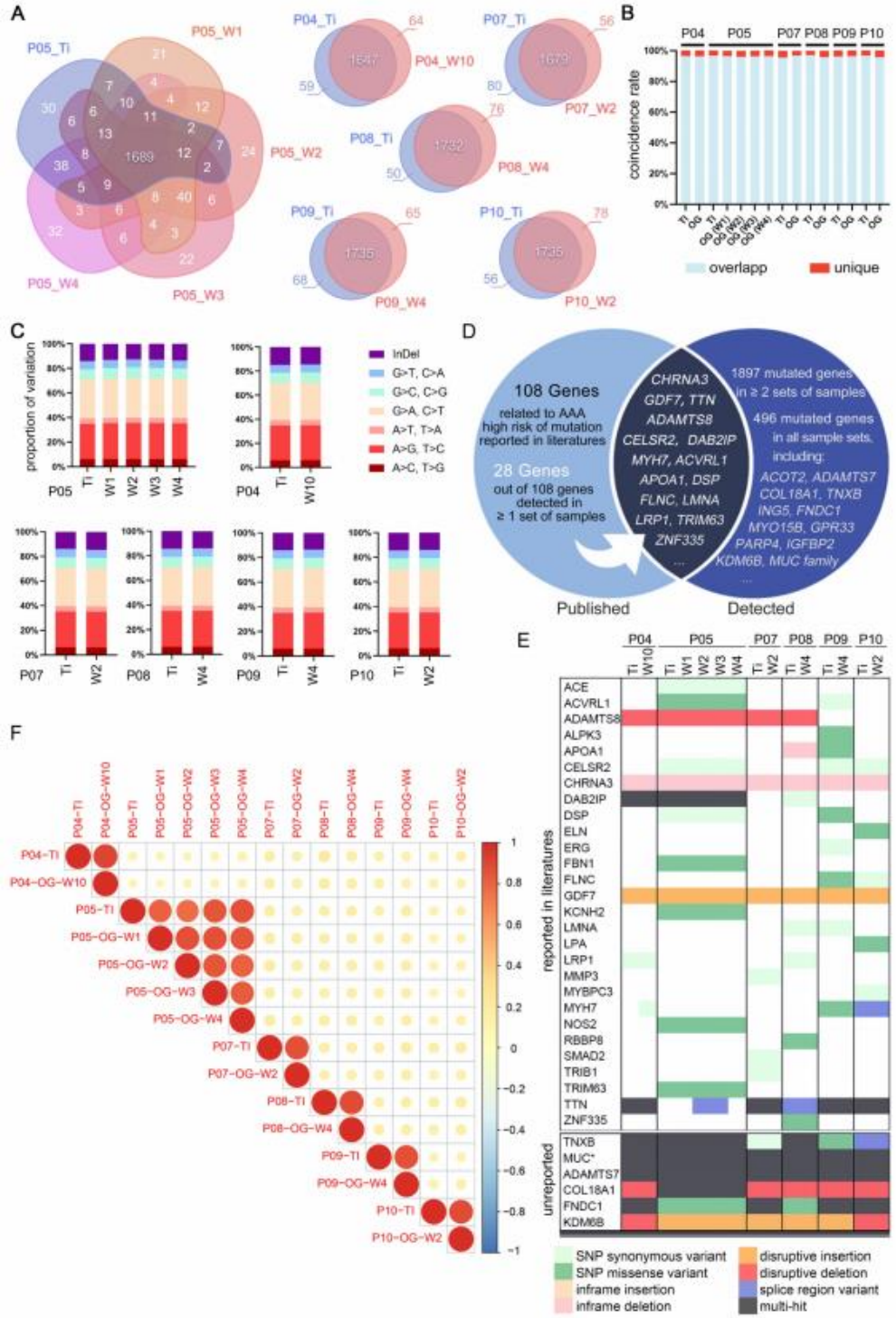

Figure 4. WES Analysis Confirming Genomic Stability. (A) Venn diagram of mutations in tissue and corresponding organoids, highlighting commonalities and differences. (B) Coincidence rate derived from Figure 4A. (C) Proportional distribution of InDels and point mutations. (D) Venn diagram comparing high-frequency mutations found in this study to those reported in literature. (E) Overview of gene mutation types, with the upper section depicting literature-consistent mutations and the lower section listing high-risk mutation genes detected, not clearly reported but associated with cardiovascular diseases. *MUC family including MUC1/2/3A/4/5AC/6/12/16/19/20/21/22. (F) Correlation of mutation frequencies between tissue and organoids samples. Pearson r values are ≥ 0.75 for all within-patient pairs, indicating strong concordance. TI = Tissue, OG = Organoids, W = week (organoid culture duration), P = patient.

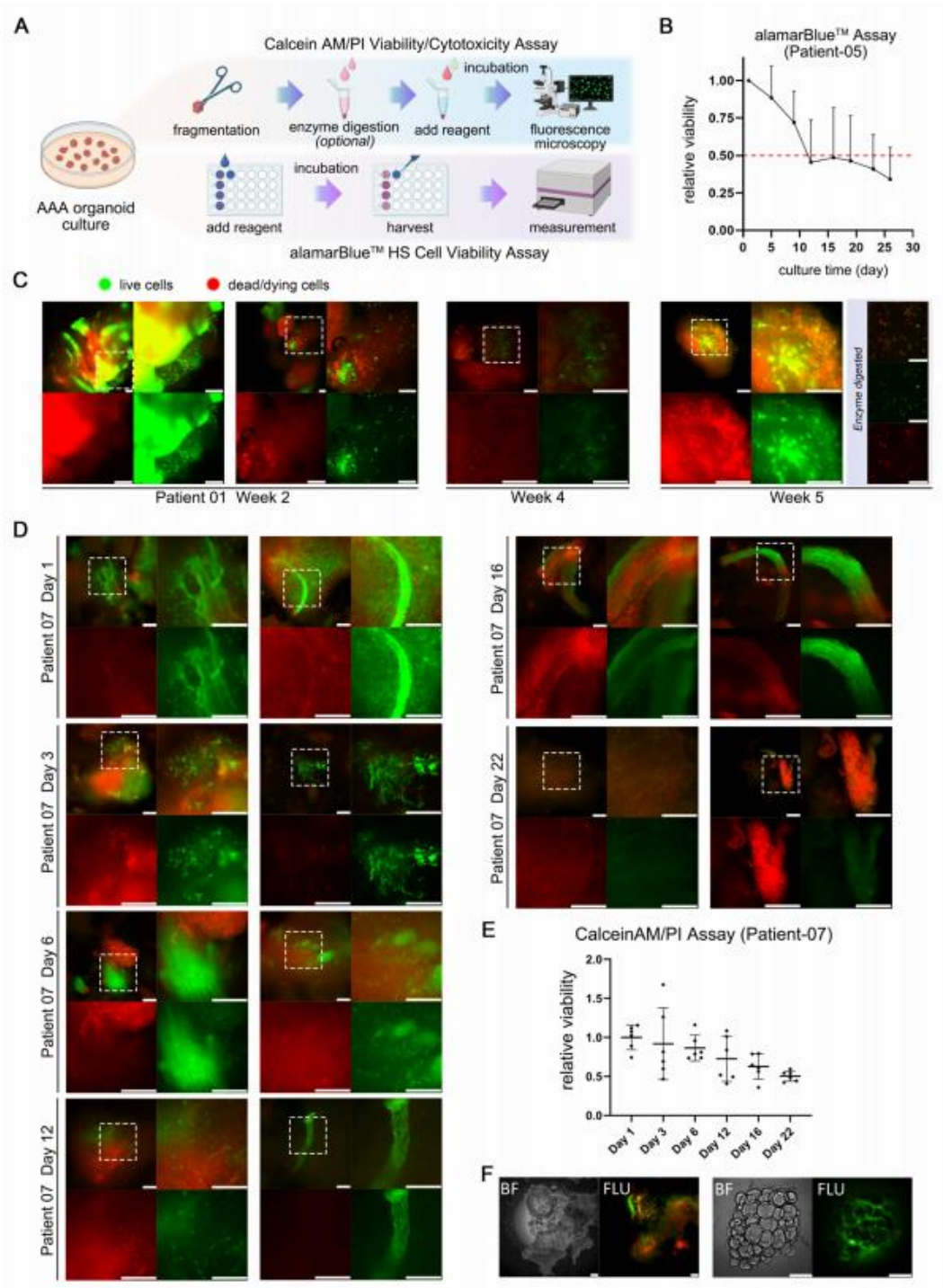

Figure 5. Viability Assessment of AAA PDO. (A) Schematic diagrams of fluorescence-based viability assays. (B) Results of the alamarBlue™ HS assay. Fluorescence units, after background subtraction, were normalized to the values from the initial test (Day 1-2) to calculate the fold change. Data are represented as the mean ± SEM. Illustration was created with GraphPad 9.0. (C, D) Results of the Calcein AM/PI assay for fragmented AAA PDO. Green fluorescence indicates live cells, red fluorescence signifies dead or dying cells. Scale bar = 200 μm. (E) Quantitative analysis of the images from Figure 6C. Images were converted to 8-bit grayscale in ImageJ, and the mean fluorescence intensity of red and green channels was measured after applied a constant threshold, respectively. Subsequently, the ratio of green to red fluorescence intensity was calculated, and then normalized to the arithmetic mean of values on Day 1. Data are represented as the mean ± SEM, with individual data points displayed. Illustration was created with GraphPad 9.0. (F) Fluorescent stained perivascular connective tissue from AAA organoid fragments. BF = Bright-field image; FLU = Merged red/green fluorescence image after Calcein AM/PI staining. Scale bar = 200 μm.

In comparison to the control groups, each drug treatment group displayed a number of proteins with markedly distinct expression profiles. A comparative analysis of the supernatants from each drug treatment group versus the control group is presented, highlighting proteins that are upregulated, downregulated, or show consistent presence or absence, respectively (Figure 6D-E). Moreover, a clustered heatmap of the proteins significantly upregulated or downregulated is provided, allowing for the determination of their distribution, differences, and clustering relationships (Figure 6F). The Venn diagram and Volcano plot (Figure 6G-H) illustrate the proteins that are significantly upregulated or newly emerged and downregulated or lost in different drug treatment groups compared to the control, highlighting both commonalities and differences. This suggests that different drug treatments could show similar effects on the expression of certain proteins. Furthermore, the impact of the RU.521 on the protein expression pattern is noticeably more pronounced than that of the other two drugs.

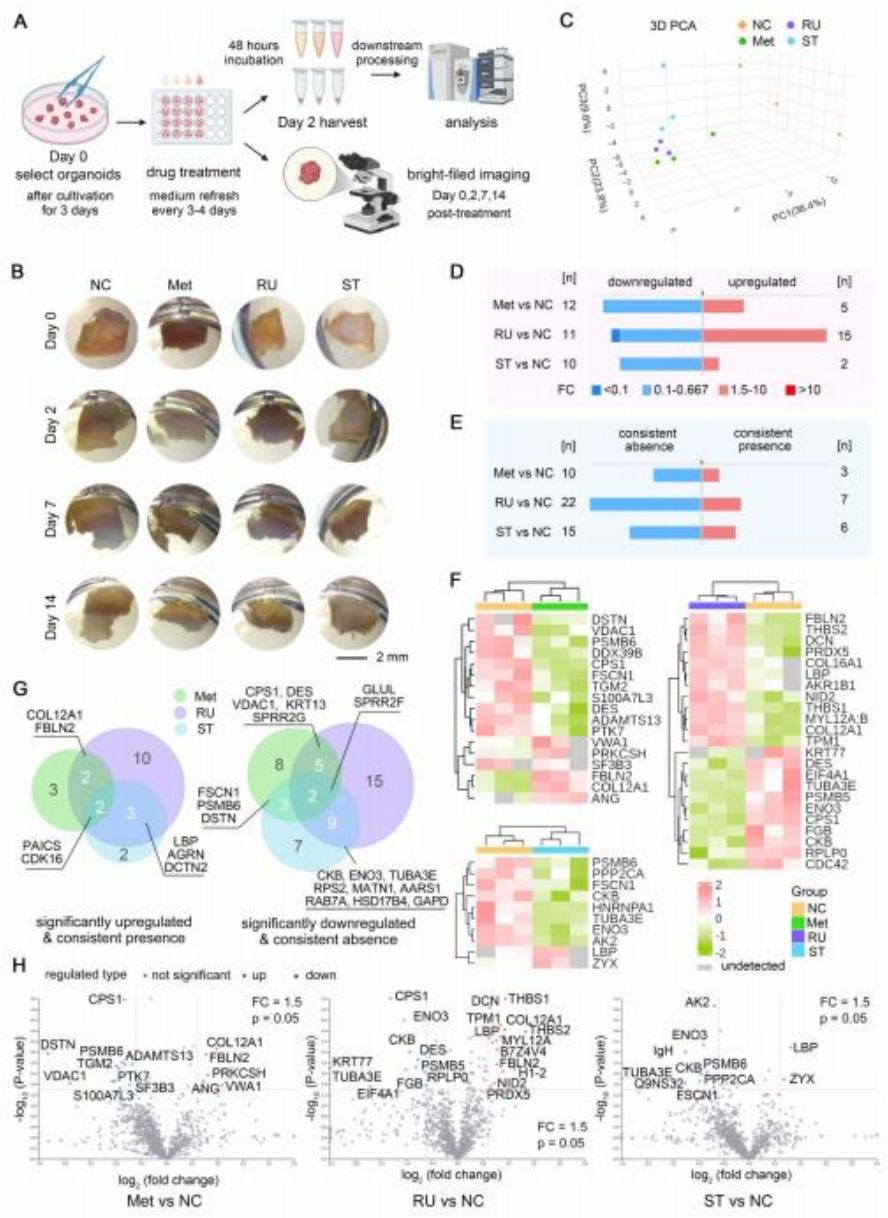

Figure 6. Drug Test in AAA PDO. (A) Schematic representation of the drug treatment process, with subsequent bright-field imaging and analysis of supernatants by mass spectrometry. (B) Bright-field images captured on days 0, 2, 7, and 14. (C) 3D PCA plot of the four test groups. (D) Number of differentially expressed proteins, with emphasis

on up- and downregulation. (E) Number of differentially expressed proteins, emphasizing consistent presence and absence across samples. (F) Heatmap of differentially expressed proteins post-hierarchical clustering, highlighting up- and downregulation. (G, H) Venn diagram and Volcano Plot illustrating the proteins significantly upregulated/emerged and downregulated/lost in different drug treatment groups compared to the control, highlighting commonalities and differences. (H) NC = negative control (solvent control 0.01% DMSO), Met = Metformin (1 μM, with 0.01% DMSO), RU = RU.521 (1 μM, with 0.01% DMSO), ST = STING-IN-2 (1 μM, with 0.01% DMSO); FC = fold change.

Discussion

The development of AAA organoid model represents a significant advancement in vascular disease research, offering a physiologically relevant platform for AAA studies. Our innovative model, engineered to replicate the intricate microenvironment of AAA, has undergone validation for multifaceted stability and has exhibited promising efficacy in initial pharmacological assessments.

Currently, the predominant focus of organoid research is on tumor-derived organoids [41]. Subsequently, considerable interest lies in organoids induced by stem cells and those derived from somatic cells or tissues with proliferative potential [42, 43]. Numerous diseases including AAA encounter limitations in developing *ex vivo* models due to their restricted proliferative capacity and the complexity of their pathology [44]. The prevalent method of investigation is currently animal-based, exemplified by the use of murine models of AAA. However, they are labor-intensive, expensive, and may not accurately reflect the pathophysiological mechanisms observed in humans [25]. Furthermore, the disparity between promising preclinical results and the absence of corresponding success in clinical trials may indicate inherent limitations in the current models for aneurysm disease representation [21]. Hence, there is a pressing demand for the development of a dependable human-derived *in vitro* AAA model.

At present, the primary method for organoid cultivation involves enzymatic dissociation into single cells, subsequent encapsulation with Matrigel [45], or the application of technologies such as microfluidics or the air-liquid interface (ALI) culture system [46]. Our cultivation system is notably innovative, offering convenience by allowing unrestricted cultivation in a standard culture dish using a specialized culture medium, thereby eliminating the requirement for enzymatic dissociation [47], or Matrigel [48, 49]. This organoid cultivation approach, by significantly retaining tissue characteristics and the microenvironment, provides a more precise reflection of the authentic physiological and pathological states *in vivo* [48-50].

The progression of AAA disease is predominantly driven by inflammation, extracellular matrix (ECM) degradation, and apoptosis of vascular smooth muscle cells (VSMCs) [51, 52]. Employing this culture system, the AAA PDO have demonstrated the structural and pathophysiological features characteristic of AAA. We have established the stability of this culture system through the following criteria: Throughout a month-long cultivation period, the PDO maintained sustained integrity, exhibiting no signs of degradation or morphological changes. The cellular and ECM phenotype was confirmed using H&E and elastic staining, and the preservation of the immune microenvironment along with the morphology of smooth muscle cells was validated through immunohistochemistry.

On the other hand, the genome of PDO has proven to be remarkably stable, showing no aberrant mutations introduced by *in vitro* cultivation, thereby validating the model's reliability and highlighting its suitability for drug exposure studies. In the present study, the samples were sourced exclusively from elderly male patients with a documented history of chronic smoking, within the age range of 61 to 73 years. Although this demographic represents a principal group at risk for AAA, additional risk factors encompass familial genetic conditions, hypertension, hyperlipidemia, and atherosclerosis. Notably, a smoking history, male gender, advanced age, and genetic predisposition are recognized as significant risk factors [53]. Consequently, genomic analysis is considered to be of considerable importance in this context. We have compiled a comprehensive list of 108 genes from extant literature that are correlated with a high risk of mutation in AAA [34-38]. A substantial overlap was noted among 28 of these genes identified in our whole-exome sequencing (WES) analysis of tissue and organoid samples from six individuals. Prominent among these overlapping genes are growth differentiation factor 7 (GDF-7) [34], a disintegrin and metalloproteinase with thrombospondin type 1 motif 8 (ADAMTS8) [35], cadherin EGF LAG seven-pass G-type receptor 2 (CELSR2) [36], Disabled homolog 2 (DAB2IP) [37], cholinergic receptor nicotinic alpha 3 (CHRNA3) [34], titin (TTN) [38], and myosin heavy chain 7 (MYH7) [38], among others. Additionally, we identified 496 mutated genes across all tissue and organoid samples, including those associated with cardiovascular diseases, such as mucin MUC family members [54], collagen type XVIII alpha 1 (COL18A1) [55], ADAMTS7 [56], tenascin XB (TNXB) [57], fibronectin type III domain containing 1 (FNDC1) [58], and lysine demethylase 6B (KDM6B, also known as JMJD3) [59]. The majority of these genes displayed multiple mutations, indicating a sophisticated genetic landscape in the etiology of AAA. This

comprehensive genetic analysis highlights the potential for a refined comprehension of the disease and could facilitate the development of targeted therapeutic strategies.

Preliminary drug testing using our AAA organoid model has produced encouraging outcomes, indicating its potential for identifying candidate therapeutic agents. In this study, we evaluated the effects of RU.521 and STING-IN-2, utilizing metformin as a positive control. Metformin, a member of the biguanide class, is well-known for its glucose-lowering effect with high safety. In addition to its action on glucose metabolism, the drug has demonstrated effects on the circulatory system and has shown participation in other biological pathways, including ECM remodeling, VSMC homeostasis, oxidative stress response, and anti-inflammatory activity [22]. It has also been associated with a reduced risk of AAA development [22, 40]. RU.521 is a small-molecule inhibitor targeting the cGAS/STING/NF-κB pathway, exerting anti-inflammatory effects [60]. Research indicates that it selectively suppresses cGAS-mediated signaling, leading to reduced interferon expression in macrophages within rodent models [61]. Likewise, STING-IN-2 is a selective covalent small molecule inhibitor that has been validated for its potent inhibitory activity against the stimulator of interferon genes (STING) protein, resulting attenuated STING-mediated inflammatory cytokine production in both human and murine cells [62].

Proteomic analysis of the supernatant from organoid cultures following drug treatment indicated that this organoid model could elicit distinct or partially overlapping responses to different drugs. Interpreting from a molecular perspective (Figure 6F-G), the expression of fibulin-2 (FBLN-2) was notably upregulated in groups treated with metformin or RU.521. FBLN-2 directs the assembly of elastic fibers and is responsible for the maintenance of the vessel wall post-injury [63]. The upregulation of collagen type XII α1 chain (COL12A1) may contribute to the remodeling of ECM [64]. Decorin (DCN), another ECM protein, regulates ECM assembly, fibrillogenesis, and biological processes, including acting as a transforming growth factor-β regulator [65, 66]. The upregulated expression of lipopolysaccharide-binding protein (LBP) in the RU.521- and STING-IN-2-treated groups may be associated with lipid droplet homeostasis and resistance to oxidative stress [67]. Thrombospondin-1 and -2 (THBS-1 and -2), uniquely upregulated in the RU.521-treated group, are implicated in vascular development, function, and exhibit anti-inflammatory activities [68]. Angiogenin (ANG), related to angiogenesis and ribonucleolytic activity, was uniquely upregulated in the metformin-treated group [69]. Zyxin (ZYX), a cytoskeletal and focal adhesion scaffold-related protein, modulates angiogenesis and cytoskeleton enlargement, was uniquely upregulated in the STING-IN-2-treated group [70]. Certain proteins, absent in the control group, emerged in drug-treated groups; for instance, agrin (AGRN), which is involved in the neuromuscular junction, inflammatory suppression and angiogenesis [71, 72], as well as cyclin-dependent kinase 16 (CDK16), which is regulated by the AMPK pathway and implicated in autophagy [73]. Conversely, several proteins were significantly downregulated in the drug-treated groups. For example, destrin (DSTN), desmin (DES), fascin (FSCN1), Ras-related protein Rab-7a (RAB7A), glutamine synthetase (GLUL) and multiple ribosomal subunits were markedly downregulated in at least two drug treated groups. Destrin and desmin have been identified as potential factors involved in aneurysm formation [74-76]. Fascin, which plays a role in the cross-linking of actin filaments [77], could potentially affect vascular smooth muscle cells and influence the integrity and function of the arterial wall. Rab-7a, involved in endocytosis and autophagy, regulates the phenotypic transformation and behavior of vascular smooth muscle cells in human aortic dissection [78]. Glutamine synthetase is implicated in angiogenesis, serving functions beyond glutamine synthesis [79]. Furthermore, the cell division cycle protein (CDC42) was specifically downregulated in the group treated with RU.521. This protein is associated with the recruitment and activation of immune cells [80, 81], potentially contributing to inflammation in AAA. Upon comparison of the list of significantly altered protein expressions with public databases, LBP, DEX, ZYX, THBS-1, and CDC42 were identified as proteins related to immune pathways. Although the underlying mechanisms necessitate additional clarification, these significant findings underscore the organoid culture system's potential for drug screening and other applications.

Despite our promising results, the study is accompanied by several limitations. Due to difficulties in sample collection, our subjects were exclusively elderly male smokers. Ideally, our sample pool should encompass a more diverse demographic, including individuals with familial genetic predispositions associated with AAA and other relevant factors, as well as those without any known risk factors. In the future, we aspire to enhance our biobank to incorporate a broader range of samples [82]. Data obtained from viability assays indicate a progressive decline in organoid viability over extended culture periods. Consequently, we opted to

conduct drug testing at an earlier stage, specifically within the initial week of cultivation. While accelerated cultivation and drug response may enhance research efficiency, future refinements must prioritize the maintenance of viability over prolonged periods, and culture methodologies should be standardized. For instance, to preserve the stratified structure of the vascular wall, efforts should be directed toward reducing the size of individual PDO to achieve greater uniformity. This approach would facilitate improved material exchange and metabolism, enhance utilization rates, and potentially increase the sample size. In the PCA analysis, a small number of proteins with different expression levels were derived solely from the supernatant, limiting further pathway studies. In the future, we intend to optimize our experimental design to attain a more effective and reproducible PCA.

Further research should consider the incorporation of more complex systems, such as Organoids-on-a-Chip [83], entailing the arrangement of the aortic wall's diverse structural layers, including perivascular adipose tissue (PVAT) and thrombi, within distinct compartments. Alternatively, microfluidic technology could be utilized to replicate blood flow and implement vacuum or pressure changes to emulate blood pressure [84]. Such advanced models could provide a more physiologically relevant context for studying the behavior of organoids and their responses to pharmacological treatments.

Conclusion

In conclusion, our AAA organoid model encapsulates a notable progression in the field, providing an innovative platform for the investigation of AAA pathophysiology and evaluating potential treatments. Characterized by its capacity to replicate key disease characteristics and maintain stability throughout an elongated timeframe, this model will be well-suited for pharmaceutical screening. As an ex vivo surrogate of the human body, it offers a unique opportunity to study the intricacies of AAA in a controlled *in vitro* microenvironment. As we further refine this model for extended applications, it is poised to augment our comprehension of AAA and contribute to the discovery of effective therapeutic strategies.

Experimental Section/Methods

Sample preparation

Aortic tissue specimens were obtained from 11 AAA patients (ages 61 to 73 years, mean age 67.2 ± 3.3 years, Table 1) who underwent resection of AAA with prosthetic graft replacement at Jiangmen Central Hospital, Guangdong Province, China. Samples were stored in a sterile vessel without tissue storage solution and transported to Shanghai LiSheng Biotech (Shanghai, China) within 24 h. The clinical samples were obtained in accordance with the ethical guidelines of Jiangmen Central Hospital and were granted institutional ethics approval with the number 2024-77 A. All procedures performed in studies involving human participants were in accordance with the ethical standards of the institutional and/or national research committee and with the 1964 Helsinki Declaration and its later amendments or comparable ethical standards. Informed consent was obtained from all individual participants included in the study.

Table 1. Collection of patient information

Patient No.	Gender	Age	Others
P01	Male	68	Smoking history 30 years
P02	Male	66	Smoking history > 30 years
P03	Male	66	Smoking history > 30 years
P04	Male	66	Smoking history 30 years; Coronary heart disease
P05	Male	73	Smoking history 50 years; Hypertension 20 years
P06	Male	61	N.A.
P07	Male	64	Smoking history 20 years; Coronary heart disease; Hypertension
P08	Male	67	Smoking history > 30 years; Hypertension
P09	Male	67	N.A.
P10	Male	73	Smoking history 30 years; Coronary heart disease; Hypertension
P11	Male	68	Smoking history > 40 years; Hypertension > 20 years

Sample processing and organoid culture

The tissue specimens were immersed in a washing buffer (LSTO01200201; Shanghai LiSheng Biotech, China) to preliminarily remove blood and then transferred to a 50 mL centrifuge tube (430829; Corning, USA) for three rounds of washing with the same buffer. Each round involved the addition of 5 mL of washing buffer and gentle agitation to rinse the tissue surface, followed by a 3 min wait. After removing the supernatant from the final round, the tissue blocks were then transferred to a 10 cm culture dish (430167; Corning, USA). The tissue blocks were sectioned into rectangles with sides measuring approximately 3-5 mm using surgical scissors and then transferred to a new 10 cm culture dish. A small portion of the tissue was reserved for sectioning and pathological staining, while another portion was retained for whole exome sequencing. Finally, 20 mL of culture medium was added to the dish (LSTO01200403; Shanghai LiSheng Biotech, China) and the cultures were maintained at 37 °C, 5% CO_2.

Throughout the organoid cultivation, partial

medium replenishment is essential, typically every 5-7 days or based on the medium's visual characteristics, including color and turbidity, to maintain the required nutrient levels for organoid metabolism. The technique for partial medium exchange involves tilting the culture dish to facilitate the removal of 8-10 mL of the old medium from the upper layer using a serological pipette. Then, 10-12 mL of freshly prepared medium was added, with an additional 1-2 mL of medium also considered to compensate for potential volume reduction due to evaporation during the cultivation.

PDO size calculation and analysis

The PDO were routinely imaged, and their sizes were quantified using ImageJ. Using a dissecting microscope with a relatively broad field of view (YZ38; Shanghai YueHe Biotech, China), the area of each organoid was calculated to track changes in size over time. Considering the limited proliferative capacity of AAA PDO, which is a distinction from the classic "spheroid" organoids, their shape, determined by the tissue processing technique, was often polygonal or rectangular. Consequently, the area analysis was conducted in ImageJ by manually tracing the organoid's perimeter.

Whole exome sequencing (WES)

For each sample, 200 ng genomic DNA was fragmented to 150-200 bp to construct libraries. Subsequently, the whole exome was captured using AIExome® Human Exome Panel V3 and TargetSeq One® Hyb & Wash Kit v2.0 (iGeneTech Co., Ltd, Beijing, China) and sequenced on DNBSEQ-T7 with 150-bp reads.

Fixation, embedding and sectioning

Routine collection of samples was performed, followed by immersion in a PBS solution with 4% paraformaldehyde (PFA) (BL539A; Biosharp, China) for 48 h fixation. Subsequently, the samples were subjected to a gradient dehydration process using a PBS solution with sucrose at concentrations of 10%, 20%, and 30% (A15583.0E; Thermo Fisher Scientific, USA) for 1 h, 2 h, and overnight, respectively. Following encapsulation of the organoids in an optimal cutting temperature compound (Tissue-Tek® O.C.T. Compound, 4583; Sakura Finetek, Japan), the samples were immediately immersed in liquid nitrogen to form embedding blocks for cryosectioning. The embedding blocks were then subjected to cryosection at -20 °C (Cryostat CM1950; Leica, Germany), with sections cut perpendicular to the vessel's lumen to expose the stratified layers of the aortic wall. Alternatively, a subset of samples was processed for paraffin embedding and sectioning. Once the fixation reagent was removed, the samples were enveloped in 2% molten agarose. After cooling and solidification, the regions containing the samples were excised, and the specimens were subjected to a dehydration (TP1020; Leica, Germany) and paraffin infiltration series as follows: 75% ethanol for 4 h, 85% ethanol for 2 h, 90% ethanol for 2 h, 95% ethanol for 1 h, 100% ethanol for 30 min (repeated three times), xylene for 5-10 min (twice), and 65 °C molten paraffin for 1 h (three times). Subsequently, the samples were embedded using an embedding machine (KD-BM IV; KEDEE, China), and the paraffin blocks were trimmed to a size conducive to sectioning (RM2016; Leica, Germany) after cooling at -20 °C.

H & E staining

Cryosectioned slides were fixed with 4% PFA in PBS for 10 min and subsequently rinsed in water. The slides were then stained with Hematoxylin and Eosin (H&E) (C0105S; Beyotime, China), beginning with a 10 min application of hematoxylin, followed by rinsing in water for 10 min. The sections were differentiated using acid alcohol (C0163M; Beyotime, China) for 5 s. Following this, the slides were rinsed again in water for 10 min and counterstained with eosin for 30 s to visualize the cytoplasm and extracellular matrix. The slides were dehydrated through a graded alcohol series and mounted with neutral balsam (Type D, G8593; Solarbio, China). Examination of the stained slides was performed using a standard microscope (YI21; Shanghai YueHe Biotech, China). On the other hand, paraffin sections necessitate an additional deparaffinization procedure prior to staining. The slides were sequentially immersed in the following solutions: xylene for 20 min (twice), 100% ethanol for 5 min (twice), and 75% ethanol for 5 min, rinse in water. After staining, the sections were dehydrated with 100% ethanol and clarified with xylene for 5 min. Following this, the slides were mounted with neutral balsam and prepared for scanning (KF-DPS-120; Kfbio, China).

For quantitative analysis based on H&E staining, ImageJ was utilized, and the ratios were calculated as the number of cell nuclei per area of the section. Images were processed using the Color Deconvolution plugin in ImageJ with the H&E Vectors to separate Hematoxylin-stained components. Subsequently, a threshold of 1-180 was applied, fine-tuning as necessary to clearly display cell nuclei without severe overlap and minimal background noise. Anatomically corresponding Regions of Interest (ROIs) were selected; six non-overlapping ROIs were selected in total, each measuring 600 μm^2 in size. Application of the Analyze Particles function

was then made to each ROI with a size range of 5-Infinity μm² for counting. For statistical analysis, GraphPad 9.0 software was employed, and a t-test was performed to compare tissue to PDO.

Verhoeff-van Gieson elastic staining

Cryosectioned slides were fixed in 4% PFA in PBS for 10 min, then rinsed in water for 10 min. The slides were subsequently stained with a mixture of 5% alcoholic hematoxylin (HE-013-100mL; BIOISCO, China), 10% ferric chloride (Iron(III) chloride, anhydrous, A600454-0500; Sangon Biotech, China), and Lugol's Iodine Solution (MM1049-100mL; MKBio, China) in a 1:1:0.5 ratio for 15 min. Following a 1 min rinse in water, slides were differentiated with 2% ferric chloride, then rinsed again for 1 min. Then, the slides were soaked in 5% sodium thiosulfate (217263-5G; Sigma-Aldrich, USA), rinsed in water for 1 min, and soaked in Van Gieson's Stain (MM1032; MKBio, China) for 30 s. After staining, the slides were dehydrated through a series of 100% alcohol and mounted using neutral balsam. The slides were examined using a standard microscope.

Quantitative analysis was performed to determine the ratio of elastic fiber staining to tissue area. The deep purple areas, corresponding to elastic fibers, were identified using the Color Deconvolution plugin in ImageJ (with the Vector set to H&E 2). ROIs containing elastic fibers, excluding cholesterol plaques, were delineated into 4 to 6 sections. A uniform threshold ranging from 1 to 200 was applied to calculate the area percentage of elastic fibers in ROI.

Immunohistochemistry (IHC)

For IHC analysis, paraffin-embedded slides (3-4 μm thick) were immunostained for CD3, CD38, CD45, CD68, MMP-9, F4/80 and α-actin. Deparaffinized sections were treated with a peroxidase-blocking solution for 10 min to quench endogenous peroxidase activity. Following rinses with PBS, the slides were immersed in pre-heated 1 mmol Tris-EDTA buffer (pH 9.0) for 15 min, then incubated at room temperature (RT) for an additional 15 min. After washing with PBS, the slides were incubated with 5% BSA for 20 min to block non-specific binding. Primary antibodies were applied and incubated at 4 °C overnight. After PBS rinses, HRP-conjugated secondary antibodies (WAS12011; World Advanced Science, China) were applied for 30 min at 37 °C. Following PBS rinses, the slides were incubated with 3,3'-Diaminobenzidine (DAB) solution (BP0770; DAKO, Denmark) and monitored under a microscope. Slides were then rinsed, counterstained with hematoxylin for 30 s at RT, dehydrated, and mounted with neutral balsam for scanning (KF-DPS-120; Kfbio, China).

The original image data were divided into four approximately equal parts with minimal overlap and blank space, each accounting for less than 20%. Using the ImageJ IHC profiler plugin, the percentage of positively stained areas was quantified. Scores from high positive, positive, and low positive areas were multiplied by factors of 3, 2, and 1, respectively, and summed for analysis.

Live-cell staining and imaging

PDO were rinsed twice using pre-warmed (37 °C) PBS and subsequently fragmented with spring scissors. In accordance with the standard protocol outlined in the Calcein/PI Cell Viability/Cytotoxicity Assay Kit (C2015M; Beyotime, China), the minced organoid fragments were stained using a shaker at 37 °C and 90 rpm for 45 min. After rinsing twice with pre-warmed (37 °C) PBS, an appropriate amount of antifading mounting medium (S2100; Solarbio, China) was added, followed by transferring the fragments to a 96-well plate (CHIMNEY WELL, μCLEAR®, WHITE, CELLSTAR®, REF 655098; Greiner Bio-One, Germany), with a 50 μL aliquot of the suspension per well. The organoid fragments were then examined under a fluorescence microscope (DMi8; Leica, Germany).

Alternatively, the initial step can be accomplished using an enzymatic cocktail to digest the extracellular matrix, thereby releasing individual cells and potentially enhancing staining outcomes. The digestion mixture comprises Collagenase Type I (5%, 150 mg/mL) (17100-017; Gibco, USA), DNase I (1%, 10 mg/mL) (A510099-0001; Sangon Biotech, China), Elastase (1%, 200 U/mL) (abs47014929; Absin, China), and Hyaluronidase (0.4%, 2 mg/mL), each dissolved in Trypsin (0.25%, 15050057; Gibco, USA). The PDO were incubated with this mixture for 1 h, rinsed twice with PBS, and then centrifuged at 500x g to pellet the cells before proceeding with the staining procedure.

The image data were converted to 8-bit grayscale in ImageJ, followed by background subtraction with a rolling ball radius of 50 and thresholding set between 10 and 128. Measurements were taken for the mean fluorescence intensity of both the red and green channels. The ratio of green to red fluorescence intensity was then calculated. These values were normalized to the arithmetic mean of the green/red fluorescence intensity on Day 1 to determine the fold change.

Organoid viability: alamarBlueTM assay

Following the protocol of the alamarBlue™ HS Cell Viability Reagent (Invitrogen A50100; Thermo

Fisher Scientific, USA), the manipulation procedure for AAA PDO was optimized. PDO were placed into individual wells of a 24-well plate (COSTAR® 3524; Corning, USA) and cultured in 1 mL of AAA organoid culture medium with 5% reagent, with a subsequent incubation for 20 h. Afterwards, the supernatant was collected, centrifuged at 3000x g for 5 min, and transferred to a 96-well plate (CHIMNEY WELL, µCLEAR®, WHITE, CELLSTAR®, REF 655098; Greiner Bio-One, Germany). The fluorescence intensity was measured using a microplate reader (Spark; TECAN, Switzerland) with excitation and emission wavelengths set at 560 nm and 595 nm, respectively. After the test, the PDO were rinsed three times with PBS and cultured in 1 mL of AAA organoid culture medium, and this medium was reused in subsequent cultivation periods. After a 2-3 days' interval, the subsequent round of testing could be initiated to monitor the activity changes of the same sample over time.

Drug treatment for AAA PDO

On the third day of cultivation, PDO underwent drug treatment. Upon transfer to a 24-well plate (COSTAR® 3524; Corning, USA), 1 mL of fresh medium containing 10 µL of the test drug solution was added to each well. The solvent of drug solution was PBS with 1% DMSO, and the solutes included 1 µM Metformin (S5958; Selleckchem, USA), 1 µM RU.521 (HY-114180; MedChemExpress, USA), 1 µM STING-IN-2 (HY-138682; MedChemExpress, USA), and solvent control, respectively. After a 48 h incubation at 37 °C with 5% CO_2, the supernatants and PDO were collected separately and stored at -80 °C.

Proteomics analysis

After drug treatment, the supernatants were concentrated and underwent quality control. From each sample, 15 µg of protein was extracted for separation by SDS-PAGE. Then, proteins were digested using the Filter Aided Sample Preparation (FASP) method. The peptides were further processed and subjected to chromatographic separation using the Vanquish Neo UHPLC system (Thermo Fisher Scientific), followed by Data-Independent Acquisition (DIA) mass spectrometry analysis with an Astral high-resolution mass spectrometer. The aforementioned assays and subsequent bioinformatics analysis were performed by APPLIED PROTEIN TECHNOLOGY (APTBIO) Co., Ltd, Shanghai, China, in accordance with their standard operating procedures.

Statistical analysis

Data were collected from at least three replicates, and quantitative results are expressed as mean ± standard deviation. Statistical analysis was conducted using GraphPad Prism version 9.0.0 (GraphPad Software, USA). Student's t-test was applied for pairwise comparisons to determine significance. For comparisons involving more than two groups, one-way ANOVA was employed. A p-value less than 0.05 was considered statistically significant. Statistical significance is indicated as: *$p < 0.05$, **$p < 0.01$, and ***$p < 0.001$. Error bars represent the standard deviation of the mean.

Supplementary Material

Supplementary methods and figures.
https://www.thno.org/v15p9029s1.pdf

Acknowledgements

This work was supported by the Project of Medical Key Construction Specialty of Shanghai Jiading District (ZK2024A07) and National Natural Science Foundation of China (No: 82000464). We also sincerely thank Guangkuo Wang from the Department of Cardiovascular Surgery, Jiangmen Central Hospital, Guangdong, for their invaluable contribution in providing the specimens. Some diagrams created and modified by BioRender.com and Adobe PhotoShop.

Competing Interests

The authors have declared that no competing interest exists.

References

1. Sakalihasan N, Limet R, Defawe OD. Abdominal aortic aneurysm. Lancet. 2005; 365: 1577-89
2. Hensley SE, Upchurch GR Jr. Repair of abdominal aortic aneurysms: JACC focus seminar, part 1. J Am Coll Cardiol. 2022; 80: 821-831
3. Kent KC, Zwolak RM, Egorova NN, Riles TS, Manganaro A, Moskowitz AJ, et al. Analysis of risk factors for abdominal aortic aneurysm in a cohort of more than 3 million individuals. J Vasc Surg. 2010; 52: 539-548
4. Sidloff D, Stather P, Dattani N, Bown MJ, Thompson J, Sayers R, et al. Aneurysm global epidemiology study: public health measures can further reduce abdominal aortic aneurysm mortality. Circulation. 2014; 129: 747-753
5. Kuivaniemi H, Shibamura H, Arthur C, Berguer R, Cole CW, Juvonen T, et al. Familial abdominal aortic aneurysms: collection of 233 multiplex families. J Vasc Surg. 2003; 37: 340-345
6. Tang W, Yao L, Roetker NS, Alonso A, Lutsey PL, Steenson CC, et al. Lifetime risk and risk factors for abdominal aortic aneurysm in a 24-year prospective study: the ARIC study (atherosclerosis risk in communities). Arterioscler Thromb Vasc Biol. 2016; 36: 2468-2477
7. Larsson E, Granath F, Swedenborg J, Hultgren R. A population-based case-control study of the familial risk of abdominal aortic aneurysm. J Vasc Surg. 2009; 49: 47-50
8. Brady AR, Thompson SG, Fowkes FG, Greenhalgh RM, Powell JT. Abdominal aortic aneurysm expansion: risk factors and time intervals for surveillance. Circulation. 2004; 110: 16-21
9. Sakalihasan N, Michel JB, Katsargyris A, Kuivaniemi H, Defraigne JO et al. Abdominal aortic aneurysms. Nat Rev Dis Primers. 2018; 4: 34
10. López-Candales A, Holmes DR, Liao S, Scott MJ, Wickline SA, Thompson RW. Decreased vascular smooth muscle cell density in medial degeneration of human abdominal aortic aneurysms. Am J Pathol. 1997; 150: 993-1007

11. Raffort J, Lareyre F, Clément M, Hassen-Khodja R, Chinetti G, Mallat Z. Monocytes and macrophages in abdominal aortic aneurysm. Nat Rev Cardiol. 2017; 14: 457-471
12. Satoh K, Nigro P, Matoba T, O'Dell MR, Cui Z, Shi X, et al. Cyclophilin a enhances vascular oxidative stress and the development of angiotensin II-induced aortic aneurysms. Nat Med. 2009; 15: 649-656
13. Cheng J, Zhang R, Li C, Tao H, Dou Y, Wang Y, et al. A targeting nanotherapy for abdominal aortic aneurysms. J Am Coll Cardiol. 2018; 72: 2591-2605
14. MA3RS Study Investigators. Aortic wall inflammation predicts abdominal aortic aneurysm expansion, rupture, and need for surgical repair. Circulation. 2017; 136: 787-797
15. Eliason JL, Hannawa KK, Ailawadi G, Sinha I, Ford JW, Deogracias MP, et al. Neutrophil depletion inhibits experimental abdominal aortic aneurysm formation. Circulation. 2005; 112: 232-240
16. Hannawa KK, Eliason JL, Woodrum DT, Pearce CG, Roelofs KJ, Grigoryants V, et al. L-selectin-mediated neutrophil recruitment in experimental rodent aneurysm formation. Circulation. 2005; 112: 241-247
17. Rateri DL, Howatt DA, Moorleghen JJ, Charnigo R, Cassis LA, Daugherty A. Prolonged infusion of angiotensin II in apoE(-/-) mice promotes macrophage recruitment with continued expansion of abdominal aortic aneurysm. Am J Pathol. 2011; 179: 1542-1548
18. Wang J, Lindholt JS, Sukhova GK, Shi MA, Xia M, Chen H, et al. IgE actions on CD4+ T cells, mast cells, and macrophages participate in the pathogenesis of experimental abdominal aortic aneurysms. EMBO Mol Med. 2014; 6: 952-969
19. Tsuruda T, Kato J, Hatakeyama K, Kojima K, Yano M, Yano Y, et al. Adventitial mast cells contribute to pathogenesis in the progression of abdominal aortic aneurysm. Circ Res. 2008; 102: 1368-1377
20. Sun J, Zhang J, Lindholt JS, Sukhova GK, Liu J, He A, et al. Critical role of mast cell chymase in mouse abdominal aortic aneurysm formation. Circulation. 2009; 120: 973-982
21. Lindeman JH, Matsumura JS. Pharmacologic management of aneurysms. Circ Res. 2019; 124: 631-646
22. Raffort J, Hassen-Khodja R, Jean-Baptiste E, Lareyre F. Relationship between metformin and abdominal aortic aneurysm. J Vasc Surg. 2020; 71: 1056-1062
23. Kim J, Koo BK, Knoblich JA. Human organoids: model systems for human biology and medicine. Nat Rev Mol Cell Biol. 2020; 21: 571-584
24. Corsini NS, Knoblich JA. Human organoids: new strategies and methods for analyzing human development and disease. Cell. 2022; 185: 2756-2769
25. Han X, Cai C, Deng W, Shi Y, Li L, Wang C, et al. Landscape of human organoids: ideal model in clinics and research. Innovation (Camb). 2024; 5: 100620
26. Zhang F, Li K, Zhang W, Zhao Z, Chang F, Du J, et al. Ganglioside GM3 protects against abdominal aortic aneurysm by suppressing ferroptosis. Circulation. 2024; 149: 843-859
27. Tian Z, Zhang Y, Zheng Z, Zhang M, Zhang T, Jin J, et al. Gut microbiome dysbiosis contributes to abdominal aortic aneurysm by promoting neutrophil extracellular trap formation. Cell Host Microbe. 2022; 30: 1450-1463
28. Wang ZY, Cheng J, Wang Y, Yuan HT, Bi SJ, Wang SX, et al. Macrophage ILF3 promotes abdominal aortic aneurysm by inducing inflammatory imbalance in male mice. Nat Commun. 2024; 15: 7249
29. Wen Y, Liu Y, Li Q, Tan J, Fu X, Liang Y, et al. Spatiotemporal ATF3 expression determines VSMC fate in abdominal aortic aneurysm. Circ Res. 2024; 134: 1495-1511
30. Miao Y, Pek NM, Tan C, Jiang C, Yu Z, Iwasawa K, et al. Co-development of mesoderm and endoderm enables organotypic vascularization in lung and gut organoids. Cell. 2025; 10.1016/j.cell.2025.05.041
31. Pan Z, Yao Q, Kong W, Ma X, Tian L, Zhao Y, et al. Generation of iPSC-derived human venous endothelial cells for the modeling of vascular malformations and drug discovery. Cell Stem Cell. 2025; 32: 227-245
32. Henriques JF, Gonçalves L, Amaro AM, Piedade AP. 3D printed polymers that mimic the mechanical properties of atherosclerotic blood vessels for training models: the advantageous degradation induced by UV radiation and hydrolysis. 3D Print Med. 2025; 11: 34
33. Bogunovic N, Meekel JP, Majolée J, Hekhuis M, Pyszkowski J, Jockenhövel S, et al. Patient-specific 3-dimensional model of smooth muscle cell and extracellular matrix dysfunction for the study of aortic aneurysms. J Endovasc Ther. 2021; 28: 604-613
34. Gyftopoulos A, Ziganshin BA, Elefteriades JA, Ochoa Chaar CI. Comparison of genes associated with thoracic and abdominal aortic aneurysms. Aorta (Stamford). 2023; 11: 125-134
35. Lamblin N, Ratajczak P, Hot D, Dubois E, Chwastyniak M, Beseme O, et al. Profile of macrophages in human abdominal aortic aneurysms: a transcriptomic, proteomic, and antibody protein array study. J Proteome Res. 2010; 9: 3720-3729
36. Steffen BT, Pankow JS, Norby FL, Lutsey PL, Demmer RT, Guan W, et al. Proteomics analysis of genetic liability of abdominal aortic aneurysm identifies plasma neogenin and kit ligand: the ARIC study. Arterioscler Thromb Vasc Biol. 2023; 43: 367-378
37. Gretarsdottir S, Baas AF, Thorleifsson G, Holm H, den Heijer M, de Vries JP, et al. Genome-wide association study identifies a sequence variant within the DAB2IP gene conferring susceptibility to abdominal aortic aneurysm. Nat Genet. 2010; 42: 692-697
38. Lenarduzzi S, Spedicati B, Alessandrini B, Cappellani S, Di Fruscio G, Tomanin R, et al. Whole-exome sequencing: clinical characterization of pediatric and adult Italian patients affected by different forms of hereditary cardiovascular diseases. Mol Genet Genomic Med. 2023; 11: e2143
39. Hinchliffe RJ. Metformin and abdominal aortic aneurysm. Eur J Vasc Endovasc Surg. 2017; 54: 679-680
40. Fujimura N, Xiong J, Kettler EB, Xuan H, Glover KJ, Mell MW, et al. Metformin treatment status and abdominal aortic aneurysm disease progression. J Vasc Surg. 2016; 64: 46-54
41. Drost J, Clevers H. Organoids in cancer research. Nat Rev Cancer. 2018; 18: 407-418
42. Vandana JJ, Manrique C, Lacko LA, Chen S. Human pluripotent-stem-cell-derived organoids for drug discovery and evaluation. Cell Stem Cell. 2023; 30: 571-591
43. Fujii M, Sato T. Somatic cell-derived organoids as prototypes of human epithelial tissues and diseases. Nat Mater. 2021; 20: 156-169
44. Andrews MG, Kriegstein AR. Challenges of organoid research. Annu Rev Neurosci. 2022; 45: 23-39
45. Gan Z, Qin X, Liu H, Liu J, Qin J. Recent advances in defined hydrogels in organoid research. Bioact Mater. 2023; 28: 386-401
46. Polak R, Zhang ET, Kuo CJ. Cancer organoids 2.0: modelling the complexity of the tumour immune microenvironment. Nat Rev Cancer. 2024; 24: 523-539
47. Hu Y, Sui X, Song F, Li Y, Li K, Chen Z, et al. Lung cancer organoids analyzed on microwell arrays predict drug responses of patients within a week. Nat Commun. 2021; 12: 2581
48. Shi Y, Liu J, Li L, Wang C, Zhang J, Rong M, et al. Patient-derived skin tumor organoids with immune cells respond to metformin. Cell Organoid. 2024; 10.26599/co.2024.9410001
49. Cao Q, Li L, Zhao Y, Wang C, Shi Y, Tao X, et al. PARPi decreased primary ovarian cancer organoid growth through early apoptosis and base excision repair pathway. Cell Transplant. 2023; 32: 9636897231187996
50. Jacob F, Salinas RD, Zhang DY, Nguyen PTT, Schnoll JG, Wong SZH, et al. A patient-derived glioblastoma organoid model and biobank recapitulates inter- and intra-tumoral heterogeneity. Cell. 2020; 180: 188-204
51. Hellenthal FA, Buurman WA, Wodzig WK, Schurink GW. Biomarkers of abdominal aortic aneurysm progression. Part 2: inflammation. Nat Rev Cardiol. 2009; 6: 543-552
52. Márquez-Sánchez AC, Koltsova EK. Immune and inflammatory mechanisms of abdominal aortic aneurysm. Front Immunol 2022; 13: 989933
53. Isselbacher EM, Preventza O, Hamilton Black J 3rd, Augoustides JG, Bolen MA, Beck AW, et al. 2022 ACC/AHA guideline for the diagnosis and management of aortic disease: a report of the American Heart Association/American College of Cardiology joint committee on clinical practice guidelines. Circulation. 2022; 146: e334-482
54. Viljoen C, Szymanski P, Osman N, Henning KL, Scholtz P, Rayner B, et al. Intimomedial mucoid degeneration causing aortic and renal artery aneurysms in a young adult. Cardiovasc J Afr. 2016; 27: 49-52
55. Moulton KS, Olsen BR, Sonn S, Fukai N, Zurakowski D, Zeng X. Loss of collagen XVIII enhances neovascularization and vascular permeability in atherosclerosis. Circulation. 2004; 110: 1330-1336
56. Arroyo AG, Andrés V. Adamts7 in cardiovascular disease: from bedside to bench and back again? Circulation. 2015; 131: 1156-1159
57. Liang G, Wang S, Shao J, Jin YJ, Xu L, Yan Y, et al. Tenascin-X mediates flow-induced suppression of EndMT and atherosclerosis. Circ Res. 2022; 130: 1647-1659
58. Song Y, Guo JF, Lan PS, Wang M, Du QY. Investigation of the pan-cancer property of FNDC1 and its molecular mechanism to promote lung adenocarcinoma metastasis. Transl Oncol. 2024; 44: 101953
59. Davis FM, Tsoi LC, Melvin WJ, denDekker A, Wasikowski R, Joshi AD, et al. Inhibition of macrophage histone demethylase JMJD3 protects against abdominal aortic aneurysms. J Exp Med. 2021; 218: e20201839
60. Shao J, Meng Y, Yuan K, Wu Q, Zhu S, Li Y, et al. RU.521 mitigates subarachnoid hemorrhage-induced brain injury via regulating microglial polarization and neuroinflammation mediated by the cGAS/STING/NF- κB pathway. Cell Commun Signal. 2023; 21: 264
61. Vincent J, Adura C, Gao P, Luz A, Lama L, Asano Y, et al. Small molecule inhibition of cGAS reduces interferon expression in primary macrophages from autoimmune mice. Nat Commun. 2017; 8: 750
62. Haag SM, Gulen MF, Reymond L, Gibelin A, Abrami L, Decout A, et al. Targeting STING with covalent small-molecule inhibitors. Nature. 2018; 559: 269-273
63. Chapman SL, Sicot FX, Davis EC, Huang J, Sasaki T, Chu ML, et al. Fibulin-2 and fibulin-5 cooperatively function to form the internal elastic lamina and protect from vascular injury. Arterioscler Thromb Vasc Biol. 2010; 30: 68-74
64. Papanicolaou M, Parker AL, Yam M, Filipe EC, Wu SZ, Chitty JL, Wyllie K, et al. Temporal profiling of the breast tumour microenvironment reveals collagen XII as a driver of metastasis. Nat Commun. 2022; 13: 4587
65. Chen S, Young MF, Chakravarti S, Birk DE. Interclass small leucine-rich repeat proteoglycan interactions regulate collagen fibrillogenesis and corneal stromal assembly. Matrix Biol. 2014; 35: 103-111
66. Yamaguchi Y, Mann DM, Ruoslahti E. Negative regulation of transforming growth factor-beta by the proteoglycan decorin. Nature. 1990; 346: 281-284
67. Zhang Q, Shen X, Yuan X, Huang J, Zhu Y, Zhu T, et al. Lipopolysaccharide binding protein resists hepatic oxidative stress by regulating lipid droplet homeostasis. Nat Commun. 2024; 15: 3213

68. Liu B, Yang H, Song YS, Sorenson CM, Sheibani N. Thrombospondin-1 in vascular development, vascular function, and vascular disease. Semin Cell Dev Biol. 2024; 155: 32-44
69. Loveland AB, Koh CS, Ganesan R, Jacobson A, Korostelev AA. Structural mechanism of angiogenin activation by the ribosome. Nature. 2024; 630: 769-776
70. He S, Zhang J, Liu Z, Wang Y, Hao X, Wang X, et al. Upregulated cytoskeletal proteins promote pathological angiogenesis in moyamoya disease. Stroke. 2023; 54: 3153-3164
71. Baehr A, Umansky KB, Bassat E, Jurisch V, Klett K, Bozoglu T, et al. Agrin promotes coordinated therapeutic processes leading to improved cardiac repair in pigs. Circulation. 2020; 142: 868-881
72. Ruegg MA, Bixby JL. Agrin orchestrates synaptic differentiation at the vertebrate neuromuscular junction. Trends Neurosci. 1998; 21: 22-27
73. Dohmen M, Krieg S, Agalaridis G, Zhu X, Shehata SN, Pfeiffenberger E, et al. AMPK-dependent activation of the cyclin Y/CDK16 complex controls autophagy. Nat Commun. 2020; 11: 1032
74. Molacek J, Mares J, Treska V, Houdek K, Baxa J. Proteomic analysis of the abdominal aortic aneurysm wall. Surg Today. 2014; 44: 142-151
75. Xu H, Chen S, Zhang H, Zou Y, Zhao J, Yu J, et al. Network-based analysis reveals novel gene signatures in the peripheral blood of patients with sporadic nonsyndromic thoracic aortic aneurysm. J Cell Physiol. 2020; 235: 2478-2491
76. Nakajima N, Nagahiro S, Sano T, Satomi J, Satoh K. Phenotypic modulation of smooth muscle cells in human cerebral aneurysmal walls. Acta Neuropathol. 2000; 100: 475-480
77. Zhang J, Fonovic M, Suyama K, Bogyo M, Scott MP. Rab35 controls actin bundling by recruiting fascin as an effector protein. Science. 2009; 325: 1250-1254
78. He K, Sun H, Zhang J, Zheng R, Gu J, Luo M, et al. Rab7-mediated autophagy regulates phenotypic transformation and behavior of smooth muscle cells via the Ras/Raf/MEK/ERK signaling pathway in human aortic dissection. Mol Med Rep. 2019; 19: 3105-3113
79. Eelen G, Dubois C, Cantelmo AR, Goveia J, Brüning U, DeRan M, et al. Role of glutamine synthetase in angiogenesis beyond glutamine synthesis. Nature. 2018; 561: 63-69
80. Allen WE, Zicha D, Ridley AJ, Jones GE. A role for Cdc42 in macrophage chemotaxis. J Cell Biol. 1998; 141: 1147-1157
81. Tian C, Wang Y, Su M, Huang Y, Zhang Y, Dou J, et al. Motility and tumor infiltration are key aspects of invariant natural killer T cell anti-tumor function. Nat Commun. 2024; 15: 1213
82. Yang H, Cheng J, Zhuang H, Xu H, Wang Y, Zhang T, et al. Pharmacogenomic profiling of intra-tumor heterogeneity using a large organoid biobank of liver cancer. Cancer Cell. 2024; 42: 535-551
83. Park SE, Georgescu A, Huh D. Organoids-on-a-chip. Science 2019; 364: 960-965
84. Quintard C, Tubbs E, Jonsson G, Jiao J, Wang J, Werschler N, et al. A microfluidic platform integrating functional vascularized organoids-on-chip. Nat Commun. 2024; 15: 1452
85. Hinterseher I, Schworer CM, Lillvis JH, Stahl E, Erdman R, Gatalica Z, et al. Immunohistochemical analysis of the natural killer cell cytotoxicity pathway in human abdominal aortic aneurysms. Int J Mol Sci. 2015; 16: 11196-11212
86. Sun P, Zhang L, Gu Y, Wei S, Wang Z, Li M, et al. Immune checkpoint programmed death-1 mediates abdominal aortic aneurysm and pseudoaneurysm progression. Biomed Pharmacother. 2021; 142: 111955
87. Curci JA. Digging in the "soil" of the aorta to understand the growth of abdominal aortic aneurysms. Vascular. 2009; 17: S21-29

礼升风采

让你的"器官"在体外试药？这家公司做到了！

上海虹口 2024年05月27日 08:01 上海

当下，深入推动科技创新引领产业创新，因地制宜发展新质生产力，是虹口坚定不移的长期战略。今年以来，虹口积极服务全市大局，在生物医药等前沿领域积极拓宽渠道，打造北科创生物技术产业园等平台载体，构筑起一个充满活力的产业集群和生态圈，加速了科技成果的转化与应用，为区域经济的持续健康发展注入了强大动力。

在人体外，我们模拟脑类器官来洞察大脑的运行机制，构建肿瘤类器官来评估药物的治疗潜力。这一曾经看似"遥不可及"的黑科技，如今在虹口落地生根，正是落户于北科创生物技术产业园的上海礼升生物科技的核心研究方向，其专业术语为"类器官"。

• 虹口区政府大力支持上海礼升生物

上海虹口

The Innovation | 人源类器官：科研突破与治疗创新的黄金选择

原创 X Han, C Cai TheInnovation创新 2024年04月26日 00:02 浙江

类器官研究的前世今生。

导读

目前，类器官在科学研究、药物开发和患者药敏等领域的应用呈指数级迅猛发展。我们梳理并深入解析近年类器官领域的重要文献，旨在为类器官领域的研究者、开发者、从业者提供全景式概览、梳理和展望，回顾已有成果，开拓应用前沿，展望未来前景，助力类器官行业的蓬勃发展。

The Innovation 类器官大综述官方报导 •

大圣的毫毛—上海礼升生物最新科教纪录片，带您走进类器官的世界

上海礼升生物 2024年08月25日 15:08 上海

#黑神话：悟空，最近最火的游戏非《黑神话：悟空》莫属，听说有人已通关，有人还在打怪升级千百遍。一夜之间，我们的传统文化瑰宝西游记火遍全球。齐天大圣孙悟空有一个特异功能大家耳熟能详，那就是拔下一根毫毛，就能幻化出无数替身。这是很多人梦寐以求的超能力。今天让我们跟随上海科教频道最新科普纪录片，和上海礼升生物一起去了解被誉为"大圣的毫毛"的类器官技术。

• 上海科教频道与上海礼升生物联合录制类器官科普宣传片

知名公众号"生物世界"多次推送 •

LISHENG
上海礼升生物
Shanghai Lisheng Biotech

北京大学
PEKING UNIVERSITY
生命科学华东产业研究院
East China Institute of Biotechnology, PKU

LiSheng Organ Regeneration Lab
East China Institute of Biotechnology, Peking University

礼升生物 学术成果已发表于

CellPress
Science that inspires

The Innovation
A Journal to See the Unseen & Change the Unchanged

清華大学出版社
Tsinghua University Press
Cell Organoid

WILEY
MedComm
Open Access

Sage
CELL TRANSPLANTATION